Synthesis, Characterization, Catalytic and Biological Applications of Bidentate Half Sandwich Ir(III), Rh(III), Ru(II) and Os(II) Complexes

by

Saravanan Thangavel

(MSc)

Dissertation submitted in fulfilment of the academic requirements for the degree of Doctor of Philosophy in the School of Chemistry & Physics, University of KwaZulu-Natal, Durban, South Africa

As the candidate's supervisor, I have approved this dissertation for submission.

Signed---------- Name---------- Date----------

December, 2015

Abstract

The complexes [Cp*MCl(**L**)]PF_6 (M = Ir (**1a**), Rh (**2a**)), (where Cp* = pentamethylcyclopentadiene) and [(η^6-arene)RuCl(**L**)]PF_6 (**3a**) [**L** = N-(pyridin-2-ylmethylene)aniline] have been synthesized and the structure and purity of these were confirmed by single crystal XRD and elemental analyses. The catalytic performance of the complexes as catalysts for the dehydrogenation of primary alcohols was investigated. The Gibbs free energy (ΔG) calculation was carried out to support the proposed reaction mechanism of the Rh complex (**2a**) using DFT study.

Six new complexes of [Cp*IrCl(**L**)]PF_6 (L = *p*-R-N-(pyridin-2-ylmethyl)aniline) (R = H (**1b**), F (**2b**), OCH_3 (**3b**)), and [Cp*RhCl(**L**)]PF_6 (R = H (**4b**), F (**5b**), OCH_3 (**6b**)) have been synthesized and characterized by various spectrometric techniques. The crystal structures of **1b** and **6b** have been resolved by X-ray crystallography. These complexes were used as catalysts for transfer hydrogenation of aromatic carbonyl compounds in water with sodium formate and formic acid as the hydrogen source under pH dependent acidic conditions.

The new carbazole N,N' ligand containing [Cp*MCl(**L**)]PF_6, (M = Ir (**1c**) and Rh (**2c**)) and [(η^6-C_6H_6)RuCl(**L**)]PF_6 (**3c**), [(η^6-*p*-cymene)RuX(**L**)]PF_6 (X = Cl (**4c**), Br (**5c**), I (**6c**)), [(η^6-C_6H_6)OsCl(**L**)]PF_6 (**7c**), [(η^6-*p*-cymene)OsX(**L**)]PF_6 X = Cl (**8c**), I (**9c**)) (**L**=9-ethyl-N-(pyridine-2-yl-methylene)-9H-carbazole-3-amine) complexes have been synthesized and characterized by various spectrometric techniques. The crystal structures of **2c** and **6c** have been confirmed by single crystal XRD. Anticancer study using complexes **1c**-**3c** clearly showed potent inhibition of MCF-7 cell lines under *in vitro* conditions.

New complexes of [$RuCl_2$(**L1**)(COD)] (**1d**)**,** [$RuCl_2$(**L2**)(COD)] (**2d**), [$RuCl_2$(**L3**)(COD)] (**3d**), [$RuCl_2$(**L4**)(COD)] (**4d**), [$RuCl_2$(**L5**)(COD)] (**5d**) (**L** = (*p*-R-N-(pyridin-2-yl-methylene)aniline), R = H (**L1**), Cl (**L2**), OCH_3 (**L3**), CH_3 (**L4**), **L5** = (9-ethyl-N-(pyridin-2-yl-methylene)-9H-carbazole-3-amine and COD = η^4-cyclooctadiene) were synthesized and characterized by various spectrometric techniques. The structures of complexes **1d**, **2d** and **3d** have been confirmed by

single crystal XRD. Interactions of complexes **1d-5d** with human serum albumin (HSA) were investigated.

Six new complexes of [Cp*IrCl(**L**)] [**L** = (*p*-R-N-benzylidene-9-ethyl-9H-carbazol-3-amine)] (R = F (**1e**), CH_3 (**2e**), OCH_3 (**3e**)), and [Cp*RhCl(**L**)] (R = F (**4e**), CH_3 (**5e**), OCH_3 (**6e**)) have been synthesized and characterized by various spectrometric techniques. The crystal structures of the [Cp*MCl(**L**)] (M = Ir (**2e**), Rh (**5e**)) were solved by X-ray crystallography.

Preface

The experimental work described in this thesis was performed in the School of Chemistry, University of KwaZulu-Natal, Durban, from February 2013 to December 2015, under the supervision of Prof. Holger B. Friedrich.

These studies represent original work by the author and have not otherwise been submitted in any form for any degree or diploma to any tertiary institution. The work of others that has been used in this study is duly acknowledged in the text.

Saravanan Thangavel
B.Sc, M.Sc (Bharathiar University, Tamilnadu, India)

Declaration 1

Plagiarism

I, ---------- hereby declare that:

1. The research reported in this thesis, except where otherwise indicated, is my original research.

2. This thesis has not been submitted for any degree or examination at any other university.

3. This thesis does not contain other person's data, pictures, graphs or other information, unless specifically acknowledged as being sourced from other persons.

4. This thesis does not contain other person's writing, unless specifically acknowledged as being sourced from other researchers. Where other written sources have been quoted, then:

    a. Their words have been re-written but the general information attributed to them has been referenced.
    b. Where their exact words have been used, then their writing has been placed in italics and inside quotation marks, and referenced.

5. This thesis does not contain text, graphics or tables copied and pasted from the Internet, unless specifically acknowledged, and the source being detailed in the thesis and in the References sections.

Signed---------- Name---------- Date----------

Declaration 2

Publications and conference Contributions

DETAILS OF CONTRIBUTION TO PUBLICATIONS that form part and/or include research presented in this thesis (include publications in preparation, submitted *in press* and published and give details of the contributions of each author to the experimental and writing of each publication).

Publications

1.

Authors: Saravanan Thangavel, Subramaniam Boopathi, N. Mahadevaiah, Ponmalai Kolandaivel, Pramod Pansuriya and Holger B. Friedrich.

Title: Catalytic Oxidation of Primary Aromatic Alcohols Using Half Sandwich Ir(III), Rh(III) and Ru(II) Complexes: A Practical and Theoretical study

Status: **Journal of Molecular Catalysis A: Chemical, 423 (2016) 160-171.**

Contribution: I carried out all experimental work and manuscript preparation under the supervision of Prof. Holger B. Friedrich.

Mr. Subramaniam Boopathi and Prof: Ponmalai Kolandaivel carried out DFT study and calculations.

Dr. N. Mahadevaiah and Dr. Pramod Pansuriya guided me during the manuscript preparation.

2.

Authors: Saravanan Thangavel, Holger B. Friedrich and Bernard Omondi.

Title: Synthesis and structural investigation of new half sandwich Ir(III) and Rh(III) amine complexes and their catalytic transfer hydrogenation of aromatic ketones and aldehydes in water

Status: Journal of Molecular Catalysis A: Chemical (Communication)

Contribution: I carried out all experimental work and manuscript preparation under the supervision of Prof. Holger B. Friedrich.

Dr. Bernard Omondi solved crystal structures for the iridium and rhodium complexes.

3.

Authors: Saravanan Thangavel, Manickam Paulpandi, Holger B. Friedrich, Kadarkarai Murugan, Kalva Sukesh and Adam A. Skelton.

Title: Synthesis and Characterization of new half sandwich Ir(III), Rh(III), Ru(II) and Os(II) complexes: Their biological applications on MCF-7 breast cancer cells

Status: **Journal of Inorganic Biochemistry, 159 (2016) 50-61.**

Title: Synthesis, characterization, antiproliferative and molecular docking study of new half sandwich Ir(III), Rh(III) and Ru(II) complexes.

Another portion of this work under manuscript preparation (**Title**: Synthesis, characterization of new half sandwich Ru(II) and Os(II) complexes).

Contribution: I carried out all experimental work and manuscript preparation under the supervision of Prof. Holger B. Friedrich.

Dr. Manickam Paulpandi and Prof: Kadarkarai Murugan carried out biological studies (Fluorescence microscopic analysis and Morphological study).

Dr. Kalva Sukesh and Dr. Adam A. Skelton guided me during the molecular docking studies.

4.

Authors: Saravanan Thangavel, Ramar Rajamanikandan, Holger B. Friedrich, Malaichamy Ilanchelian and Bernard Omondi.

Title: Binding interaction, conformational change, and molecular docking study of N-(pyridin-2-ylmethylene)aniline derivatives and carbazole Ru(II) complexes with human serum albumin

Status: **Polyhedron, 107 (2016) 124-135.**

Contribution: I carried out all experimental work and manuscript preparation under the supervision of Prof. Holger B. Friedrich.

Mr. Ramar Rajamanikandan and Dr. Malaichamy Ilanchelian carried out binding interaction studies.

Dr. Bernard Omondi solved the crystal structures of the ruthenium complexes.

5.

Authors: Saravanan Thangavel and Holger B. Friedrich.

Title: Synthesis and characterization of C,N cyclometalated new half sandwich Ir(III) and Rh(III) Complexes.

Status: Manuscript in preparation

Contribution: I carried out all experimental work and manuscript preparation under the supervision of Prof. Holger B. Friedrich.

Conferences

1. Poster titled “Synthesis and Structural Investigation of New Ru(II) imine complexes containing N,N' bidentate ligands” Saravanan Thangavel, Holger B. Friedrich, presented at the CATSA 2013 conference, University of KwaZulu-Natal, Durban, November 2013.

2. Poster titled “Catalytic oxidation of benzyl alcohol over M^{n+} Complexes (M= Ir, Rh, Ru and n= 2 or 3)” Saravanan Thangavel, Holger B. Friedrich, presented at the ICCC-41 conference, Suntec City, Singapore, July 2014.

3. Poster titled “Transfer Hydrogenation of Aromatic Ketones and Aldehydes by New Half Sandwich Metal Complexes using Water as a Solvent” Saravanan Thangavel, Holger B. Friedrich, presented at the CATSA 2014 conference, University of Witswatersrand, Johannesburg, November 2014.

Signed---------- Name---------- Date----------

Table of Contents

List of Abbreviations

Abbreviation	Full Meaning
acac	acetylacetonate
Ala	Alanine
$aneS_2$	1,4-dithiacyclohexane
AO	Acridine orange
APT	Attached proton test
ATR	Attenuated total reflectance
bpy	Bipyridine
CD	Circular dichroism
CIF	Crystallographic information file
COD	1,5 Cyclooctadiene
COSY	Correlation spectroscopy
COX-2	Cyclooxygenase-2
Cp*	1,2,3,4,5-Pentamethylcyclopentadiene
Cp^{xbiph}	biphenylphenyltetramethylcyclopentadienyl
Cp^{xph}	phenyltetramethylcyclopentadienyl
d	Doublet
dab	1,2-diaminobenzene
danp	2,3-diaminonaphthalene
DAPTA	3,7 diacetyl-1, 3, 7-triaza-5-phophabicyclo[3.3.1]nonane
dec.	Decompose
DFT	Density functional theory
dmdtc	dimethyldithiocarbamate
DMF	Dimethyl formamide
DMSO	Dimethyl sulfoxide
DNA	Deoxyribonuclei acid
dppn	benzo[i]dipyrido[3,2-a:2',3'-c]phenazine
dppz	dipyrido[3,2-a:2',3'-c]phenazine
dpq	dipyrido[3,2-d:2',3'-f]quinoxaline
DSC	Differential scanning calorimetry
en	ethylenediamine

ESI	Electron spray ionization
Et_3N	Triethylamine
EtBr	Ethidium bromide
FT-IR	Fourier transform-Infra red spectroscopy
GC	Gas chromatography
Glu	Glutamine
Gly	Glycine
HOMO	Highest occupied molecular orbital
HR-MS	High Resolution Mass Spectroscopy
HSA	Human serum albumin
IR	Infrared
L	Ligand
Leu	Leucine
LUMO	Lowest unoccupied molecular orbital
m	Multiplet
MCF-7	Michigan cancer foundation-7
MHz	Mega Hertz
Mp	Melting point
MTT	3-(4,5-dimethylthiazol-2-yl)-2,5 diphenyltetrazolium bromide
NBO	Natural bond orbital
NHC	N-Heterocyclic Carbene
NMR	Nuclear magnetic resonance
NOE	Nuclear overhauser effect
NOESY	Nuclear overhauser effect spectroscopy
NPA	Natural population analysis
ORTEP	Oak ridge thermal ellipsoid plot
PBS	Phosphate buffered solution
PEI	2-pyridinalethylimine
Ph	phenyl
phby	2-phenylpyridine
Phe	Phenylalanine
phen	1,10-phenanthroline
phpy	2-phenylpyridine
$Phpy^-$	2-phenypyridinate

pico	picolinate
PIP	2-pyridinalisopropylimine
PTA	1, 3, 5-triaza-7-phosphaadamantane
pTs-dpen	Poly(N-(*p*-toluenesulfonyl)-1,2-diphenylethylenediamine)
q	Quartet
RT	Room Temperature
salen	Salicylaldehyde & ethylenediamine
Ser	Serine
SI	Supplementary Information
SI	Supporting Information
t	Triplet
tBu	Tertiary Butyl
TEMPO	2,2,6,6-tetramethyl-1-piperidinyloxyl
TGA	Thermogravimetric analysis
TH	Transfer Hydrogenation
TOF	Turnover frequency
TON	Turnover number
Trp	Tryptophan
Ts-cydn	N-(*p*-toluenesulfonyl)-1,2-cyclohexanediamine
Ts-cydn	N-Touenesulfonyl-1,2-diaminocyclohexane
Ts-dach-dmss	1,2-diaminocyclohexane core shell structured mesoporous silica
Ts-dpen-dmss	Diphenyl-1,2-ethylenediamine core shell structured mesoporous silica
Tyr	Tyrosine
Val	Valine

List of Figures

List of Schemes

List of Tables

Acknowledgements

- First and foremost I thank God for his blessings, kindness and support throughout my life and in particular during this study.
- I would like to acknowledge my supervisor Prof Holger B. Friedrich for taking me into his research group, providing me with all I needed to carry out this work and in particular I am grateful for the freedom he allowed me in designing the focus of this study, under this guidance and using his experience to help me throughout this work.
- I gratefully thank the NRF, THRIP (Grant no. TP 1208035643) and the University of KwaZulu - Natal, Durban, South Africa for financial support and facilities. Thank you very much for funding.
- I also thank Dr B. Omondi, Mr S. Zamisa and Ms U. Bongoza for X-ray crystallographic data collection and refinement.
- I am also thankful to, Mrs Charmaine Magwaza, Ms C. Nkosi and Mrs Jayambal Govender for their efficient assistance with the handling of my orders.
- I would like to thank to the technical staff at the School of Chemistry (Westville campus): Mrs Anita Naidoo, Mr Dilip Jagjivan, Mr Gregory Moodley, Mr Raj Somaru, and Mrs Malini Padayachee.
- My special thanks go to my CRG group members, your input in my studies and everyday atmosphere has been immeasurable. We have had some eventful group meetings, team buildings and fun-filled CATSA trips. I really appreciate all your help and support that you have given me.
- My extended thanks goes to: Dr N. Mahadevaiah, Mrs L. Soobramoney, Mr M. N. Pillay, Mr V. Moodly, Ms D. Naicker, Mr E. Kadwa, Mr P. Mpungose, Mrs E. Nyawade, Mr J. Gichumbi, Mr Z. Mohamed, Mr D. Padayachee, Ms L. Deeplal, Mr H. Bandaru, Dr A. Golandaj, Dr P. Pansuriya, Ms S. Naidoo, Ms R. Chanerika and Dr A. Krishnan for their help, encouragement and support throughout my Ph.D.
- I dedicate this thesis to my beloved family who always put my name in their prayers. Without my Family, Friends and God's blessing I would not be where I am today.

Chapter 1

Introduction

Background Discussion

1.1 Scope of the bidentate Schiff base ligands

Over the past century, there has been substantial growth in the area of Schiff base and bidentate nitrogen donor ligands and the application of their transition metal complexes in homogeneous catalysis. Schiff base compounds were first prepared in 1879 at the Chemical Institute of the University of Florence by Hugo Schiff, a German chemist, born in 1834, in Frankfurt [1]. Schiff base compounds are synthesized by the condensation of primary amines with carbonyl groups forming a >C=N double bond [2-4] (Scheme 1.1). The imine group of Schiff base ligands plays an important role in biological applications as well as in catalysis. In comparison to ketones, aldehydes react readily with amines to form Schiff base compounds. These types of compounds are unstable unless they have an aryl group attached to either the carbon or nitrogen atom [5, 6]. The formation of Schiff base compounds is dependent on various factors such as: the order in which reagents are added, reactivity of the substrates, solvents used and the reaction temperature. Equilibrium of these reactions is achieved after a short time when the metal salts are added last to the reaction mixture [7]. Formation of the Schiff base ligands are mainly determined by two factors: (i) facilitating removal of the N-H protons from the substrate and, (ii) enhancing nucleophilic attack at the carbonyl group present in the substrate [7]. Schiff bases are intermediates in biological systems involving interactions with amino or carbonyl groups of a substrate. There is a certain degree of flexibility in the structure of these ligands mainly due to their electronic nature and the presence of additional donor atoms apart from the imine nitrogen atoms [8].

Attractive features of Schiff base ligands include their electronic fine tunability, structure flexibility and straight forward synthetic reaction routes. Research into Schiff base compounds has extended enormously, and embraces wide and diversified areas of organometallic chemistry. Schiff bases are widely associated with diverse inorganic and organic ligands such as chloride, arenes, various carbenes and cyclodienes [9]. Thus, Schiff bases are of great interest for making new active, versatile and selective metal complexes for catalytic and biological applications.

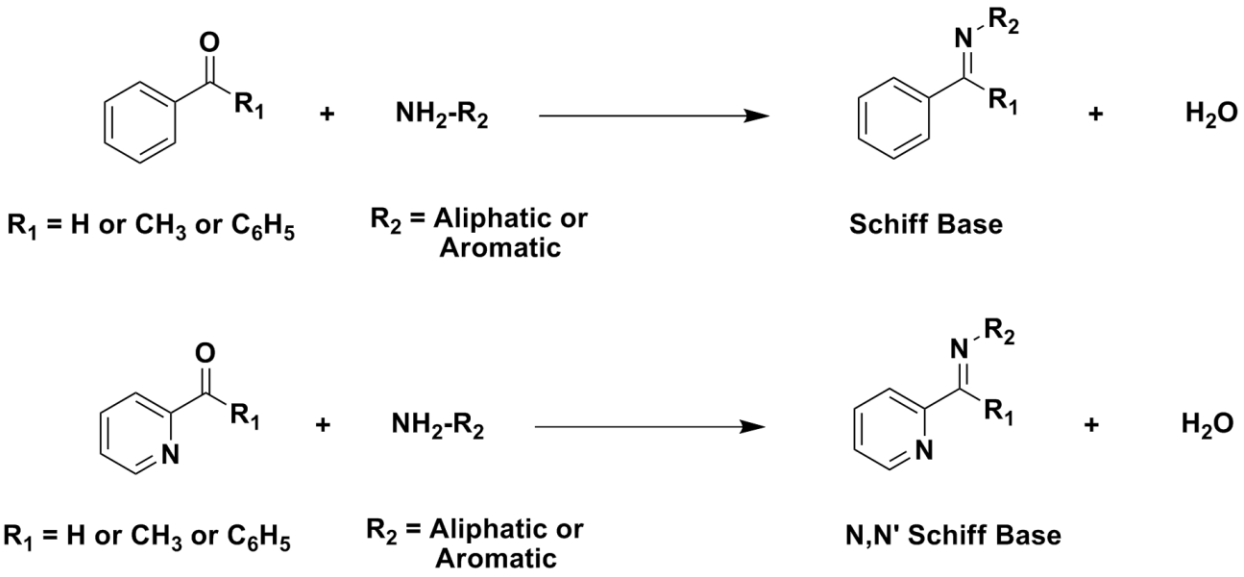

Scheme 1.1: Schematic diagram of the formation of Schiff bases.

1.2 Scope of the Schiff base metal complexes for catalytic and biological applications

Schiff bases are an important class of ligands in organometallic chemistry which can coordinate to main group and transition metals through azomethine nitrogen atoms. The nitrogen based Schiff base N,N′ bidentate ligands containing metal complexes are widely used in bioinorganic, inorganic and organometallic chemistry [10-12].

Schiff base compounds coordinate to transition metal ions in either bidentate or multidentate modes, yielding stable or highly active complexes for different catalytic and biological applications [13-15]. Interestingly, Schiff base compounds form stable five or six-membered chelate rings with different transition metal precursors (Figs. 1.1-1.3), due to the second functional group in the vicinity of the metal coordination site [16]. The lone pair of electrons on the nitrogen atoms play an important role in the formation of highly stable chelated complexes with versatile applications in bioinorganic chemistry and catalysis [8] (Fig. 1.4). The orbital present in Schiff base nitrogen atoms is either sp^3 or sp^2, depending on the substituent on the nitrogen atom (alkyl or aryl), and their steric hindrance alters the behavior of the nitrogen atom in potential chemical applications [17]. The central metal atom present in these complexes act as an active site in biological applications and chemical transformation reactions [17] (Fig. 1.5).

The oxidation of alcohols and the transfer hydrogenation of carbonyl compounds are among the important transformations in synthetic chemistry. High selectivity and productivity are important aspects for industrial processes and it can be achieved by tuning the ligand design and synthetic route to optimize the versatility of the catalysts. On the other hand adjusting the reaction temperature, solvents and co-

catalysts can help to improve the activity of the catalyst for multi-organic transformation reactions. In homogeneous catalysis, pyridine-based Schiff base ligands play an important role due to their ability to coordinate to different transition, non-transition, lanthanide and actinide metals in different oxidation states [18]. Over the last decade, Schiff base complexes have become attractive compounds for the development of a new generation of catalysts with high activity and selectivity. Hence, the development of metal mediated catalytic oxidation of alcohols and transfer hydrogenation of carbonyl compounds under mild conditions are important [19, 20]. Oxidation of aromatic alcohols to their respective aldehydes and transfer hydrogenation of carbonyl compounds have been the focus of numerous articles and reviews [19, 20].

In bioinorganic chemistry, the scope of Schiff base complexes has been widely investigated due to their ability to offer synthetic models for metal containing sites for metalloproteins [2]. Transition metal complexes containing heterocyclic scaffold Schiff base ligands which have been reported have a wide range of biological applications in medicinal chemistry, especially for designing new drugs [10]. According to biological views, DNA is the primary pharmacological target of anticancer compounds to damage tumor cells. Transition metal complexes containing Schiff base ligands have shown a strong binding interaction with DNA through surface association or intercalation, and DNA cleavage via hydrolytic or oxidative mechanisms [21]. The N,N' ancillary ligands, such as bipyridine, phenanthroline, dipyrido-quinoxaline and dipyridophenazine presented metal complexes also play pivotal roles in their binding nature and intercalation with DNA. Planarity of the ancillary ligands can improve the nature of intercalation of complexes with DNA and, in turn, increase the binding potential. Furthermore, the N,N' bidentate phenanthroline ligand present in some complexes has drawn much attention to biological systems in which they exhibit high nucleolytic efficiency [22].

In recent years, various scientific research groups have shown interest in the functionalization of Schiff base complexes with nanomaterials for therapeutic applications [14]. Many of the antharacene moieties and their derivatives present in Schiff base compounds are known to possess significant anti-cancer activities against certain cancer cells, with their fluorescent chromophores acting as photo-signalers for charge transfer complexes. Therefore, the antharacene chromophore present in metal complexes provides significant information about cellular processes because of their intrinsic fluorescence property within cells [23]. Hence, Schiff base complexes are widely used for biological applications such as antifungal, antibacterial, antiviral and anticancer activities [14, 15]. Schiff base complexes are also involved in different biochemical processcs like haloperoxidation, nitrogen fixation, phosphorylation, glycogen metabolism and insulin mimicking [24-26].

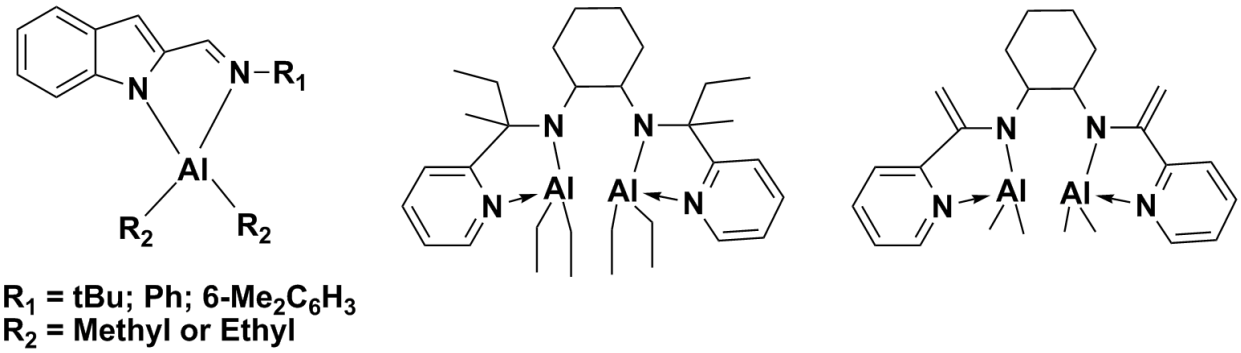

Fig. 1.1 Aluminum Schiff base complexes for guanylation of aromatic amines.

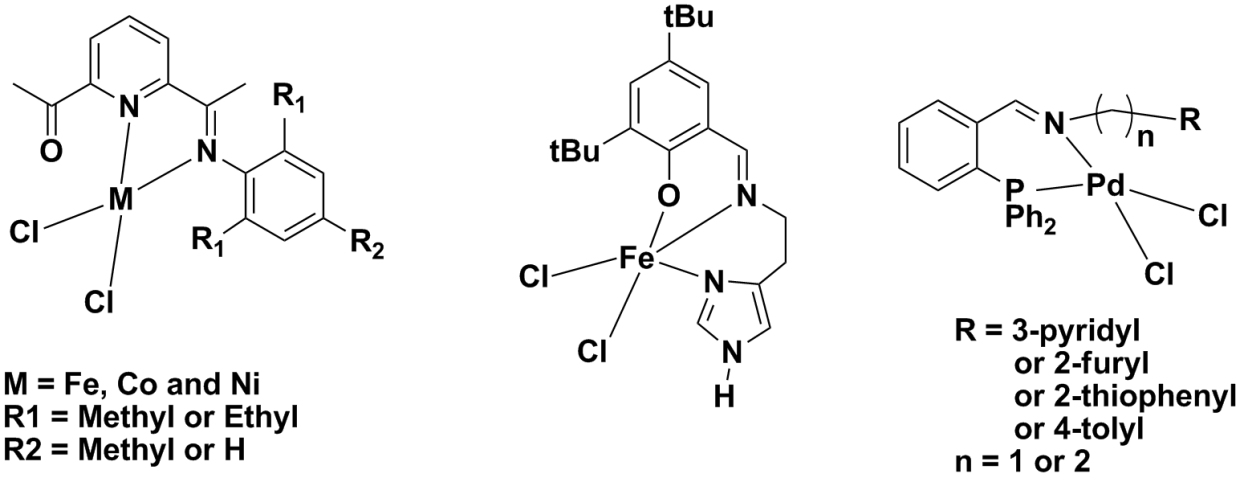

Fig. 1.2 Some Schiff base transition complexes for ethylene oligomerization.

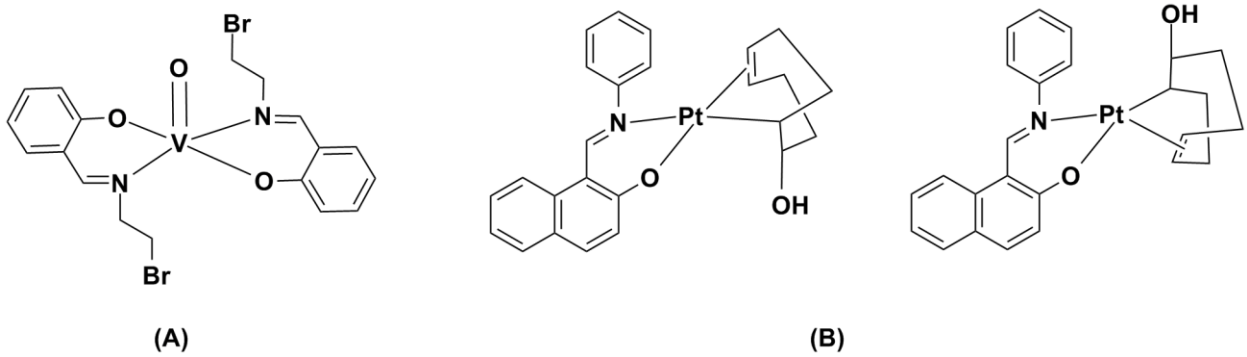

Fig. 1.3 (A) Vanadium Schiff base catalysts for the epoxidation of alkenes and (B) platinum Schiff base catalysts for hydrosilylation reactions.

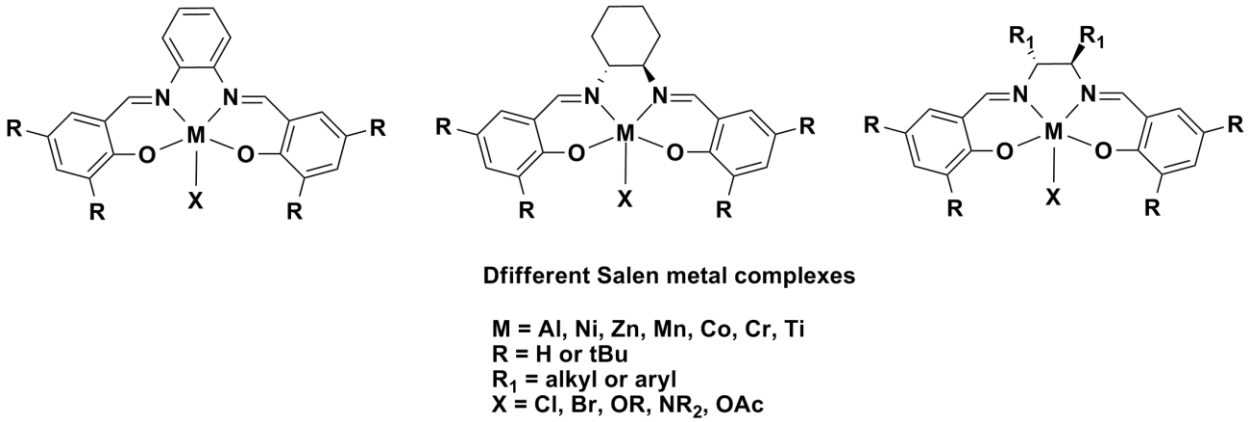

Fig. 1.4 Different Salen Schiff base metal complexes for various enantioselective chemical transformation reactions.

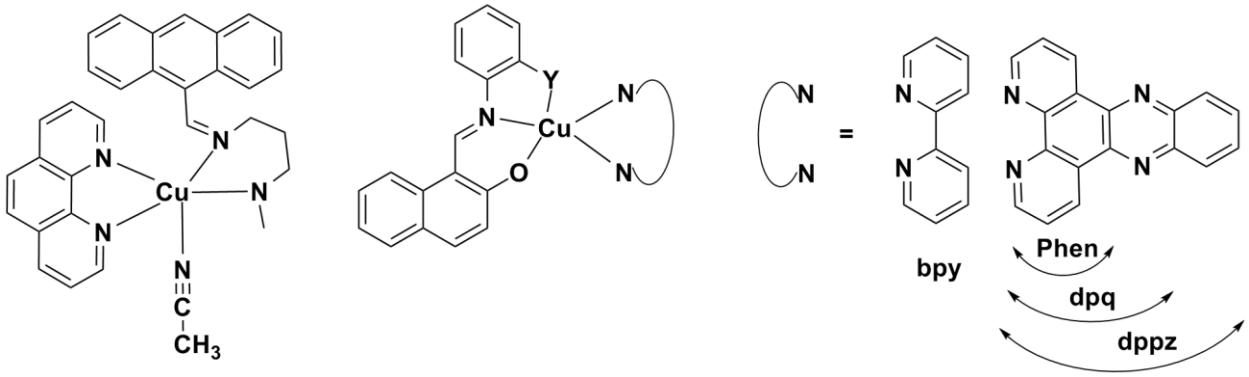

Fig. 1.5 Some biologically active copper N,N' Schiff base ligand complexes.

1.3 Schiff base coordinated Ru(II), Ir(III) and Rh(III) complexes in homogeneous catalysis

1.3.1 Ru(II) complexes containing N,N'-, N,S-, N,Se-, P,P'- and N,P ligands for catalytic transfer hydrogenation and oxidation reactions

The catalytic activities of Ir(III), Rh(III) and Ru(II) N,N' bidentate complexes were widely investigated by different research groups around the world using different reaction conditions and reagents (Scheme 1.2). Furthermore, catalytic TH is one of the widely accepted methods in industry as a green process for the production of a number of aromatic alcohols. Noyori and co-workers [27] first reported ruthenium metal complex systems which accelerate the catalytic TH of aromatic ketones to their respective alcohols under mild conditions. The chiral Ru(II)-Ts-dpen (Where Ts-dpen = N-(*p*-toluenesulfonyl)-1,2-diphenylethylenediamine) catalyst is known for asymmetric transfer hydrogenation of aromatic ketones with high enantiomeric excess [28]. The Noyori-Ikariya Ru(II)-dpen modulated catalyst is highly active (Substrate/Catalyst = 1000/1) for asymmetric transfer hydrogenation of aromatic

ketones with a high enantiomeric excess in water using HCOOH-Et_3N and HCOONa hydrogen sources under pH controlled reaction conditions [28-30]. Thus, the Ru(II)-Ts-dpen catalyst showed a catalytic TH process through a concerted delivery of an N-H proton as well as a Ru-H, via a six-membered transition state in an outer sphere mechanism.

Transfer hydrogenation

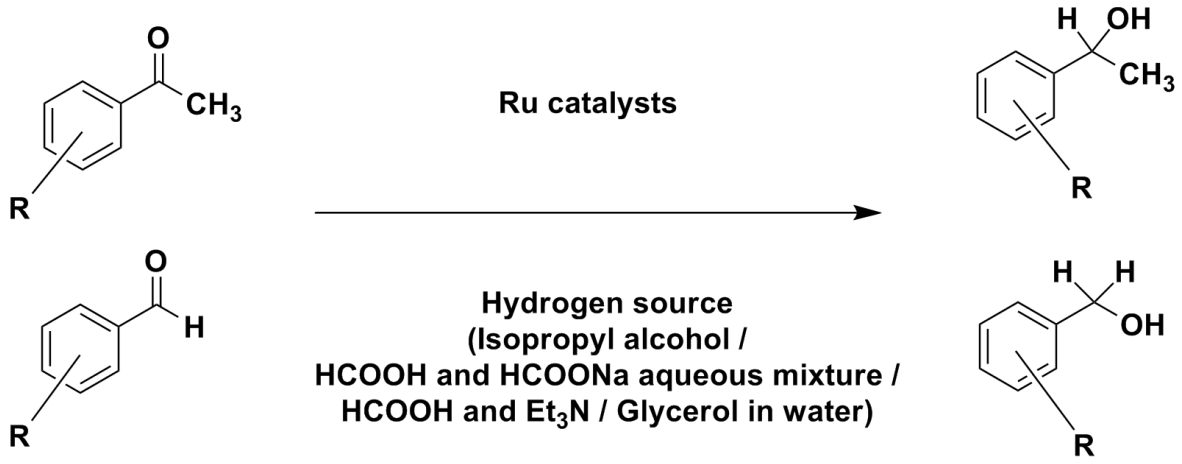

Oxidation reaction

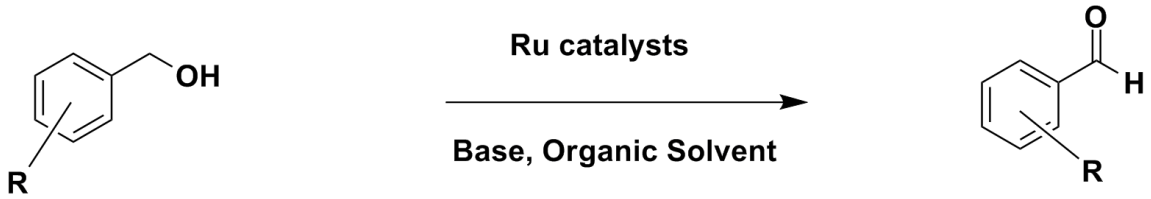

Scheme 1.2: Catalytic oxidation and transfer hydrogenation by ruthenium catalysts.

In 1999, Mizushima *et al.* first reported the use of Ru(II) complexes chelated to both aminomethyl pyridine derivatives and phosphine ligands which exhibited good catalytic activity for asymmetric TH of aromatic ketones [31]. Recently, Ru(II) arene complexes bearing chalcogenated pyridine-based bidentate and tridentate N, S or Se ligands showed good catalytic TH activity towards aromatic ketones and they were also active in the oxidation of different aromatic alcohols [32, 33]. The same group reported the use of glycerol as a hydrogen donor for TH of carbonyl groups in water, catalyzed by Ir(III), Rh(III) and Ru(II) chalcogenated bidentate complexes [34]. Very recently, water soluble Ru(II) complexes bearing naphthyridine-carboxylate N,N' ligands showed catalytic TH of aromatic ketones, as reported by Huang *et al*. [35] (Fig. 1.6).

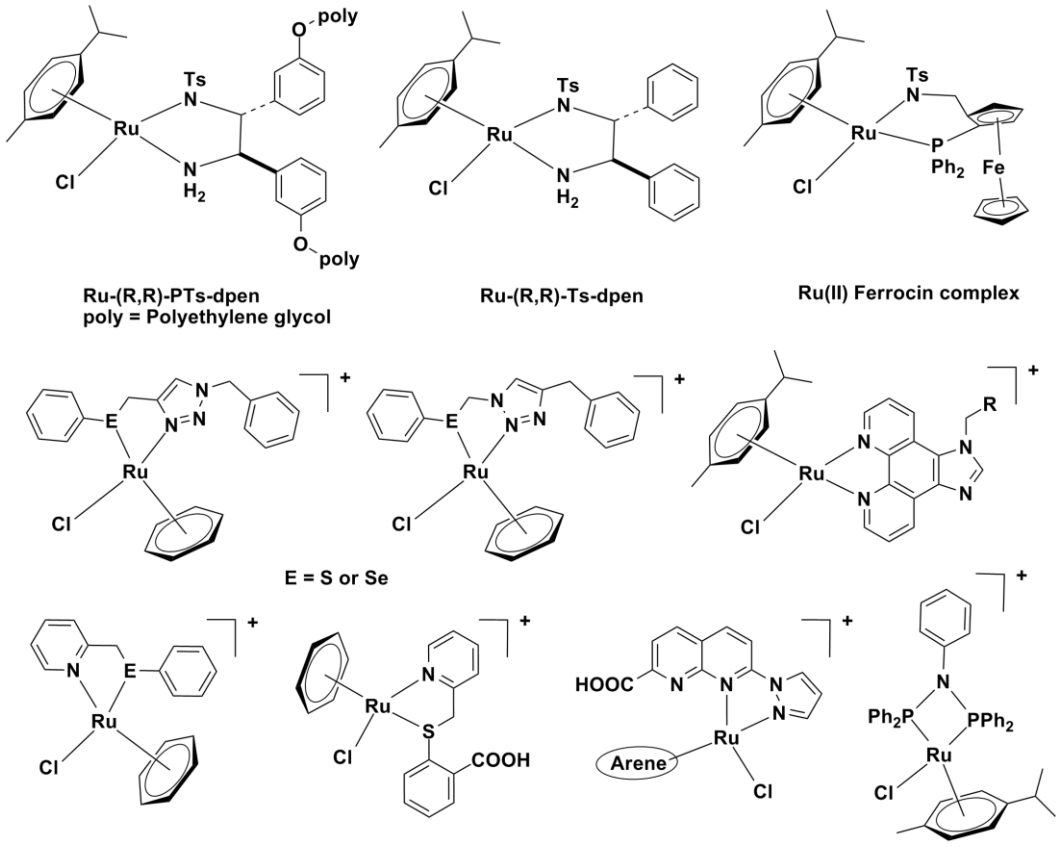

Fig. 1.6 Ru(II) catalysts containing different bidentate ligands for oxidation and transfer hydrogenation reactions.

In TH reactions the reaction medium and hydrogen sources play an important role in achieving desirable reduced products. Metal complex catalyzed TH reactions have been executed in isopropyl alcohol or HCOOH-HCOONa in water or in an azeotropic mixture of HCOOH-Et_3N (F/T), in which the molar ratio of F/T is 2.5:1 [36]. The advantage of the HCOOH-HCOONa and azeotropic mixture of HCOOH-Et_3N is that it acts as a hydrogen donor as well as a base, which does not allow the reversibility of the reduction process of the ketone like the isopropyl alcohol does. HCOOH-HCOONa and HCOOH-Et_3N mixtures are good hydrogen donors compared to isopropyl alcohol due to the resulting CO_2, which is thermodynamically stable and can be easily removed from the system, which results in the reactions being irreversible [36]. Moreover, a wide range of substrates are soluble in an acidic medium and HCOOH-HCOONa / HCOOH-Et_3N is miscible with many organic solvents in the temperature range of 20-60 °C [36]. This process is thus an environmentally benign process for TH applications.

Nitrogen donor atoms present in ruthenium based organometallic complexes have recently been shown to play an important role in the oxidation of alcohols [37]. Notably, (η^6-arene)Ru(II) complexes were among the best catalysts for this transformation, which can be performed on a wide range of

alcohols and amines [38, 39]. Furthermore, Prades *et al.* reported N-Heterocyclic carbene (NHC) triazolylidene ligands coordinated to Ru(II) complexes, which showed excellent reactivity in the catalytic oxidation of alcohols and cross coupling reactions of alcohols and amines under different reaction conditions [40]. The functionalized NHC-triazolylidene moieties act as potential nitrogen donor ligands for transition metal complexes and organometallic species. The advantage of NHC-based ligands is that they have a number of possible coordination modes of the carbene to the metal and accommodate positive and negative charges in the triazole moiety. A number of reported triazole based Ru(II) half sandwich complexes were active for the catalytic oxidation of alcohols [41]. Ohzu *et al*. reported photocatalytic primary alcohol oxidation reactions by Ru(II)-pyridylamine complexes with the use of $[Ru(II)(bpy)_3]$ as a photosensitizer [42].

1.3.2 Ir(III) complexes for catalytic transfer hydrogenation and oxidation reactions

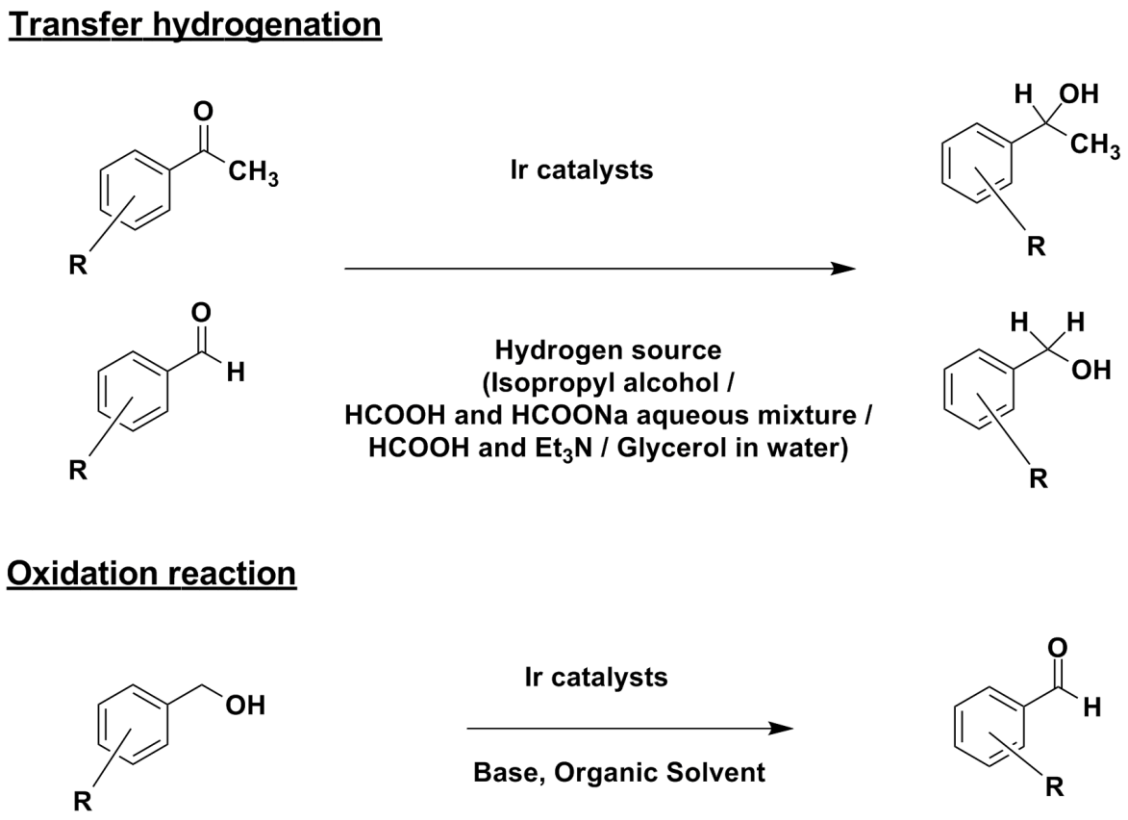

Scheme 1.3: Catalytic oxidation and transfer hydrogenation by iridium catalysts.

Iridium is a third row transition metal, in a group that also contains, cobalt and rhodium. Ir shows different oxidation states, commonly Ir(I), Ir(III), Ir(IV), coordination numbers (4, 6) and coordination geometries during organoiridium complex formation [43]. Some Ir(III) half-sandwich complexes are

reported as highly versatile catalysts for catalytic TH and oxidation reactions (Scheme 1.3), which contain an electron rich Cp* moiety, N,N' and C,N ligands [43].

The importance of green chemistry has drawn attention to the reduction of carbonyl compounds in water as a solvent, using Ir(III) and Rh(III) metal complexes. Half sandwich IrCp* complexes are versatile catalysts for the oxidative amine addition, TH and alcohol oxidation reactions. Half sandwich IrCp* complexes are versatile catalysts for the oxidative amine addition, TH and alcohol oxidation reactions. Yamaguchi *et al.* reported that the IrCp*(2-OH-pyridine)Cl and IrCp*(6-phenyl-2-pyridone)Cl complexes are highly active catalysts for the oxidation of aromatic alcohols [44, 45]. A turnover number of up to 700 for these catalysts was achieved in the oxidation of the aromatic alcohols, refluxing in toluene. Fujita and Yamaguchi reported several alcohol activation reactions and Oppenauer-type oxidations of primary and secondary alcohols using IrCp* complexes [46]. Brewster *et al.* reported a series of half-sandwich IrCp* and RhCp* compounds containing N,N'-, C,N- and carbene ligands that act as versatile catalysts for the hydrogenation of carboxylic acids under relatively mild conditions [47]. A wide range of substrates, including primary and secondary alcohols as well as different aromatic and aliphatic carbonyl compounds, catalyzed by IrCp* complexes under mild and harsh conditions have been investigated [20] (Fig. 1.7).

Ogo *et al.* first developed the water soluble $[Ir(\eta^5\text{-}Cp^*)(H_2O)_3]^{2+}$ and $[Ru(\eta^6\text{-}C_6Me_6)(H_2O)_3]^{2+}$ compounds for transfer hydrogenation of carbonyl compounds in water using HCOONa as a hydrogen source [48]. Recently, IrCp* diamine and cyclometalated IrCp* imine complexes were reported as highly versatile catalysts by Villa *et al.* [49] and Wei *et al.* [50] for catalytic transfer hydrogenation in water using formic acid as a hydrogen source. Apart from water, many solvents meet the green protocol criteria and glycerol has attracted the attention of many researchers, due to its chemical properties, being readily available and cost effective. Recently, Ir(I) and Ir(III) NHC based complexes with 3,4,5-trimethoxybenzyl N-substituted complexes have been reported for catalytic transfer hydrogenation with glycerol as a solvent [51]. In a number of examples reported, glycerol has replaced isopropyl alcohol as a hydrogen source in ruthenium and iridium catalyzed transfer hydrogenation reactions [34]. The catalytic activities for a series of $[IrCl_2Cp^*(NHC)]$ complexes were reported as being high for several C-O and C-N coupling reactions [52]. The protic NHC complexes bearing an ionizable proton at the β-position to the metal center can be regarded as versatile and active β-bifunctional catalysts [52-54].

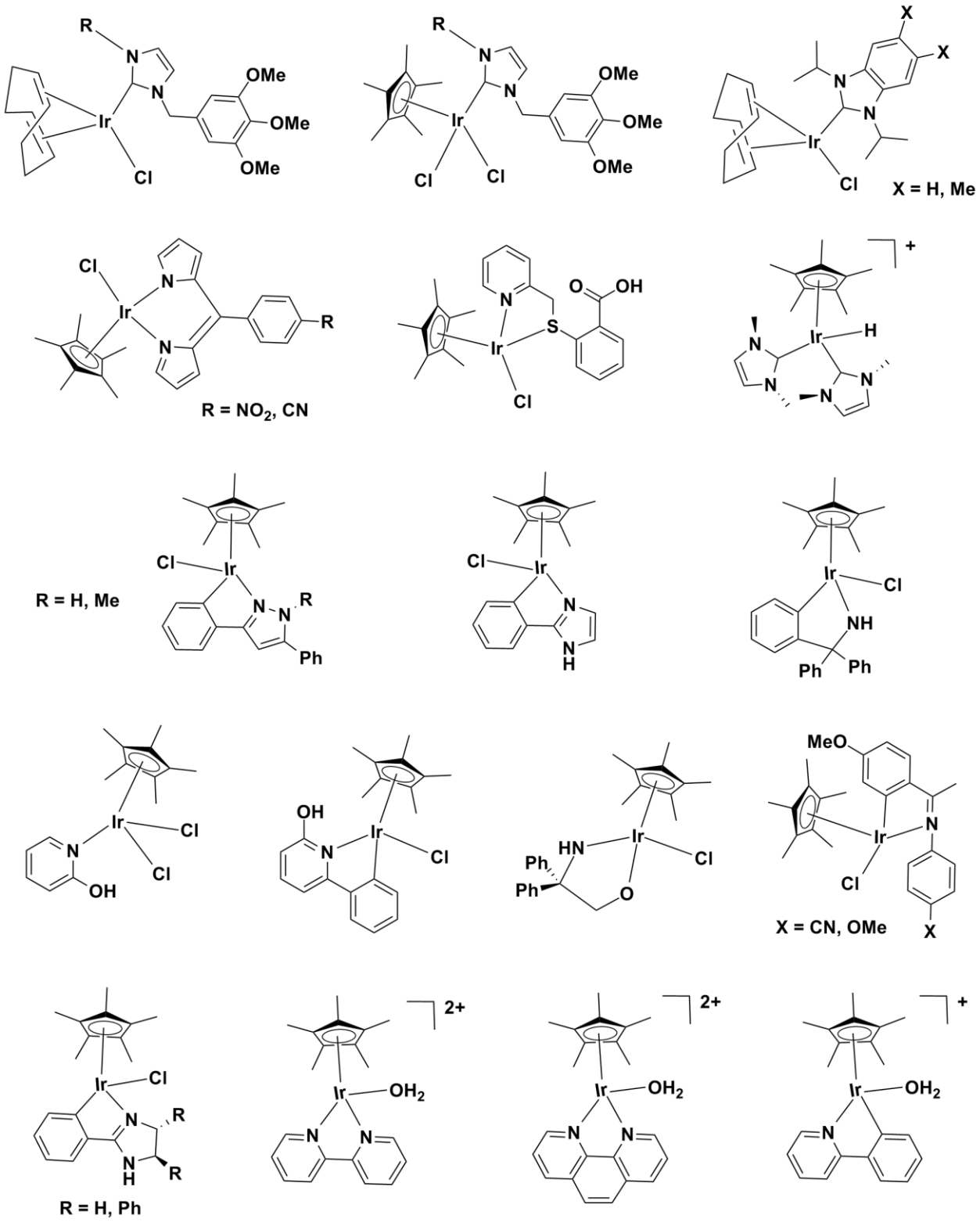

Fig. 1.7 Ir(III) catalysts with bidentate ligands for catalytic oxidation and transfer hydrogenation reactions.

1.3.3 Rh(III) complexes containing bidentate ligands for catalytic transfer hydrogenation and oxidation reactions

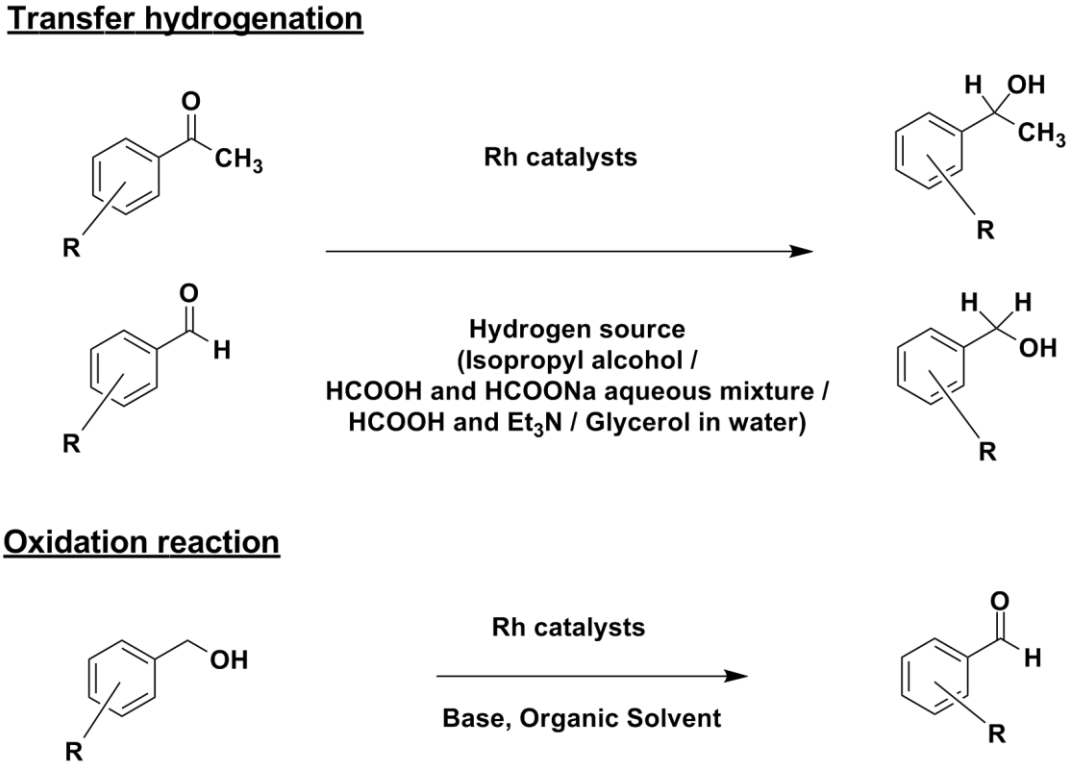

Scheme 1.4: Catalytic oxidation and transfer hydrogenation by rhodium catalysts.

The η^5-C_5Me_5 rhodium complexes are of great scientific interest because they can be used as precursors in the synthesis of many rhodium complexes, as well as be applied in a wide range of catalytic reactions [55] (Scheme 1.4). The pioneering work by Noyori *et al.* reported highly active enantioselective Ru(II)-(Ts-dpen) for asymmetric transfer hydrogenation reactions [27, 28]. After the remarkable discovery of this catalyst, new N,N' chiral ligands have been developed with Rh(III) and Ir(III) complexes for catalytic transfer hydrogenation reactions (Fig. 1.8). Rh(III)-(1R,2R)(Ts-cydn) has been reported as an excellent and stable catalyst for the asymmetric transfer hydrogenation of aromatic carbonyl compounds in water under air using HCOONa as a hydrogen source [56]. Recently Singh *et al.* have reported water soluble RhCp* complexes containing a (phenylthio)methyl-2-pyridine scaffold which showed promising results as an efficient catalyst for transfer hydrogenation of carbonyl compounds with a low catalyst loading (0.5 mol%) [34]. Moreover, when the reaction is carried out in water, the organic substrates can be easily separated by liquid-liquid extraction. However, most of the transition metal complexes were not stable toward hydrolysis or water as this hinders the transition states of the catalytic cycles through coordination of H_2O molecules to the metal center [57]. Therefore, the design of a catalyst that is not only active in the aqueous phase, but also could be stable and completely soluble in this system would be most

desirable [57]. A core-shell structured heterogeneous Rh(III) catalysts (Fig. 1.8 (B)) have also been reported as a versatile and recoverable catalyst for asymmetric transfer hydrogenation reactions in aqueous media [58].

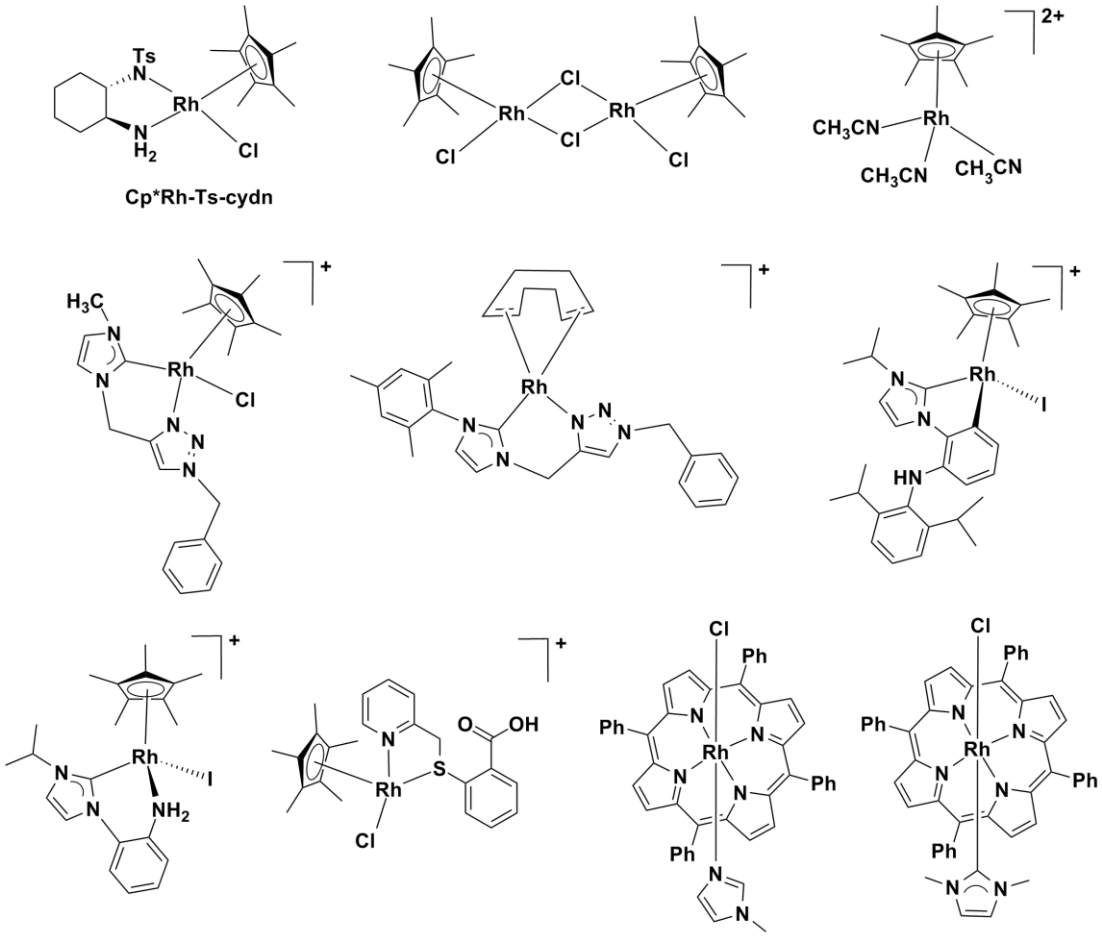

Fig. 1.8 Some of the homogeneous (A) and heterogeneous (B) rhodium catalysts for catalytic oxidation and transfer hydrogenation reactions.

Studies carried out by Qi *et al.* showed rhodium catalyzed efficient oxidative coupling between aromatic C-H bonds and allylic alcohols [59]. The synthesis of a functionalized *β*-aryl ketone and aldehyde achieved by a Rh catalyzed process afforded the products in good yields. Rhodium complexes normally show high catalytic activity in constructing $C(sp^2)$-$C(sp^3)$ compounds via cleavage of unactivated C-H bonds, as reported by Li and Shi. [60]. Recently, oxidative coupling of monosubstituted arenes with alkynes to form benzannulated heterocyclic compounds catalyzed by Rh(III) compounds was reported by Wei *et al.* [61] and Wang *et al.* [62]. RhCp* compounds are also found as versatile catalysts for coupling reactions of benzylic alcohols with alkynes through OH directed C-H bond cleavage [63]. Recently, rhodium complexes containing hybrid NHC-phosphine and NHC-pyrazole bidentate ligands showed promising results as catalysts for hydroamination reactions, as demonstrated by Field *et al.* [54] and Gray *et al.* [64]. The coupling of amines with alkenes is known and has been an active field of interest for the last 40 years, with Coulson being the first to demonstrate the addition of ethylene to secondary amines catalyzed by rhodium homogeneous catalysts in 1971 [65].

1.4 Biologically important Schiff base ligands-containing transition metal complexes

Transition metals, such as ruthenium, iridium, rhodium and osmium, with N,N' bidentate ligands exhibit diverse applications in the pharmaceutical, agrochemical, dye, and food industry, as well as in photo sensitizer, photo luminescence and fluorescence studies, in addition to catalysis and biological studies (anti-inflammatory and potential *in vitro & in vivo* studies) [13, 14, 66-68].

1.4.1 Organoruthenium compounds for different biological applications

Over the last few decades, ruthenium complexes have become of great interest in the field of chemotherapeutic studies with regard to the development of anti-cancer drugs [68]. In 1976, Durig *et al.* discovered biologically active Ru(III) complexes such as *fac*-$Ru(NH_3)_3Cl_3$ which induces filamentous growth of *E. coli* at a similar concentration to cis-platin [69, 70]. These results suggested Ru could be considered as an alternative metal to platinum, to overcome the drawbacks of the platinum anti-cancer drugs in cancer treatment. Interestingly, many of the Ru compounds are not very toxic and some of the ruthenium compounds have been shown to be highly selective for cancer treatment [70, 71]. This high selectivity towards cancer cells suggested Ru has the ability to mimic iron in binding to biological cells [72]. Thus KP1019 (indazolium trans-[tetrachloridobis(1H-indazole)ruthenate(III)]) and NAMI-A (imidazolium trans-[tetrachlorido(dimethyl sulfoxide)(1H-imidazole)ruthenate-(III)]) are pioneering ruthenium compounds (Fig. 1.9) for potential anticancer and antitumor activity in biological systems [71-73]. Ru complexes containing Schiff base ligands have been involved in various biological studies, such

as protein binding, antifungal, antibacterial, antiviral, antimalarial, antiparasitic, antimetastatic, antiangiogenic and anti-inflammatory studies in medicinal chemistry [73-77]. Sadler and co-workers reported numerous N,N' bidentate ligands containing cationic arene Ru(II) complexes with potential cytotoxicity activities under *in vitro* and *in vivo* conditions [78-80].

Recently arene scaffold modified ruthenium(II)-arene PTA complexes RAPTA-C [(Ru(η^6-*p-cymene*)Cl_2(PTA)], RAPTA-T [(Ru(η^6-*p-toluene)*Cl_2(PTA)] (where PTA = 1,3,5-triaza-7-phosphaadamantane), DAPTA-C [(Ru(η^6-*p-cymene*)Cl_2(DAPTA)], and DAPTA-T [(Ru(η^6-*p-toluene)*Cl_2(DAPTA)] (where DAPTA = 3,7 diacetyl-1, 3, 7-triaza-5-phosphabicyclo[3.3.1]nonane) showed low toxicity profiles and antiproliferative effects in endothelial cells [75]. In recent years, organometallic ruthenium half sandwich octahedral low spin d^6 metal complexes have been of great interest in chemotherapeutic studies because of the hydrophilic and hydrophobic nature of carbon bound π bonded arenes and substituted moieties. This arene moiety emerged as a versatile tool to develop novel compounds for antitumor activity studies, which is responsible for cell intake, targeting tumor cells and kinetic inertness of the complexes [78, 81].

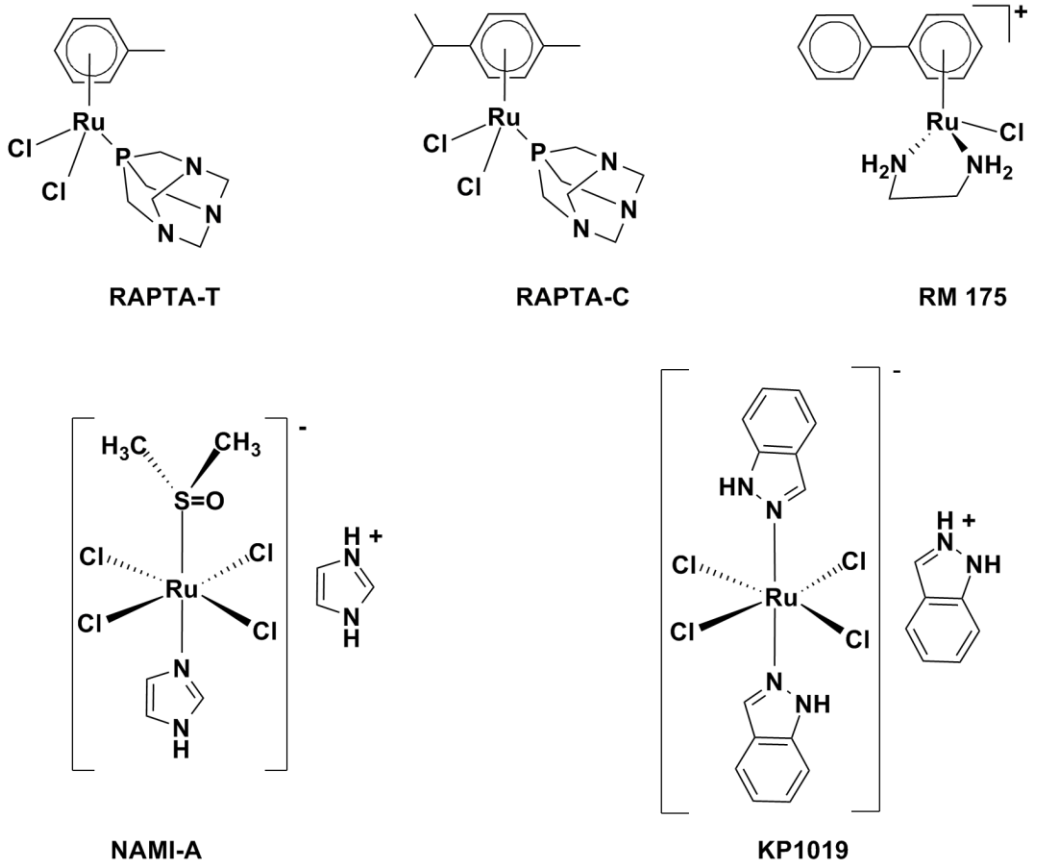

Fig. 1.9 Structure of organoruthenium(II) and (IV) anticancer compounds.

1.4.2 Organoiridium compounds containing N,N'-, C,N-, and N,O- ligands for anti-cancer studies

In recent years iridium metal complexes have become important in their application in chemotherapeutic studies, in which they show high antiproliferative activity towards cancer cells [82]. Iridium is an inert and corrosion-resistant metal with several common oxidation states (Ir(I), Ir(III) and Ir(IV)) and coordination geometries [83]. The Ir(III) oxidation state is one of the most stable low-spin inert d^6 states while forming complexes with bidentate chelated ligands [84]. This stability and inertness also plays an important role in the design of anti-cancer drugs. Ir compounds were first investigated for anti-cancer studies in the later 1970s after the discovery of cis-platin [85]. The Ir(I) compounds, [Ir(acac)(COD)] and dinuclear $[IrCl(COD)]_2$, were investigated for anti-tumor activity studies in mice, because of their square planner geometry like cis-platin [85, 86]. Comparatively, Ir(III) is more stable than Ir(I) with higher coordination numbers, which can be stabilized by electron-rich pentamethylcyclopentadienyl (Cp*) and substituted Cp* moieties [87].

[Ir(acac)(COD)] and dinuclear $[IrCl(COD]_2$ were investigated for anti-tumor activity properties and for targeted delivery of complexes to specific cancer tumor [88]. Sadler *et al.* have also recently investigated neutral N,N' ligands, such as bipyridine, 1,10-phenanthroline and ethylenediamine, chelated Ir(III) complexes which exhibited moderate anticancer activity against certain cancer cell lines [89]. The chelating N,N' ligands provide additional stability for the metal complex and contribute to tuning the electronic nature of the iridium metal center. The anticancer activity of metal complexes could be considerably increased by tuning via small modification in the ligands chelated to the metal center. The cytotoxicity effect of IrCp* complexes was increased drastically when phenyl or biphenyl groups were introduced in place of the methyl group on the Cp* moiety. Half-sandwich organometallic Ir(III) complexes bearing the substituted Cp* moiety $[(\eta^5\text{-}Cp^x)Ir(N,N')Cl]$ (where Cp^x = Cp*, Cp^{xph} (phenyltetramethylcyclopentadienyl) and Cp^{xbiph} (biphenyltetramethylcyclopentadienyl) with N,N' donor ligands exhibited excellent anticancer activities against cancer cell lines. The electron rich Cp* and substituted Cp* (Cp^{xph} & Cp^{xbiph}) moieties could facilitate rapid hydrolysis by increasing the negative charge on the metal, making it easy for the chlorine group to dissociate from the complex [43]. The replacement of neutral N,N' chelated ligands by cationic C,N donor ligands in Ir(III) complexes significantly increases the antiproliferative activity against A2780 cancer cell lines [43] (Fig. 1.10).

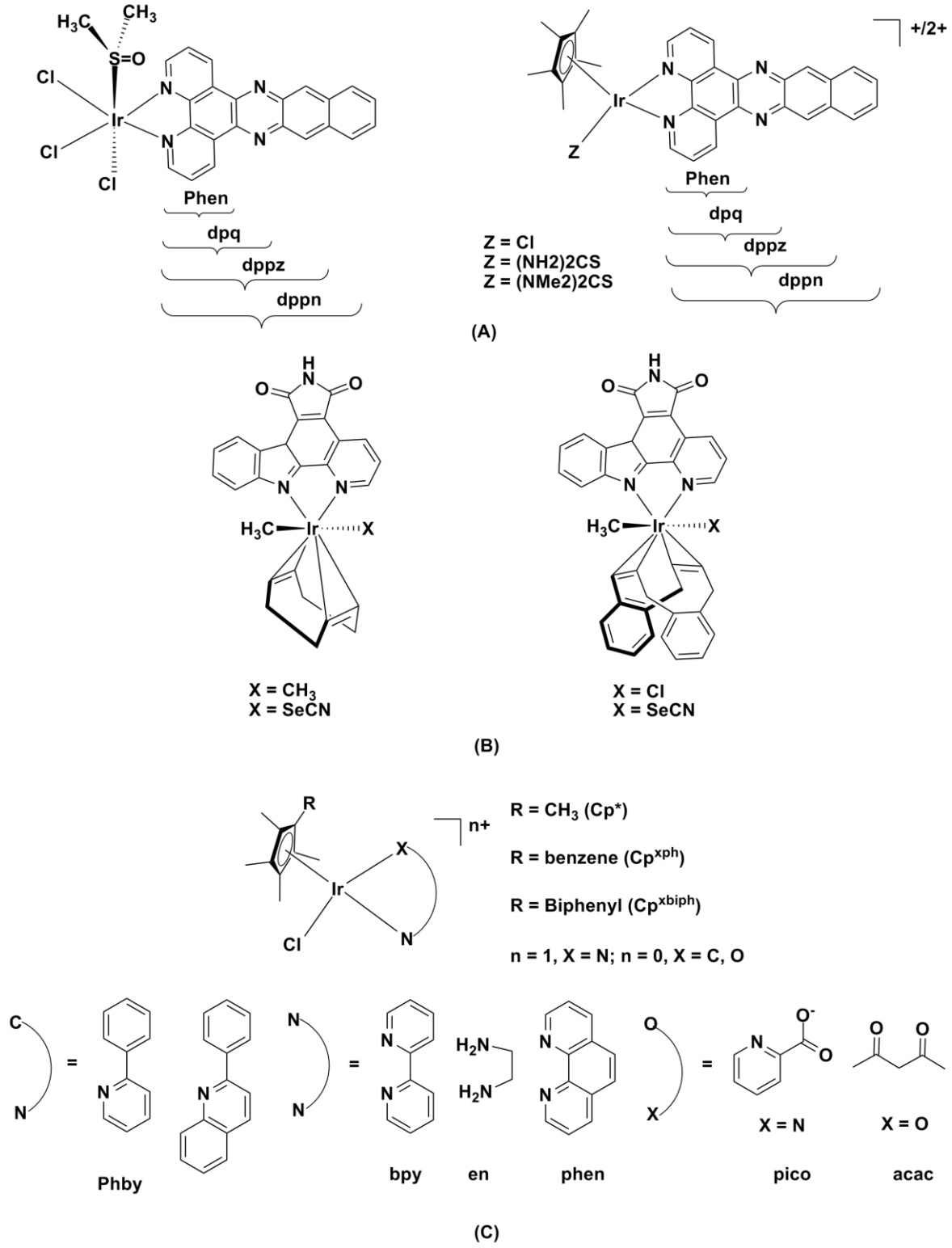

Fig. 1.10 (A) Anti-cancer organoiridium polypyridyl complexes against MCF-7, HT-29 and HEK-293. (B) Photocytotoxic (diene)Ir(III) protein kinase inhibitors. (C) Anti-cancer organoiridium(III) complexes containing different bidentate ligands.

A significant number of (diene)Ir(III) complexes were reported in phototoxic activity studies towards cancer cells, protein and lipid kinase inhibitors [84]. The development of luminescent cellular probes containing organometallic complexes is important to understanding the assorted structures and functions of biological systems. There has been interest in studying luminescent inorganic and organometallic complexes in cellular systems through emission spectroscopy and scanning microscopy techniques. Recently, Zhang *et al.* reported a series of luminescent cyclometalated Ir(III) dipyridoquinoxaline complexes [$(Ir(N,C)_2(N,N'))PF_6$] (where N,N' = polypyridines) which were successfully investigated for cellular uptake studies [90].

1.4.3 Biologically active organorhodium compounds containing N,N'- and S,S' ligands

In the past decade structure-activity relationships of rhodium (Rh) compounds and their cytotoxicity effects on cancer cells were extensively studied by various research groups [91]. Rh(I), Rh(II) and Rh(III) compounds showed potential anti-tumor activity against human oral carcinoma, leukemia L1210 and P388, sarcoma 180, lung carcinoma, lymphocytic leukemia, L1210 and B16 melanoma, and Ehrlich ascites carcinoma [92]. Upon the discovery of potential carcinostatic activity of Rh(II) carboxylates, investigations based on their chemical properties and biological activities have accelerated. The dirhodium tetracarboxylate complexes [$(RCOO)_4L_2Rh_2(II)$] (where R = Me, Et, Ph or CF_3; L = H_2O or other solvents) exhibit anti-tumor activity against various tumor cells, but the toxicity of these complexes prevented their use [93]. The dirhodium tetraacetate complex [$(CH_3COO)_4(H_2O)_2Rh_2(II)$] and [$(RCOO)_4Rh_2(II)$] (R = CH_3, CH_2CH_3, $CH_2CH_2CH_3$, $CH_2CH_2CH_2CH_3$) showed considerable anti-tumor activity against *E. coli* DNA polymerase I and Ehrlich ascites tumors [94-97]. The neutral and square planar rhodium(I) cyclooctadiene complexes [$Cl(COD)NH_3Rh(I)$], [Rh(acac)(COD)] and [Cl(COD)-piperidineRh(I)] (COD = cis- 1,5 cyclooctadiene) displayed potential anti-tumor activity against the Ehrlich ascites tumor under *in vivo* conditions [98]. The square-planer Rh(I) complexes ([(COD)(PMI)Rh]Cl (where PMI = 2-pyridinalmethylimine), [(COD)(PEI)Rh]Cl (where PEI = 2-pyridinalethylimine), and [(COD)(PIP) Rh]Cl (where PIP = 2-pyridinalisopropylimine)) were also investigated for anti-tumor and anti-metastatic activities [99] (Fig. 1.11).

A number of Rh(III) analogues of Ru(III) antitumor complexes also show significant antineoplastic activity in cancer treatment by reduction of Ru(III) to Ru(II) [100]. The N,N' bidentate 2,6-diaminepyridine Rh(III) complex showed high activity on the humoral immune response of white mice [101].

Furthermore, anti-malarial drugs containing cationic rhodium complexes, such as $[L_4Cl_2Rh(III)]^+Cl^-$ (where L = primaquine, mepacrine, amodiaquine, lepidine, plasmoquine, pentaquine,

and isopentaquine) have also been investigated for different anti-tumor activities [102]. Morrison and co-workers reported potential phototoxic agents for the destruction of cancer cells using N,N' ligands containing bis(bipyridyl)Rh(III) complexes such as cis-[$RhCl_2$(dppz)(phen)]Cl and cis-[$RhCl_2$(3, 4, 7, 8 - Me_4phen)$_2$]Cl [103]. These photoluminescent activated drugs introduced a new kind of attractive drug treatment in chemotherapeutic studies, causing no harm to the living cells by attacking cancer affected cells only.

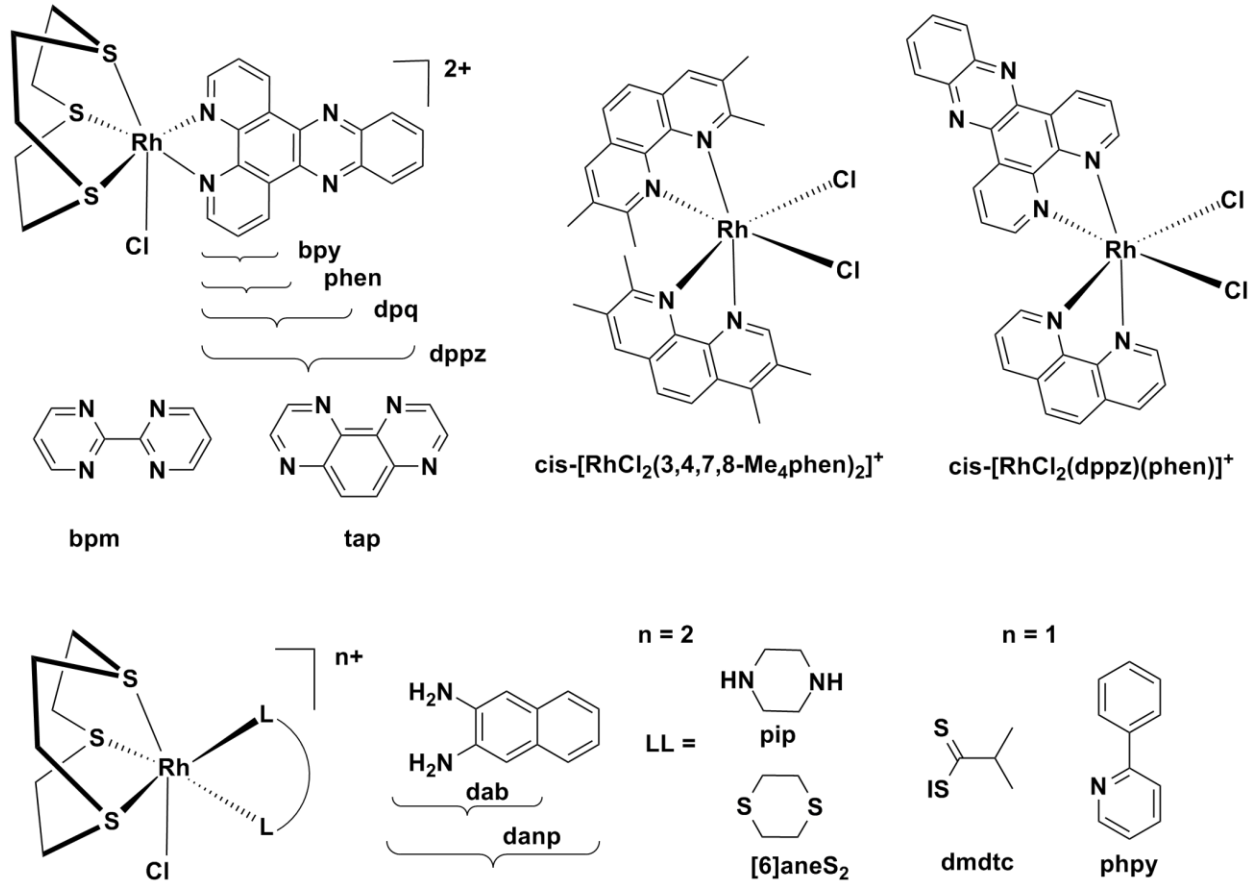

Fig. 1.11 Biologically active organorhodium(III) complexes for various cancer cell lines.

1.4.4 Organoosmium compounds containing N,N'-, O,O'- and sulphur ligands

Since 2006, osmium compounds have become an emerging field for developing anti-cancer drugs as an alternative to the ruthenium analogues, due to their antiproliferative effect against cancer cells and activity towards DNA [104, 105]. Among the transition metals, Os compounds are less explored in medicinal chemistry compared to their ruthenium analogues. Biological studies of osmium complexes appear to have been restricted to osmium carbohydrate polymers which exhibit antiarthritic activity [79, 105]. Normally, third row transition metal ions are relatively inert compared to the first and second row transition metal ions. Fine tuning the properties of N,N' O,O' and N,O ligands chelated Os(II)-arene

compounds, gave complexes with potential anti-tumor activity and which showed promising pharmacological properties for pro-drugs, like solubility in water and plasma, behavior of drug absorption, distrubtion, excretion and non-sterile bioavailability in biological systems [106].

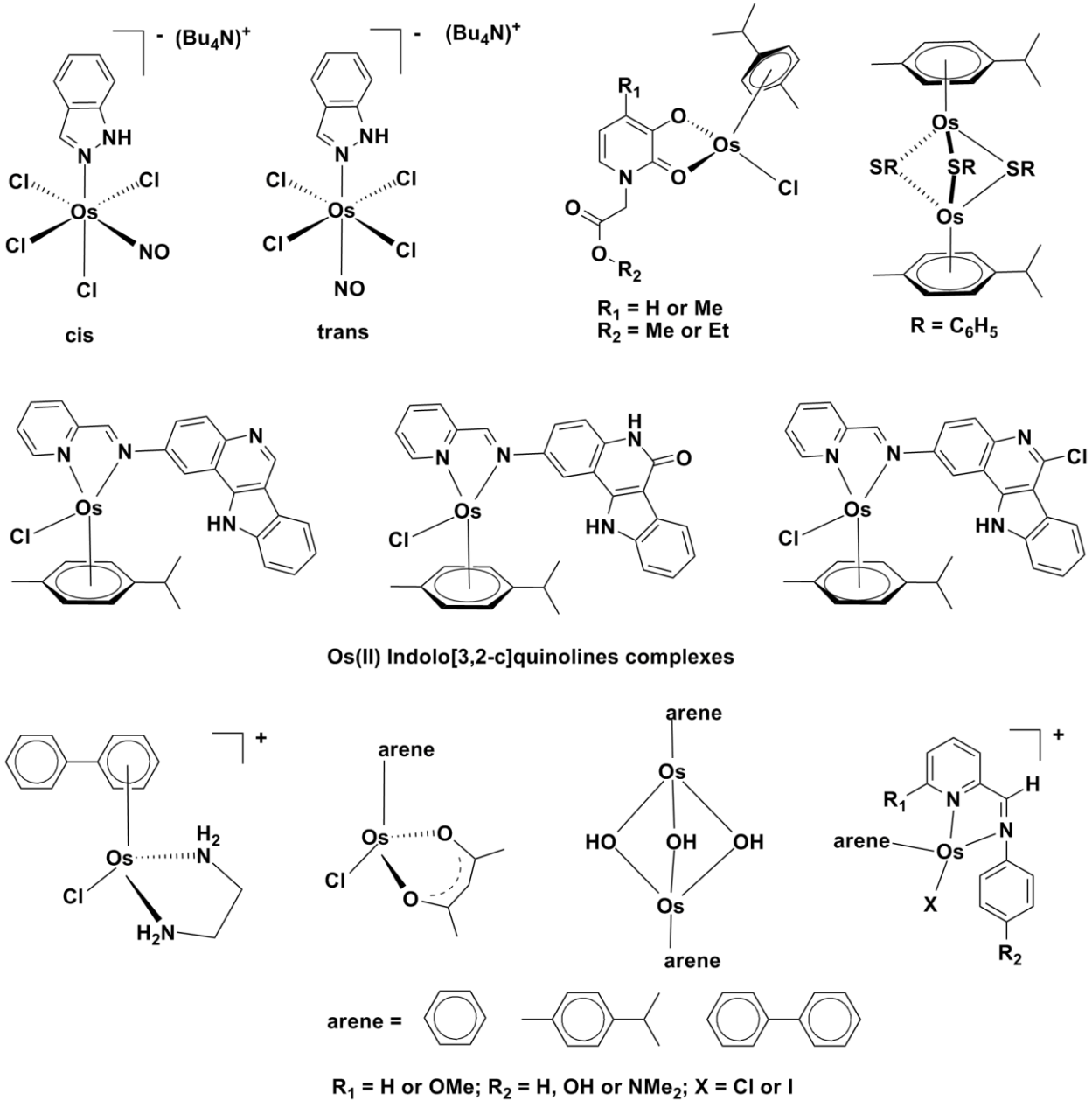

Fig. 1.12 Structure of some anti-cancer organoosmium(IV) and Os(II) compounds containing different bidentate ligands.

Os(II)–arene compounds with bidentate ligands, such as those with N,N'-, N,O-, O,O'-, or S,O-heteroatom have shown potential anticancer activity against different cancer cell lines [79, 104, 107, 108]] (Fig. 1.12). Complexes containing N,N' chelating ligands show promising potential anticancer activity in *in vitro* studies, regardless of the metal center (Ru or Os) in comparison to those with N,O- and O,O'-ligands [79]. N,N' chelating $[\eta^6$-arene)Os(LL)Cl$]^{n+}$ complexes (Where LL = ethylenediamine or acetylacetonate) showed promising effects after hydrolysis and reactivity toward DNA nucleobases, like 9-ethylguanine and 9-methyladenine, in biological systems. In general, the aqueous chemistry of (O,O')-, (N,O)- and (N,N')- chelated Os(II)-arene complexes are less studied than their congener Ru(II)-arene analogues [79, 107].

1.5 Biologically active Ir(III) and Rh(III) compounds containing C,N ligands

Cyclometalated complexes were synthesized by intramolecular C-H activation of C,N Schiff base ligands [108, 109]. The strong C–M sigma bond improved the stability of the complexes against biological reduction, ligand exchange and organic chemical transformation reactions [110, 111]. The biological properties and reaction rate of organic reactions are enhanced by introducing different substitutions in ancillary ligands. Normally, these complexes are kinetically inert. The activity, electronic and kinetic properties are changed by altering the structure of the C–N complexes or fine-tuning the properties of the ligands [43, 88, 112]. These complexes have opened a new field in organometallic and coordination chemistry due to this versatile application in chemical transformation reactions, such as in hydrogenation [113], TH [114], oxidation reactions [44], N-alkylation and carbon-heteroatom forming reactions [20] under relatively mild conditions, which may be difficult to achieve by conventional organic reactions.

Sadler and his co-workers reported different C,N and N,N' Ir complexes which exhibited anticancer activity against A2780 human ovarian cancer cell lines [85, 88, 115] (Fig. 1.13). Rh(III) cyclometalated complexes showed janus kinase 2 enzyme phosphorylation activity and cytotoxicity towards human erythroleukemia cancer cells, as reported by Leung *et al.* [116]. Recently Yellol *et al.* reported high antitumor activities of novel cyclometalated benzimidazole Ru(II), Rh(III) and Ir(III) complexes against HT29, T47D, A2780, A2780cisR cancer cell lines [111].

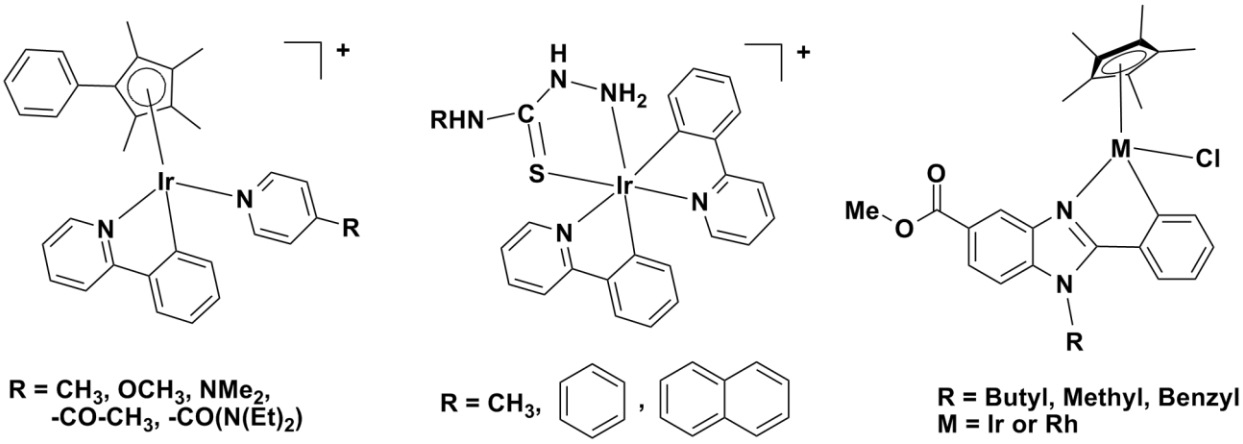

Fig. 1.13 Some C,N ligands coordinated organoiridium(III) and organorhodium(III) complexes for anti-cancer studies.

1.6 Project aims and goals

The aims of this project are to synthesize and characterize a series of bidentate N,N' imine, N,N' amine and C,N Schiff base ligands and coordinate these ligands to different metal atoms such as iridium, rhodium, ruthenium and osmium in a bidentate manner. In order to investigate the catalytic behaviour of the synthesised novel metal complexes, they were used in catalytic transfer hydrogenation and oxidation reactions of primary aromatic alcohols. Furthermore, some of these novel metal complexes were chosen to determine whether these complexes could potentially inhibit cancer cells and bind with human serum albumin in biological systems.

The definitive goal of this project was to prepare catalysts which are active in environmently benign reaction conditions, as well as versatile for different catalytic applications. Being eco-friendly, the catalysts will be active under relatively mild reaction conditions in greener solvents when compared to other catalytic systems, which require harsh reaction conditions to obtain desired products. The correct choice of the metal atom or ion was essential to obtain desired and satisfactory results under the required criteria. Thus, iridium, rhodium, ruthenium and osmium were chosen to give versatile catalytic and biological applications, since these metals can fit the expected criteria (Fig. 1.14).

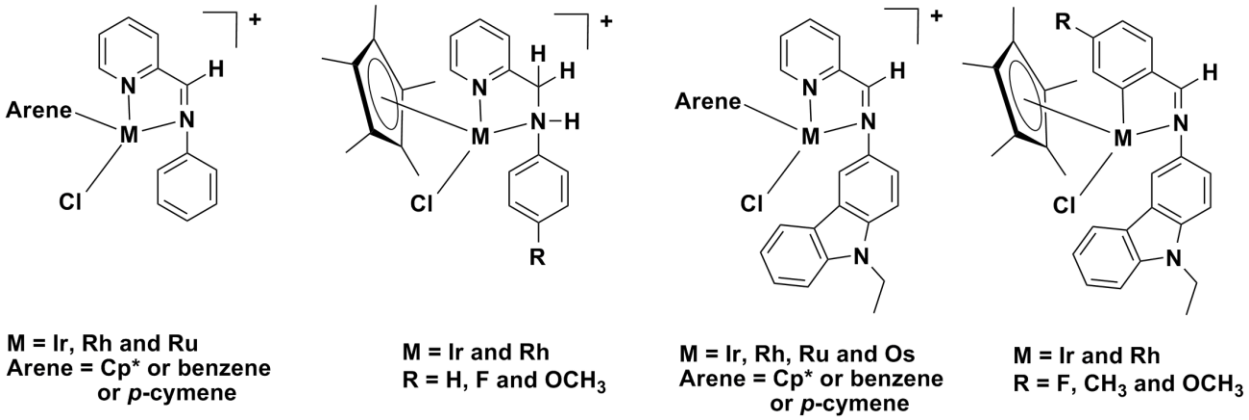

Fig. 1.14 Structures of the N,N' and C,N bidentate ligands and complexes that are presented in this thesis.

1.7 Scope of the thesis and graphical abstracts

This thesis summarizes and presents research carried out involving the synthesis and characterization of different half-sandwich Ir(III), Rh(III), Ru(II) and Os(II) complexes coordinated to a series of N,N' and C,N bidentate ligands. Catalytic and biological investigations of the respective complexes were also carried out. The graphical abstracts of the respective chapters of this thesis are shown here.

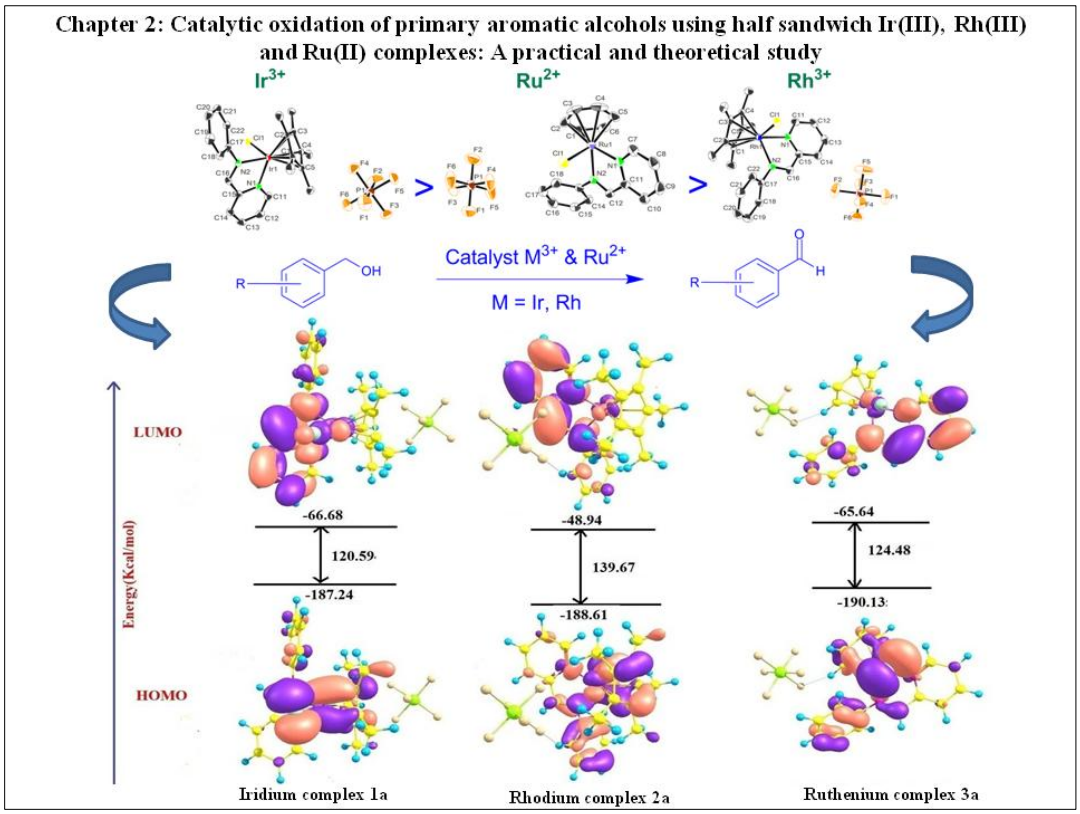

Chapter 3: Synthesis and structural investigation of new half sandwich Ir(III) and Rh(III) amine complexes and their catalytic transfer hydrogenation of aromatic ketones and aldehydes in water

Synthesis of the Ir(III) and Rh(III) complexes

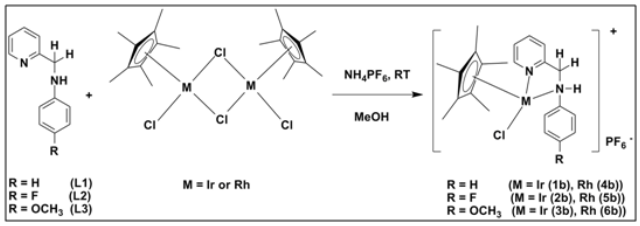

Transfer hydrogenation

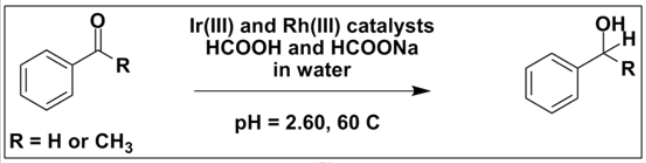

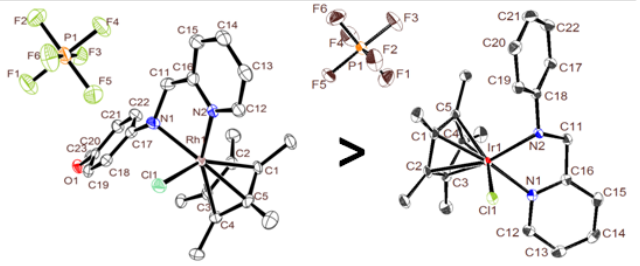

1D NOE contacts of complexes

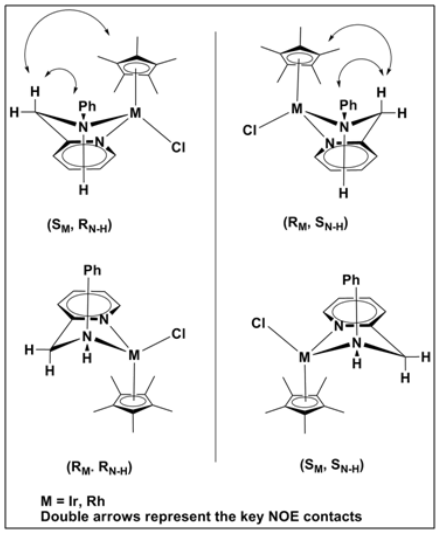

Catalytic activity of the complexes

Rh(III) complexes > Ir(III) complexes

Chapter 4: Synthesis and characterization of new half Ir(III), Rh(III), Ru(II) and Os(II) complexes: Their biological application on MCF-7 breast cancer cells

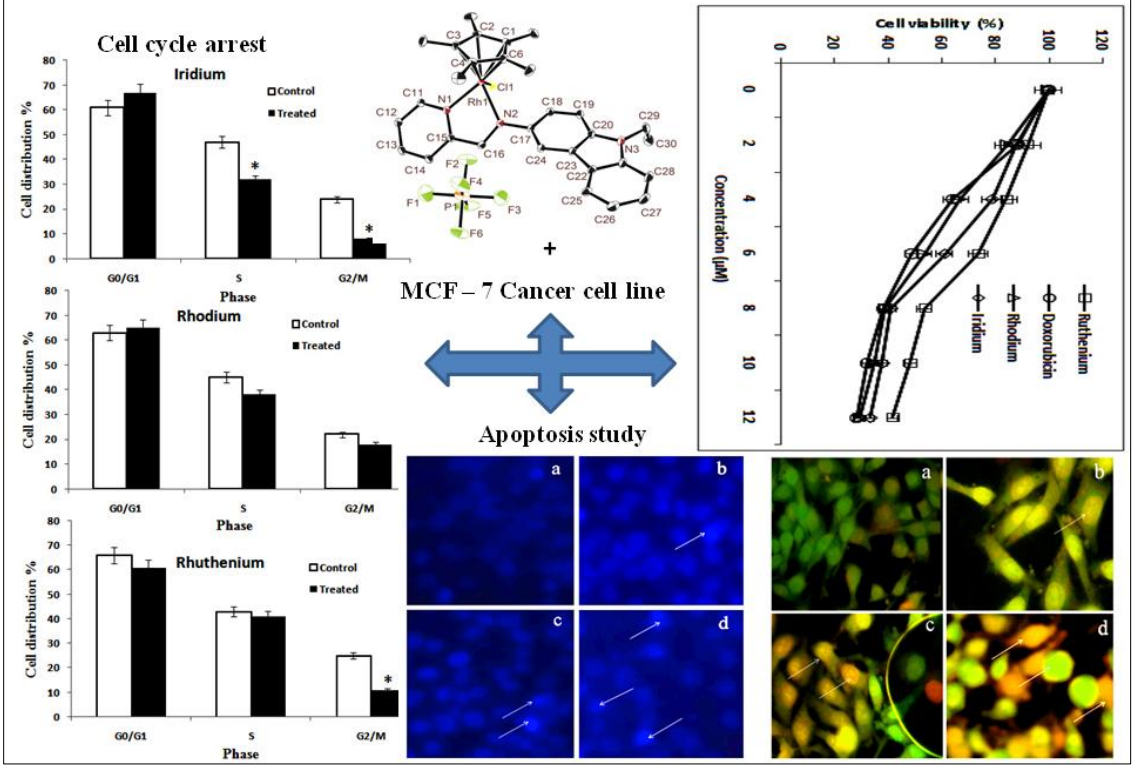

Chapter 5: Binding interactions, conformational change and docking studies of new Ru(II) complexes with human serum albumin

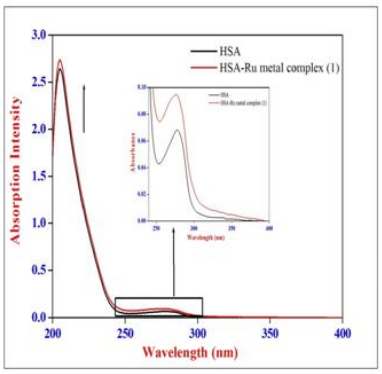

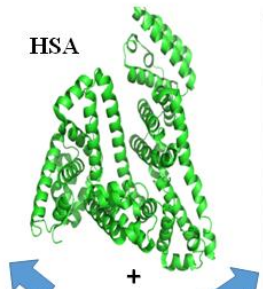

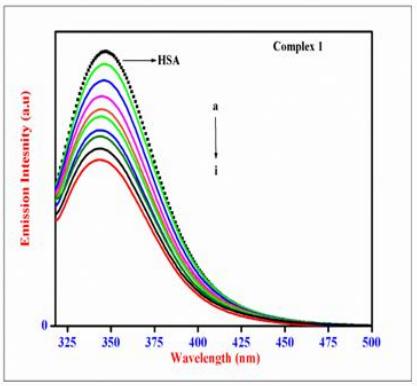

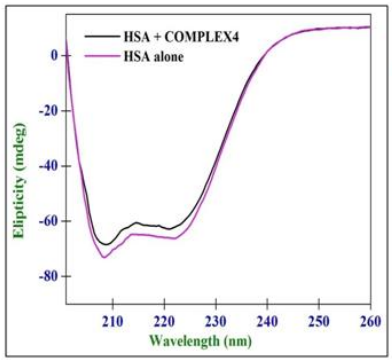

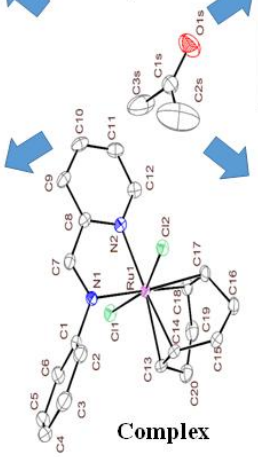

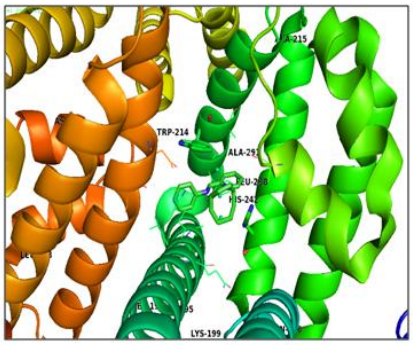

Chapter 6: Synthesis and characterization of C,N cylcometalated new half sandwich Ir(III) and Rh(III) complexes

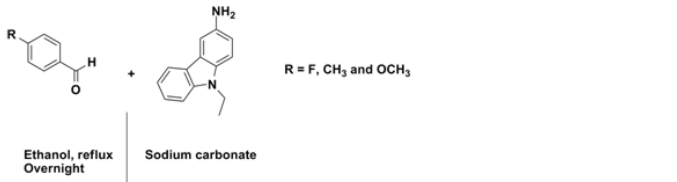

R = F (L1), CH_3 (L2) and OCH_3 (L3) M = Ir or Rh

R = F (M = Ir (1e), Rh (4e))
R = CH_3 (M = Ir (2e), Rh (5e))
R = OCH_3 (M = Ir (3e), Rh (6e))

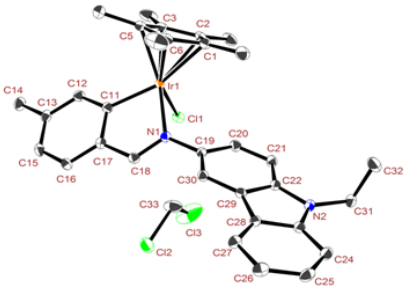

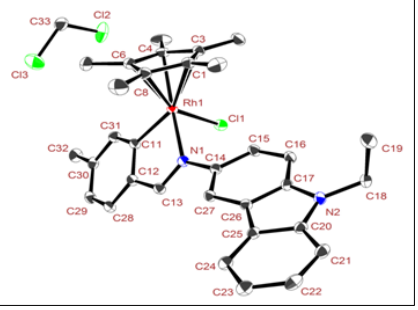

References

[1] F.A. Carey, Adv. Org. Chem., Springer, McGraw-Hill, New York 2003.

[2] J. Costamagna, J. Vargas, R. Latorre, A. Alvarado, G. Mena, Coord. Chem. Rev. 119 (1992) 67-88.

[3] A.D. Garnovskii, A.L. Nivorozhkin, V.I. Minkin, Coord. Chem. Rev. 126 (1993) 1-69.

[4] P.A. Vigato, S. Tamburini, Coord. Chem. Rev. 248 (2004) 1717-2128.

[5] K.N. Campbell, A.H. Sommers, B.K. Campbell, J. Am. Chem. Soc. 66 (1944) 82-84.

[6] J. Hine, C.Y. Yeh, J. Am. Chem. Soc. 89 (1967) 2669-2676.

[7] L.J. Nunez, G.L. Eichhorn, J. Am. Chem. Soc. 84 (1962) 901-906.

[8] S. Yamada, Coord. Chem. Rev. 190–192 (1999) 537-555.

[9] R. Drozdzak, N. Ledoux, B. Allaert, I. Dragutan, V. Dragutan, F. Verpoort, Cent. Eur. J. Chem. 3 (2005) 404-416.

[10] E. Ritter, P. Przybylski, B. Brzezinski, F. Bartl, Curr. Org. Chem. 13 (2009) 241.

[11] G. Ellis, L. Chang, B. Cogionis, D. Daneman, Clin. Chem. 43 (1997) 2437-2439.

[12] M.P. Sathisha, U.N. Shetti, V.K. Revankar, K.S.R. Pai, Eur. J. Med. Chem. 43 (2008) 2338-2346.

[13] G. Chelucci, S. Baldino, W. Baratta, Coord. Chem. Rev. 300 (2015) 29-85.

[14] P. Goel., D. Kumar., S. Chandra., J. Chem. Bio. Phy. Sci. Sec. A. 4 (2014) 1946-1964.

[15] A.A. El-Sherif, M.S. Aljahdali, J. Coord. Chem. 66 (2013) 3423-3468.

[16] P. Steel, Molecules 9 (2004) 440.

[17] C.P. Pradeep, S.K. Das, Coord. Chem. Rev. 257 (2013) 1699-1715.

[18] P.G. Cozzi, Chem. Soc. Rev. 33 (2004) 410-421.

[19] W. Adam, C.R. Saha-Möller, P.A. Ganeshpure, Chem. Rev. 101 (2001) 3499-3548.

[20] G.E. Dobereiner, R.H. Crabtree, Chem. Rev. 110 (2009) 681-703.

[21] D.K. Chand, H.-J. Schneider, A. Bencini, A. Bianchi, C. Giorgi, S. Ciattini, B. Valtancoli, Chem. Eur. J. 6 (2000) 4001-4008.

[22] T. Kiran, V.G. Prasanth, M.M. Balamurali, C.S. Vasavi, P. Munusami, K.I. Sathiyanarayanan, M. Pathak, Inorg. Chim. Acta 433 (2015) 26-34.

[23] P. Jaividhya, M. Ganeshpandian, R. Dhivya, M.A. Akbarsha, M. Palaniandavar, Dalton Trans. 44 (2015) 11997-12010.

[24] D.C. Crans, J.J. Smee, E. Gaidamauskas, L. Yang, Chem. Rev. 104 (2004) 849-902.

[25] K.H. Thompson, J.H. McNeill, C. Orvig, Chem. Rev. 99 (1999) 2561-2572.

[26] J.H. McNeill, V.G. Yuen, H.R. Hoveyda, C. Orvig, J. Med. Chem. 35 (1992) 1489-1491.

[27] S. Hashiguchi, A. Fujii, J. Takehara, T. Ikariya, R. Noyori, J. Am. Chem. Soc. 117 (1995) 7562-7563.

[28] X. Wu, X. Li, F. King, J. Xiao, Angew. Chem. Int. Ed. Engl. 44 (2005) 3407-3411.

[29] X. Li, X. Wu, W. Chen, F.E. Hancock, F. King, J. Xiao, Org. Lett. 6 (2004) 3321-3324.

[30] S.V. Slungård, T.-A. Krakeli, T.H.K. Thvedt, E. Fuglseth, E. Sundby, B.H. Hoff, Tetrahedron 67 (2011) 5642-5650.

[31] E. Mizushima, H. Ohi, M. Yamaguchi, T. Yamagishi, J. Mol. Catal. A: Chem. 149 (1999) 43-49.

[32] O. Prakash, K.N. Sharma, H. Joshi, P.L. Gupta, A.K. Singh, Dalton Trans. 42 (2013) 8736-8747.

[33] P. Singh, A.K. Singh, Organometallics 29 (2010) 6433-6442.

[34] O. Prakash, H. Joshi, K.N. Sharma, P.L. Gupta, A.K. Singh, Organometallics 33 (2014) 3804-3812.

[35] C.-Y. Huang, K.-Y. Kuan, Y.-H. Liu, S.-M. Peng, S.-T. Liu, Organometallics 33 (2014) 2831-2836.

[36] X. Zhou, X. Wu, B. Yang, J. Xiao, J. Mol. Catal. A: Chem. 357 (2012) 133-140.

[37] F. Saleem, G.K. Rao, A. Kumar, G. Mukherjee, A.K. Singh, Organometallics 32 (2013) 3595-3603.

[38] D. Hollmann, S. Bahn, A. Tillack, M. Beller, Chem. Commun. (2008) 3199-3201.

[39] D. Hollmann, S. Bähn, A. Tillack, M. Beller, Angew. Chem. Int. Ed. 46 (2007) 8291-8294.

[40] A. Prades, E. Peris, M. Albrecht, Organometallics 30 (2011) 1162-1167.

[41] A. Bolje, S. Hohloch, D. Urankar, A. Pevec, M. Gazvoda, B. Sarkar, J. Košmrlj, Organometallics 33 (2014) 2588-2598.

[42] S. Ohzu, T. Ishizuka, Y. Hirai, S. Fukuzumi, T. Kojima, Chem. Eur. J. 19 (2013) 1563-1567.

[43] Z. Liu, P.J. Sadler, Acc. Chem. Res. 47 (2014) 1174-1185.

[44] K.-i. Fujita, T. Yoshida, Y. Imori, R. Yamaguchi, Org. Lett. 13 (2011) 2278-2281.

[45] K.-i. Fujita, N. Tanino, R. Yamaguchi, Org. Lett. 9 (2006) 109-111.

[46] R. Yamaguchi, S. Kawagoe, C. Asai, K.-i. Fujita, Org. Lett. 10 (2008) 181-184.

[47] T.P. Brewster, A.J.M. Miller, D.M. Heinekey, K.I. Goldberg, J. Am. Chem. Soc. 135 (2013) 16022-16025.

[48] S. Ogo, N. Makihara, Y. Watanabe, Organometallics 18 (1999) 5470-5474.

[49] H. Vázquez-Villa, S. Reber, M.A. Ariger, E.M. Carreira, Angew. Chem. Int. Ed. 50 (2011) 8979-8981.

[50] Y. Wei, D. Xue, Q. Lei, C. Wang, J. Xiao, Green Chem. 15 (2013) 629-634.

[51] A. Azua, J.A. Mata, E. Peris, F. Lamaty, J. Martinez, E. Colacino, Organometallics 31 (2012) 3911-3919.

[52] A. Prades, R. Corberán, M. Poyatos, E. Peris, Chem. Eur. J. 14 (2008) 11474-11479.

[53] S. Kuwata, T. Ikariya, Chem. Eur. J. 17 (2011) 3542-3556.

[54] L.D. Field, B.A. Messerle, K.Q. Vuong, P. Turner, Organometallics 24 (2005) 4241-4250.

[55] M. Yadav, A.K. Singh, D.S. Pandey, Organometallics 28 (2009) 4713-4723.

[56] X. Wu, D. Vinci, T. Ikariya, J. Xiao, Chem. Commun. (2005) 4447-4449.

[57] G. Kang, S. Lin, A. Shiwakoti, B. Ni, Catal. Commun. 57 (2014) 111-114.

[58] H. Zhang, R. Jin, H. Yao, S. Tang, J. Zhuang, G. Liu, H. Li, Chem. Commun. 48 (2012) 7874-7876.

[59] J. Qi, L. Huang, Z. Wang, H. Jiang, Org. Biomol. Chem. 11 (2013) 8009-8013.

[60] B.-J. Li, Z.-J. Shi, Chem. Sci. 2 (2011) 488-493.

[61] X. Wei, M. Zhao, Z. Du, X. Li, Org. Lett. 13 (2011) 4636-4639.

[62] Y.-F. Wang, K.K. Toh, J.-Y. Lee, S. Chiba, Angew. Chem. Int. Ed. 50 (2011) 5927-5931.

[63] K. Morimoto, K. Hirano, T. Satoh, M. Miura, J. Org. Chem. 76 (2011) 9548-9551.

[64] K. Gray, M.J. Page, J. Wagler, B.A. Messerle, Organometallics 31 (2012) 6270-6277.

[65] D.R. Coulson, Tetrahedron Lett. 12 (1971) 429-430.

[66] M.J. Genin, C. Biles, B.J. Keiser, S.M. Poppe, S.M. Swaney, W.G. Tarpley, Y. Yagi, D.L. Romero, J. Med. Chem. 43 (2000) 1034-1040.

[67] Y. Cui, X. Dong, Y. Li, Z. Li, W. Chen, Eur. J. Med. Chem. 58 (2012) 323-331.

[68] C.-M. Che, J.-S. Huang, Coord. Chem. Rev. 242 (2003) 97-113.

[69] J.R. Durig, J. Danneman, W.D. Behnke, E.E. Mercer, Chem. Biol. Interact. 13 (1976) 287-294.

[70] C.S. Allardyce., P.J. Dyson, Platinum Met. Rev. 45 (2001) 62.

[71] I. Kostova, Curr. Med. Chem. 13 (2006) 1085-1107.

[72] C.S. Allardyce, A. Dorcier, C. Scolaro, P.J. Dyson, App. Organomet. Chem. 19 (2005) 1-10.

[73] G. Suss-Fink, Dalton Trans. 39 (2010) 1673-1688.

[74] D. Gambino, L. Otero, Inorg. Chim. Acta 393 (2012) 103-114.

[75] P. Nowak-Sliwinska, J.R. van Beijnum, A. Casini, A.A. Nazarov, G. Wagnières, H. van den Bergh, P.J. Dyson, A.W. Griffioen, J. Med. Chem. 54 (2011) 3895-3902.

[76] R. Pettinari, C. Pettinari, F. Marchetti, B.W. Skelton, A.H. White, L. Bonfili, M. Cuccioloni, M. Mozzicafreddo, V. Cecarini, M. Angeletti, M. Nabissi, A.M. Eleuteri, J. Med. Chem. 57 (2014) 4532-4542.

[77] F. Aman, M. Hanif, W.A. Siddiqui, A. Ashraf, L.K. Filak, J. Reynisson, T. Söhnel, S.M.F. Jamieson, C.G. Hartinger, Organometallics 33 (2014) 5546-5553.

[78] A.L. Noffke, A. Habtemariam, A.M. Pizarro, P.J. Sadler, Chem. Commun. 48 (2012) 5219-5246.

[79] A.F.A. Peacock, A. Habtemariam, R. Fernández, V. Walland, F.P.A. Fabbiani, S. Parsons, R.E. Aird, D.I. Jodrell, P.J. Sadler, J. Am. Chem. Soc. 128 (2006) 1739-1748.

[80] T. Bugarcic, A. Habtemariam, R.J. Deeth, F.P.A. Fabbiani, S. Parsons, P.J. Sadler, Inorg. Chem. 48 (2009) 9444-9453.

[81] M.L.B. Tobe, J, in: A. Bakac (Ed.), Physical Inorganic Chemistry: Reactions, Processes, and Applications, Addison Wesley Longman Inc, UK, 1999.

[82] J. Ruiz, C. Vicente, C. de Haro, D. Bautista, Inorg. Chem. 52 (2013) 974-982.

[83] M.K. Helms, C.E. Petersen, N.V. Bhagavan, D.M. Jameson, FEBS Lett. 408 (1997) 67-70.

[84] A. Wilbuer, D.H. Vlecken, D.J. Schmitz, K. Kräling, K. Harms, C.P. Bagowski, E. Meggers, Angew. Chem., Int. Ed. Engl. 49 (2010) 3839-3842.

[85] T. Giraldi, G. Sava, G. Mestroni, G. Zassinovich, D. Stolfa, Chem. Biol. Interact. 22 (1978) 231-238.

[86] G. Sava, S. Zorzet, L. Perissin, G. Mestroni, G. Zassinovich, A. Bontempi, Inorg. Chim. Acta 137 (1987) 69−71.

[87] Z. Liu, A. Habtemariam, A.M. Pizarro, S.A. Fletcher, A. Kisova, O. Vrana, L. Salassa, P.C.A. Bruijnincx, G.J. Clarkson, V. Brabec, P.J. Sadler, J. Med. Chem. 54 (2011) 3011-3026.

[88] Z. Liu, A. Habtemariam, A.M. Pizarro, G.J. Clarkson, P.J. Sadler, Organometallics 30 (2011) 4702-4710.

[89] Z. Liu, I. Romero-Canelón, B. Qamar, J.M. Hearn, A. Habtemariam, N.P.E. Barry, A.M. Pizarro, G.J. Clarkson, P.J. Sadler, Angew. Chem. 126 (2014) 4022-4027.

[90] Kenneth Yin Zhang, Steve Po-Yam Li, Nianyong Zhu, Iyana Wai-Shan Or, Maggie Shau-Ha Cheung, Yun-Wah Lam, K.K.-W. Lo., Inorg. Chem. 49 (2010) 2530–2540.

[91] N. Cutillas, G.S. Yellol, C. de Haro, C. Vicente, V. Rodríguez, J. Ruiz, Coord. Chem. Rev. 257 (2013) 2784-2797.

[92] N. Katsaros, A. Anagnostopoulou, Crit. Rev. Oncol. Hematol. 42 (2002) 297-308.

[93] A. Erck, L. Rainen, J. Whileyman, I.M. Chang, A.P. Kimball, J. Bear, Proc. Soc. Exp. Biol. Med. 145 (1974) 1278-1283.

[94] A. Erck, E. Sherwood, J.L. Bear, A.P. Kimball, Cancer Res. 36 (1976) 2404-2409.

[95] R.A. Howard, E. Sherwood, A. Erck, A.P. Kimball, J.L. Bear, J. Med. Chem. 20 (1977) 943-946.

[96] R.A. Howard, A.P. Kimball, J.L. Bear, Cancer Res. 39 (1979) 2568-2573.

[97] H. LM., S. RJ., R. HJ., J. Clin. Hematol. Oncol. 10 (1980) 25-27.

[98] G. T., Z. G., M. G., Chem. Biol. Interact. 9 (1974) 389-394.

[99] G. Sava, S. Zorzet, S. Pacor, G. Mestroni, G. Zassinovich, Cancer Chemother. Pharmacol. 24 (1989) 302-306.

[100] K.S. McCully, M.P. Vezeridis, Cancer Invest. 5 (1987) 25-30.

[101] A.S. Salameh, N. Nassif, H.A. Tayim, Arab. J. Sci. Eng. Sect A. 23 (1998) 175-182.

[102] C. DG., M. C., P.I. E., A. MP., D.-V.J.e. al., An. R. Acad. Farm. 56 (1990) 453-467.

[103] E.L. Menon, R. Perera, M. Navarro, R.J. Kuhn, H. Morrison, Inorg. Chem. 43 (2004) 5373-5381.

[104] G. Gupta, N. Nagesh, B.S. Murray, P.J. Dyson, B. Therrien, Inorg. Chim. Acta 423, Part A (2014) 31-35.

[105] B. Boff, C. Gaiddon, M. Pfeffer, Inorg. Chem. 52 (2013) 2705-2715.

[106] G.E. Büchel, A. Gavriluta, M. Novak, S.M. Meier, M.A. Jakupec, O. Cuzan, C. Turta, J.-B. Tommasino, E. Jeanneau, G. Novitchi, D. Luneau, V.B. Arion, Inorg. Chem. 52 (2013) 6273-6285.

[107] B.C.E. Makhubela, M. Meyer, G.S. Smith, J. Organomet. Chem. 772–773 (2014) 229-241.

[108] D.L. Davies, O. Al-Duaij, J. Fawcett, M. Giardiello, S.T. Hilton, D.R. Russell, Dalton Trans. (2003) 4132-4138.

[109] L. Li, W.W. Brennessel, W.D. Jones, Organometallics 28 (2009) 3492-3500.

[110] F. Monti, F. Kessler, M. Delgado, J. Frey, F. Bazzanini, G. Accorsi, N. Armaroli, H.J. Bolink, E. Ortí, R. Scopelliti, M.K. Nazeeruddin, E. Baranoff, Inorg. Chem. 52 (2013) 10292-10305.

[111] G.S. Yellol, A. Donaire, J.G. Yellol, V. Vasylyeva, C. Janiak, J. Ruiz, Chem. Commun. 49 (2013) 11533-11535.

[112] C.L. Ho, K.L. Wong, H.K. Kong, Y.M. Ho, C.T.L. Chan, W.M. Kwok, K.S.Y. Leung, H.L. Tam, M.H.W. Lam, X.F. Ren, A.M. Ren, J.K. Feng, W.Y. Wong, Chem. Commun. 48 (2012) 2525-2527.

[113] S. Arita, T. Koike, Y. Kayaki, T. Ikariya, Organometallics 27 (2008) 2795-2802.

[114] W.B. Cross, C.G. Daly, Y. Boutadla, K. Singh, Dalton Trans. 40 (2011) 9722-9730.

[115] Z. Liu, L. Salassa, A. Habtemariam, A.M. Pizarro, G.J. Clarkson, P.J. Sadler, Inorg. Chem. 50 (2011) 5777-5783.

[116] C.-H. Leung, H. Yang, V.P.-Y. Ma, D.S.-H. Chan, H.-J. Zhong, Y.-W. Li, W.-F. Fong, D.-L. Ma, MedChemComm 3 (2012) 696-698.

Chapter 2

Catalytic oxidation of primary aromatic alcohols using half sandwich Ir(III), Rh(III) and Ru(II) complexes: A practical and theoretical study

Abstract

The complexes [Cp*IrCl(N-(pyridin-2-ylmethylene)aniline)]PF_6 (**1a**), [Cp*RhCl(N-(pyridin-2-ylmethylene)aniline)]PF_6 (**2a**), (where Cp* = 1,2,3,4,5-pentamethylcyclopentadiene) and [η^6-areneRuCl(N-(pyridin-2-ylmethylene)aniline)]PF_6 (**3a**) have been synthesized and the structure and purity of these were confirmed by single crystal XRD and elemental analyses respectively. Iridium and rhodium complexes exhibit the monoclinic P21/n space group, the ruthenium complex the P21/c space group and all three complexes show the expected pseudo octahedral "piano-stool" geometry. The performance of these complexes as catalysts for the dehydrogenation of primary alcohols to their respective aldehydes with different bases and solvents was investigated. The complexes of iridium and ruthenium gave good conversions in different alkaline solutions. Density functional theory was applied to determine the respective MO energy levels, bond lengths, bond angles and binding energies of all the metal complexes. It was also used to study the activity, stability and intermediates of the complexes. A Gibbs free energy (ΔG) DFT calculation was carried out to help understand the reaction mechanism / catalytic cycle of the Rh complex (**2a**). The energy barrier for oxidation of aromatic alcohols by the rhodium hydride complex is much lower (-8.50 kcal/mol) than the barrier for hydride transfer of the corresponding Rh benzyloxo species (21.41 kcal/mol), in agreement with mechanisms proposed for related systems.

Keywords: Catalytic oxidation; N,N' bidentate ligand; half sandwich metal complexes; primary alcohols; DFT.

2.1 Introduction

Oxidation of primary aromatic alcohols to their respective aldehydes is an important chemical transformation in synthetic chemistry [1]. Alcohols are generally inactive and require harsh methods to activate the hydroxyl group present [2-5]. In transition metal chemistry, the metal can mediate the dehydrogenation of alcohols to yield the aldehydes [5-9] and there are many reports on the oxidation of alcohols to aldehydes and ketones. Indeed, metal catalyzed aromatic alcohol oxidation reactions are

recognized as one of the greener methods [10-13]. There are several water soluble homogeneous metal complexes that have been reported for the oxidation of alcohols, such as those of copper, palladium and gold [14, 15]. Many classical methods and reagents are available for these reactions, like "activated DMSO" methods, NaOCl/TEMPO (TEMPO = 2,2,6,6-tetramethyl-1-piperidinyloxyl), hypervalent iodine reagents and chromium and manganese oxides [16-18].

The N,N' chelating donor ligands containing (η^5-C_5Me_5)Ir(III), (η^5-C_5Me_5)Rh(III) and (η^6–arene)Ru(II) half sandwich complexes exhibit a wide range of applications in homogeneous catalysis due to their high stability in solution, rapid formation of metal-hydride intermediate, steric and electronic properties around the metal center can be easily tuned by these ligands [18, 19]. To explore the metal complex systems, researchers also have developed eco-friendly and efficient catalytic metal complex systems for the oxidation of alcohols using less toxic oxidants such as oxygen, hydrogen peroxide and acetone [19-21].

In a homogeneous catalytic system, the borrowing of hydrogen and hydrogen auto transfer reactions usually occur via the formation of a metal hydride intermediate to complete the catalytic cycle [22, 23]. In recent years the hydrogen gas evolved alcohol dehydrogenation process has generated great interest from the view point of atom economy [22, 23]. There are different homogeneous catalytic systems which effectively dehydrogenate primary alcohols to their respective aldehydes, which include metals such as iridium, rhodium and ruthenium [24-26]. As per existing literature, many of the complexes were reported with high catalyst loading and using oxidizing agents for oxidation of alcohols under harsh reaction conditions. In this study we compared the catalytic activity of iridium, rhodium and ruthenium complexes containing N,N' functional bidentate N-(pyridin-2-ylmethylene)aniline ligand over oxidation of alcohols without oxidizing agents under mild reaction conditions using inexpensive bases such as Cs_2CO_3, K_2CO_3, Na_2CO_3 and $NaHCO_3$. We also report a DFT modelling study of the complexes, HOMO-LUMO energy differences and reactivity.

2.2 Experimental section

2.2.1 Methods and analysis

Unless otherwise noted, all manipulations were performed using standard Schlenk tube techniques under argon atmosphere. The reagents and solvents were purchased from Sigma-Aldrich, Fluka and Merck and used without further purification. The solvents were dried by standard procedures and distilled prior to use. Gas chromatography (GC) analysis was performed using a Perkin-Elmer Clarus 500 GC with a HP-Pona-50m*0.2mm, 0.5µ capillary column. The NMR solvent DMSO-d_6 was

purchased from Merck Germany. ^{1}H NMR (400 MHz) and ^{13}C (100 MHz) NMR were recorded in DMSO-d_6 solvent systems using a Bruker Topspin 400 spectrometer. Solid and liquid state infrared spectra were recorded using an FT-IR Perkin Elmer Spectrum 100 spectrophotometer between 4000 - 400 cm^{-1}. Elemental analyses were performed on a Thermo-Scientific Flash 2000 CHNS/O analyser.

Single-crystal X-ray diffraction data were collected on a Bruker KAPPA APEX II DUO diffractometer using graphite-monochromated Mo-Kα radiation (χ = 0.71073 Å). Data collection was carried out at 173(2) K. Temperature was controlled by an Oxford Cryostream cooling system (Oxford Cryostat). Cell refinement and data reduction were performed using the program SAINT [27]. The data were scaled and absorption corrections performed using SADABS. The structure was solved by direct methods using SHELXS-97 and refined by full-matrix least-squares methods based on F^2 using SHELXL-97 [28]. For the structures and graphics, *ORTEP-3* [29] and DIAMOND [30] programs were used. The crystals of all the metal complexes were obtained by slow evaporation of a mixture of hexane and acetonitrile at ambient temperature. The electronic absorption spectroscopy (UV-Vis) studies were recorded using a Perkin Elmer precisely Lambda35 instrument. The TGA-DSC analyses were performed using a Thermal Analyser SDT Q600 instrument and a heating rate of 10 °C.min^{-1} and nitrogen flow of 100 mL.min^{-1}. The metal precursors $(IrCl_2Cp^*)_2$, $(RhCl_2Cp^*)_2$ and $(RuCl_2C_6H_6)_2$ were prepared according to the literature methods [31-33].

2.2.2 Synthesis and characterization of complexes 1a-3a.

A mixture of $(MCl_2Cp^*)_2$ (M = Ir / Rh) (0.13 / 0.16 mmol), the Schiff base imine ligand **L** (0.26 / 0.32 mmol) and NH_4PF_6 (0.26 / 0.32 mmol) was stirred at room temperature in methanol (15 mL) for 2 hours. The yellow precipitate was separated out and filtered off through filter paper, washed with cold methanol and diethyl ether and dried under vacuum. The above common procedure was followed to synthesize complexes **1a**-**2a**.

2.2.2.1 [(η^5-C_5Me_5)IrCl(**L**)] **(1a)**

$(IrCl_2Cp^*)_2$ (100 mg), the Schiff base imine ligand (46 mg) and NH_4PF_6 (41 mg). Yield (140mg, 0.21 mmol, 70 %). Mp. 270.0 °C (dec). ^{1}H NMR (400 MHz, DMSO-d_6, 25 °C, ppm) δ = 9.38 (s, 1H, imine CH), 9.05 (d, 1H, J_{H-H} = 5.40 Hz, α proton of Py), 8.45 (d, 1H, J_{H-H} = 7.52 Hz Py), 8.32 (m, 1H, Py), 7.95 (m, 1H, Py), 7.68 (d, 2H, J_{H-H} = 7.60 Hz, ph), 7.61 (t, J = 7.45 Hz, 2H, ph), 7.52 (t, J = 7.24 Hz, 1H, ph), 1.43 (s, 15H, C_5Me_5) ^{13}C NMR (100 MHz, DMSO-d_6, 25 °C, ppm) δ = 169.12 (imine C-H), 155.33 (Py), 152.26 (Py), 148.69 (Py), 140.52 (Py), 130.47 (ph), 130.01 (ph), 129.54 (ph), 129.33 (Ph), 122.45 (ph),

89.69 (C, C_5Me_5), 7.98 (CH_3, C_5Me_5). FT-IR (γ/cm^{-1}): 1615 (s, C=N), 830 (s, P-F). MS (ESI^+): *m/z* 545.20 $(M\text{-}PF_6)^+$. Anal. Calcd for $C_{22}H_{25}ClF_6IrN_2P$: C, 38.29; H, 3.65; N, 4.06. Found: C, 38.34; H, 3.66; N, 3.89.

2.2.2.2 [(η^5-C_5Me_5)RhCl(**L**)] (**2a**)

$(RhCl_2Cp^*)_2$ (100 mg), the Schiff base imine ligand (59 mg) and NH_4PF_6 (53 mg). Yield (132 mg, 0.22 mmol, 68%). Mp. 275.0 °C (dec). ^{1}H NMR (400 MHz, DMSO-d_6, 25 °C, ppm) δ = 9.07 (s, 1H, imine CH), 8.96 (d, 1H, $J_{H\text{-}H}$ = 2.48 Hz, Py), 8.37 (m, 1H, Py), 8.31 (d, 1H, $J_{H\text{-}H}$ = 6.92 Hz, Py), 7.97 (m, 1H, Py), 7.72 (d, 2H, $J_{H\text{-}H}$ = 7.56 Hz, Ph), 7.64 (t, 2H, *J* = 8.00 Hz, Ph), 7.54 (t, 1H, *J* = 7.36 Hz, Ph), 1.43 (s, 15H, C_5Me_5). ^{13}C NMR (100 MHz, DMSO-d_6, 25 °C, ppm) δ = 167.78 (imine C-H), 153.74 (Py), 152.76 (Py), 148.35 (Py), 140.48 (Py), 129.94 (ph), 129.87 (Ph), 129.48 (ph), 129.35 (ph), 122.38 (ph), 97.11 - 97.03 (C, C_5Me_5), 8.23 (CH_3, C_5Me_5). FT-IR (γ/cm^{-1}): 1595 (s, C=N), 830 (s, P-F). MS (ESI^+): *m/z* 455.10 $(M\text{-}PF_6)^+$. Anal. Calcd for $C_{22}H_{25}ClF_6N_2PRh$: C, 43.98; H, 4.19; N, 4.66. Found: C, 44.21; H, 4.11; N, 4.53.

2.2.2.3 [(η^6-C_6H_6)RuCl(**L**)] (**3a**)

To a suspension $(RuCl_2C_6H_6)_2$ (100mg, 0.15 mmol), and the Schiff base ligand 1a (58mg, 0.32 mmol) was dissolved and stirred at room temperature in acetonitrile solvent (10ml) for 1 hour. The mixture was evaporated and dryness, the residue was treated with NH_4PF_6 (52mg, 0.32 mmol) in ethanol (10ml) one hour. The yellow color solid of **3a** (140mg, 0.26 mmole, 83%) was separated out and filtered through filter paper, washed with diethyl ether and dried in vacuum. Mp. 232.0°C (dec). ^{1}H NMR (400 MHz, DMSO-d_6, 25 °C, δ) 9.67 (d, 1H, $J_{H\text{-}H}$ = 5.4 Hz, α proton of Py) 8.91 (s, 1H, imine CH), 8.31 - 8.27 (m, 2H, Py), 7.88 (m, 1H, Py), 7.82 (d, 2H, $J_{H\text{-}H}$ = 7.48 Hz, ph), 7.65 – 7.58 (m, 3H, ph), 5.95 (s, 6H, C_6H_6). ^{13}C NMR (100 MHz, DMSO-d_6, 25°C, δ) 168.01 (imine C-H), 156.22 (Py), 154.64 (Py), 151.77 (Py), 140.04 (Py), 129.95 (ph), 129.65 (ph), 129.45 (Ph), 128.73 (ph), 128.28 (ph), 122.38 (Ph), 87.20 (C, C_6H_6). FT-IR (γ/cm^{-1}): 1591 (s, C=N), 824 (s, P-F). MS (ESI^+): *m/z* 397.0 $(M\text{-}PF_6)^+$. Anal. Calcd. for $C_{22}H_{25}ClF_6N_2PRu$: C, 39.90; H, 2.98; N, 5.17; Found: C, 39.97; H, 2.95; N, 5.00.

2.2.3 DFT calculations

All the calculations were performed using the Guassian 09 program package [34]. The structural and energetic results calculated using M05-2X were more consistent with the experimental observations [35]. The hybrid exchange-correlation functional M05-2X, developed by Zhao and Truhlar [36, 37], have been shown to describe weak bonding interaction better than the other density functionals such as M06

classes, M05, B3LYP, and PBE functional. So, all the complex structures were optimized at M05-2X level of theory using the LANL2DZ basis set. Frequency calculation was carried out at the same level of theory and to characterize the structures to be the minima or transition states. The one imaginary frequencies confirmed that (A)TS_1 transition state had stable minima. The HOMO and LUMO energy gap was calculated from the DFT method. The frontier molecular orbital plot was drawn using the chemcraft program package *(http://www.chemcraftprog.com)*. Using Gaussian NBO (ver. 3.1), natural population analysis (NPA) and natural bond orbital (NBO) analysis has been performed to investigate the change in electron density from proton donor to proton acceptor for optimized metal complexes at the M05-2X/LANL2DZ level of theory. Second order perturbation energy ($E^{(2)}$) was used to estimate the magnitude of electron delocalization [38].

2.2.4 General procedure for the oxidation of benzyl alcohol

Benzyl alcohol (1 mmol), catalyst (2 mol%), base (5 mol%) and solvent (20 mmol) were placed in a Schlenk tube under argon or nitrogen atmosphere. The mixture was stirred magnetically under reflux over the specified time. The yield of the benzaldehyde was determined by GC analysis using chlorobenzene as an internal standard.

2.2.5 Procedure for the oxidation of benzyl alcohol derivatives catalysed by complexes 1a and 3a

The benzyl alcohol derivatives (1 mmol), catalyst **1a** or **3a** (2 mol%), base (5 mol%) and toluene or *p*-xylene (20 mmol) were added to a Schlenk tube under argon or nitrogen atmosphere. The mixture was stirred magnetically at reflux temperature. The yields of the products were analyzed by GC chromatography using chlorobenzene as an internal standard.

2.3 Results and discussion

2.3.1 Synthesis of ligand and metal complexes

The N,N' bidentate ligand precursor N-(pyridin-2-ylmethylene)aniline and metal complexes of iridium, rhodium and ruthenium were synthesised according to methods discussed elsewhere [39-41]. The structure and purity of the synthesized metal complexes, along with the ligands were confirmed by single crystal XRD, NMR, IR and electronic absorption spectral studies. The thermal stability of the prepared compounds was confirmed by TGA analysis. The structures of the metal complexes are shown (Fig. 2.1).

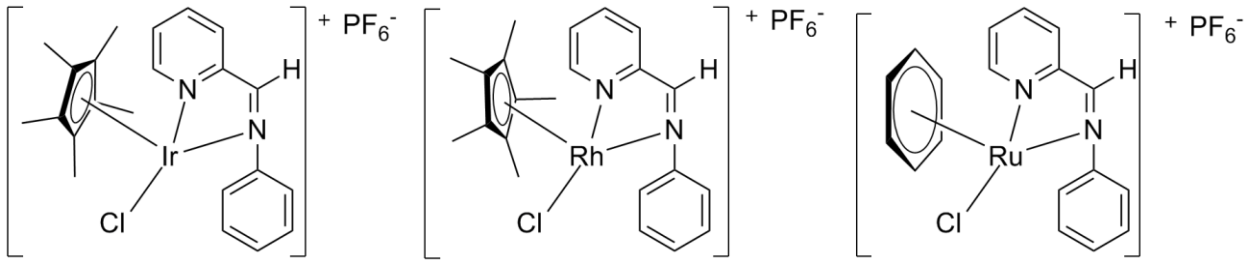

Fig. 2.1 The metal complexes of Ir(III) (**1a**), Rh(III) (**2a**) and Ru(II) (**3a**).

2.3.2 X –Ray crystallography

The crystallographic data of complexes **1a**-**3a** are given in Table 2.1. The *ORTEP* view of the metal complexes iridium (**1a**), rhodium (**2a**) and ruthenium (**3a**) are shown in Figs. 2.2-2.4. In complexes **1a** and **2a**, the iridium and rhodium metal centers are coordinated via the nitrogen atoms of the ligand, five carbon atoms of the Cp* moiety and a Cl. In complex (**3a**), the ruthenium metal is coordinated via the nitrogen atoms of the ligand, η^6 coordination to the benzene ring and to chloride. This gives pseudo-octahedral half sandwich "piano-stool" structures around the iridium, rhodium and ruthenium metal centers in the complexes [41]. The Cp*/arene moieties of complexes **1a, 2a** and **3a** occupy the triangular face of an octahedron. The N1, N2 nitrogen atoms form a five membered chelate ring with the metal center. A chloride completes the coordination sphere. The M-Cl bond length in complexes **1a**-**3a** are 2.400(10) Å, 2.393(8) Å and 2.393(10) Å, respectively. These values are consistent with related reported metal complexes in literature, like $[(\eta^5\text{-}C_5Me_5)IrCl(C_5H_5N\text{-}2\text{-}CH{=}NC_6H_4\text{-}P\text{-}NO_2)]PF_6$ [40], $[(\eta^5\text{-}C_5Me_5)RhCl(C_5H_5N\text{-}2\text{-}CH{=}NC_6H_4\text{-}P\text{-}Cl)]BF_4$ [40] and $[(\eta^6\text{-}C_6H_6)RuCl(C_5H_5N\text{-}2\text{-}CH{=}NC_6H_4\text{-}P\text{-}CH_3)]PF_6$ [41]. The M-C (Cp*/arene) bond lengths in the complexes are 2.153(3) - 2.205(3) Å (**1a**), 2.136(3) - 2.192(3) Å (**2a**) and 2.171(4) - 2.192(4) Å (**3a**), respectively. Non-covalent interactions of C-H···F and C-H···Cl bonds in the complexes of **1a**, **2a** and **3a** are observed. In the crystal structure of complexes **1a**-**3a** C-H···Cl and C-H···F non-covalent intra and intermolecular interactions are seen (Figs. 2.5-2.7). In all three complexes, the counter ion PF_6 is involved in C-H···F non-covalent inter-molecular interactions. The P-F···π intermolecular interaction is observed in complexes **1a** and **3a** and C-H···π intermolecule interaction is observed in complex **2a** (Tables 2.2 & 2.3).

Table 2.1 Crystallographic data and summary of structural refinement of the metal complexes **1a, 2a** and **3a**

	1a	**2a**	**3a**
Empirical formula	$C_{22}H_{25}ClF_6IrN_2P$	$C_{22}H_{25}ClF_6N_2PRh$	$C_{18}H_{16}ClF_6N_2PRu$
Formula weight	690.06	600.77	541.82
Crystal colour	Orange	Yellow	Yellow
Temperature/K	173(2)	173(2)	173(2)
Crystal system	monoclinic	monoclinic	monoclinic
Space group	$P2_1/n$	$P2_1/n$	$P2_1/c$
a (Å)	8.694(4)	8.7080(4)	7.7407(3)
b (Å)	13.312(6)	13.2046(3)	17.0759(4)
c (Å)	20.664(9)	20.6563(8)	15.3185(6)
α (°)	90.00	90.00	90.00
β (°)	94.244(9)	94.4670(10)	101.7610(10)
γ (°)	90.00	90.00	90.00
Volume ($Å^3$)	2385.0(18)	2367.96(15)	1982.28(12)
Z	4	4	4
ρ_{calc} (mg/mm^3)	1.922	1.685	1.816
μ(Mo$K\alpha$) [mm^{-1}]	5.837	0.962	1.068
F(000)	1336.0	1208.0	1072.0
Crystal size/mm^3	0.16 × 0.14 × 0.12	0.18 × 0.14 × 0.11	0.16 × 0.12 × 0.11
2θ range for data collection	3.96 to 57.26°	7.34 to 54.92°	7.22 to 55.76°
Reflections collected	81251	94755	94614
Independent reflections	6006[R(int) = 0.0495]	5403[R(int) = 0.0806]	4716[R(int) = 0.0847]
Data/restraints/parameters	6006/0/303	5403/0/303	4716/0/262
Goodness-of-fit on F^2	1.034	1.072	1.132
Final R indexes [I>=2σ (I)]	R_1 = 0.0225, wR_2 = 0.0458	R_1 = 0.0344, wR_2 = 0.0692	R_1 = 0.0450, wR_2 = 0.0960
Final R indexes [all data]	R_1 = 0.0374, wR_2 = 0.0514	R_1 = 0.0656, wR_2 = 0.0807	R_1 = 0.0751, wR_2 = 0.1109
Largest diff. peak/hole (e $Å^{-3}$)	1.31/-0.68	1.20/-0.66	1.59/-0.77

Table 2.2 C-H···X intermolecular interactions in complexes **1a-3a**

C-H···X	D-H	H···A	D···A	D-H···A
Complex **1**				
C(8)-H(8a) ···F(4)	0.98	2.54	3.502(4)	167
C(10)-H(10C) ···F(1)	0.98	2.44	3.332(5)	151
C(11)-H(11) ···F(2)	0.95	2.35	3.093(5)	135
C(13)-H(13)…Cl(1)	0.95	2.79	3.622(4)	146
C(14)-H(14) ···F(5)	0.95	2.50	3.235(4)	134
C(21)-H(21) ···F(2)	0.95	2.54	3.313(4)	138
Complex **2**				
C(10)-H(10A) ···F(6)	0.98	2.43	3.341(4)	154
C(11)-H(11) ···F(5)	0.95	2.35	3.122(4)	137
C(13)-H(13) ···Cl(1)	0.95	2.79	3.607(3)	145
C(14)-H(14) ···F(2)	0.95	2.51	3.227(4)	132
C(21)-H(21) ···F(5)	0.95	2.54	3.315(4)	139
Complex **3**				
C(4)-H(4) ···F(6)	0.95	2.35	3.295(6)	172
C(17)-H(17) ···F(5)	0.95	2.48	3.374(6)	157

Table 2.3 Y-X···π intermolecular interactions in complexes **1a-3a**

Y-X···Cg(Pi-Ring)	X···Cg (Bond length (Å))	Y-X···Cg (Bond angles (°))
Complex **1**		
P(1)-F(1) ···Cg(2)	3.111(3)	128.00(13)
Complex **2** (C-H···Cg)		
C(7)-H(7B) ···Cg(3)	2.89	137
Complex **3**		
P(1)-F(5) ···Cg(1)	3.329(4)	129.22(18)
P(1)-F(6) ···Cg(3)	3.755(4)	141.34(17)

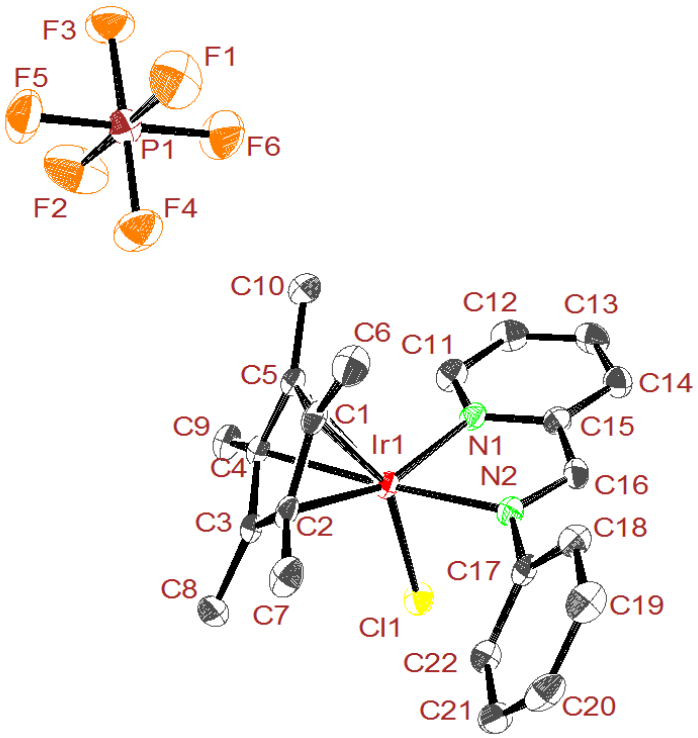

Fig. 2.2 *ORTEP* diagram of the metal complex **1a** with atom numbering scheme. Displacement ellipsoids are drawn at the 50% probability level and hydrogen atoms are omitted for clarity.

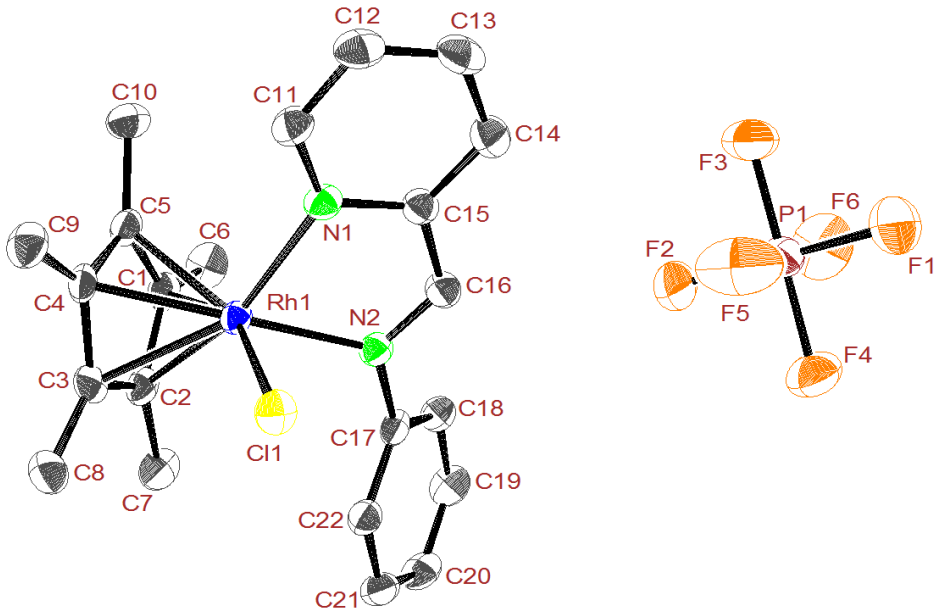

Fig. 2.3 *ORTEP* diagram of the metal complex **2a** with atom numbering scheme. Displacement ellipsoids are drawn at the 50% probability level and hydrogen atoms are omitted for clarity.

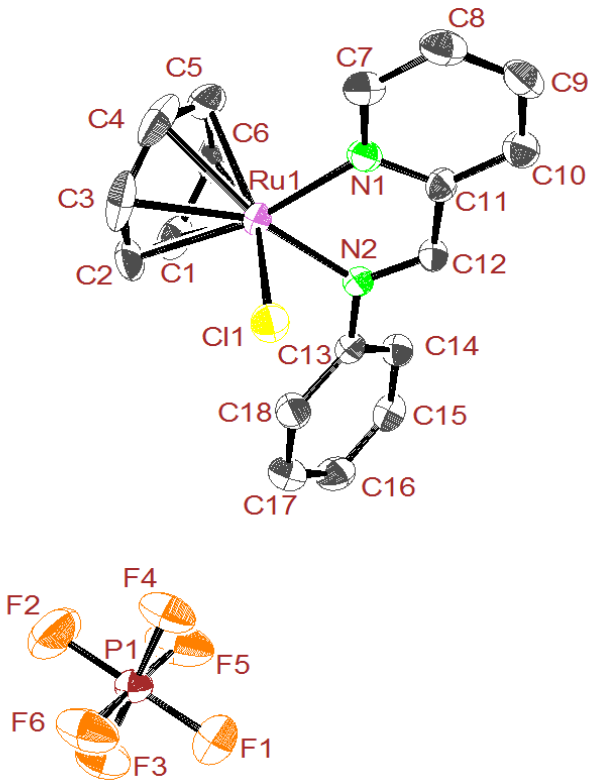

Fig. 2.4 *ORTEP* diagram of the metal complex **3a** with atom numbering scheme. Displacement ellipsoids are drawn at the 50% probability level and hydrogen atoms are omitted for clarity.

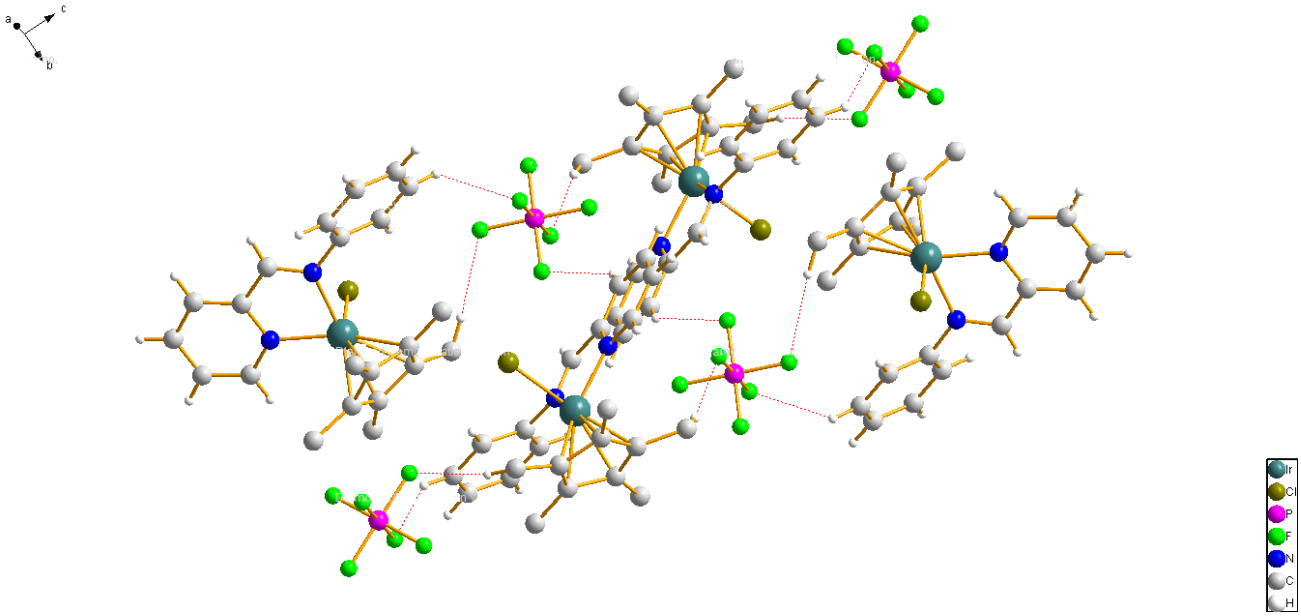

Fig. 2.5 Non-covalent C-H···F (2.585 Å) interactions in the metal complex **1a**.

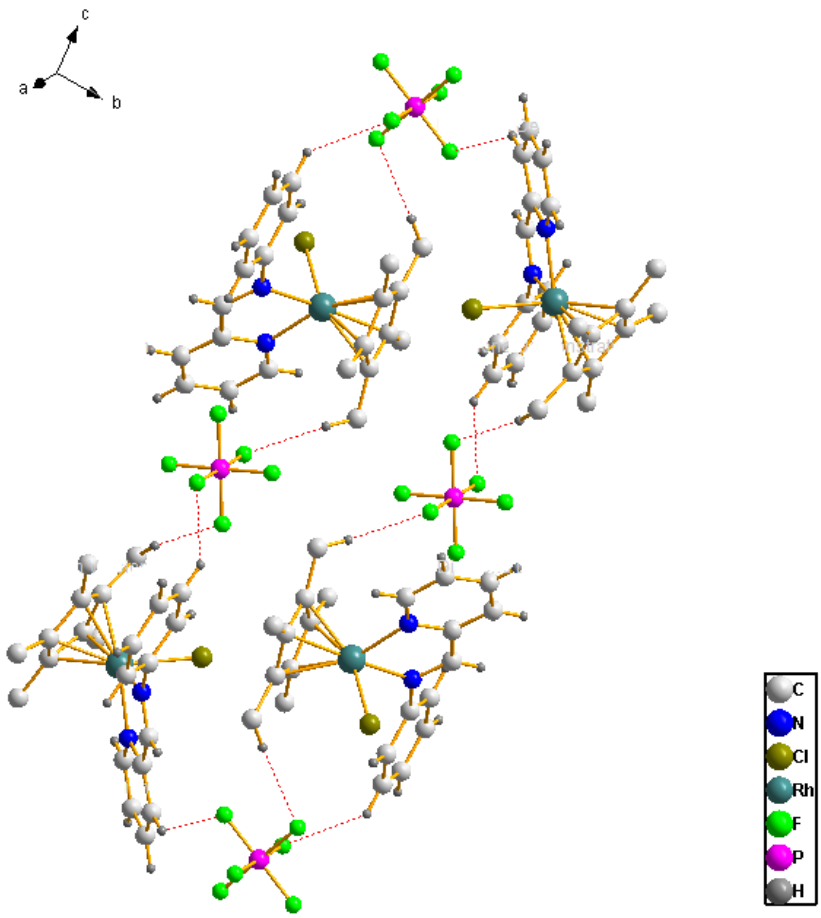

Fig. 2.6 Non-covalent C-H···F and C-H···Cl interactions in the metal complex **2a**.

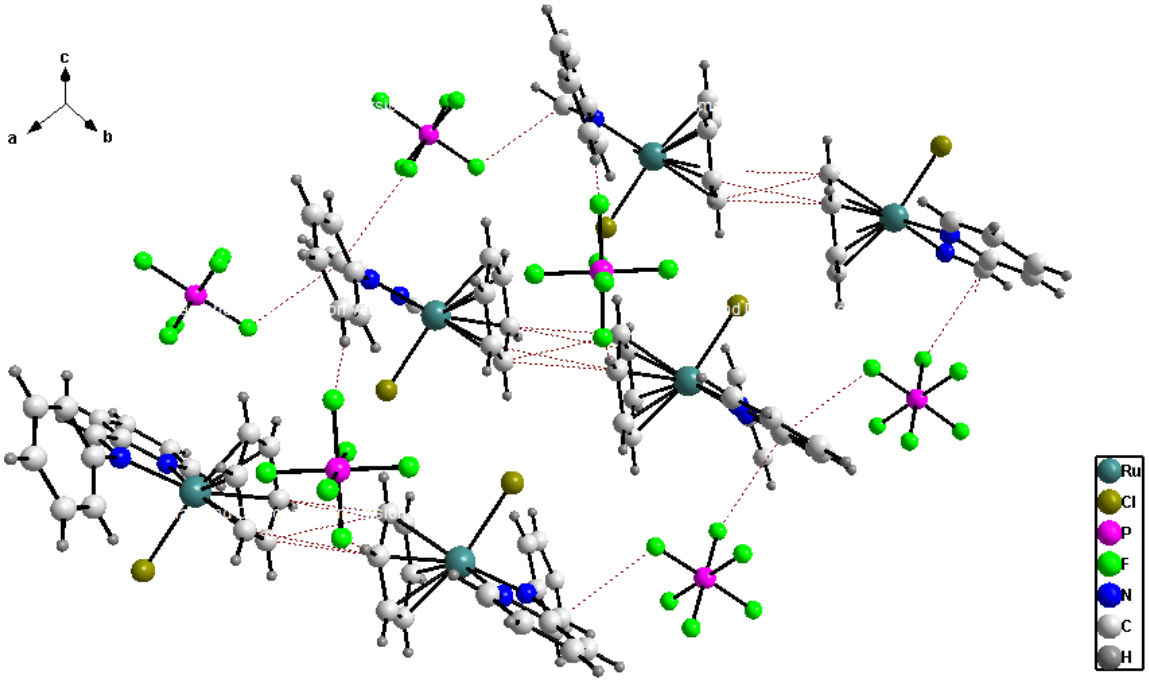

Fig. 2.7 Non-covalent π···π and C-H···F interactions in the metal complex **3a**.

2.3.3 Electronic absorption spectroscopy

The electronic absorption spectra of all the metal complexes were recorded by preparing a 10 µM (v/v DCM) solution. The resulting spectra of the metal complexes are depicted in the wavelength range between 200 nm to 600 nm (Fig. 2.8). The low energy bands of the metal complexes appeared at 382.92 nm (**1a**), 369.77 nm (**2a**), 416.27 nm (**3a**) and the conjugated intra ligand based π-π* and metal ligand charge transfer (MLCT) transitions were observed in the region of 315.23 to 284.92 nm for (**1a**), 324.17 to 274.82 nm for (**2a**) and 313.87 to 261.25 nm for (**3a**) [43].

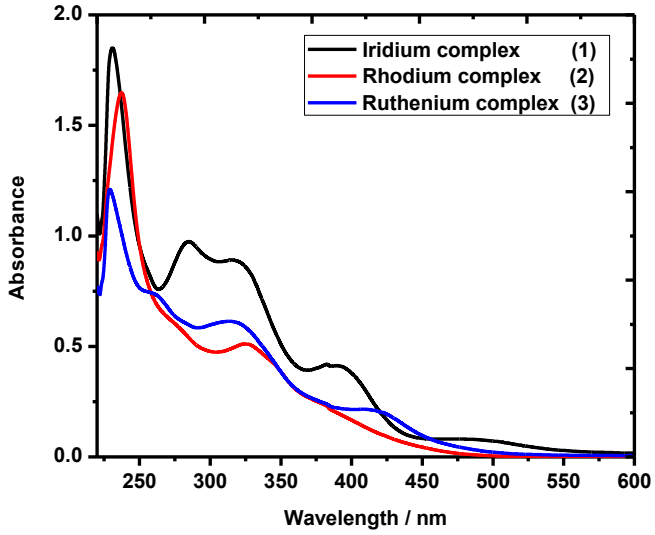

Fig. 2.8 UV-vis spectra of the metal complexes **1a, 2a** and **3a** (Dichloromethane, 10µM, v/v).

2.3.4 TG-DSC studies

TG curves of all complexes are shown in Figs. 2.9-2.10. In the TG curves, no degradation was observed until ~270º C, which indicates the high inherent stability of complexes **1a**-**3a**. The calculated weight loss of the complexes at ~270 ºC was 2.28% (**1a**), 3.12% (**2a**) and 7.85% (**3a**) respectively. The DSC curves of exothermic peaks indicates the complexes undergoes phase transition (might be Chloride cleavge) on melting at 290 ºC (**1a**), 280 °C (**2a**) and 270 °C (**3a**) and the following exothermic peaks indicates possible phase transition during which the complexes are completely decomposed as metal oxides [44b]. The sharp exothermic peaks presented in the DSC curves (Fig. 2.10) further confirms the crystalline nature of the metal complexes [44].

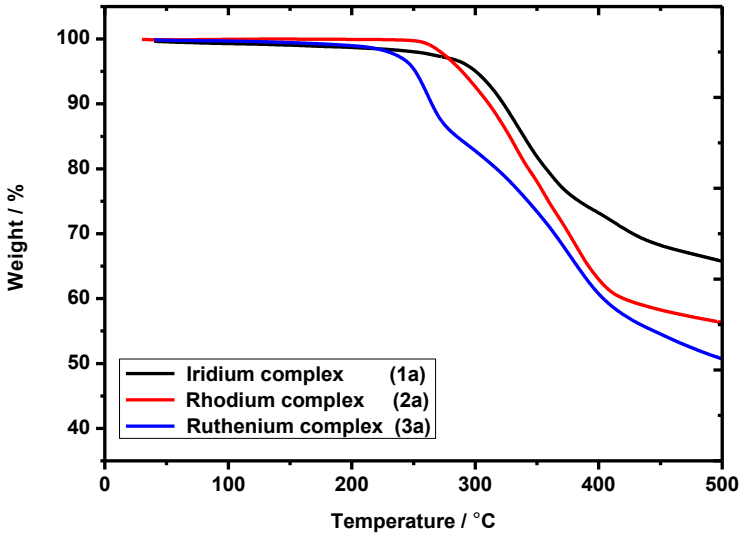

Fig. 2.9 TGA curves of the complexes **1a, 2a** and **3a**. Heating rate 10 °C min^{-1}.

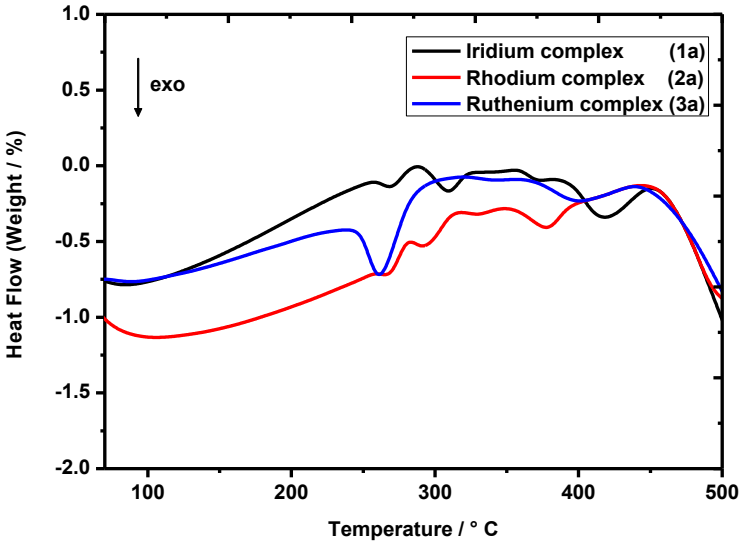

Fig. 2.10 DSC curves of the complexes **1a, 2a** and **3a**. Heating rate 10 °C min^{-1}.

2.3.5 Catalytic activity studies

2.3.5.1 Oxidation of primary alcohols

The oxidation of benzyl alcohol under reflux conditions was carried out with various bases and solvents using the three complexes of iridium (**1a**), rhodium (**2a**) and ruthenium (**3a**) (Table 2.4). No

benzyl alcohol conversion was achieved in the absence of catalysts **1a**-**3a**. In the presence of catalysts **1a**-**3a** (1 mol% or 2 mol%) and bases (5 mol%) in toluene under reflux, benzyl alcohol to benzaldehyde conversion reached up to 90% (Table 2.4). In the presence of the catalyst **1a** (2 mol%) and the bases (5 mol%) Na_2CO_3, $NaHCO_3$, K_2CO_3 and Cs_2CO_3, the yield of benzaldehyde reached 44%, 33%, 63% and 89% respectively (Entries 3-6). In the presence of catalysts **2a** (2 mol%) and **3a** (2 mol%) with Na_2CO_3 as the base in toluene, the benzaldehyde yield obtained was 49% and 44% respectively (Entries 9 and 15). For catalyst **3a** with $NaHCO_3$, the yield further increased to 58% (Entry 16). When catalysts **2a** (2 mol%) and **3a** (2 mol%) were refluxed with K_2CO_3 as the base in toluene, a 60% yield of the benzaldehyde was achieved in both systems (Entries 11 and 17). However, overall catalyst **1a** with Cs_2CO_3 as base under reflux in toluene gave the best yield to benzaldehyde (89%) (Entry 6).

When the reaction was carried out with different solvents, the benzaldehyde yield varied. In the presence of K_2CO_3 as base and *p*-xylene as a solvent, the maximum benzaldehyde yields of 29% and 56% were achieved over catalysts **1a** and **2a** respectively (Entries 19 and 22). In the presence of all three catalysts, the use of 1,4 dioxane and DMSO as solvents gave a lower yield of benzaldehyde. The yield of benzaldehyde obtained from all the reactions using different solvents and K_2CO_3 as base are summarized in the Table 2.4 (Entries 19-27). However, in the case of catalyst **3a**, the yield of benzaldehyde was as high as 76% (Entry 25), likely due to the higher solubility of catalyst **3a** in *p*-xylene than catalysts **1a** and **2a**.

Table 2.4 Screening and optimization for the oxidation of benzyl alcohol[a]

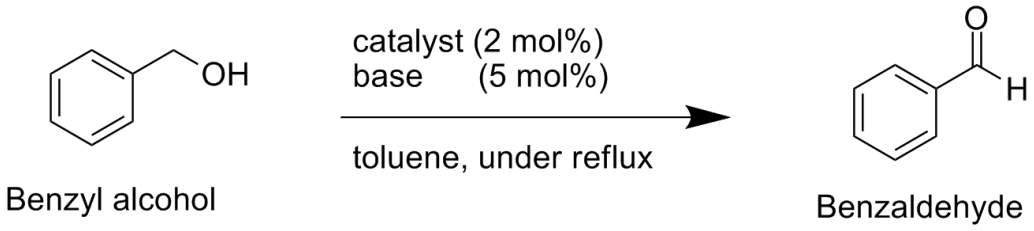

Entry	Catalyst	Base	Conversion (%)[c]	Yield (%)[c]	TON	TOF
1	1a	None	24[b]	24	24	1
2	1a	None	39	39	20	1
3	1a	Na_2CO_3	44	44	22	1
4	1a	$NaHCO_3$	34	33	17	1
5	1a	K_2CO_3	64	63	32	1
6	1a	Cs_2CO_3	90	89	45	2

7	2a	None	36[b]	36	36	1
8	2a	None	38	38	19	1
9	2a	Na_2CO_3	52	49	26	1
10	2a	$NaHCO_3$	26	25	13	1
11	2a	K_2CO_3	63	60	32	1
12	2a	Cs_2CO_3	62	60	31	1
13	3a	None	16[b]	16	16	<1
14	3a	None	26	26	13	1
15	3a	Na_2CO_3	48	44	24	1
16	3a	$NaHCO_3$	60	58	30	1
17	3a	K_2CO_3	63	60	32	1
18	3a	Cs_2CO_3	46	45	23	1
19	1a	K_2CO_3	31[d]	29	16	1
20	1a	K_2CO_3	9[e]	8	5	<1
21	1a	K_2CO_3	25[f]	23	13	1
22	2a	K_2CO_3	58[d]	56	29	1
23	2a	K_2CO_3	24[e]	20	12	1
24	2a	K_2CO_3	22[f]	21	11	<1
25	3a	K_2CO_3	78[d]	76	39	2
26	3a	K_2CO_3	27[e]	24	14	1
27	3a	K_2CO_3	40[f]	37	20	1

[a] Benzyl alcohol (1 mmol) and catalyst (2 mol%) in toluene (20 mmol) under reflux 48 hrs.

[b] Benzyl alcohol (1 mmol) and catalyst (1 mol%) in toluene (20 mmol) under reflux 48 hrs.

[c] Determined by GC (average of two runs). [d] *p*-xylene (20 mmol). [e] 1,4 dioxane (20 mmol).

[f] DMSO (20 mmol). Turnover number (TON) = [(mol of product)/(mol of catalyst)].

Turnover frequency (TOF) = [TON/h].

2.3.5.2 Effect of substituents on the oxidation of benzyl alcohol over the catalysts 1a and 3a

Catalyst **1a** showed good activity for oxidizing substituted benzyl alcohols in the presence of Cs_2CO_3 as base and toluene as solvent (Table 2.5). It is evident that substrates with groups present in the *para* position (Entries 2, 5, 7 and 8) were oxidized faster than those with steric *ortho*-substituted groups present in benzyl alcohol, in the presence of base [24, 44] (Entries 3 and 6). A bulky *ortho* substitution could cause a decrease in the benzyl alcohol oxidation rate [46] (Entries 2 and 5). On the other hand, bulky 3,4- and 2,5-OCH_3 substituted benzyl alcohol also showed moderate conversion with catalyst **1a** (Entries 9 - 11). In contrast, *para* dimethylaminobenzyl alcohol showed lower conversion due to the high electron donating ability of dimethylamino group on the aromatic ring (Entry 12). The electronic nature of the aromatic ring present in the substrate plays a big role in oxidation reactions [15]. The efficient catalytic activity of the iridium complex (**1a**) could be explained by the electronic effect of the ligand on the iridium metal. The N,N' ligand gives a greater donor strength than in the rhodium and ruthenium complexes [47]. The theoretical natural atomic populations study for the iridium complex coincides well with this statement (Section 3.6). Catalyst **1a** showed 100% and 97% (Entries 2 and 8) conversion of electron rich and poor benzyl alcohols.

The mesomeric effect is a permanent effect and operates in compounds containing at least one double bond and another double bond or a lone pair separated by a single bond. The mesomeric effect is a result of *p*-orbital overlap (resonance) and has absolutely no effect on this inductive effect, as the inductive effect purely deals with the electronegativity of the atoms. Hence, mesomeric effect might be influencing a phenyl ring rather than a reacting alcohol group. The strength of the inductive effect is also dependant on the distance between the substituent group and the main group that react, the greater the distance, the weaker the effect. Hence, para substituted alcohols have no effect by inductive effects (Entries 2, 5, 7 and 8). It may be possible to ortho substitute alcohols due to a short distance between substituent and the reacting alcohol group. The lower conversion of ortho substituted alcohols might be due to steric, inductive and mesomeric effects (Entries 3 and 6).

Table 2.5 Catalytic oxidation of benzyl alcohol derivatives mediated by catalyst **1a**[a]

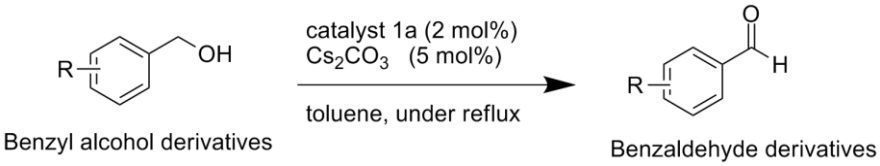

Benzyl alcohol derivatives — Benzaldehyde derivatives

Entry	Benzyl alcohol derivaties	Conversion (%)[c]	Yield (%)[c]	TON	TOF
1	R – H	90[b]	89	45	1
2	R –*4*-NO_2	100	98	50	2
3	R –*2*-NO_2	83[b]	80	42	1
4	R –*2*-OH	100	95	50	2
5	R –*4*-Cl	91	89	46	2
6	R –*2*-Cl	80[b]	78	40	1
7	R –*4*-CH_3	90	89	45	2
8	R –*4*-OCH_3	97	96	49	2
9	R –*3,4* –OCH_3	72[b]	70	36	1
10	R –*2,5* –OCH_3	48[b]	46	24	1
11	R –*4*-OH *3*–OCH_3	64	62	32	1
12	R –*4*–$N(CH_3)_2$	33[b]	30	17	<1

[a] Substrate (1 mmol) in toluene (20 mmol) under reflux 24 hrs. [b] Substrate (1 mmol) in toluene (20 mmol) under reflux 48 hrs. [c] Determined by GC (average of two runs). Turnover number (TON) = [(mol of product)/(mol of catalyst)]. Turnover frequency (TOF) = [TON/h].

Catalyst **3a** showed up to 96% (Entry 4, Table 2.6) conversion in the oxidation of primary alcohols to their corresponding aldehydes using K_2CO_3 as base with *p*-xylene as the solvent (Table 2.6). In this catalytic system, the electron rich *para* substituted benzyl alcohols (Entries 7, 8 and 11) oxidized better than electron poor *para* substituted benzyl alcohols (Entries 2 and 5). The bulky groups present in the *ortho* position of benzyl alcohol caused lower conversion of these substituted benzyl alcohols (Entries 3, 6 and 10). A plausible coordination site for the substrate is the electronically unsaturated ruthenium center, which is generated after liberation of the labile chloride atom. The base K_2CO_3 is expected to promote the formation of the metal-alkoxide species, which could then undergo *β*-hydride elimination to form a ruthenium-hydride complex [48, 49]. A faster oxidation rate of the *ortho*-hydroxy benzyl alcohol

to the corresponding aldehyde in both catalytic systems **1a** and **3a** was observed (Entry 4, Table 2.5 and Entry 4, Table 2.6).

Table 2.6 Catalytic oxidation of benzyl alcohol derivatives mediated by catalyst **3a**[a]

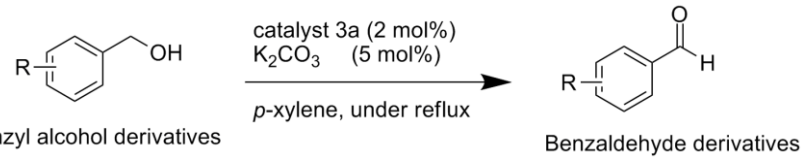

Benzyl alcohol derivatives — Benzaldehyde derivatives

Entry	Benzyl alcohol derivatives	Conversion (%)[c]	Yield (%)[c]	TON	TOF
1	R –H	78[b]	76	39	1
2	R –*4*-NO_2	45[b]	44	23	<1
3	R –*2*-NO_2	40[b]	37	20	<1
4	R –*2*-OH	96	92	48	2
5	R –*4*-Cl	65[b]	63	33	1
6	R –*2*-Cl	50[b]	47	25	1
7	R –*4*-CH_3	77	76	39	2
8	R –*4*-OCH_3	85	84	43	2
9	R –*3,4*–OCH_3	68[b]	64	34	1
10	R –*2,5*-OCH_3	51[b]	48	26	1
11	R –*4*-OH *3*–OCH_3	91	90	46	2
12	R –*4*–$N(CH_3)_2$	no reaction[b]	-	-	-

[a] Substrate (1 mmol) in *p*-xylene (20 mmol) under reflux for 24 hrs. [b] Substrate (1 mmol) in *p*-xylene (20 mmol) under reflux for 48 hrs. [c] Determined by GC (average of two runs). Turnover number (TON) = [(mol of product)/(mol of catalyst)]. Turnover frequency (TOF) = [TON/h].

2.3.5.3 Proposed catalytic reaction mechanism for oxidation of primary alcohols

A proposed reaction mechanism (supported by theoretical calculations, Section 3.6) for the oxidation of primary alcohols by catalysts **1a-3a** is illustrated in Scheme 2.1. The first step of this reaction cycle is the generation of the metal benzyloxo species (A) from the base. In the second step, the *β*-hydride elimination occurs to form the dehydrogenated product of benzaldehyde and a metal hydride (B) complex. In step 3, the metal hydride (B) intermediate promotes a protonolysis to form the metal complex (C) intermediate, followed by dihydrogen release from the metal complex (C) intermediate to form the $16e^-$ species (D) in step 4. The key steps of this catalytic cycle is the generation of the metal hydride

intermediate in step 2. A similar kind of iridium hydride intermediate has been characterized and reported by Fujita *et al.* [46].

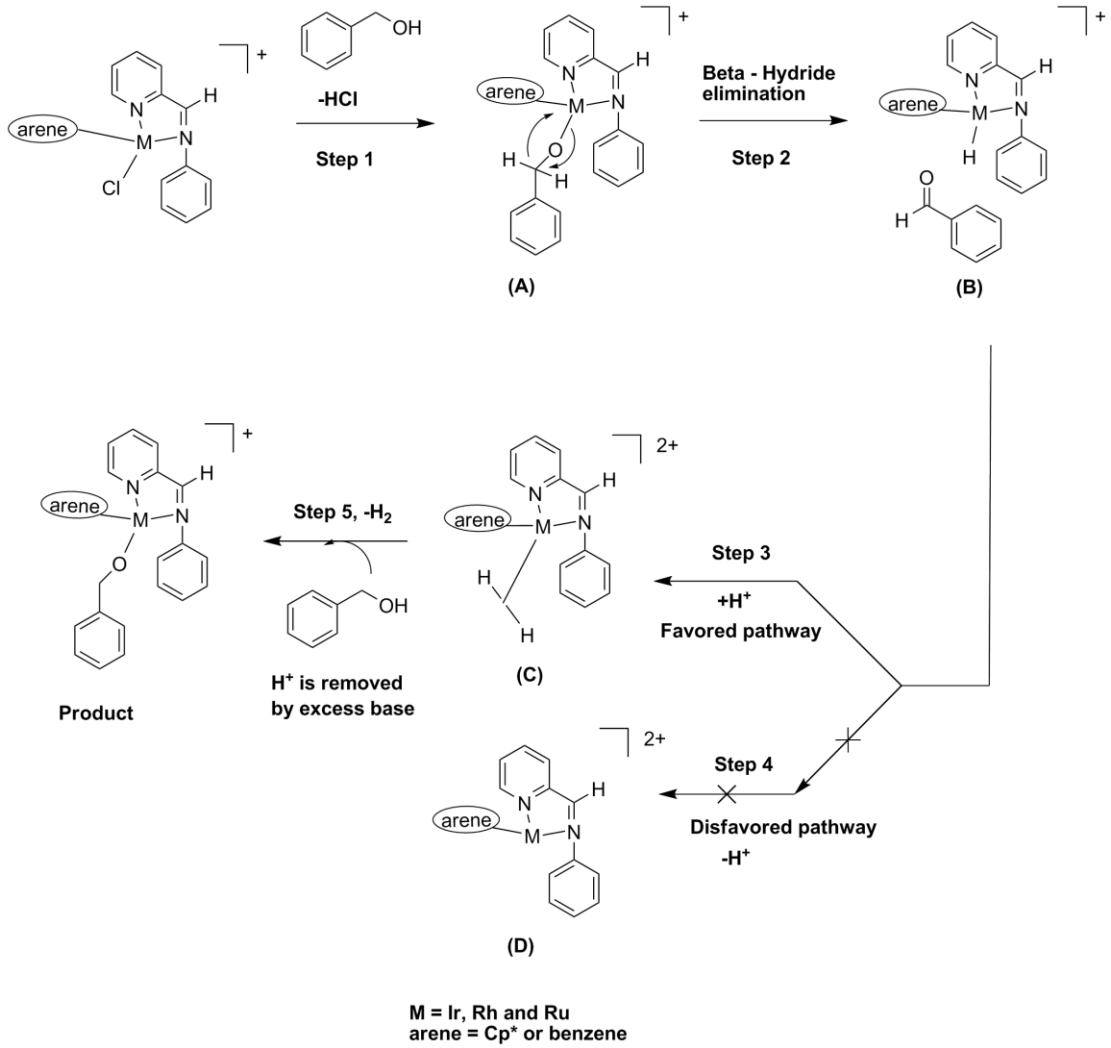

Scheme 2.1 Proposed reaction mechanism of the oxidation of primary alcohols by catalysts **1a-3a**.

2.3.6 Density Functional Theory (DFT) Calculations

DFT calculations were carried out to understand structural properties, such as type of molecular energy levels, bond lengths, bond angles and the binding nature of the metal complexes. A Gibbs free energy calculation on the rhodium catalytic cycle was carried out to support the proposed mechanism given in Scheme 2.1. The energy difference between the HOMO (highest occupied molecular orbitals) and the LUMO (lowest unoccupied molecular orbitals) orbitals is called the energy gap, which is important to understand the stability of the structures of the metal complexes. The analysis of the orbitals indicates that the electron absorption corresponds to the transition state from the ground state to the first excited state, which mainly describes the one electron excitation from the HOMO to the LUMO, which is

correlated to the energy gap and the chemical reactivity. A larger energy gap between HOMO and LUMO indicates good stability of the structure and lower reactivity, and a smaller energy gap difference implies higher reactivity of the complexes [50] (Figs. 2.11 and 2.13).

The HOMO is highly concentrated over the metal centers, benzene or the Cp* ring, but with a small contribution from the Cl atom. Consequently, the LUMO is localized over the N1 and N2 atoms. The HOMO is constituted of a π-orbital in the Cp* ring or benzene. The LUMO is dominated by the π* orbital of the pyridine ring. This suggests that the higher value of the HOMO of a d orbital of the metal has a tendency to donate electrons to the p orbital of the N1, N2 acceptor atoms. Calculated bond lengths and bond angles are given in the Table 2.7. The experimentally obtained results of bond distances and bond angles are close to the theoretical values, except for the angle C(5)-Ir(1)-Cl(1). The lone pair electrons of the Cl coordinated with the iridium center are placed closer to the N1 and N2 atoms, as compared to the rhodium (**2a**) and ruthenium (**3a**) complexes, which causes repulsion between Cl and the nitrogen atoms. Thus, the DFT method could not predict the C(5)-Ir(1)-Cl(1) bond angle accurately, due to the presence of the lone pair electrons of the Cl [52].

The calculated energy gaps from HOMO-LUMO for the iridium complex (**1a**), rhodium complex (**2a**) and ruthenium complex (**3a**) were 120.59 kcal/mol, 130.67 kcal/mol and 124.49 kcal/mol respectively. The higher energy gap of the rhodium complex (**2a**) indicates that it is more stable and less reactive when compared to the iridium and ruthenium complexes. Lowest vibrational frequency calculations have been carried out to predict the minimum energy structure with the lowest vibrational frequency for the Ir(III) complex (17.731 cm^{-1}), the Rh(III) complex (30.332 cm^{-1}) and the Ru(II) complex (3.797 cm^{-1}) and this is shown in the SI S2.

NPA analysis describes the charge transfer from chloride or nitrogen atoms to the metal (Ir(III), Rh(III) and Ru(II)) ions, which plays a pivotal role in determining metal complex properties (Fig. 2.12). The atomic charges of each atom in the complexes collected from NPA are presented in the SI S3, the metal ions gain charges of 2.79e (Ir(III)), 2.73e (Rh(III)) and 1.94e (Ru(II)) in the metal complexes. The positive charge of the metal ions decreases significantly in all the complexes and especially the iridium metal ion strongly co-ordinated with neighboring atoms. The bidentate ligand N,N' donor electron strength on the iridium (N1 = -0.441 & N2 = -0.405) is higher than on rhodium and ruthenium and this would account for the iridium complex being more reactive than the other complexes. On the complexes **1a**-**3a**, the chloride group transfers higher charges of 0.66e to the Ru(II) metal ion when compared with lesser charge transfer from chloride (0.59e) to the Rh(III) and 0.61e to the Ir(III) metal ion (S5, Table

2.3). The electron densities of the Cl group attached to the iridium (0.212) and ruthenium (0.057) are less than that of the Cl group attached to the rhodium (0.273). These electron density values confirm that the Rh-Cl (**2**) bond is stronger and this would account for it being a less reactive complex compared to the latter two complexes [51].

The proposed reaction mechanism for the complexes is given in Scheme 2.1. The iridium benzyloxo (**A**) complex has a higher energy gap (116.59 kcal/mol) than the iridium hydride (**B**) complex (106.83 kcal/mol), which indicates that A is more stable (less reactive) than complex **B**. A similar iridium hydride (**B**) complex has been studied and reported as being a highly active species by Fujita *et al.* [46] and its frontier orbital diagram is shown in Fig. 2.13.

Gibbs free energy calculations of the rhodium catalytic cycle, thus support the proposed mechanism (Scheme 2.1). The result of the Gibbs free-energy (ΔG) DFT calculation for the reaction mechanism of catalyst **2a** is shown in Fig. 2.14. Gibbs free-energy (ΔG) profile calculations rationalize the stability and reactivity of various transformations of catalyst **2a** as per the proposed mechanism. In the reaction mechanism, the Rh-H step was processed via β-hydride elimination with a high activation free energy barrier of 21.41 kcal/mol. The calculated activation free energy barrier of the Rh-H intermediate (**B**) was lower (-8.50 kcal/mol) than the corresponding Rh-benzyloxo (**A**) species, which correlates to the rate-determining step of the proposed reaction cycle. The Rh-H intermediate is the thermodynamically more favored stable state in the proposed reaction mechanism. The calculated Gibbs free energy barrier for the Rh-H species (-8.50 kcal/mol) was in good agreement with a reported value for a similar species [52]. The calculated activation free energy barrier of the $16e^-$ Rh complex **D** was higher (31.85 kcal/mol) than the respective Rh complex **C** (20.34 kcal/mol), which indicates that the proposed reaction mechanism is more favorable through the **C** transition state than the **D** $16e^-$ Rh complex **D**. The calculated Gibbs free energy values of the reaction intermediates fall in the following order: **A** > **B** (Stable state) < **C** < **D**, which confirms that the calculated low activation free energy transition intermediates (Rh-H species) can facilitate the oxidation of aromatic benzyl alcohols to their respective aldehydes. The Gibbs free-energy profile (ΔG) and the structures of the optimized rhodium catalytic cycle transition states are given in the SI S14.

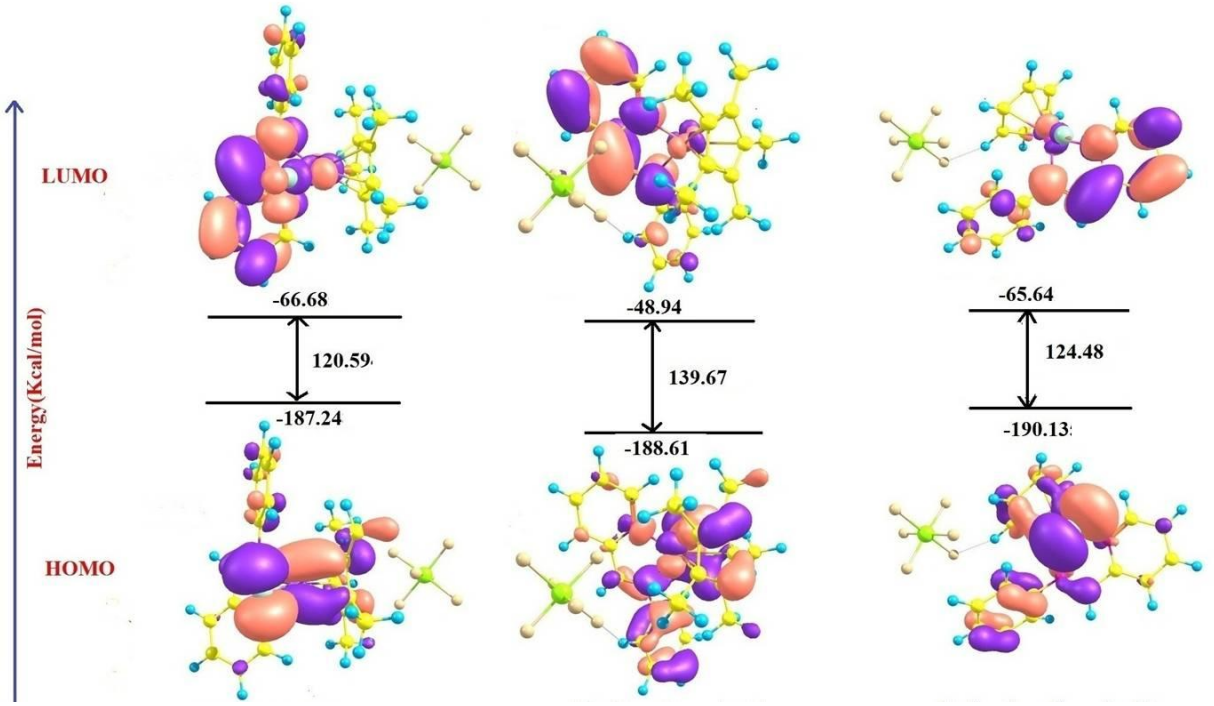

Fig. 2.11 Molecular orbital diagrams of the metal complexes **1a**, **2a** and **3a**.

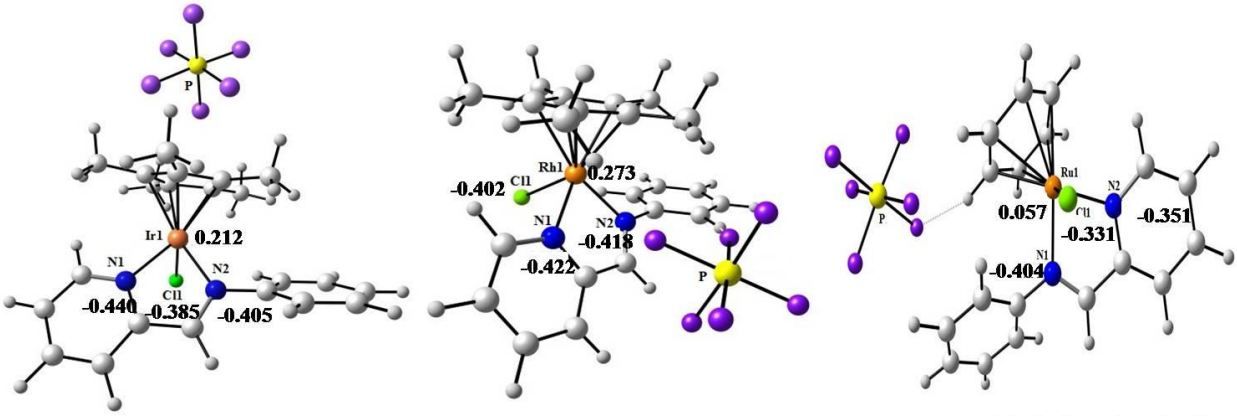

Fig. 2.12 Natural atomic population charges of complexes **1a**, **2a** and **3a**.

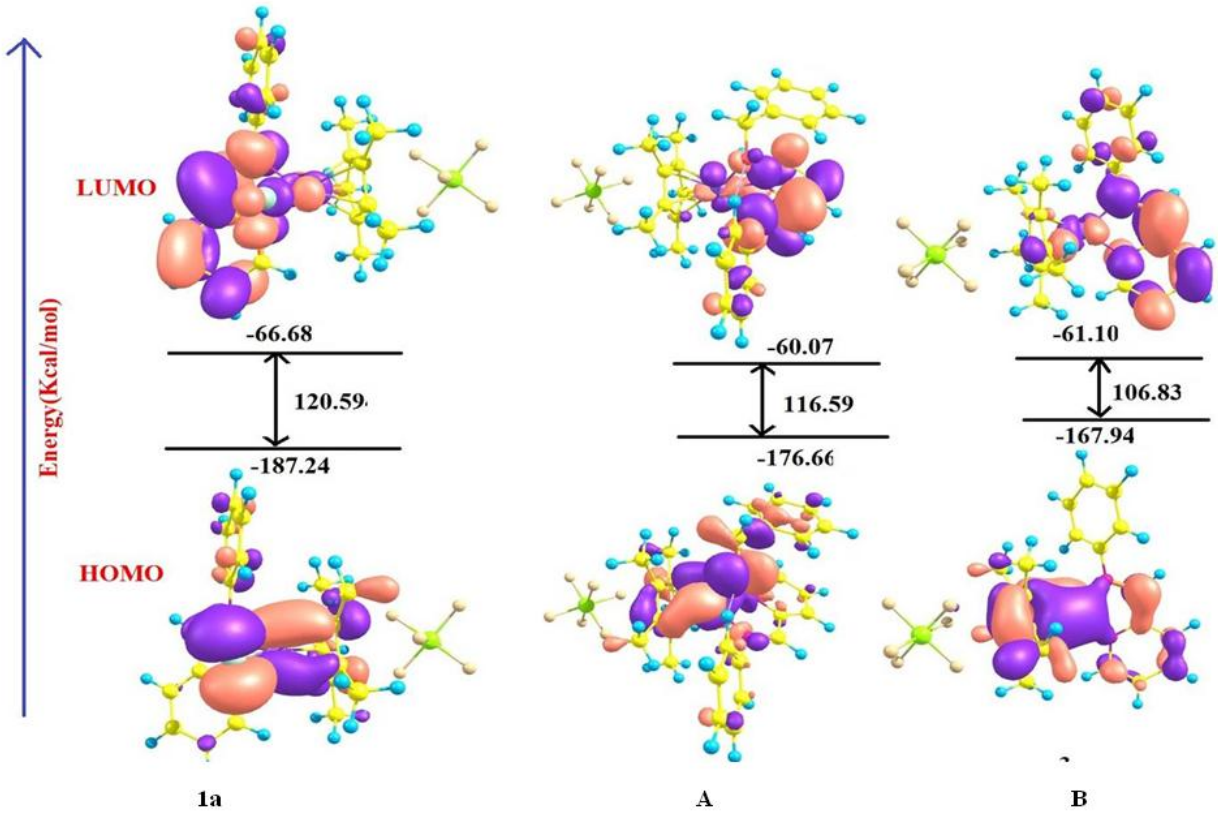

Fig. 2.13 Molecular orbital diagrams of catalyst **1a** reaction intermediates.

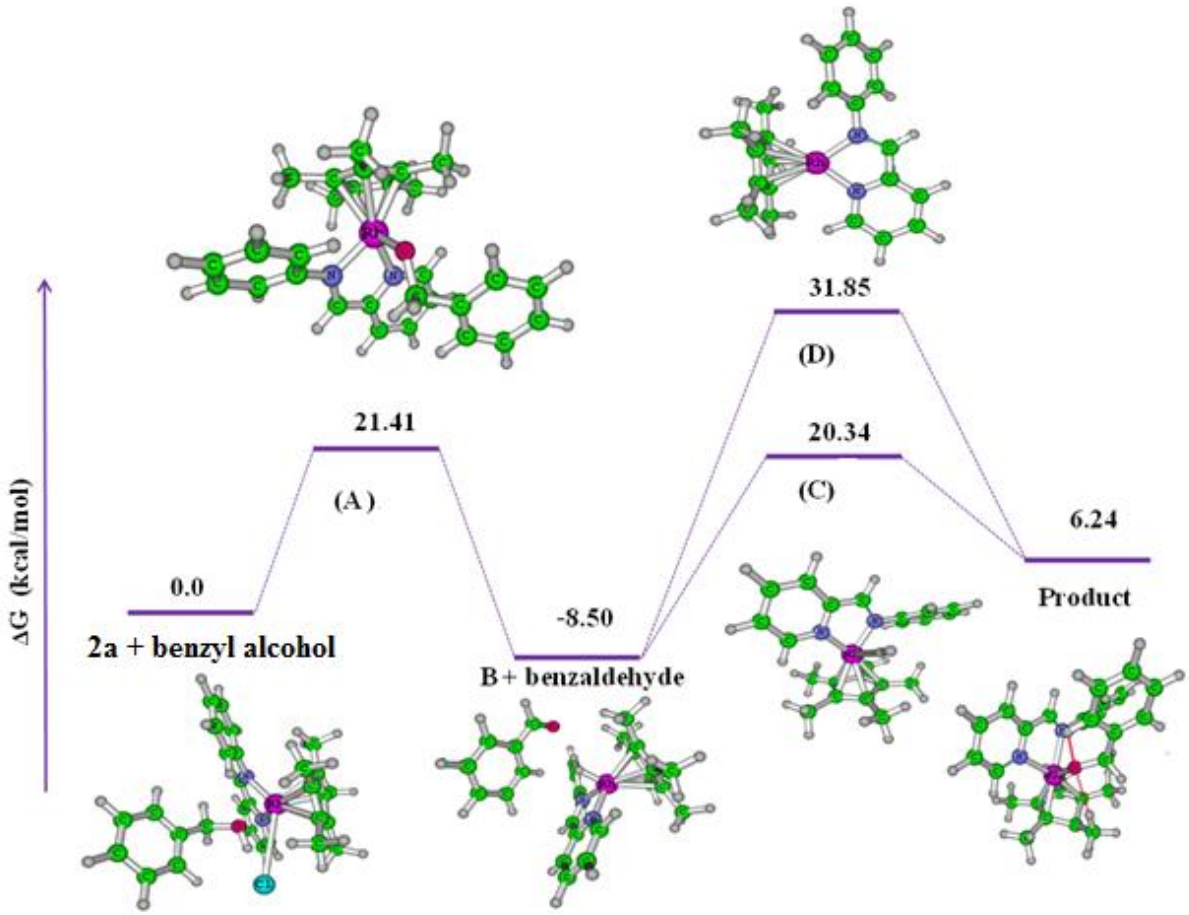

Fig. 2.14 Gibbs free energy profile of the Rh catalyst (**2a**) catalyzed reaction mechanism shown in Scheme 2.1.

Table 2.7 Selected bond lengths (Å), bond angles (°) and calculated DFT data for metal complexes **1a**, **2a** and **3a**

Complex **1a**	Crystal data	DFT	Complex **2a**	Crystal data	DFT	Complex **3a**	Crystal data	DFT
Distances (Å)			Distances (Å)			Distances (Å)		
Ir(1) – C1 (Cp*)	2.174(3)	2.229	Rh(1) – C1 (Cp*)	2.157(3)	2.267	Ru(1) – C1 (arene)	2.192(4)	2.42
Ir(1) – C2 (Cp*)	2.204(3)	2.265	Rh(1) – C2 (Cp*)	2.192(3)	2.286	Ru(1) – C2 (arene)	2.192(4)	2.405
Ir(1) – C3 (Cp*)	2.205(3)	2.233	Rh(1) – C3 (Cp*)	2.192(3)	2.271	Ru(1) – C3 (arene)	2.185(4)	2.387
Ir(1) – C4 (Cp*)	2.153(3)	2.256	Rh(1) – C4 (Cp*)	2.136(3)	2.224	Ru(1) – C4 (arene)	2.192(4)	2.393
Ir(1) – C5 (Cp*)	2.171(3)	2.268	Rh(1) – C5 (Cp*)	2.157(3)	2.275	Ru(1) – C5 (arene)	2.171(4)	2.374
Ir(1) – Centroid (Cp*)	1.803	1.858	Rh(1) – Centroid (Cp*)	1.789	1.970	Ru(1) – C6 (arene)	2.192(4)	2.388
Ir(1) – Cl(1)	2.400(10)	2.468	Rh(1) – Cl(1)	2.393(8)	2.439	Ru(1) – Centroid (arene)	1.681	1.766
Ir(1) – N(1)	2.096(3)	2.077	Rh(1) – N(1)	2.106(2)	2.064	Ru(1) – Cl(1)	2.393(10)	2.426
Ir(1) – N(2)	2.106(2)	2.059	Rh(1) – N(2)	2.119(2)	2.085	Ru(1) – N(1)	2.093(3)	2.063
						Ru(1) – N(2)	2.084(3)	2.049
Angles (°)			Angles (°)			Angles (°)		
N(1)-Ir(1)-Cl(1)	84.76(7)	84.251	N(1)-Rh(1)-Cl(1)	85.88(7)	86.533	N(1)-Ru(1)-Cl(1)	86.34(9)	83.31
N(2)-Ir(1)-Cl(1)	86.67(8)	86.710	N(2)-Rh(1)-Cl(1)	87.74(6)	91.300	N(2)-Ru(1)-Cl(1)	86.12(9)	86.807
N(1)-Ir(1)-N(2)	76.21(10)	77.117	N(1)-Rh(1)-N(2)	76.58(9)	77.932	N(1)-Ru(1)-N(2)	76.99(12)	78.165
C(1)-Ir(1)-Cl(1)	155.43(9)	156.906	C(1)-Rh(1)-Cl(1)	155.14(8)	153.452	C(1)-Ru(1)-Cl(1)	123.09(14)	120.139
C(2)-Ir(1)-Cl(1)	116.77(9)	122.115	C(2)-Rh(1)-Cl(1)	116.74(8)	117.742	C(2)-Ru(1)-Cl(1)	94.29(13)	93.505
C(3)-Ir(1)-Cl(1)	93.29(8)	93.316	C(3)-Rh(1)-Cl(1)	92.76(8)	91.904	C(3)-Ru(1)-Cl(1)	89.23(14)	90.532
C(4)-Ir(1)-Cl(1)	103.85(9)	97.505	C(4)-Rh(1)-Cl(1)	103.32(8)	100.223	C(4)-Ru(1)-Cl(1)	112.12(16)	113.687
C(5)-Ir(1)-Cl(1)	141.65(8)	131.308	C(5)-Rh(1)-Cl(1)	141.06(8)	136.014	C(5)-Ru(1)-Cl(1)	149.46(16)	148.727
Centroid (Cp*)-Ir(1)-Cl(1)	126.13	122.930	Centroid (Cp*)-Rh(1)-Cl(1)	125.68	124.258	C(6)-Ru(1)-Cl(1)	160.77(13)	154.42
						Centroid (arene)-Ru(1)-Cl(1)	127.19	127.429

2.4 Conclusions

In summary, the catalytic activity of half sandwich Ir(III), Rh(III) and Ru(II) complexes in the oxidation of primary aromatic alcohols to their respective aldehydes was demonstrated. It is clear that the Ir(III) complex in the presence of Cs_2CO_3 and the Ru(II) complex in the presence of K_2CO_3 improved the oxidation of benzyl alcohol significantly. In the proposed reaction mechanism, the iridium-hydride intermediate was more reactive than iridium-benzyloxo species, which is supported by HOMO and LUMO energy gap differences. DFT calculation of selected bond lengths and angles essentially matched the obtained crystal data. Furthermore, the calculated electron density of the metal complexes and the calculated energy differences between the HOMO and LUMO coincide with the observed reactivity of the Ir(III) and Ru(II) complexes. The HOMO and LUMO energy gap difference of complex **1a** is lower than those of **2a** and **3a**, which indicates the following order of reactivity: **1a** > **3a** > **2a**. Gibbs free energy calculations for Rh(III) catalytic cycle further confirmed the proposed reaction mechanism processed via a Rh-H intermediate.

Acknowledgements

Authors would like to thank the NRF, THRIP (Grant no. TP 1208035643) and the University of KwaZulu - Natal, Durban, South Africa for financial support and facilities.

Appendix A. Supplementary Information

The vibrational free energy, HOMO-LUMO calculations and NBO analysis for complexes **1a-3a**, iridium reaction intermediate and rhodium catalytic cycle Gibbs free energy calculations are also shown in the SI. CCDC-1020802 (**1a**), CCDC-1020803 (**2a**), and CCDC-1020804 (**3a**) contain the supplementary crystallographic data for this paper. These data can be obtained free of charge from the Cambridge crystallographic data center via *www.ccdc.cam.ac.uk/data_request/cif.*

References

[1] (a) R.A. Sheldon, J.K. Koch, Metal-Catalyzed Oxidations of Organic Compounds, first ed., Academic Press, New York, 1981.

(b) M. Vazylyev, D. Sloboda Rozner, A. Haimov, G. Maayan, R. Neumann. Top. Catal. 34 (2005) 93-99.

[2] H. Qin, N. Yamagiwa, S. Matsunaga, M. Shibasaki, Angew. Chem. Int. Ed. 46 (2007) 409-413.

[3] Y. Tao, B. Wang, B. Wang, L. Qu and Qu, Org. Lett. 12 (2010) 2726-2729.

[4] T. Ohshima, Y. Miyamoto, J. Ipposhi, Y. Nakahara, M. Utsunomiya, K. Mashima, J. Am. Chem. Soc. 131 (2009) 14317-14328.

[5] G.E. Dobereiner, R.H. Crabtree, Chem. Rev. 110 (2010) 681-703.

[6] A.J.A. Watson, J.M.J. Williams, Science 329 (2010) 635-636.

[7] G. Tojo, M. Fern-andez, Oxidation of Alcohols to Aldehydes and Ketones, A Guide to Current Common Practice, Springer Press, New York, 2006.

[8] H. B. Friedrich, N. Singh, Tetrahedron Lett. 41 (2000) 3971-3974.

[9] T. Seki, A. Baiker, Chem. Rev. 109 (2009) 2409-2454.

[10] A.S.K. Hashmi, Chem. Rev. 107 (2007) 3180-3211.

[11] T. Naota, H. Takaya, S.I. Murahashi, Chem. Rev. 98 (1998) 2599-2660.

[12] S.S. Stahl, Angew. Chem, Int. Ed.,43 (2004) 3400-3420.

[13] E.T.T. Kumoulainen, A.M.P. Koskinen, Chem. Eur. J. 15 (2009) 10901-10911.

[14] G. Tojo, M. Fern-andez, Oxidation of Primary Alcohols to Carboxylic Acids. Basic Reactions in Organic Synthesis, first ed., Springer, New York, 2010.

[15] L. Liu, M. Yu, B.B. Wayland, X. Fu, Chem. Commun. 46 (2010) 6353-6355.

[16] (a) J.W. Ladbury, C.F. Cullis, Chem. Rev. 58 (1958) 403-438.
(b) R.J.K. Taylor, M. Reid, J. Foot, S.A. Raw, Acc. Chem. Res. 38 (2005) 851-869.

[17] (a) A.J. Mancuso, S.L. Huang, D. Swern, J. Org. Chem. 43 (1978) 2480-2482.
(b) T.T. Tidwell, Synthesis (1990) 857-870.

[18] (a) J.M. Hoover, S.S. Stahl, J. Am. Chem. Soc. 133 (2011) 16901-16910.
(b) M. Uyanik, K. Ishihara, Chem. Commun. (2009) 2086-2099.

[19] O.L.E. Mark, P.R. Giles, M. Tsukazaki, S.M. Brown, C. Urch, Science 274 (1996) 2044-2046.

[20] (a) H.B. Friedrich, V. Gokul, J. Mol. Catal, A: Chem. 271 (2007) 277-283.
(b) R. Noyori, M. Aoki, K. Sato, Chem. Commun. (2003), 1977-1986.

[21] (a) M.G. Coleman, A.N. Brown, B.A. Bolton, H. Guan, Adv. Synth. Catal. 352 (2010) 967-970.
(b) S.A. Moyer, T.W. Funk, Tetrahedron Lett. 51 (2010) 5430-5433.

[22] (a) Guillena, G. Ramon, D.J. Yus, Angew. Chem, Int. Ed. 46 (2007) 2358-2364.
(b) K.I. Fujita, R. Yamaguchi, Synlett. (2005) 560-571.

[23] (a) K. Fujita, N. Tanino, R. Yamaguchi, Org. Lett. 9 (2007) 109-111.
(b) A.M. Royer, T.B. Rauchfuss, S.R. Wilson, Inorg. Chem. 47 (2008) 395-397.

[24] A.M. Royer, T.B. Rauchfuss, D.L. Gray, Organometallics 29 (2010) 6763-6768.

[25] Y. Sawama, K. Morita, T. Yamada, S. Nagata, Y. Yabe, Y. Monguchi, H. Sajiki, Green Chem. 16 (2014) 3439-3443.

[26] S. Ohzu, T. Ishizuka, Y. Hirai, S. Fukuzumi, T. Kojima, Chem. Eur. J. 19 (2013) 1563-1567.

[27] SAINT Version 7.60a, Bruker AXS Inc, Madison, WI, USA, 2006.

[28] G. M. Sheldrick, SHELXS-97, SHELXL-97.

[29] *ORTEP-3* for Windows. Farrugia, L.J.J. Appl. Crystallogr. 30 (1997) 565.

[30] K. Brandenburg, H. Putz, DIAMOND. Crystal Impact GbR, Bonn, Germany, 2005.

[31] (a) R. Lenz, S.V. Ley, J. Chem. Soc, Perkin Trans. 1 (1997) 3291-3292.
(b) N. Mizuno, K. Yamaguchi, Catal. Today. 132 (2008) 18-27.

[32] C. White, A. Yates, P.M. Maitlis, Inorg. Synth. 29 (1992) 228-234.

[33] M. Bennet, A. Smith, J. Chem. Soc, Dalton Trans. (1974) 233-241.

[34] M.J. Frisch *et al*. Gaussian,Inc., Gaussian 09, Revision D.01, Wallingford, CT, USA, 2009.

[35] F. Huang, G. Lu, L. Zhao, H. Li, Z. X. Wang, J. Am. Chem. Soc. 132 (2010) 12388-12396.

[36] Y. Zhao, D. G. Truhlar, Acc. Chem. Res. 41 (2008) 157-167.

[37] Y. Zhao, D. G. Truhlar, Theor. Chem. Acc. 120 (2008) 215-241.

[38] NBO analysis was performed using the NBO Version 3.1, as implemented in the Gaussian 09 package by Glendening, E. D. Badenhoop, J. K. Reed, A. E. Carpenter, J. E. Weinhold, F.

[39] C.H. Chien, S. Fujita, S. Yamoto, T. Hara, T. Yamagata, M. Watanabe, K. Mashima, Dalton Trans. (2008) 916-923.

[40] P. Govindaswamy, Y.A. Mozharivskyj, M.R. Kollipara, Polyhedron 24 (2005) 1710-1716.

[41] J. Gomez, G.G. Herbosa, J.V. Cuevas, A. Arnaiz, A. Carbayo, A. Munoz, L. Falvello, P.E. Fanwick, Inorg. Chem. 45 (2006) 2483-2493.

[42] O. Prakash, H. Joshi, K.N. Sharma, P.L. Gupta, A.K. Singh, Organometallics 33 (14) (2014) 3804-3812.

[43] M. Yadav, A.K. Singh, D.S. Pandey, Organometallics 28 (2009) 4713-4723.

[44] (a) M. Jiang, J. Li, Y.Q. Huo, Y. Xi, J.F. Yan, F.X. Zhang, J. Chem. Eng. Data. 56 (2011) 1185-1190.
(b) J. M. Gichumbi, H. B. Frierich, B. Omondi, J. Organomet. Chem. 808 (2016) 87-96.

[45] N.A. Owston, A.J. Parker, J.M.J. Williams, Org. Lett. 9 (1) (2007) 73-75.

[46] K.I. Fujita, T. Yoshida, Y. Imori, R. Yamaguchi, Org. Lett. 13 (9) (2011) 2278-2281.

[47] S. Gulcemal, A.G. Gokce, B. Cetinkaya, Dalton Trans. 42 (2013), 7305-7311.

[48] S. Gauthier, R. Scopelliti, K. Severin, Organometallics 23 (2004) 3769-3771.

[49] T. Ohkuma, N. Utsumi, K. Tsutsumi, K. Murata, C. Sandoval, R. Noyori, J. Am. Chem. Soc. 128 (2006) 8724-8725.

[50] F. Saleem, G.K. Rao, A. Kumar, G. Mukherjee, A.K. Singh, Organometallics 32 (2013) 3595-3603.

[51] P. Kolandaivel, K. Senthilkumar, J. Mol. Struct. (Theochem) 535 (2001) 61-70.

[52] Cheng Hou, Jingxing Jiang, Shidong Zhang, Guo Wang, Zhihan Zhang, Zhuofeng Ke, Cunyuan Zhao, ACS Catal. 4 (2014), 2990−2997.

Chapter 3

Synthesis and structural investigation of new half sandwich Ir(III) and Rh(III) amine complexes and their catalytic transfer hydrogenation of aromatic ketones and aldehydes in water

Abstract

Six new complexes, [Cp*IrCl(*para*-R-N-(pyridin-2-ylmethyl)aniline)]PF_6 (R = H (**1b**); F (**2b**); OCH_3 (**3b**)), and [Cp*RhCl(*para*-R-N-(pyridin-2-ylmethyl)aniline)]PF_6 (R = H (**4b**); F (**5b**); OCH_3 (**6b**)), (where Cp* = pentamethylcyclopentadiene) have been synthesized. The synthesized complexes were characterized by ^{1}H NMR, 2D NMR, ^{13}C NMR, HR-MS spectroscopy, IR spectroscopy and elemental analysis. ^{1}H NMR studies revealed that the N,N' amine bidentate ligands coordinated to the Ir(III) and Rh(III) metals ions and complexes **1b**-**6b** exhibit diastereoisomerism in DMSO-d_6 solution at room temperature. Time dependent ^{1}H NMR studies show that the Ir(III) amine complexes **1b**-**3b** are oxidized to imine complexes by molecular oxygen, due to the highly acidic hydrogen bonded to the nitrogen atom. The crystal structures of the [Cp*IrCl(N-(pyridin-2-ylmethyl)aniline)]PF_6 (**1b)** and [Cp*RhCl(*para*-OCH_3-N-(pyridin-2-ylmethyl)aniline)]PF_6 (**6b**) complexes have been resolved by single crystal X-ray diffraction. The Ir(III) and Rh(III) amine complexes were used in catalytic transfer hydrogenation reaction. The Rh(III) catalyst loadings used to reduce the aromatic ketones and aromatic aldehydes were 0.5 and 0.1 mol%, respectively. The Rh(III) amine and imine complexes were found to be versatile and particularly effective for the catalytic transfer hydrogenation of aromatic carbonyl groups in water with sodium formate and formic acid as the hydrogen source under pH dependent acidic conditions.

Keywords: Half sandwich complexes; Transfer hydrogenation; N,N' chiral ligands; Ir(III), Rh(III) amine complexes; sodium formate / formic acid.

3.1 Introduction

Transfer hydrogenation (TH) of carbonyl groups using organometallic compounds is an emerging field in transition metal chemistry as well as in industry [1]. Using an aqueous medium for TH reactions

is of great interest in chemistry due to water having important advantages over conventional organic solvents [2, 3]. Water is readily available, inexpensive, non-toxic, non-carcinogenic, non-flammable and easy to handle.

Conventional TH reactions require neither explosive hydrogen gas nor high pressure vessels for reducing carbonyl groups. Generally, isopropyl alcohol is used as a hydrogen source for reducing carbonyl groups in catalytic TH reactions [4]. The reversibility of the reaction equilibrium using isopropyl alcohol as a solvent is a major drawback in this system. To overcome the drawbacks, alternative hydrogen sources such as HCOOH-HCOONa mixtures, formic acid-Et_3N azeotropic mixtures, and HCOONa were used in aqueous TH reactions [5-7]. Recently, in a number of examples reported, glycerol has replaced isopropyl alcohol as a hydrogen source for aqueous TH reactions using Ir(III), Rh(III) and Ru(II) metal complexes[8, 9]. The advantage of the HCOOH / HCOONa mixture is that it acts as both hydrogen source and base in the aqueous reaction medium. A HCOOH / HCOONa mixture is a better hydrogen source compared to isopropyl alcohol due to the resulting CO_2 being thermodynamically more stable and easily removed from system, which results in the reactions becoming irreversible. Moreover, it offers wide range of the substrates solubility in acidic medium and miscibility with many organic solvents in the range of 20-60 ºC [10]. This process is an example of an environmentally benign process for TH applications.

Noyori, Ikariya and co-workers have reported many of the metal-ligand bifunctional ruthenium catalysts that reduce organic carbonyl compounds under aqueous reaction conditions [11-14]. Indeed, the majority of catalytic TH reactions reported used ruthenium species rather than iridium or rhodium species [10, 15-18]. Recently, Talwar *et al.* explored iridium cyclometalated compounds for transfer hydrogenative reductive amination using ammonium formate both as a nitrogen and hydrogen source [19]. Yadav *et al.* have reported an effective and versatile N,N' dipyrrin ligand coordinated to Ir(III) and Rh(III) half sandwich catalysts for aqueous catalytic TH reactions [20]. There are very few reported rhodium complexes with coordinated N,N' chelated ligands for homogeneous or heterogeneous catalytic TH reactions carried out in aqueous medium [8, 21-23].

Using half sandwich complexes of iridium, rhodium and ruthenium for TH reactions can give high selective reactivity of one functional (carbonyl) group in the presence of others in organic compounds and can show a broad range of the substrate scope in the aqueous medium [24]. A β-protic pyrazole containing metal-ligand bifunctional iridium catalysts was reported by Kuwata and Ikariya [25], in which the labile N-H proton at the β-position to the metal may be activated to give a potential and more

accessible β-protic bifunctional catalyst [25]. Several pyridinebisimidazolines coordinated ruthenium, iridium and rhodium catalysts have been reported, where the effect of the N-H groups on enantioselectivity of products as well as their effects on TH reactions was reported [4, 26, 27]. The nature of the nitrogen atom is sp^2 or sp^3 and the lability and hemilability of the nitrogen donor atom is defined by the electronic nature of the substituent groups present on nitrogen.

The chiral ligands present in the catalysts may undergo easy association or dissociation during the reaction conditions, which may influence the selectivity of the reaction, but it is controlled by metal stereochemistry [28]. This statement is strongly supported when the metal is an additional center of chirality in the ligand-associated form [29]. For the TH reactions mainly, N-H bond bearing N,N' bidentate ligands were used and they control the TH reaction mechanism according to Noyori's proposal [10]. The pH dependence of TH reactions catalyzed by iridium and ruthenium complexes was reported by Ogo *et al.* [30, 31]. Recently Wei *et al.* reported cyclometalated Ir(III) complexes for TH of carbonyl groups under pH controlled reactions conditions [5]. To the best of our knowledge, only a few homogeneous and heterogeneous rhodium catalyzed TH reactions in water have been reported in literature [8, 21, 32].

In this chapter, we report the synthesis and characterization of new amine Ir(III) and Rh(III) half sandwich complexes with a chiral metal center coordinated to N,N' chelated ligands. The highly acidic N-H bond in the ligand allows oxidation from the amine to the imine in the iridium complexes. The labile N-H bond is present on the β position with respect to the metal. The coordination nature and stereochemistry of the complexes were studied by single crystal XRD, ^{1}H NMR and 1D NOE studies. Their catalytic TH was carried out in pH dependent aqueous medium using a HCOOH / HCOONa mixture as a hydrogen donor.

3.2 Experimental section

3.2.1 Reagents and Methods

Unless otherwise noted, all manipulations were performed using standard Schlenk tube techniques under an argon atmosphere. The reagents 2-pyridinecarboxaldehdye, $IrCl_3 \cdot 3H_2O$ (≥99% purity), $RhCl_3 \cdot 3H_2O$ (≥99% purity), KOH pellets and solvents were purchased from Sigma-Aldrich, Capital Labs, South Africa and were used without further purification. HCOONa and HCOOH (85 wt%) were purchased from Fluka chemicals. The solvents were dried by standard procedures and distilled prior to use [33]. Melting points were recorded on a Stuart™ Scientific apparatus SMP 3 and are uncorrected.

The NMR solvent DMSO-d_6 was purchased from Merck, Germany. Solid and liquid state infrared spectra were recorded using an FT-IR Perkin Elmer Spectrum 100 spectrophotometer between 4000 - 400 cm^{-1}. Low and high resolution mass spectra were recorded using a Waters Micromass LCT Premier TOF-MS instrument. Optical rotations were measured using an ADP410 Polarimeter that operated at λ = 589.3 nm, which corresponds to the LED / interference filter and at ambient temperature. Elemental analyses were performed on a Thermo-Scientific Flash 2000 CHNS/O analyser. Gas chromatography (GC) analysis was performed using a Perkin-Elmer Clarus 500 GC with a HP-Pona-50 m*0.2 mm, 0.5µ capillary column. pH measurements of a HCOOH / HCOONa mixture was carried out using a pH 211 microprocessor pH meter equipped with a glass electrode calibrated with Sigma–Aldrich buffer solutions at pH 4, 7 and 10.

Time dependent ^{1}H NMR (400 MHz) stability studies and ^{13}C (100 MHz) and 2D NMR were recorded in DMSO-d_6 solvent systems using a Bruker Topspin 400 spectrometer. The variant temperature ^{1}H NMR (600 MHz) and 1D NOE studies were performed by a Bruker Topspin 600 spectrometer using TXLZ/AV 600 probe. X-ray single crystal intensity data were collected on a Bruker Smart *APEX11* Nonius Kappa-CCD diffractometer using graphite monochromated MoKα radiation (λ = 0.71073 Å). The precursors $(IrCl_2Cp^*)_2$ and $(RhCl_2Cp^*)_2$ were prepared according to literature methods [34-36]. Iridium complexes **1b**-**3b** were completely oxidized to imine complexes during the synthesis of the amine complexes in room temperature by molecular oxygen [37]. The oxidized imine Ir(III) (**1a**) and Rh(III) (**2a**) complexes were synthesized [38], in order to compare the catalytic activity of the amine and imine complexes for catalytic TH reactions.

3.2.2 Synthesis and characterization of complexes 1b-6b

A mixture of $(MCl_2Cp^*)_2$ (M = Ir / Rh) (0.13 / 0.16 mmol), the amine ligands **L1**-**L3** (0.26 / 0.32 mmol) and NH_4PF_6 (0.26 / 0.32 mmol) was stirred at room temperature in methanol (15 mL) for 2 hours. The pale yellow precipitate was separated out and filtered off through filter paper, washed with cold methanol and diethyl ether and dried under vacuum. The above common procedure was followed to synthesize complexes **1b**-**6b**.

3.2.2.1 $[(\eta^5\text{-}C_5Me_5)IrCl(\mathbf{L1})]PF_6$ (**1b**)

$(IrCl_2Cp^*)_2$ (100 mg), amine ligand **L1** (48 mg) and NH_4PF_6 (43 mg). Yield (126 mg, 0.18 mmol, 73 %). Mp. 274.0 °C (dec.). ^{1}H NMR (400 MHz, DMSO-d_6, 25 ºC, ppm); Major isomer (73 %) (δ = 8.71 (d, 1H, $J_{H\text{-}H}$ = 5.48 Hz, α proton of Py), 8.16 (t, 1H, Py), 7.93 (d, 1H, $J_{H\text{-}H}$ = 7.68 Hz, Py), 7.73 (d, 1H, $J_{H\text{-}H}$ = 7.92 Hz, Py), 7.69 - 7.60 (m, 2H, Ph), 7.53 - 7.41 (m, 3H, Ph), 7.29 (t, 1H, N-H), 5.02 - 4.99 (d-d, 1H,

$^{3}J_{CH\text{-}NH}$ = 11.20 Hz, -CH_2), 4.63 - 4.56 (d-d, 1H, $^{3}J_{CH\text{-}NH}$ = 2.72 Hz, -CH_2), 1.24 (s, 15H, C_5Me_5); Minor isomer (27 %) δ = 8.79 (d, 1H, $J_{H\text{-}H}$ = 5.52 Hz, α proton of Py), 8.18 (t, 1H, Py), 7.97 (d, 1H, $J_{H\text{-}H}$ = 6.08 Hz, Py), 7.80 (d, 1H, $J_{H\text{-}H}$ = 7.72 Hz, Py), 7.70 (m, 2H, Ph), 7.57 - 7.54 (m, 2H, Ph), 7.48 (d, 1H, $J_{H\text{-}H}$ = 7.96 Hz, Py), 7.34 (t, 1H, N-H), 4.89 - 4.82 (d-d, 1H, $^{3}J_{CH\text{-}NH}$ = 10.12 Hz, -CH_2), 4.64 (d-d, 1H, $^{3}J_{CH\text{-}NH}$ = 6.08 Hz, -CH_2), 1.40 (s, 15H, C_5Me_5); ^{13}C NMR (100 MHz, DMSO-d_6, 25 °C, ppm); Major isomer δ = 159.53, 151.66, 145.94, 139.90, 129.44 (Py), 129.21, 126.45, 126.15, 122.49, 122.38, 119.85 (Ph), 87.32 (C, C_5Me_5), 58.15 (C, CH_2), 7.58 (CH_3, C_5Me_5); Minor isomer δ = 155.33, 150.69, 146.22, 140.66, 130.52 (Py), 129.61, 129.29, 127.19, 126.34, 122.12, 120.33 (Ph), 87.08 (C, C_5Me_5), 61.05 (C, CH_2), 7.76 (CH_3, C_5Me_5). FT-IR (γ/cm^{-1}): 3128 (s, N-H), 3042, 1616, 1598, 1403, 1033, 831 (s, P-F). HR-MS (TOF MS ES$^+$) $C_{22}H_{27}ClIrN_2$ Calculated: 547.1492, Found: 547.1475. $[\alpha]_{\lambda}^{25}$ = –1.94 (c = 2.05, CH_3CN). Anal. Calcd for $C_{22}H_{27}ClF_6IrN_2P$: C, 38.18; H, 3.93; N, 4.05; Found: C, 37.83; H, 4.02; N, 3.89.

3.2.2.2 [(η^5-C_5Me_5)IrCl(**L2**)]PF_6 (**2b**)

($IrCl_2Cp^*$)$_2$ (100 mg), amine ligand **L2** (53 mg) and NH_4PF_6 (43 mg). Yield (130 mg, 0.18 mmol, 73 %). Mp. 286.0 °C (dec.). ^{1}H NMR (400 MHz, DMSO-d_6, 25 ºC, ppm); Major isomer (64 %) δ = 8.71 (d, 1H, $J_{H\text{-}H}$ = 5.52 Hz, α proton of Py), 8.16 (t, 1H, Py), 7.92 (d, 1H, $J_{H\text{-}H}$ = 7.80 Hz, Py), 7.68 (t, 1H, Py), 7.48 - 7.44 (m, 4H, Ph), 7.35 (t, 1H, N-H), 4.95 - 4.93 (d-d, 1H, $^{3}J_{CH\text{-}NH}$ = 10.92 Hz, -CH_2), 4.61 - 4.58 (d-d, 1H, $^{3}J_{CH\text{-}NH}$ = 2.32 Hz, -CH_2), 1.26 (s, 15H, C_5Me_5). Minor isomer (36 %) δ = 8.78 (d, 1H, $J_{H\text{-}H}$ = 5.48 Hz, α proton of Py), 8.18 (t, 1H, Py), 7.82 (d, 1H, $J_{H\text{-}H}$ = 7.64 Hz, Py), 7.64 (t, 1H, Py), 7.47 (m, 4H, Ph), 7.33 (t, 1H, N-H), 4.84 - 4.78 (d-d, 1H, $^{3}J_{CH\text{-}NH}$ = 10.00 Hz, -CH_2), 4.63 - 4.62 (d-d, 1H, $^{3}J_{CH\text{-}NH}$ = 2.48 Hz, -CH_2), 1.41 (s, 15H, C_5Me_5). ^{13}C NMR (100 MHz, DMSO-d_6, 25 °C, ppm); major isomer δ = 160.99, 159.33, 151.71, 142.35, 139.98 (Py), 126.51, 124.26, 122.39, 121.71, 116.04, 115.82 (Ph), 87.37 (C, C_5Me_5), 58.48 (C, CH_2), 7.67 (CH_3, C_5Me_5).); minor isomer δ = 160.57, 158.56, 150.71, 142.35, 139.98 (Py), 126.42, 124.18, 122.33, 121.79, 116.14, 115.91 (Ph), 87.17 (C, C_5Me_5), 61.20 (C, CH_2), 7.83 (CH_3, C_5Me_5). FT-IR (γ/cm^{-1}): 3212 (s, N-H), 1613, 1510, 1471, 1449, 1027, 833 (s, P-F). HR-MS (TOF MS ES$^+$) $C_{22}H_{24}ClFIrN_2$ Calculated: 563.1241, Found: 563.1251. $[\alpha]_{\lambda}^{25}$ = –4.85 (c = 2.06, CH_3CN). Anal. Calcd for $C_{22}H_{26}ClF_7IrN_2P$: C, 37.21; H, 3.69; N, 3.95; Found: C, 37.17; H, 3.22; N, 3.83.

3.2.2.3 [(η^5-C_5Me_5)IrCl(**L3**)]PF_6 (**3b**)

($IrCl_2Cp^*$)$_2$ (100 mg), amine ligand **L3** (56 mg) and NH_4PF_6 (43 mg). Yield (127 mg, 0.18 mmol, 70 %). Mp. 279.0 °C (dec.). ^{1}H NMR (400 MHz, DMSO-d_6, 25 ºC, ppm); Major isomer (70 %) δ = 8.70 (d, 1H, $J_{H\text{-}H}$ = 5.48 Hz, α proton of Py), 8.15 (t, 1H, Py), 7.91 (d, 1H, $J_{H\text{-}H}$ = 7.68 Hz, Py), 7.66 (t, 1H, Py), 7.36 (d, 2H, $J_{H\text{-}H}$ = 8.96 Hz, Ph), 7.19 (d, 2H, $J_{H\text{-}H}$ = 8.92 Hz, Ph), 7.06 (t, 1H, N-H), 4.97 - 4.91 (d-d, 1H,

$^{3}J_{CH\text{-}NH}$ = 11.00 Hz, -CH_2), 4.59 - 4.56 (d-d, 1H, $^{3}J_{CH\text{-}NH}$ = 2.80 Hz, -CH_2), 3.78 (s, 3H, OCH_3), 1.26 (s, 15H, C_5Me_5); Minor isomer (30 %) δ = 8.79 (d, 1H, $J_{H\text{-}H}$ = 5.56 Hz, α proton of Py), 8.17 (t, 1H, Py), 7.81 (d, 1H, $J_{H\text{-}H}$ = 7.64 Hz, Py), 7.69 (t, 1H, Py), 7.37 (m, 2H, Ph), 7.19 (m, 2H, Ph), 7.03 (t, 1H, N-H), 4.80 - 4.74 (d-d, 1H, $^{3}J_{CH\text{-}NH}$ = 10.24 Hz, -CH_2), 4.55 - 4.52 (d-d, 1H, $^{3}J_{CH\text{-}NH}$ = 4.04 Hz, -CH_2), 3.77 (s, 3H, OCH_3), 1.40 (s, 15H, C_5Me_5). ^{13}C NMR (100 MHz, DMSO-d_6, 25 °C, ppm); Major isomer δ = 159.58, 157.20, 151.66, 149.25, 139.87, (Py), 138.99, 126.41, 123.43, 122.30, 120.97, 114.16 (Ph), 87.33 (C, C_5Me_5), 58.60 (C, CH_2), 55.46 (C, OCH_3), 7.70 (CH_3, C_5Me_5); Minor isomer δ = 160.73, 157.91, 150.61, 149.43, 139.90, (Py), 139.15, 126.31, 124.10, 122.26, 114.42, 114.24 (Ph), 87.08 (C, C_5Me_5), 61.56 (C, CH_2), 55.44 (C, OCH_3), 7.82 (CH_3, C_5Me_5). FT-IR (γ/cm^{-1}): 3214 (s, N-H), 1613, 1512, 1451, 1253, 1031, 837 (s, P-F). HR-MS (TOF MS ES$^+$) $C_{23}H_{27}ClIrN_2O$ Calculated: 575.1441, Found: 575.1445. $[\alpha]_{\lambda}^{25}$ = –3.05 (c = 1.97, CH_3CN). Anal. Calcd for $C_{23}H_{29}ClF_6IrN_2OP$: C, 38.25; H, 4.05; N, 3.88; Found: C, 38.49; H, 4.17; N, 4.13.

3.2.2.4 [(η^5-C_5Me_5)RhCl(**L1**)]PF_6 (**4b**)

($RhCl_2Cp^*$)$_2$ (100 mg), amine ligand **L1** (59 mg) and NH_4PF_6 (53 mg). Yield (130 mg, 0.22 mmol, 67 %). Mp. 242.0 °C (dec.). ^{1}H NMR (400 MHz, DMSO-d_6, 25 ºC, ppm); Major isomer (72 %) δ = 8.72 (d, 1H, $J_{H\text{-}H}$ = 5.40 Hz, α proton of Py), 8.13 (t, 1H, Py), 7.82 (d, 1H, $J_{H\text{-}H}$ = 7.80 Hz, Py), 7.74 - 7.70 (m, 2H, Py & Ph), 7.51 (d, 2H, $J_{H\text{-}H}$ = 7.44 Hz, Ph), 7.46 (d, 2H, $J_{H\text{-}H}$ = 8.08 Hz, Ph), 7.29 (t, 1H, N-H), 5.01 - 4.95 (d-d, 1H, $^{3}J_{CH\text{-}NH}$ = 11.60 Hz, -CH_2), 4.34 - 4.31 (d-d, 1H, $^{3}J_{CH\text{-}NH}$ = 4.24 Hz, -CH_2), 1.27 (s, 15H, C_5Me_5); Minor isomer (28 %) δ = 8.80 (d, 1H, $J_{H\text{-}H}$ = 5.48 Hz, α proton of Py), 8.15 (t, 1H, Py), 7.68 (m, 1H, Py), 7.74 - 7.64 (m, 2H, Py & Ph), 7.55 (d, 2H, $J_{H\text{-}H}$ = 5.52 Hz, Ph), 7.48 (s, 1H, Ph), 7.34 (t, 1H, N-H), 4.63 - 4.56 (d-d, 1H, $^{3}J_{CH\text{-}NH}$ = 10.44 Hz, -CH_2), 4.42 - 4.38 (d-d, 1H, $^{3}J_{CH\text{-}NH}$ = 3.20 Hz, -CH_2), 1.43 (s, 15H, C_5Me_5). ^{13}C NMR (100 MHz, DMSO-d_6, 25 ºC, ppm) Major isomer δ = 158.85, 151.89, 150.35, 145.65, 139.74 (Py), 129.29, 126.07, 125.57, 122.65, 121.95, 119.58 (Ph), 95.59 (d, C, C_5Me_5), 56.47 (C, CH_2), 7.81 (CH_3, C_5Me_5); Minor isomer δ = 158.96, 150.35, 146.25, 139.79, 129.48 (Py), 129.34, 126.82, 125.98, 122.39, 122.22, 119.61 (Ph), 95.36 (d, C, C_5Me_5), 59.89 (C, CH_2), 8.01 (CH_3, C_5Me_5). FT-IR (γ/cm^{-1}): 3138 (s, N-H), 2973, 2918, 1614, 1599, 1494, 1444, 1024, 830 (s, P-F). HR-MS (TOF MS ES$^+$) $C_{22}H_{27}ClN_2Rh$ Calculated: 457.0918, Found: 457.0905. $[\alpha]_{\lambda}^{25}$ = +3.16 (c = 1.90, CH_3CN). Anal. Calcd for $C_{22}H_{27}ClF_6N_2PRh$: C, 43.84; H, 4.51; N, 4.65; Found: C, 43.52; H, 4.10; N, 4.70.

3.2.2.5 [(η^5-C_5Me_5)RhCl(**L2**)]PF_6 (**5b**)

($RhCl_2Cp^*$)$_2$ (100 mg), amine ligand **L2** (65 mg) and NH_4PF_6 (53 mg). Yield (141 mg, 0.23 mmol, 70 %). Mp. 274.0 °C (dec.). ^{1}H NMR (400 MHz, DMSO-d_6, 25 ºC, ppm); Major isomer (66 %) δ

= 8.73 (d, 1H, $J_{H\text{-}H}$ = 5.36 Hz, α proton of Py), 8.13 (t, 1H, Py), 7.80 (d, 1H, $J_{H\text{-}H}$ = 7.72 Hz, Py), 7.71 (t, 1H, Py), 7.57 (d, 1H, $J_{H\text{-}H}$ = 10.84 Hz, Ph), 7.48 (t, 1H, Ph), 7.39 (d, 1H, $J_{H\text{-}H}$ = 8.72 Hz, Ph), 7.39 (t, 1H, N-H), 4.98 - 4.91 (d-d, 1H, $^{3}J_{CH\text{-}NH}$ = 11.44 Hz, -CH_2), 4.34 - 4.30 (d-d, 1H, $^{3}J_{CH\text{-}NH}$ = 2.28 Hz, -CH_2), 1.29 (s, 15H, C_5Me_5); Minor isomer (34 %) δ = 8.79 (d, 1H, $J_{H\text{-}H}$ = 5.40 Hz, α proton of Py), 8.15 (t, 1H, Py), 7.77 (m, 3H, Py & Ph), 7.66 (d, 2H, $J_{H\text{-}H}$ = 7.72 Hz, Ph), 7.51 (m, 1H, Ph), 7.39 (d, 1H, $J_{H\text{-}H}$ = 8.72 Hz, Ph), 7.32 (t, 1H, N-H), 4.58 - 4.51 (d-d, 1H, $^{3}J_{CH\text{-}NH}$ = 10.40 Hz, -CH_2), 4.41 - 4.37 (d-d, 1H, $^{3}J_{CH\text{-}NH}$ = 3.72 Hz, -CH_2), 1.44 (s, 15H, C_5Me_5). ^{13}C NMR (100 MHz, DMSO-d_6, 25 °C, ppm); Major isomer δ = 158.62, 151.90, 150.34, 142.05, 139.79 (Py), 126.12, 124.05, 122.66, 121.43, 116.10, 115.88 (Ph), 95.64 (d, C, C_5Me_5), 56.81 (C, CH_2), 7.87 (CH_3, C_5Me_5); Minor isomer δ = 158.80, 150.35, 142.60, 140.26, 139.22 (Py), 126.03, 123.96, 122.23, 121.33, 116.18, 115.96 (Ph), 95.45 (d, C, C_5Me_5), 56.47 (C, CH_2), 8.07 (CH_3, C_5Me_5). FT-IR (γ/cm^{-1}): 3152 (s, N-H), 1610, 1509, 1480, 1213, 1084, 1030, 829 (s, P-F). HR-MS (TOF MS ES$^+$) $C_{22}H_{24}ClFN_2Rh$ Calculated: 473.0667, Found: 473.0669. $[\alpha]_{\lambda}^{25}$ = –1.93 (c = 2.07, CH_3CN). Anal. Calcd for $C_{22}H_{26}ClF_7N_2PRh$: C, 42.57; H, 4.22; N, 4.51; Found: C, 42.32; H, 4.17; N, 4.56.

3.2.2.6 [(η^5-C_5Me_5)RhCl(**L3**)]PF_6 (**6b**)

($RhCl_2Cp^*$)$_2$ (100 mg), amine ligand **L3** (69 mg) and NH_4PF_6 (53 mg). Yield (170 mg, 0.27 mmol, 83 %). Mp. 285.0 °C (dec.). ^{1}H NMR (400 MHz, DMSO-d_6, 25 ºC, ppm); Major isomer (65 %) δ = 8.72 (d, 1H, $J_{H\text{-}H}$ = 5.36 Hz, α proton of Py), 8.12 (t, 1H, Py), 7.80 - 7.78 (d, 1H, $J_{H\text{-}H}$ = 7.76 Hz, Py), 7.71 - 7.69 (t, 1H, Py), 7.48 (t, 1H, Ph), 7.39 (d, 1H, $J_{H\text{-}H}$ = 8.72 Hz, Ph), 7.07 (t, 1H, N-H), 4.96 - 4.89 (d-d, 1H, $^{3}J_{CH\text{-}NH}$ = 11.40 Hz, -CH_2), 4.32 - 4.28 (d-d, 1H, $^{3}J_{CH\text{-}NH}$ = 2.44 Hz, -CH_2), 3.78 (s, 3H, -OCH_3), 1.29 (s, 15H, C_5Me_5); Minor isomer (35 %) δ = 8.79 (d, 1H, $J_{H\text{-}H}$ = 5.40 Hz, α proton of Py), 8.33 (d, 1H, $J_{H\text{-}H}$ = 9.76 Hz, Py), 8.14 (t, 2H, Py), 7.65 (d, 1H, $J_{H\text{-}H}$ = 7.84 Hz, Ph), 7.41 (broad, 2H, Ph), 7.03 (t, 1H, N-H), 4.55 - 4.48 (d-d, 1H, $^{3}J_{CH\text{-}NH}$ = 10.56 Hz, -CH_2), 4.35 - 4.32 (d-d, 1H, $^{3}J_{CH\text{-}NH}$ = 3.60 Hz, -CH_2), 3.77 (s, 3H, -OCH_3), 1.44 (s, 15H, C_5Me_5). ^{13}C NMR (100 MHz, DMSO-d_6, 25 °C, ppm); Major isomer δ = 159.40, 152.38, 150.78, 140.20, 140.17 (Py), 139.15, 126.53, 123.84, 123.09, 121.24, 114.82 (Ph), 96.08 (d, C, C_5Me_5), 57.49 (C, CH_2), 55.95 (C, OCH_3), 8.41 (CH_3, C_5Me_5); Minor isomer δ = 158.24, 157.39, 154.45, 140.97, 140.19 (Py), 139.68, 126.43, 124.51, 122.66, 121.20, 114.99 (Ph), 95.83 (d, C, C_5Me_5), 60.99 (C, CH_2), 55.88 (C, -OCH_3), 8.59 (CH_3, C_5Me_5). FT-IR (γ/cm^{-1}): 3232 (s, N-H), 1610, 1600, 1514, 1482, 1448, 1284, 1253, 1182, 1070, 1018, 824 (s, P-F). HR-MS (TOF MS ES$^+$) $C_{23}H_{27}ClN_2ORh$ Calculated: 485.0867, Found: 485.0867. $[\alpha]_{\lambda}^{25}$ = –3.98 (c = 2.01, CH_3CN). Anal. Calcd for $C_{23}H_{29}ClF_6N_2OPRh$: C, 43.65; H, 4.62; N, 4.43; Found: C, 43.48; H, 4.41; N, 4.47.

3.2.3 Crystallography

Suitable crystals for X-ray analysis were grown by slow evaporation of hexane into an acetonitrile solution. The crystals were selected and glued onto the tip of glass fibers, then mounted in a stream of cold nitrogen at 173 (2) K and centered in the X-ray beam by using a video camera. The crystal refinement and data collection were performed on a Bruker Smart *APEX11* diffractometer using graphite crystal monochromatised Mo - Kα radiation (ʎ = 0.71073 Å) and a diffractometer to crystal distance of 4.00 cm. The initial cell matrix was obtained from three series of scans at different starting angles. Each series consisted of 12 frames collected at intervals of 0.5° in a 6° range with the exposure time of about 10 seconds per frame. The reflections were successfully indexed by an automated indexing routine built in the APEXII program suite. The final cell constants were calculated from a set of 6460 strong reflections from the actual data collection. The data collection method involved ω scans of width 0.5°. Data reduction was carried using the program *SAINT*+ [39]. The structure of crystal was resolved by the SHELX [40] program. The full-matrix least-squares on F^2 refinement method with the SHELX program package was used to refine the positions and thermal parameters of all non-hydrogen atoms in the crystal [40]. All H atoms were positioned geometrically and allowed to ride on their respective parent atoms. All H atoms were refined isotropically. The structure and graphics of the crystals and N-H···Cl interactions were generated by *ORTEP-3* [41] and MERCURY [42] programs. Structural refinement data as well as crystal data for compound **1b** are given in Table 3.1. Those of compound **6b** are provided in the supplementary information and are only reported to support connectivity to the metal center, as the data acquired fairly low quality.

Table 3.1 Structure refinement and crystal data of complex **1b**

Complex	**1b**
Empirical formula	$C_{22}H_{29}ClF_6IrN_2P$
Formula weight	692.07
Temperature/K	173(2) K
Crystal system	triclinic
Space group	P-1
a/Å	9.4334(2)
b/Å	11.5851(3)
c/Å	12.2190(3)
α/°	74.1290(10)
β/°	70.2610(10)
γ/°	82.7480(10)
Volume/Å^3	1208.15(5)
Z	2
ρ_{calc}g/cm^3	1.902
μ(Mo Kα)/mm^{-1}	5.762
F(000)	672
Crystal size/mm^3	0.220 × 0.190 × 0.180
Radiation	Mo Kα (λ = 0.71073)
2ɵ range for data collection/°	3.654 to 57.56
Index ranges	$-10 \le h \le 12$, $-15 \le k \le 15$, $-16 \le l \le 16$
Reflections collected	26957
Independent reflections	6157 [R_{int} = 0.0314, R_{sigma} = 0.0223]
Data/restraints/parameters	6157/0/303
Goodness-of-fit on F^2	1.116
Final R indexes [I>=2σ (I)]	R_1 = 0.0157, wR_2 = 0.0407
Final R indexes [all data]	R_1 = 0.0159, wR_2 = 0.0408
Largest diff. peak/hole / e Å^{-3}	0.81/-1.38

3.2.4 General procedure for catalytic transfer hydrogenation of aromatic ketones

Ketone (1 mmol), catalyst (0.5 mol%) and a mixture of HCOOH (85 wt%) (3.75 mmol) and HCOONa (2 mmol) in 2 mL of deionized water were placed in a Schlenk tube under argon or nitrogen atmosphere. The mixture was stirred magnetically at specified temperature over the specified time. After

completion of the reaction, the reaction mixture was cooled to room temperature, quenched with aqueous $NaHCO_3$ solution, and extracted with diethyl ether. The organic layer was washed with brine solution, dried over $MgSO_4$, the solvent was removed by rotary evaporator and the resulting residue passed through a short silica column. The fractions were collected and the conversion of the respective products was determined by GC analysis using chlorobenzene as an internal standard. All experiments were done at least in duplicate.

3.2.5 General procedure for catalytic transfer hydrogenation of aromatic aldehydes

The above-mentioned procedure was followed to carry out the TH of aromatic aldehydes. Aldehyde (5 mmol), catalyst (0.5 mol%) and a mixture of HCOOH (85 wt%) (7.50 mmol) and HCOONa (4 mmol) in 4 mL of deionized water were placed in a Schlenk tube under argon or nitrogen atmosphere.

3.2.6 General procedure for catalyst recyclability and catalytic activity

Acetophenone (1 mmol), catalyst (0.5 mol%) and a mixture of HCOOH / HCOONa (3.75 mmol / 2.0 mmol) were dissolved in 2 mL deionized water in a Schlenk tube under an argon or nitrogen atmosphere. The mixture was stirred magnetically at 60 ºC over the specified time. After completion of the reaction, the reaction mixture was cooled to room temperature and the organic phase was extracted with ethyl acetate. The solvent was removed by distillation and the resulting residue was treated with diethyl ether to precipitate the catalyst which was dried under vacuum overnight. A new TH reaction was started by introducing acetophenone (1 mmol), recovered catalyst (0.5 mol%) and a mixture of HCOOH / HCOONa in 2 mL of deionized water. After degassing with nitrogen or argon, the mixture was stirred magnetically at 60 ºC over required time.

3.3 Results and discussion

3.3.1 Complex synthesis

In the present work, the new half sandwich metal complexes **1b**-**6b** have been synthesised using N,N' amine bidentate ligands (Scheme. 3.1). The reaction between the chloro bridged dimer $(MCl_2Cp^*)_2$ (M = Ir and Rh) with N,N' *para*-R-N-(pyridine-2-ylmethyl)-aniline (R = H (**L1**), F (**L2**), OCH_3 (**L3**)) and NH_4PF_6 afforded the new $[(\eta^5\text{-}C_5Me_5)MCl(L1\text{-}L3)]PF_6$ (M = Ir (**1**-**3**) and Rh (**4b**-**6b**)) complexes **1b**-**6b** in good yield in methanol. Complexes **1b**-**3b** are pale yellow and **4b**-**6b** are yellow crystalline solids which are air stable, non-hygroscopic and highly soluble in common polar solvents such as DMSO, DMF,

acetonitrile, dichloromethane, acetone, ethyl acetate, methanol, ethanol and soluble in water up to 3 mg / mL at room temperature. These complexes are insoluble in diethyl ether, petroleum ether and hexane.

During the synthesis of the iridium complexes **1b**-**3b**, small amounts of the amine oxidized products, i.e. imine complexes, were observed to form when molecular oxygen was not totally eliminated from the reaction medium. When the reaction was done in air, the iridium amine complexes were oxidized to the corresponding imine complexes completely over time. This reaction was monitored and the amine and imine complexes were confirmed by ^{1}H NMR (See SI S17-S19). The highly acidic N-H proton present on the ligand promoted the formation of the oxidized product of the imine iridium complexes in the reaction medium. In contrast, this was not observed during the synthesis of the rhodium complexes **4b**-**6b**. We were unable to separate the iridium amine and imine complexes by chromatography [43]. The mechanism of the amine to imine oxidation is unknown [27]. Gomez *et al.* reported that ruthenium coordinated to secondary amine ligands activates their oxidation to imines by molecular oxygen in a base-catalyzed reaction [37].

Characterization of the ligand and metal complexes **1b**-**6b** were carried out by ^{1}H NMR, 2D NMR (COSY, NOESY), ^{13}C NMR, IR spectroscopy, melting point analysis, HR-MS spectroscopy and elemental analyses. The crystal structures of complexes **1b** and **6b** have been further authenticated by single crystal X-ray crystallography.

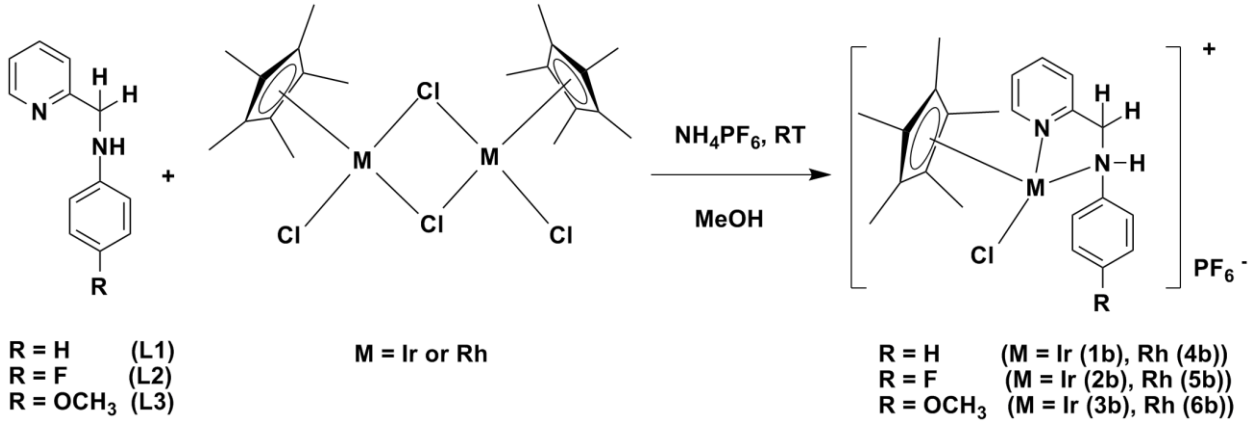

Scheme 3.1: Synthesis of complexes **1b**-**6b**.

3.3.2 Solution NMR studies

Spectral details of complexes **1b**-**6b** have been summarized in the Experimental section. The ^{1}H NMR spectra of the free N,N' amine ligands, **L1**-**L3**, showed a CH_2 group proton doublet in the range of 4.29 - 4.33 ppm and a doublet for the α proton in the pyridine ring appeared in the range of 8.53 - 8.50

ppm. The N-H proton present in ligands **L1**-**L3** coupled with the CH_2 protons and showed a triplet in the ^{1}H NMR spectra. When the N,N' amine ligands **L1**-**L3** were coordinated with the iridium and rhodium precursors, the doublet of the α proton in the pyridine ring shifted down-field to 8.71 (**1b** & **2b**), 8.70 (**3b**), 8.73 (**4b** & **5b**), and 8.72 (**6b**) ppm. The aromatic region and N-H signal of complexes **1b**-**6b** were also shifted down-field compared to the free ligand signals. The secondary amine ligands **L1**-**L3** have chiral nitrogen atoms and hence complexes **1b**-**6b** are found as a mixture of diastereomers (R_M, S_{N-H}) and (S_M, R_{N-H}) in solution. Interestingly, distinct peaks for the major and minor isomers were seen in the ^{1}H NMR and ^{13}C NMR spectra of complexes **1b**-**6b**. Unfortunately, some aromatic phenyl group signals of the major and minor diastereomers overlapped together in the ^{1}H NMR spectra, and the distinct signals of complexes **1b**-**6b** and the respective peaks of each diastereomer were resolved by 2D NMR studies (See SI S2-S16). The dd coupling constant of the CH_2 protons present in the complexes **1b**-**6b** are 11-12 and 2-3 Hz, which may be associated to the diastereomers present in solution.

Interestingly, the signals of each proton of the CH_2 fragment appeared separately as doublets of doublets (dd) in the range of 4.28 - 5.03 ppm for complexes **1b**-**6b**. This is as a result of the two diastereomeric protons present in the CH_2 group. The diastereoselectivity of complexes **1b**-**6b** have been determined by interpretation of the respective ^{1}H NMR signals of each isomer and the diastereomeric ratios of the major and minor diastereomers in solution are given in Table 3.2. The Cp* ($\mathbf{C}(CH_3)$)$_5$ carbons in the ^{13}C NMR spectra showed a doublet instead of a singlet for complexes **4b**-**6b**, which could be due to rhodium coupling with the Cp* ($\mathbf{C}(CH_3)$)$_5$ carbon atoms [44]. By lowering the temperature of the solutions of the complexes **1b** and **4b** to 293 K, these inter conversion was "frozen", according to variable-temperature ^{1}H NMR experiment. At 293 K, the CH_2 signal split into two peaks, as did the Cp* signal, which relates to the two possible diastereomers present in solution (Figs. 3.1-3.3).

The ^{1}H - ^{1}H COSY and 1D NOE analyses of complexes **1b** and **4b** showed the interaction between the CH_2 protons and Cp* protons (See SI S20 & S21) (Schem 3.2). The diastereomers of the complexes **1b**-**6b** could not be isolated as pure species and were only characterized by solution ^{1}H NMR, ^{13}C NMR and 2D NMR studies. Pfeffer and co-workers [43, 45, 46] also reported chiral primary and secondary amines cyclometalated with Ir(III), Rh(III) and Ru(II) half sandwich complexes showing diastereomeric behavior in solution. Their solution NMR analysis showed the characteristic key NOE interactions between the Cp* protons and the aromatic or benzylic protons.

The stereochemistry of complexes **1b** and **4b** can be explained as follows: the N-H proton is coupled to the CH_2 protons with coupling constants of $^3J_{CHNH}$ = 2.72 (**1b**), 4.24 (**4b**), 11.20 (**1b**), and

11.60 (**4b**) Hz, where the latter two values suggest the *anti*-positioning of one CH_2 proton to the N-H group, as per the Karplus law [43]. A low value of $^3J_{CHNH}$ (2.72 (**1b**) & 4.24 (**4b**) Hz) is associated with the *syn*-position of the other CH_2 proton to the N-H group. The configuration of the nitrogen atom is assigned as *S*, as per the above observation. The analysis of the single crystal XRD further confirms the configuration of the nitrogen, which correlates with the NMR studies.

With regard to the configuration around the metal of complex **1b** (S_M, $R_{(N-H)}$), we assume the following decreasing priority sequence: 1 (η^5-C_5Me_5), 2 (Cl), 3 (N_{aryl}), 4 (N-H) [46]. The determination of the metal configuration is important in order to understand the TH activities and selectivity [46]. Strong 1D NOE cross interaction of the signals Ph/CH_2 and Cp*/CH_2 are observed in complexes **1b** and **4b**, which strongly indicates that the metal configuration is S_m. This means that the (S_M, R_{N-H}) diastereomer exists as a major diastereomer in solution compared to the (R_M, S_{N-H}) minor diastereomer [45]. Moreover, no conversion of (R_M, S_{N-H} / S_M, R_{N-H}) to (S_M, S_{N-H} / R_M, R_{N-H}) was observed in solution by ^{1}H NMR at room temperature over 24 hours. This observation indicates that the absolute configuration around the metal center remains unchanged in solution, which is important for asymmetric TH reactions [29]. A similar stereochemistry was observed for the rest of the complexes.

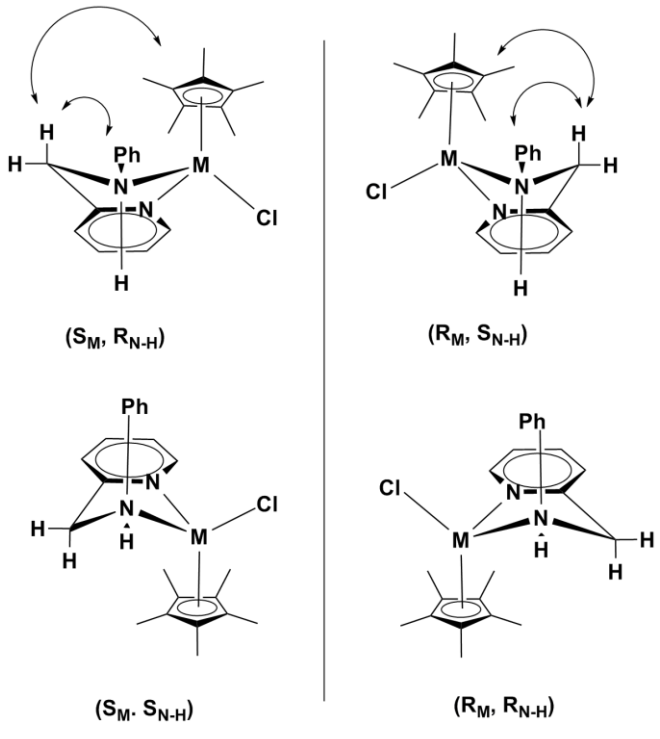

Scheme 3.2: Possible conformations of the complexes **1b** and **4b**. For clarity, the charges on the complex and counter ion PF_6 were omitted.

Table 3.2 Proportions of the diasteromers present in the complexes **1b**-**6b** [a]

Complex	Major isomer (%)	Minor isomer (%)
1	73	27
2	64	36
3	70	30
4	72	28
5	66	34
6	65	35

[a] Determined by ^{1}H NMR in DMSO-d_6 at ambient temperature as per distinct signal of Cp* peaks of both isomers

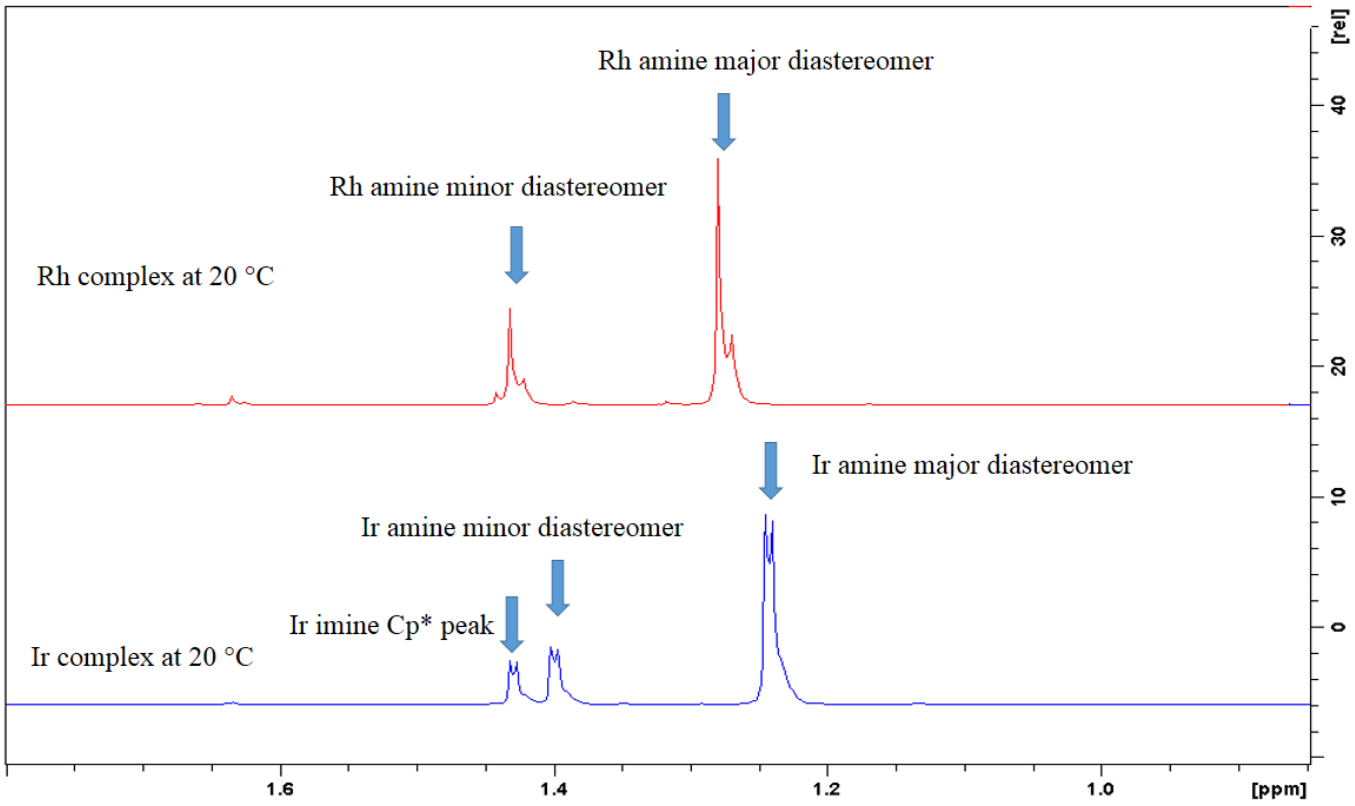

Fig. 3.1 ^{1}H NMR spectra showing the Cp* splitting pattern of complexes **1b** (blue) and **4b** (blue) at 20 °C.

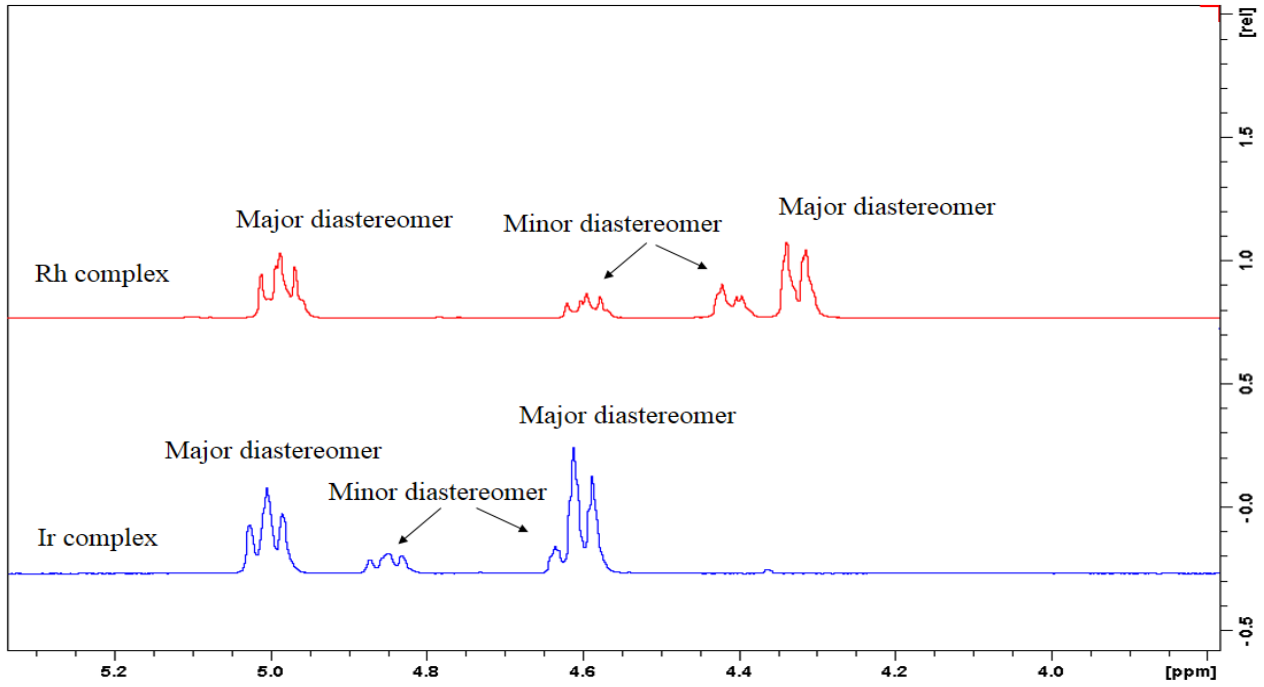

Fig. 3.2 ^{1}H NMR spectra for the CH_2 protons of the complexes **1b** and **4b** at 20 °C.

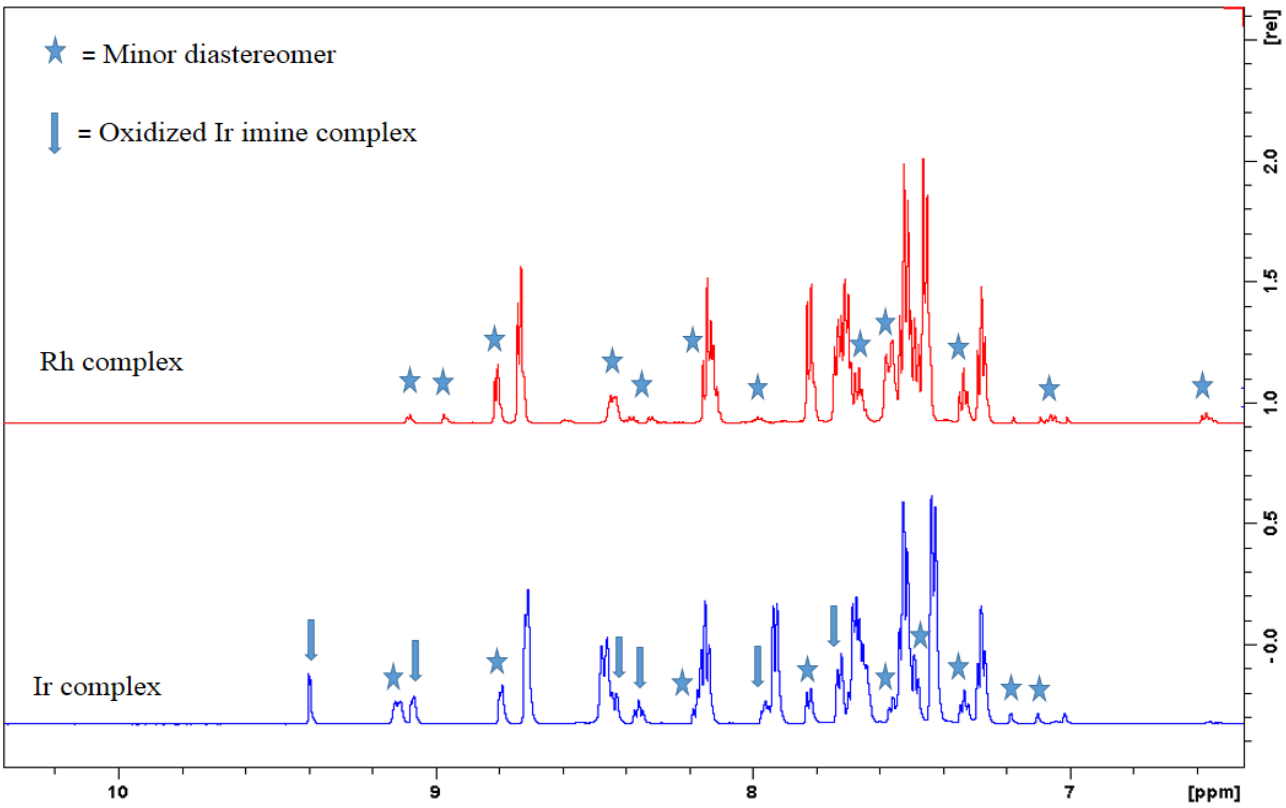

Fig. 3.3 ^{1}H NMR spectra of the aromatic protons of the complexes **1b** and **4b** at 20 °C.

3.3.3 IR spectroscopy

IR spectra of the ligands **L1-L3** exhibit a sharp peak for the N-H stretch in the range 3279 - 3367 cm^{-1}, and the equivalent N-H bands of complexes **1b-6b** were shifted to lower frequencies in the range of 3128 - 3232 cm^{-1}. This is attributed to the nitrogen atom of the N-H group now being coordinated to iridium or rhodium. The PF_6 stretching frequency was observed for all the complexes in the range of 824 - 837 cm^{-1}, which indicates that the PF_6 counter ion is present in the metal complexes. Thus, IR data show that the Schiff base ligands were coordinated to iridium and rhodium through the N,N' nitrogen atoms.

3.3.4 Molecular structure of complex 1b

Single crystal of the (R_M, S_{N-H}) iridium complex **1b** was grown by slow evaporation of hexane into their acetonitrile solution and analyzed by X-ray diffraction. The *ORTEP* drawings for the complex **1b** is shown in Fig. 3.4, while selected bond lengths and bond angles, as well as hydrogen bonds in the crystal, are given in Tables 3.3 and 3.4 for **1b**.

The molecular structure of complex **1b** show the N-(pyridin-2-ylmethyl) aniline ligand which coordinated to the Ir(III) center via it is two N atoms in a bidentate manner forming five member metallacycles. The geometries around the two metal centers of complex is pseudooctahedral in which the two N atoms and a Cl atom form the base, while the π-bonds of the Cp* ring form the apex of a piano stool. The average Ir-Cp* centroid bond distances is 1.785 (Å), while the Ir-N_{amine}, Ir-N1 and Ir-Cl bond distances are 2.167(16), 2.112(17) and 2.405(6) (Å) respectively and fall within the expected ranges of related compounds [8, 17, 20, 27, 43, 47]. The Ir-amine bond is relatively longer than that of the Ir-N_{aryl} bond. H_{11a} is in a *syn*-position to the N-H proton, while H_{11b} is in an *anti*-position to the N-H proton based on the torsion angles involving the two protons, H-C(11)-N(2)-H_{11a} and H-C(11)-N(2)-H_{11b} (-57.12° and -177.28°) respectively, as observed also by coupling constants shown in the ^{1}H NMR.

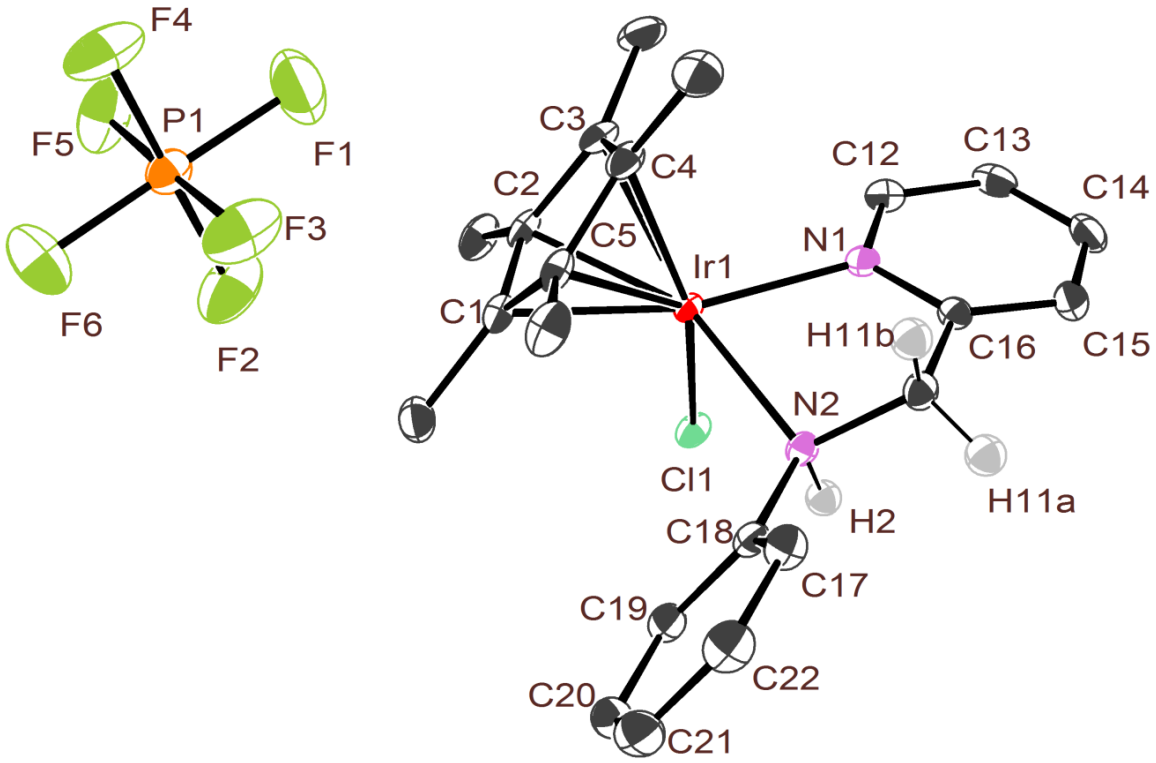

Fig. 3.4 *ORTEP* view of the complex **1b** with atom numbering scheme. Displacement of the ellipsoids are drawn at the 50% probability level.

Table 3.3 Selected bond distances (Å), bond angles (°) and torsion angles (°) of complex **1b**

Selected bond distances (Å)		**Selected bond angles (°)**	
N(1) – Ir(1)	2.112(17)	Cp* Centroid – Ir(1) – N(2)	135.53
N(2) – Ir(1)	2.167(16)	**Torsion angles (°)**	
Cl(1) – Ir(1)	2.405(5)	H_{11a} – C(11) – N(2) - H	-57.12
Cp* centroid – Ir(1)	1.785	H_{11b} – C(11) – N(2) - H	-177.28
Selected bond angles (°)		H_{11a} – C(16) – N(1)	156.05
N(1) – Ir(1) – N(2)	75.40(6)	H_{11b} – C(16) – N(1)	-83.82
N(1) – Ir(1) – Cl(1)	85.73(5)	H – N(2) – Ir(1) – N(1)	-75.42
N(2) – Ir(1) – Cl(1)	83.56(5)	H – N(2) – Ir(1) – Cl(1)	11.82
Cp* Centroid – Ir(1) - Cl	165.70	Ir(1) – N(1) – C(16) – C(11)	-6.11
Cp* Centroid – Ir(1) – N(l)	105.22	Ir(1) – N(2) – C(11) – C(16)	-47.41

Table 3.4 Hydrogen bonds present in the complex **1b**

C-H···F	**D-H (Å)**	**H···A (Å)**	**D···A (Å)**	**D-H···A (º)**
N(2)-H(2) ···Cl(1)	1.00	2.34	3.2032(17)	144
Cl(1)-H(11b) ···F(3)	0.99	2.46	3.424(3)	164
C(15)-H(15) ···F(5)	0.95	2.42	3.112(3)	129
N(2)-H(2) ···Cl(1)	1.00	2.34	3.2032(17)	144
Cl(1)-H(11b) ···F(3)	0.99	2.46	3.424(3)	164
C(15)-H(15) ···F(5)	0.95	2.42	3.112(3)	129

3.3.5 Catalytic activity studies

3.3.5.1 Transfer hydrogenation (TH) of aromatic ketones and aldehydes

The synthesised Ir(III) and Rh(III) amine half sandwich complexes were investigated for catalytic transfer hydrogenation (TH) of aromatic ketones and aldehydes under pH dependent reaction conditions in water as a solvent (Table 3.5).

The experiments were carried out using a mixture of acetophenone, catalyst and an aqueous solution of HCOOH / HCOONa in water and were heated to the required temperature. A HCOOH / HCOONa mixture was used as hydrogen source and base for this catalytic TH, to create an environmentally benign process. The catalyst loading was also optimized at different pH in water. As seen from the results, aromatic ketones required a higher catalyst loading (0.5 mol%, Table 3.5) than aromatic aldehydes (0.1 mol%, Table 3.6), likely due to the steric hindrance of the methyl group. Low pH reaction conditions may increase the activation of ketones by hydrogen bonding with the highly acidic N-H proton in the catalyst through a six numbered transition state [2, 48] (Scheme 3.3). However, at low pH the reaction rate of the postulated metal-hydride intermediate was also expected to be fast. Thus low pH reaction conditions offer a wide range of substrate scope in TH.

The complexes **1b** and **4b** were investigated as pre-catalysts for catalytic TH to establish the optimized reaction conditions. The different aqueous pH reaction conditions *vs* acetophenone conversions are summarized in Table 3.5. The pH of the aqueous solutions was changed by varying the quantity of HCOONa. No conversion of acetophenone was achieved without catalysts **1b** and **4b**. In buffer solutions at pH = 2.60, the reduction of acetophenone took longer at 40 ºC with 0.1 and 0.5 mol% catalyst loading of **1b** or **4b** compared to the reaction at 60 ºC (Entries 1-4 & 13-16). The complexes **1b** and **4b** showed better catalytic activity at the lower pH of 2.60 compared to a pH of 3.60 and 4.60 in aqueous solution of

HCOOH / HCOONa with 0.5 mol% catalyst loading at 60 °C (Entries 4, 5, 6, 16, 17 & 18). Overall, at pH = 2.60, 99% of acetophenone conversion was achieved within an hour by complex **4b** (Entry 16).

Other hydrogen sources also examined for acetophenone reduction under different reaction conditions. The complexes **1b** and **4b** showed poor conversion (26 & 28%) of acetophenone in HCOOH and Et_3N azotropic mixture over 48 h at 60 °C (Entries 7 & 19). With isopropyl alcohol and KOH as base, complexes **1b** and **4b** showed 98 and 93% conversion of acetophenone respectively, but this system required longer reaction times (4 h) and higher catalyst loading (2 mol%) than the HCOOH / HCOONa system (0.5 mol%) (Entries 12 & 24).

Under the acidic conditions (pH = 2.60 to 4.60) the aromatic carbonyl compounds reduced faster than under basic conditions with complexes **1b** and **4b**. The complexes **1b** and **4b** decomposed under the basic conditions (pH = 8.70), which is indicated by the formation of a black precipitate in the reaction mixture (Entries 8, 9, 20 & 21). It can be seen that TH of acetophenone smoothly increased with decreasing pH values with 0.5 mol% catalyst loading (Entries 4-6 & 16-18). In the presence of the Rh complex **4b** (0.5 mol%), acetophenone was reduced completely (99%) in aqueous pH = 2.60 solution of HCOOH / HCOONa at 60 ºC (Entry 16). Complexes Ir(III) and Rh(III) (**2b**, **3b**, **5b** & **6b**) with electron donating (OCH_3) and withdrawing groups (F) substituted on the ligand showed the best conversion (96, 95, 98 & 99%) of acetophenone to 1-phenyl ethanol with 0.5 mol% catalyst loading (Entries 25-28) under aqueous pH = 2.60 reaction conditions.

The Ir(III) complexes (**1b**-**3b**) normally required longer reaction times (4 to 6 h) than the Rh(III) complexes (**4b**-**6b**) under the specified reaction conditions. This is due to the highly acidic N-H proton, which promotes the formation of imine Ir(III) complexes in the reaction medium [37]. The oxidized Ir(III) imine (**1a**) and Rh(III) imine (**2a**) complexes were also synthesized and investigated for the TH of acetophenone (Entries 29 & 30), in order to compare their catalytic activity with the Ir(III) (**1b**) and Rh(III) (**4b**) amine complexes. The oxidized Ir(III) (**1a**) and Rh(III) (**2a**) imine complexes showed 96% and 99% conversion of acetophenone respectively, but this imine complexes required longer reaction times in aqueous pH of 2.60 solution of HCOOH / HCOONa at 60 ºC (Entries 29 & 30). The catalytic activity of the Ir(III) and Rh(III) imine complexes lower than respective amine complexes. However, overall optimization results showed a HCOOH / HCOONa mixture in aqueous solution at pH = 2.60 is an ideal reaction condition for this catalytic system at 60 ºC. These reaction conditions are also applicable for different substituted benzaldehyde derivatives. The chirality of the product was analysed by chiral GC and the ratio of the isomers 49:51 (racemic mixture) were obtained in all the cases (See SI S21-S22).

Table 3.5 Optimization conditions of TH for acetophenone by complexes **1b**-**6b**

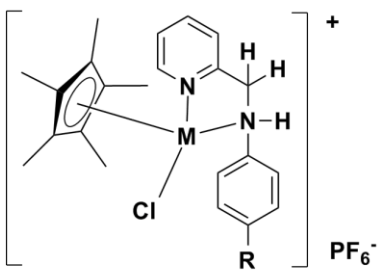

R = H M = Ir (1b); M = Rh (4b)
R = F M = Ir (2b); M = Rh (5b)
R = OCH_3 M = Ir (3b); M = Rh (6b)

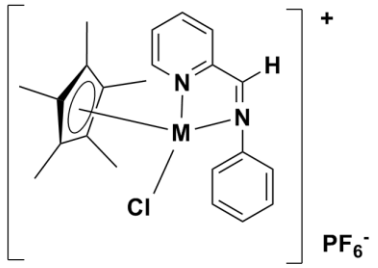

M = Ir (1a); M = Rh (2a)

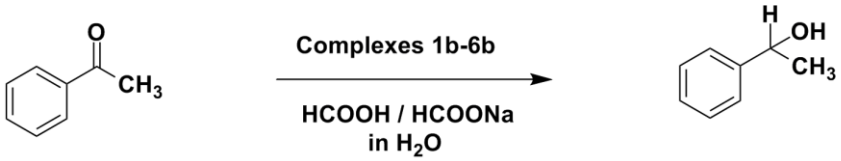

Entry	Complex	Catalyst loading (mol%)	Hydrogen source / Base	Temperature (ºC)	Reaction time (hrs)	Conversion by GC	TON	TOF
1	**1b**	0.1	[a]HCOOH/HCOONa	40	24	28	280	12
2	**1b**	0.1	[a]HCOOH/HCOONa	60	24	30	300	13
3	**1b**	0.5	[a]HCOOH/HCOONa	40	7	88	176	25
4	**1b**	0.5	[a]HCOOH/HCOONa	60	4	96	192	48
5	**1b**	0.5	[b]HCOOH/HCOONa	60	4	90	180	45
6	**1b**	0.5	[c]HCOOH/HCOONa	60	4	73	146	37
7	**1b**	0.5	[d]HCOOH/Et_3N	60	48	26	52	1
8	**1b**	0.5	[e]HCOONa	60	48	12	24	<1
9	**1b**	0.5	[e]HCOONa	100	48	27	54	1
10	**1b**	0.5	[f]IPA/KOH	60	48	25	50	1
11	**1b**	1	[f]IPA/KOH	82	12	87	87	7
12	**1b**	2	[f]IPA/KOH	82	4	98	49	12
13	**4b**	0.1	[a]HCOOH/HCOONa	40	24	44	440	18
14	**4b**	0.1	[a]HCOOH/HCOONa	60	24	47	470	20
15	**4b**	0.5	[a]HCOOH/HCOONa	40	3	98	196	65
16	**4b**	0.5	[a]HCOOH/HCOONa	60	1	99	198	198
17	**4b**	0.5	[b]HCOOH/HCOONa	60	1	92	184	184
18	**4b**	0.5	[c]HCOOH/HCOONa	60	1	80	160	160

19	**4b**	0.5	[d]$HCOOH/Et_3N$	60	48	28	56	1
20	**4b**	0.5	[e]HCOONa	60	48	14	28	1
21	**4b**	0.5	[e]HCOONa	100	48	31	62	1
22	**4b**	0.5	[f]IPA/KOH	60	48	34	68	1
23	**4b**	1	[f]IPA/KOH	82	12	84	84	7
24	**4b**	2	[f]IPA/KOH	82	4	93	47	12
25	**2b**	0.5	[a]HCOOH/HCOONa	60	6	96	192	32
26	**3b**	0.5	[a]HCOOH/HCOONa	60	6	95	190	32
27	**5b**	0.5	[a]HCOOH/HCOONa	60	2	98	196	98
28	**6b**	0.5	[a]HCOOH/HCOONa	60	2	96	192	96
29	[g]**1a**	0.5	[a]HCOOH/HCOONa	60	24	96	192	8
30	[g]**2a**	0.5	[a]HCOOH/HCOONa	60	2	99	198	99

[a] HCOOH (7.50 mmol) / HCOONa (3.50 mmol) in 2 mL H_2O pH = 2.60)

[b] HCOOH (7.50 mmol) / HCOONa (11.0 mmol) in 2 mL H_2O pH = 3.60)

[c] HCOOH (7.50 mmol) / HCOONa (29.0 mmol) in 2 mL H_2O pH = 4.60)

[d] Azeotropic mixture (0.2 mL / 1 mL of F/T)

[e] HCOONa (5.0 mmol) in 2 mL H_2O pH = 8.70

[f] IPA (5 mL), KOH (5.0 mol%) (where IPA = isopropyl alcohol)

[g] **1a** = Ir(III) imine complex; **2a** = Rh(III) imine complex

Turnover number (TON) = [(mol of product)/(mol of catalyst)]

Turnover frequency (TOF) = [TON/h]

From the optimization results, the rhodium complexes **4b** and **2a** showed the best conversion of acetophenone in the aqueous HCOOH / HCOONa mixture at pH = 2.60 at 60 °C. This reaction condition was investigated for further substituted acetophenone derivatives (Table 3.6). Generally, the electronic nature of the aromatic ring present on the substrate plays a big role in TH reactions. Generally, the electron-withdrawing groups (4-NO_2, 4-F & 4-Cl) on the acetophenone ring promotes the reaction rate of TH reactions rather than electron-donating groups (4-I, 4-OMe & 4-Me) under pH dependent reaction conditions [5, 21]. This is also observed here, where substrates with *p*-electron-withdrawing substituents (Table 3.6, Entries 1-4) were more easily reduced than substrates with *p*-electron-donating groups (Table 3.6, Entries 5-7) on the acetophenone. Both rhodium amine (**4b**) and imine (**2a**) complexes reduced acetophenone derivatives with good yield under aqueous reaction conditions (Table 3.6). But generally rhodium amine (**4b**) complex is reduced acetophenone derivatives faster than the respective rhodium imine (**2a**) complex.

Table 3.6 Transfer hydrogenation of aromatic ketones by complexes **4b** and **2a**[a]

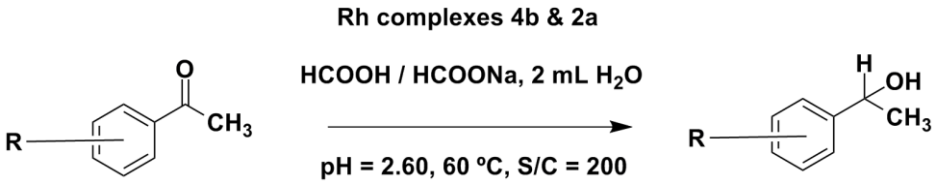

Entry	Substrate	Complex	Reaction time (hrs)	Conversion [b]	TON	TOF
1	Acetophenone	**4b**	1	99 (96)	198	198
		2a	2	99 (94)	198	99
2	4-NO_2 acetophenone	**4b**	1	99	198	198
		2a	2	99	198	99
3	4-F acetophenone	**4b**	2	99 (93)	198	99
		2a	2	100 (95)	200	100
4	4-Cl acetophenone	**4b**	2	100	200	100
		2a	6	92	184	31
5	4-I acetophenone	**4b**	24	54	108	5
		2a	24	50	100	4
6	4-OMe acetophenone	**4b**	5	99 (95)	198	40
		2a	6	98 (92)	196	33
7	4-Me acetophenone	**4b**	8	92	184	23
		2a	14	88	176	13

[a] 1 mmol substrate, 0.5 mol% catalyst, HCOOH (7.50 mmol) / HCOONa (3.50 mmol)

[b] Determined by GC

Isolated yields mentioned in parenthesis

Turnover number (TON) = [(mol of product)/(mol of catalyst)]

Turnover frequency (TOF) = [TON/h]

The rhodium complexes **4b** and **2a** showed efficient TH of aromatic aldehydes to their respective alcohols with lower catalyst loading (S/C = 1000) in the aqueous HCOOH / HCOONa system (Table 3.7). The aromatic aldehydes containing both electron-donating and electron-withdrawing groups reduced to the respective alcohols faster over the rhodium amine (4b) and imine (**2a**) complexes compared to the benzaldehyde substrate (Table 3.6). Thus, rhodium complexes **4b** and **2a** showed versatile reducing activity for the aromatic ketones and aldehydes. The catalytic loading (0.1 mol%) equivalent for effective aromatic aldehyde TH is lower than that required for aromatic ketones (0.5 mol%). Overall the studies

demonstrated that the rhodium amine **4b** and imine **2a** complexes reduced aromatic ketones and aldehydes to their respective alcohols faster than the iridium complexes.

A possible reduction reaction pathway for rhodium catalyzed TH is explained in Scheme 3.3 [3, 13]. Metal catalyzed transfer hydrogenation of aromatic ketones in aqueous solution is a well documented process [2, 3, 13, 30]. In the reaction mechanism, β-hydride elimination occurs to form a metal hydride complex, which interacts with the carbonyl group of acetophenone to form a six membered transition state as per Noyori's proposal [13]. Thus, the further reduction takes place and gives the final product of 1-phenyl ethanol.

Table 3.7 Transfer hydrogenation of aromatic aldehydes by complexes **4b** and **2a**[a]

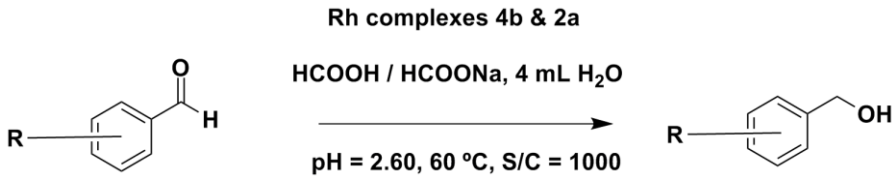

Entry	Substrate	Complex	Reaction time (hrs)	Yield [b]	TON	TOF
1	Benzaldehyde	**4b**	2.5	94	940	376
		2a	4	96	960	240
2	4-NO_2 benzaldehyde	**4b**	1	94	940	940
		2a	1.5	92	920	613
3	4-F benzaldehyde	**4b**	1	96	960	960
		2a	2	93	930	465
4	4-Cl benzaldehyde	**4b**	1	92	920	920
		2a	3	94	940	313
5	4-OMe benzaldehyde	**4b**	1	93	930	930
		2a	2	90	900	450
6	4-Me benzaldehyde	**4b**	1	91	910	910
		2a	3	87	870	290

[a] 5 mmol substrate, 0.5 mol% catalyst, HCOOH (15.0 mmol) / HCOONa (7.0 mmol)

[b] Isolated yields

Turnover number (TON) = [(mol of product)/(mol of catalyst)]

Turnover frequency = [TON/h]

3.3.6 Recyclability of the catalyst 4b

One important feature of this system is that the catalyst can be recovered due to easy organic layer separation of the catalyst from the aqueous reaction medium. The upper organic layer was extracted with ethylacetate and the solvent was removed by vacuum distillation. The obtained residue was treated with diethylether to precipitate the catalyst. A sticky solid was obtained, which was dried under vacuum overnight and examined by ^{1}H NMR. The ^{1}H NMR analysis of the fresh, recovered and recovered catalyst **4b** after 3rd cycle in DMSO-d_6 is shown in Fig. 3.6. The ^{1}H NMR spectra of the recovered catalyst **4b** show all the characteristic peaks present for the fresh catalyst **4b**.

The catalytic activity of the recovered catalyst **4b** was examined for TH of acetophenone (Table 3.8). The recovered catalyst **4b** showed similar conversion of acetophenone in 1 h for the 1st recycle, no significant loss in the catalytic activity was observed (Table 3.8, Entry 2). To achieve a similar conversion, took 1.5 h on the 2nd recycle (Table 3.8, Entry 3). However, it required 5 h to achieve this conversion in the 3rd recycle (Table 3.8, Entry 4). This decrease in catalytic activity is due to the partial decomposition of catalyst in the reaction mixture, which is supported by the ^{1}H NMR spectra of the recovered catalyst after the third catalytic cycle (Fig. 3.6).

Table 3.8 Catalytic activity of the recovered catalyst **4b** [a]

Entry	Catalytic recycle	Substrate	Conversion [b]	Reaction time (hrs)
1	Fresh catalyst	Acetophenone	99	1
2	1st	Acetophenone	98	1
3	2nd	Acetophenone	96	1.5
4	3rd	Acetophenone	95	5

[a] 1 mmol substrate, 0.5 mol% recovered catalyst, HCOOH (7.50 mmol) / HCOONa (3.50 mmol) in 2 mL H_2O at 60 °C

[b] Determined by GC

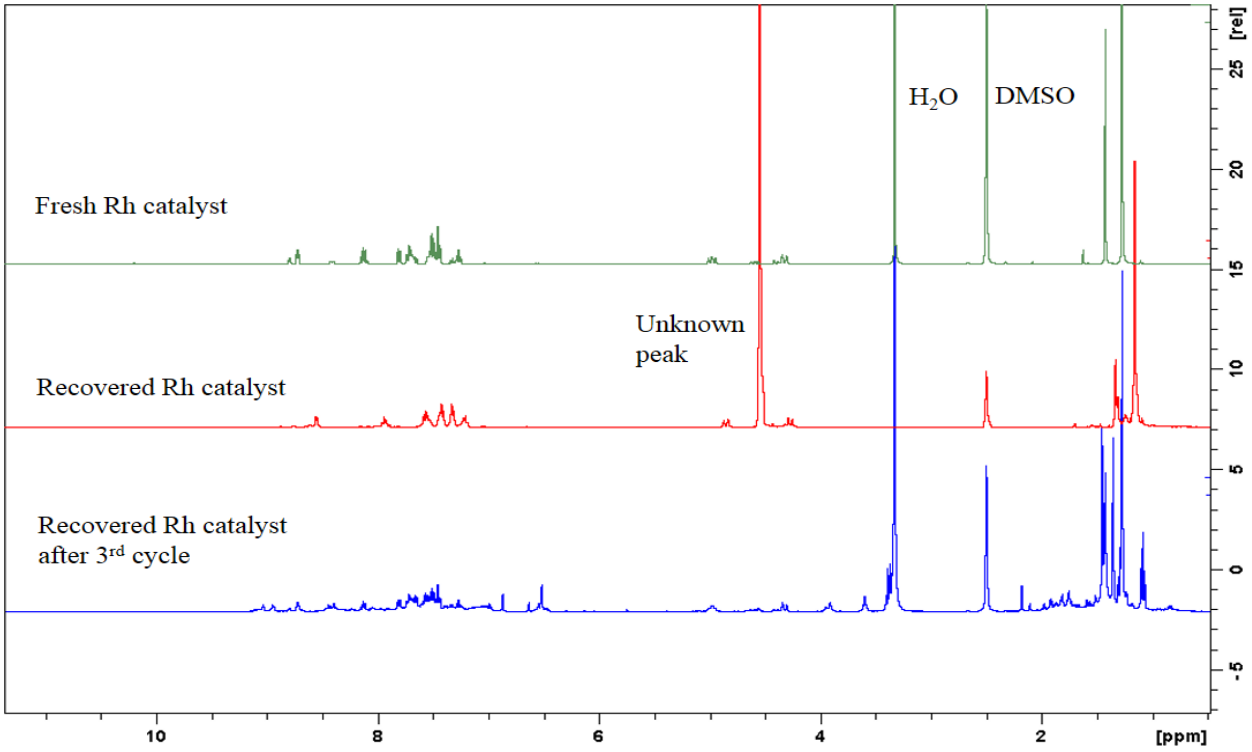

Fig. 3.5 ^{1}H NMR spectra of the fresh, recovered and recovered catalyst **4b** after 3rd cycle in DMSO-d_6.

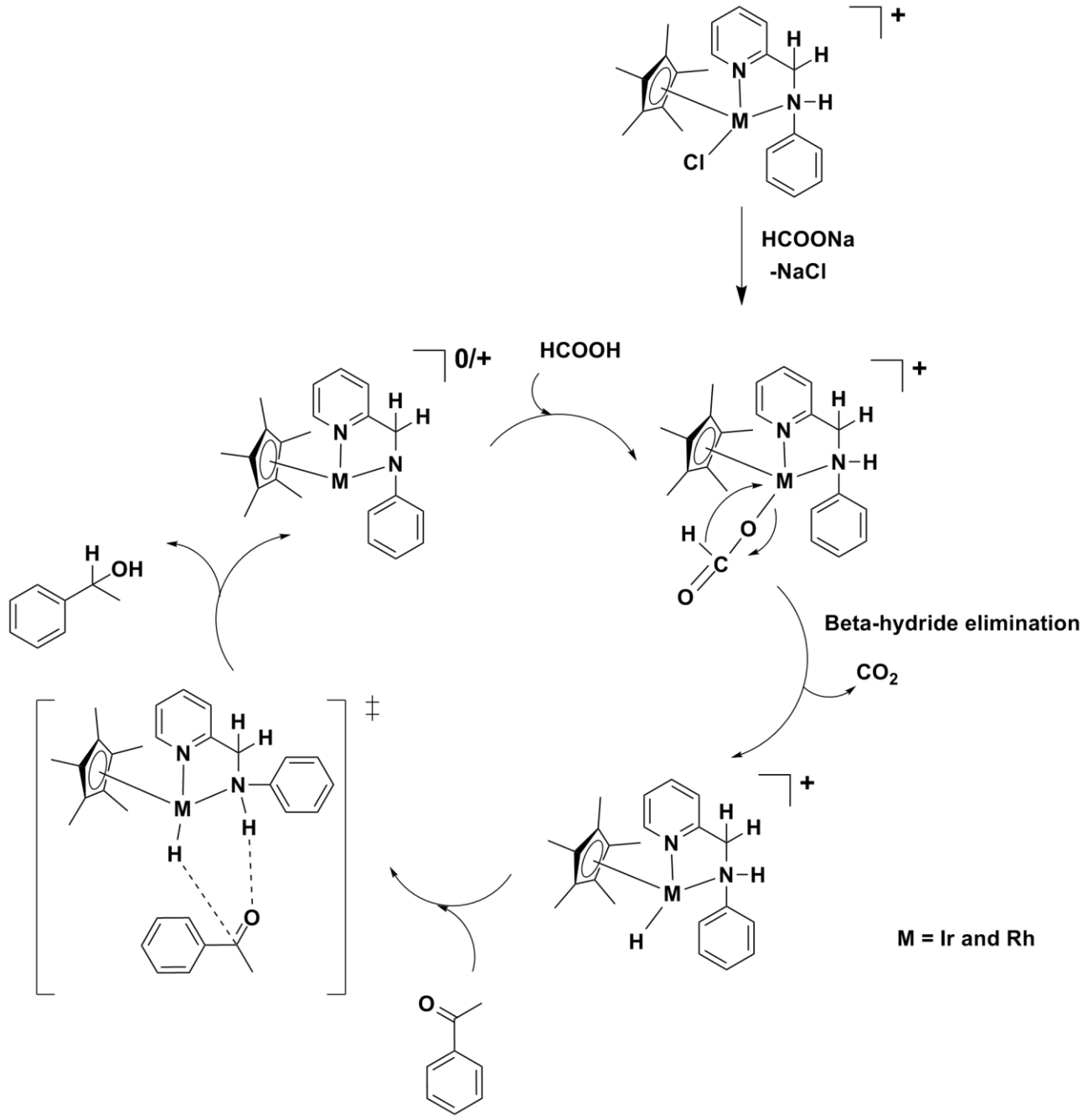

Scheme 3.3: Proposed reaction mechanism for the TH of aromatic ketones.

3.4 Conclusions

In conclusion, new half sandwich Ir(III) and Rh(III) complexes were synthesized and characterized. The crystal structure further confirms that the iridium **1b** exhibited a pseudooctahedral geometry. Solution NMR studies revealed that the iridium and rhodium complexes are diasteromers in solution. It was further confirmed that the (R_M, S_{N-H}) diastereomer exists as the major diastereomer in solution compared to the minor (S_M, R_{N-H}) diastereomer. Interestingly, we indentified the cross interactions between the CH_2 to Cp* moiety as well as CH_2 to phenyl ring by 1D NOE NMR studies.

The catalytic activity of the Ir(III) and Rh(III) amine complexes in the TH of aromatic ketones and aldehydes was demonstrated in water, with no need of organic solvents. Among the complexes, the rhodium amine **4b** and imine **2a** complexes in an aqueous HCOOH and HCOONa mixture at pH = 2.60 at 60 °C showed the best catalytic activity for the TH reactions. These catalysts achieved good TON for TH of aromatic ketones (200 / 200) and aldehydes (960 / 1000) under optimized reaction conditions. The highly acidic N-H proton present in the rhodium amine complex facilitated the TH of aromatic ketones and aldehydes more effectively. The aromatic aldehydes normally required lower catalyst loading (S/C = 1000) than aromatic ketones (S/C = 200) for effective TH reactions under the specified reaction conditions. The recovered catalyst showed good catalytic activity up to three catalytic recycles. These studies offer new possibilites for developing versatile catalysts for catalytic TH and other applications in water or organic solvents.

Acknowledgements

Authors would like to thank the NRF, THRIP (Grant no. TP 1208035643) and the University of KwaZulu - Natal, Durban, South Africa for financial support.

Appendix A. Supplementary Information

The ^{1}H and ^{13}C NMR, 2D NMR, NMR stability data, 1D NOE analysis and crystal data of the complexes are also shown in the SI.

References

[1] S. Hashiguchi, A. Fujii, J. Takehara, T. Ikariya, R. Noyori, J. Am. Chem. Soc. 117 (1995) 7562-7563.

[2] X. Wu, X. Li, F. King, J. Xiao, Angew. Chem. Int. Ed. Engl. 44 (2005) 3407-3411.

[3] X. Li, X. Wu, W. Chen, F.E. Hancock, F. King, J. Xiao, Org. Lett. 6 (2004) 3321-3324.

[4] W. Du, P. Wu, Q. Wang, Z. Yu, Organometallics 32 (2013) 3083-3090.

[5] Y. Wei, D. Xue, Q. Lei, C. Wang, J. Xiao, Green Chem. 15 (2013) 629-634.

[6] C.-Y. Huang, K.-Y. Kuan, Y.-H. Liu, S.-M. Peng, S.-T. Liu, Organometallics 33 (2014) 2831-2836.

[7] S.V. Slungård, T.-A. Krakeli, T.H.K. Thvedt, E. Fuglseth, E. Sundby, B.H. Hoff, Tetrahedron 67 (2011) 5642-5650.

[8] O. Prakash, H. Joshi, K.N. Sharma, P.L. Gupta, A.K. Singh, Organometallics 33 (2014) 3804-3812.

[9] A. Azua, J.A. Mata, E. Peris, F. Lamaty, J. Martinez, E. Colacino, Organometallics 31 (2012) 3911-3919.

[10] X. Zhou, X. Wu, B. Yang, J. Xiao, J. Mol. Catal. A: Chem. 357 (2012) 133-140.

[11] R. Noyori, C.A. Sandoval, K. Muniz, T. Ohkuma, Philos. Trans. Ser. A, Mathematical, physical, and engineering sciences 363 (2005) 901-912; discussion 1035-1040.

[12] S. Hashiguchi, A. Fujii, K.-J. Haack, K. Matsumura, T. Ikariya, R. Noyori, Angew. Chem. Int. Ed. Engl. 36 (1997) 288-290.

[13] R. Noyori, S. Hashiguchi, Acc. Chem. Res. 30 (1997) 97-102.

[14] N. Uematsu, A. Fujii, S. Hashiguchi, T. Ikariya, R. Noyori, J. Am. Chem. Soc. 118 (1996) 4916-4917.

[15] P. Singh, A.K. Singh, Organometallics 29 (2010) 6433-6442.

[16] O.R. Allen, L.D. Field, A.M. Magill, K.Q. Vuong, M.M. Bhadbhade, S.J. Dalgarno, Organometallics 30 (2011) 6433-6440.

[17] O. Prakash, K.N. Sharma, H. Joshi, P.L. Gupta, A.K. Singh, Dalton Trans. 42 (2013) 8736-8747.

[18] T. Marimuthu, H.B. Friedrich, ChemCatChem 4 (2012) 2090-2095.

[19] D. Talwar, N.P. Salguero, C.M. Robertson, J. Xiao, Chem. Eur. J. 20 (2014) 245-252.

[20] M. Yadav, A.K. Singh, D.S. Pandey, Organometallics 28 (2009) 4713-4723.

[21] X. Wu, D. Vinci, T. Ikariya, J. Xiao, Chem. Commun. (2005) 4447-4449.

[22] G. Kang, S. Lin, A. Shiwakoti, B. Ni, Catal. Commun. 57 (2014) 111-114.

[23] F. Gao, R. Jin, D. Zhang, Q. Liang, Q. Ye, G. Liu, Green Chem. 15 (2013) 2208-2214.

[24] Y.-M. He, Q.-H. Fan, ChemCatChem 7 (2015) 398-400.

[25] S. Kuwata, T. Ikariya, Chem. Eur. J. 17 (2011) 3542-3556.

[26] F. Zeng, Z. Yu, Organometallics 28 (2009) 1855-1862.

[27] E. Féghali, L. Barloy, J.-T. Issenhuth, L. Karmazin-Brelot, C. Bailly, M. Pfeffer, Organometallics 32 (2013) 6186-6194.

[28] T. Ikariya, A.J. Blacker, Acc. Chem. Res. 40 (2007) 1300-1308.

[29] M.-M. Wei, M. García-Melchor, J.-C. Daran, C. Audin, A. Lledós, R. Poli, E. Deydier, E. Manoury, Organometallics 31 (2012) 6669-6680.

[30] S. Ogo, T. Abura, Y. Watanabe, Organometallics 21 (2002) 2964-2969.

[31] S. Ogo, N. Makihara, Y. Watanabe, Organometallics 18 (1999) 5470-5474.

[32] H. Zhang, R. Jin, H. Yao, S. Tang, J. Zhuang, G. Liu, H. Li, Chem. Commun. 48 (2012) 7874-7876.

[33] D.D.A. Perrin, W. L. F.; Perrin, D. R, Purification of laboratory chemicals, Pergamon: Oxford, UK, 1986.

[34] S.J. Dickson, M.J. Paterson, C.E. Willans, K.M. Anderson, J.W. Steed, Chem. Eur. J. 14 (2008) 7296-7305.

[35] R. Lenz, S. V. Ley, J. Chem. Soc., Perkin Trans. 1. (1997) 3291-3292.

[36] C. White, A. Yates, P.M. Maitlis, Inorg. Synth. 29 (1992) 228-234.

[37] J. Gómez, G. García-Herbosa, J.V. Cuevas, A. Arnáiz, A. Carbayo, A. Muñoz, L. Falvello, P.E. Fanwick, Inorg. Chem. 45 (2006) 2483-2493.

[38] P. Govindaswamy, Y.A. Mozharivskyj, M.R. Kollipara, Polyhedron 24 (2005) 1710-1716.

[39] Bruker-AXS, Bruker-AXS, Madison, Wisconsin, USA, 2009.

[40] G.M.Sheldrick, Acta. Crystallogr. A64 (2008) 112-122.

[41] L. J. Farrugia, *ORTEP-3* for Windows. J. Appl. Crystallogr. 30 (1997) 565.

[42] C.F. Macrae, P.R. Edgington, P. McCabe, E. Pidcock, G.P. Shields, R. Taylor, M. Towler, J. van de Streek, J. Appl. Crystallogr. 39 (2006) 453-457.

[43] L. Barloy, J.-T. Issenhuth, M.G. Weaver, N. Pannetier, C. Sirlin, M. Pfeffer, Organometallics 30 (2011) 1168-1174.

[44] H. Nakai, T. Nonaka, Y. Miyano, M. Mizuno, Y. Ozawa, K. Toriumi, N. Koga, T. Nishioka, M. Irie, K. Isobe, J. Am. Chem. Soc. 130 (2008) 17836-17845.

[45] J.-B. Sortais, N. Pannetier, N. Clément, L. Barloy, C. Sirlin, M. Pfeffer, N. Kyritsakas, Organometallics 26 (2007) 1868-1874.

[46] J.-B. Sortais, N. Pannetier, A. Holuigue, L. Barloy, C. Sirlin, M. Pfeffer, N. Kyritsakas, Organometallics 26 (2007) 1856-1867.

[47] M. Yadav, A.K. Singh, D.S. Pandey, J. Organomet. Chem. 696 (2011) 758-763.

[48] Y. Huang, V.H. Rawal, J. Am. Chem. Soc. 124 (2002) 9662-9663.

Chapter 4

Synthesis and characterization of new half sandwich Ir(III), Rh(III), Ru(II) and Os(II) complexes: Their biological application on MCF-7 breast cancer cells

Abstract

A new carbazole N,N' ligand containing [(η^5-C_5Me_5)MCl(**L**)]PF_6, (M = Ir (**1c**) and Rh (**2c**)) and [(η^6-C_6H_6)RuCl(**L**)]PF_6 (**3c**), [(η^6-*p*-cymene)RuX(**L**)]PF_6 (X = Cl (**4**), Br (**5c**), I (**6c**)), [(η^6-C_6H_6)OsCl(**L**)]PF_6 (**7**), [(η^6-*p*-cymene)OsX(**L**)]PF_6 X = Cl (**8c**), I (**9c**)) (**L** = 9-ethyl-N-(pyridine-2-yl methylene)-9H-carbazole-3-amine) complexes have been synthesized and characterized by ^{1}H NMR, ^{13}C NMR, 2D NMR, melting point analysis, infrared spectroscopy, HR-MS and elemental analyses. The structures of the **3c** and **6c** have been determined by single crystal XRD. Anticancer study of the synthesized complexes **1c**-**3c** clearly showed them as potent inhibitors of human breast cancer cells (MCF-7) under *in vitro* conditions. The inhibitory concentrations (IC_{50}) of complexes **1c**-**3c** were determined at low (5, 6 and 8 μM) concentration against the MCF-7 human breast cancer cell line. Further cytotoxic, cell cycle and nuclear studies confirmed that the novel half sandwich Ir(III), Rh(III) and Ru(II) complexes could be effective against MCF-7 human breast cancer cell proliferation. Moreover the results indicate that anticancer *in vitro* activity of complexes **1c**-**3c** follows the order of **1c** > **2c** > **3c**. Molecular docking study of the complexes **1c**-**3c** showed the nature of binding energy, H-bond and hydrophobic interactions with the COX-2 receptor.

Keywords: Half sandwich complexes; MCF-7 cancer cell line; cytotoxicity; cell morphology; molecular docking

4.1 Introduction

Since the remarkable discovery of cis-platin for anticancer treatment, metal mediated anticancer drugs have received great attention in the treatment of various types of cancers for chemotherapeutic studies [1, 2]. Various platinum based metallo-drugs, such as carboplatin and oxalioplatin [3, 4] are available. Toxicity, side effects and platinum drug resistance of living cells lead to the discovery and

design of novel organometallic drugs for the therapeutic treatment of cancer. To replace the classic platinum based metallodrugs, various transition metals have been investigated to identify suitable metallodrugs for *in vitro* and *in vivo* anticancer studies [5, 6]. For example, Zeglis *et al*. developed Cu(II) complexes containing α-heterocyclic-N^4-substituted thiosemicarbazone ligands promoting excellent topoisomerase-IIα inhibition and antiproliferative activity [7]. Among the transition metals, ruthenium metal based metallodrugs KP1019 (indazolium trans-[tetrachloridobis(1H-indazole)ruthenate(III)] and NAMI-A (imidazolium trans-[tetrachlorido(dimethyl sulfoxide)(1H-imidazole)ruthenate-(III)]) showed high antitumor activity under *in vitro* and *in vivo* conditions in clinical trials [8, 9]. Recently arene scaffold modified ruthenium(II)-arene PTA complexes RAPTA-C [(Ru(η^6-*p-cymene*)Cl_2(PTA)], RAPTA-T [(Ru(η^6-*p-toluene)*Cl_2(PTA)] (where PTA = 1,3,5-triaza-7-phosphaadamantane), DAPTA-C [(Ru(η^6-*p-cymene*)Cl_2(DAPTA)], and DAPTA-T [(Ru(η^6-*p-toluene)*Cl_2(DAPTA)] (where DAPTA = 3,7 diacetyl-1, 3, 7-triaza-5-phosphabicyclo[3.3.1]nonane) showed low toxicity profiles and antiproliferative effects in endothelial cells [10]. In recent years, organometallic half sandwich octahedral low spin d^6 metal complexes have been of great interest in chemotherapeutic studies because of the hydrophilic and hydrophobic nature of carbon bound π bonded arenes and the cyclopentadienyl moieties respectively. This arene and cyclopentadienyl moieties emerged as versatile tool to develop novel compounds for antitumor activity studies, which is responsible for cell intake, targeting and kinetic inertness of the complexes [11, 12].

The half sandwich [(η^6-arene)M(LL)X][Z] (M = Ru or Os, LL = ethylenediamine or acetylacetonate (Ru), LL = N-(2-pyridylmethylene)-(S)-1-phenylethylamine or N-(2-pyridylmethylene)-(R)-1-phenylethylamine (Os), X = Cl^- (Ru), I^- (Os), and Z = counter ion) complexes exhibit excellent anti-cancer activities and their activities were in some cases found to be higher than those of cis-platin and carbo-platin [13-15]. Recently, half sandwich and cyclometalated isoelectronic Ir(III) complexes containing a pentamethylcyclopentadienyl (Cp*) stabilizing moiety were found to exhibit high antitumor activity against human ovarian A2780 due to their rapid hydrolysis in solution and direct binding to DNA nucleobases, which is accompanied by Cp* intercalation between the nucleobases like 9-ethylguanine and 9-methyladenine [16, 17].

The N,N' chelating donor ligands containing Cp*Ir(III), Cp*Rh(III) and (η^6–arene)Ru(II) half sandwich complexes exhibit a wide range of applications in bio-organometllic chemistry due to their air stability, rapid hydrolysis, cell accumulation, hydrophobicity, effective distribution within cells, intercalation with DNA and anticancer activity [16, 18]. Furthermore, recently reported C,N cyclometalated Cp*Ir(III), Cp*Rh(III) and (η^6-arene)Ru(II) complexes containing novel benzimidazole

chelating ligands exhibit anticancer activities against HT29, T47D, A2780 and A2780cisR cancer cell lines which were almost comparable to that of the cis-platin drug [19].

The 5H-benzo*[b]*carbazoles, 3,6-dibromocarbazole piperazine, 9-hydroxy-5,6-dimethyl-6H-pyrido[4,3-*b*]carbazole-1-carboxylic acid (2-(dimethylamino)ethyl)amide and their derivatives exhibit various biological activities in chemotherapeutic studies, such as antitumor, inhibition of cytochrome *c*, inhibition of DNA topoisomerase II and intercalation into DNA. The carbazole core moiety present, 9-hydroxy-2-methylellipticinium acetate III (ellipticinium), has been used for osteolytic metastases of breast cancer [20-24]. There are a number of carbazole based drugs reported in literature, such as carvedilol for antioxidative [25], P7C3 for neuroprotective [26], carbazomycin B for antibiotic [27], caprofen for anti-inflammatory [28] activity and carbazomadurin A as a neuronal cell-protecting agent [29]. These biological applications of carbazole moiety drugs influenced us to synthesize and evaluate the anticancer activity of new metal carbazole complexes. This work describes the synthesis and characterization of new N,N' carbazole chelating ligand containing compounds $[(\eta^5\text{-}C_5Me_5)M(III)(L)]PF_6$ (M = Ir (**1c**) and Rh (**2c**)) and $[(\eta^6\text{-}C_6H_6)Ru(II)(L)]PF_6$ (**3c**) and morphological studies on MCF-7 cancer cells using fluorescence and DAPI staining methods, as well as *in vitro* anticancer activity studies against the MCF-7 human breast cancer cell lines. In order to understand the binding interactions of these metal complexes with the COX-2 receptor, molecular docking studies was carried out.

4.2 Experimental Section

4.2.1 Reagents and Methods

Unless otherwise noted, all manipulations were performed using standard Schlenk tube techniques under nitrogen atmosphere. The reagents 2-pyridinecarboxaldehdye, glacial acetic acid, $IrCl_3{\cdot}3H_2O$ (≥99% purity), $RhCl_3{\cdot}3H_2O$ (≥99% purity), hydrated $RuCl_3{\cdot}xH_2O$ (≥99% purity), $OsCl_3{\cdot}xH_2O$ (≥99% purity) and solvents were purchased from Sigma-Aldrich, Capital Labs, South Africa and were used without further purification. The NMR solvent DMSO-d_6 and D_2O was purchased from Merck Germany. The solvents were dried by standard procedures and distilled prior to use [30]. Melting points were recorded on a Stuart™ Scientific apparatus SMP 3 and are uncorrected. Time-dependent ^1H NMR (400 MHz) stability studies and ^{13}C (100 MHz) NMR were recorded in DMSO-d_6 / D_2O and DMSO-d_6 solvent systems respectively using a Bruker Topspin 400 spectrometer. Elemental analyses were performed on a Thermo-Scientific Flash 2000 CHNS/O analyser. Solid and liquid state infrared spectra were recorded using an FT-IR Perkin Elmer Spectrum 100 spectrophotometer between 4000 - 400 cm^{-1}. High resolution mass spectra were recorded using a Waters Micromass LCT Premier TOF-MS instrument. UV-Vis studies were recorded using a Perkin Elmer precisely Lambda35 instrument. X-ray single crystal intensity

data were collected on a Bruker Smart *APEX11* Nonius Kappa-CCD diffractometer using graphite monochromated MoKα radiation (λ = 0.71073 Å). The Eclipse E400 biological microscope (Nikon Eclipse, Inc, Japan) at 400x magnification with an excitation filter at 480 nm used to visualize the MCF-7 cells. The ligand precursor 3-amino-9-ethyl-9*H*-carbazole [31] and metal precursors $(IrCl_2Cp^*)_2$, $(RhCl_2Cp^*)_2$, $[RuX(\eta^6\text{-arene})_2]_2$ (arene = benzene or *p*-cymene, X = Cl or Br or I) and $[OsX(\eta^6\text{-arene})_2]_2$ (arene = benzene or *p*-cymene, X = Cl or I) were prepared according to literature methods [15, 32-35].

4.2.2 Synthesis and Characterization of the ligand and complexes

4.2.2.1 Synthesis procedure for 9-ethyl-N-(pyridine-2-yl methylene)-9H-carbazole-3-amine (L)

A mixture of the 9-ethyl-9H-carbazole-3-amine (2.5 mmol, 530 mg), 2-pyridinecarboxaldehyde (2.5 mmol, 0.25 mL) and 2 drops of the glacial acetic acid in toluene (10 mL) was stirred at room temperature for 24 h. The reaction was monitored by TLC. Once the reaction was completed, diluted $NaHCO_3$ solution was added to the reaction mixture to neutralize the glacial acetic acid. The solvent was distilled off under reduced pressure to leave the crude product. The crude product was dissolved in diethylether (30 mL) and the organic layer was washed with brine solution (15 mL) twice and dried over anhydrous Na_2SO_4. The combined organic layer was concentrated under vacuum and the resulting residue was purified by column chromatography on silica gel [ethyl acetate:n-hexanes] yielding a dark brown oil as the product. Yield (700 mg, 93%). ^{1}H NMR (400 MHz, DMSO-d_6, 25 ºC, ppm) δ = 8.83 (s, 1H, imine CH), 8.73 (d, 1H, $J_{H\text{-}H}$ = 4.72 Hz, α proton of Py), 8.30 (d, 1H, $J_{H\text{-}H}$ = 1.92 Hz, Carb 1st ring), 8.24 (t, 2H, Py & Carb 3rd ring), 7.97 (t, 1H, Py), 7.66 (d, 1H, $J_{H\text{-}H}$ = 8.64 Hz, Carb 1st ring), 7.61 - 7.59 (m, 2H, Carb 1st & 3rd ring), 7.51 - 7.49 (m, 1H, Py), 7.48 (t, 1H, Carb 3rd ring), 7.23 (m, 1H, Carb 3rd ring), 4.47 - 4.42 (q, 2H, N - CH_2), 1.33 (t, 3H, N -CH_3). ^{13}C NMR (100 MHz, DMSO-d_6, 25 °C, ppm) δ = 157.52 (imine C-H), 154.63, 149.58, 136.91, 126.04 (Py), 141.91, 140.14, 138.28, 125.06, 122.77, 122.37, 120.73, 120.70, 120.32, 118.90, 113.29, 109.53, 109.29 (Carb), 37.08 (CH_2, N - CH_2CH_3), 13.69 (CH_3, N - CH_2CH_3). FT-IR (γ/cm^{-1}): 3050, 2974, 2931, 1733, 1581 (s, C=N), 1478 (s), 1469 (s), 1234 (s) 744 (s), 728 (s). UV-Vis (dichloromethane, v/v): λ_{max}(nm) = 242, 291, 321, 377.

4.2.2.2 Synthesis of complexes 1c and 2c

A common procedure was followed to synthesize $[(\eta^5\text{-}C_5Me_5)IrCl(\mathbf{L})]$ (**1c**) and $[(\eta^5\text{-}C_5Me_5)RhCl(\mathbf{L})]$ (**2c**) (L = 9-ethyl-N-(pyridine-2-yl methylene)-9H-carbazole-3-amine). A mixture of $(IrCl_2Cp^*)_2$ (100 mg, 0.13 mmol), the Schiff base carbazole ligand (78 mg, 0.26 mmol) and NH_4PF_6 (41 mg, 0.25 mmol) was stirred at room temperature in methanol (15 mL) for five hours. The orange colored

precipitate separated out and was filtered with filter paper, washed with cold methanol and diethyl ether and dried under vacuum.

4.2.2.3 [(η^5-C_5Me_5)IrCl(**L**)] (**1c**)

Yield (145 mg, 0.18 mmol, 72%). Mp. 287.0 °C (dec.). ^{1}H NMR (400 MHz, DMSO-d_6, 25 ºC, ppm) δ = 9.44 (s, 1H, imine CH), 9.07 (d, 1H, J_{H-H} = 5.44 Hz, α proton of Py), 8.51 (s, 1H, Carb 1st ring), 8.44 (d, 1H, J_{H-H} = 7.48 Hz, Py), 8.37 (t, 1H, Py), 8.17 (d, 1H, J_{H-H} = 7.68 Hz, Carb 3rd ring), 7.96 (t, 1H, Py), 7.87 (s, 2H,Carb 1st ring), 7.74 (d, 1H, J_{H-H} = 8.28 Hz Carb 3rd ring), 7.58 (t, 1H, Carb 3rd ring), 7.32 (t, 1H, Carb 3rd ring), 4.57 - 4.51 (q, 2H, N - CH_2), 1.46 (s, 15H, C_5Me_5), 1.38 (t, 3H, N -CH_3). ^{13}C NMR (100 MHz, DMSO-d_6, 25 °C, ppm) δ = 167.02 (imine C-H), 155.70, 152.28, 140.99, 140.65, 140.51 (Py), 139.74, 130.07, 129.40, 126.83, 121.83, 121.77, 121.01, 120.42, 119.68, 114.68, 109.94, 109.57 (Carb), 89.74 (C, C_5Me_5), 37.36 (CH_2, N - CH_2CH_3), 13.69 (CH_3, N - CH_2CH_3), 8.05 (CH_3, C_5Me_5). FT-IR (γ/cm^{-1}): 3069, 2983, 2941, 1596 (s, C=N), 1479 (s), 1470, 1459, 1231, 826 (s, P-F). HR-MS (TOF MS ES$^+$) $C_{30}H_{32}ClIrN_3$ Calculated: 662.1914, Found: 662.1907. Anal. Calcd for $C_{30}H_{32}ClF_6IrN_3P$: C, 44.64; H, 4.00; N, 5.21; Found: C, 44.59; H, 4.10; N, 5.33.

4.2.2.4 [(η^5-C_5Me_5)RhCl(**L**)] (**2c**)

($RhCl_2Cp^*$)$_2$ (100 mg, 0.16 mmol), Schiff base carbazole ligand (96 mg, 0.32 mmol) and NH_4PF_6 (53 mg, 0.32 mmol). Yield (195 mg, 0.27 mmol, 84%). Mp. 306.0 °C (dec.). ^{1}H NMR (400 MHz, DMSO-d_6, 25 ºC, ppm) δ = 9.08 (d, 1H, J_{H-H} = 5.32 Hz, α proton of Py), 9.05 (s, 1H, imine CH), 8.55 (d, 1H, J_{H-H} = 1.92 Hz, Carb 1st ring), 8.40 (t, 1H, Py), 8.32 (d, 1H, J_{H-H} = 6.88 Hz, Carb 3rd ring), 8.17 (d, 1H, J_{H-H} = 7.76 Hz, Py), 7.97 (d-d, 1H, Carb 1st ring), 7.94 (t, 1H, Py), 7.88 (d, 1H, J_{H-H} = 8.76 Hz Carb 1st ring), 7.74 (d, 1H, J_{H-H} = 8.16 Hz, Carb 3rd ring), 7.58 (t, 1H, Carb 3rd ring), 7.33 (t, 1H, Carb 3rd ring), 4.57 - 4.51 (q, 2H, N - (CH_2)CH_3), 1.44 (s, 15H, C_5Me_5), 1.39 (t, 3H, N - CH_2(CH_3)). ^{13}C NMR (100 MHz, DMSO-d_6, 25 °C, ppm) δ = 165.62 (imine C-H), 154.11, 152.74, 140.60, 140.49, 139.65 (Py), 129.42, 129.37, 126.80, 121.88, 121.05, 120.41, 119.65, 114.40, 109.92, 109.61 (Carb), 97.14 (C, C_5Me_5), 37.35 (CH_2, N - CH_2CH_3), 13.70 (CH_3, N - CH_2CH_3), 8.31 (CH_3, C_5Me_5). FT-IR (γ/cm^{-1}): 3094, 2971, 2939, 1581 (s, C=N), 1490, 1478 (s), 1240 (s), 1022, 833 (s, P-F). HR-MS (TOF MS ES$^+$) $C_{30}H_{32}ClN_3Rh$ Calculated: 572.1340, Found: 572.1334. Anal. Calcd for $C_{30}H_{32}ClF_6N_3PRh$: C, 50.19; H, 4.49; N, 5.85; Found: C, 49.86; H, 4.51; N, 6.10.

4.2.2.5 Synthesis of complexes 3c-9c

The following common procedure was followed for the syntheses of complexes **3c**-**9c**. A mixture of [MX(η^6-arene)]$_2$ (M = Ru or Os; arene = benzene or *p*-cymene; X = Cl or Br or I) and Schiff base carbazole ligand was dissolved in acetonitrile. The resulting mixture was stirred at room temperature for three hours, and the solvent was evaporated and treated with NH_4PF_6 in ethanol for an hour. The orange colored precipitate was separated and filtered through filter paper, washed with cold methanol and diethylether and dried in vacuum.

4.2.2.6 [(η^6-C_5H_6)RuCl(**L**)] (**3c**)

($RuCl_2(\eta^6$-$C_6H_6)$)$_2$ (100 mg, 0.20 mmol), Schiff base carbazole ligand (120 mg, 0.40 mmol) and NH_4PF_6 (65 mg, 0.40 mmol). Yield (180 mg, 0.27 mmol, 87%). Mp. 270.0 °C (dec.). ^{1}H NMR (400 MHz, DMSO-d_6, 25 ºC, ppm) δ = 9.68 (d, 1H, J_{H-H} = 5.48 Hz, α proton of Py), 8.99 (s, 1H, imine CH), 8.57 (d, 1H, J_{H-H} = 2.08 Hz, Carb 3rd ring), 8.34 (d-d, 1H, Carb 1st ring), 8.28 - 8.24 (m, 2H, Py), 8.04 (d-d, 1H, Carb 3rd ring), 7.89 (t, 1H, Py), 7.85 (d, 1H, J_{H-H} = 8.84 Hz, Carb 3rd ring), 7.74 (d, 1H, J_{H-H} = 8.24 Hz, Carb 3rd ring), 7.58 (t, 1H, Carb 1st ring), 7.36 (t, 1H, Carb 3rd ring), 5.99 (s, 6H, C_6H_6), 4.58 - 4.53 (q, 2H, N - (CH_2)CH_3), 1.41 (t, 3H, N - CH_2(CH_3)). ^{13}C NMR (100 MHz, DMSO-d_6, 25 °C, ppm) δ = 165.86 (imine C-H), 156.14, 154.95, 139.99, 129.31, 128.28 (Py), 144.30, 140.49, 139.81, 126.76, 122.04, 121.93, 120.72, 119.56, 113.77, 109.84, 109.51 (Carb), 87.32 (C_6H_6), 37.34 (CH_2, N - CH_2CH_3), 13.81 (CH_3, N - CH_2CH_3). FT-IR (γ/cm^{-1}): 3089, 3061, 3027, 2980, 1627, 1611, 1595 (s, C=N), 1494, 1477 (s), 1244 (s) 837, 822, 810 (m, P-F), 766, 753. HR-MS (TOF MS ES$^+$) $C_{26}H_{23}ClN_3Ru$ Calculated: 514.0624, Found: 514.0634. Anal. Calcd for $C_{26}H_{23}ClF_6N_3PRu$: C, 47.39; H, 3.52; N, 6.38; Found: C, 47.62; H, 3.60; N, 6.04.

4.2.2.7 [(η^6-p-cymene)RuCl(**L**)] (**4c**)

($RuCl_2(\eta^6$-*p*-cymene)$)_2$ (100 mg, 0.16 mmol), Schiff base carbazole ligand (96 mg, 0.32 mmol) and NH_4PF_6 (53 mg, 0.32 mmol). Yield (185 mg, 0.20 mmol, 79%). Mp. 260.0 °C (dec.). ^{1}H NMR (400 MHz, DMSO-d_6, 25 ºC, ppm) δ = 9.59 (d, 1H, J_{H-H} = 5.44 Hz, α proton of Py), 8.99 (s, 1H, imine CH), 8.60 (d, 1H, J_{H-H} = 1.60 Hz, Carb 3rd ring), 8.32-8.25 (m, 3H, Carb 1st ring and Py), 8.01 (d-d, 1H, Carb 3rd ring), 7.89-7.84 (m, 1H, Py and Carb 3rd ring), 7.75 (d, 1H, J_{H-H} = 8.28 Hz, Carb 3rd ring), 7.59 (t, 1H, Carb 1st ring), 7.34 (t, 1H, Carb 3rd ring), 6.12 (d, 1H, J_{H-H} = 6.20 Hz, *p*-cymene), 5.79 (d, 1H, J_{H-H} = 6.16 Hz, *p*-cymene), 5.67 (d, 1H, J_{H-H} = 6.12 Hz, *p*-cymene), 5.62 (d, 1H, J_{H-H} = 6.08 Hz, *p*-cymene), 4.58 - 4.53 (q, 2H, N - (CH_2)CH_3), 2.21 (s, 3H, *p*-cymene), 1.42 (t, 3H, N - CH_2(CH_3)), 1.03 (d, 3H, J_{H-H} = 6.88 Hz, *p*-cymene), 0.99 (d, 3H, J_{H-H} = 6.84 Hz, *p*-cymene). ^{13}C NMR (100 MHz, DMSO-d_6, 25 °C, ppm) δ =

165.53 (imine C-H), 155.89, 154.85, 139.89, 129.33, 128.41 (Py), 144.17, 140.52, 139.91, 126.80, 122.02, 121.97, 121.32, 120.77, 119.59, 114.03, 109.84, 109.54 (Carb), 105.07, 102.96, 86.44, 85.90, 85.49, 85.40 (Ph, *p*-cymene), 37.37 (CH_2, N - CH_2CH_3), 30.48 (CH, ($CH(CH_3)_2$), *p*-cymene), 21.82, 21.43 (($CH_3)_2$ ($CH(CH_3)_2$), *p*-cymene), 18.26 (CH_3, *p*-cymene), 13.83 (CH_3, N - CH_2CH_3). FT-IR (γ/cm^{-1}): 3054, 2979, 1627, 1598(s, C=N), 1491, 1481 (s), 1242 (s) 829 (s, P-F), 780, 755, 555. HR-MS (TOF MS ES^+) $C_{30}H_{31}ClN_3Ru$ Calculated: 570.1250, Found: 570.1238. Anal. Calcd for $C_{30}H_{31}ClF_6N_3PRu$: C, 50.39; H, 4.37; N, 5.88; Found: C, 50.52; H, 4.19; N, 5.56.

4.2.2.8 [(η^6-p-cymene)RuBr(**L**)] (**5c**)

($RuBr_2(\eta^6$-*p*-cymene))$_2$ (100 mg, 0.13 mmol), Schiff base carbazole ligand (78 mg, 0.26 mmol) and NH_4PF_6 (42 mg, 0.32 mmol). Yield (170 mg, 0.22 mmol, 88%). Mp. 250.0 °C (dec.). ^{1}H NMR (400 MHz, DMSO-d_6, 25 ºC, ppm) δ = 9.58 (d, 1H, $J_{H\text{-}H}$ = 5.48 Hz, α proton of Py), 8.98 (s, 1H, imine CH), 8.63 (d-d, 1H, $J_{H\text{-}H}$ = 1.64 Hz, Carb 3rd ring), 8.30 (d, 2H, $J_{H\text{-}H}$ = 4.24 Hz, Carb 1st ring), 8.26 (d, 1H, $J_{H\text{-}H}$ = 7.72 Hz, Py), 8.05 (d-d, 1H, Carb 3rd ring), 7.87-7.84 (m, 2H, Py), 7.75 (d, 1H, $J_{H\text{-}H}$ = 8.28 Hz, Carb 3rd ring), 7.59 (t, 1H, Carb 1st ring), 7.34 (t, 1H, Carb 3rd ring), 6.10 (d, 1H, $J_{H\text{-}H}$ = 6.24 Hz, *p*-cymene), 5.80 (d, 1H, $J_{H\text{-}H}$ = 6.20 Hz, *p*-cymene), 5.67 (d, 1H, $J_{H\text{-}H}$ = 6.12 Hz, *p*-cymene), 5.63 (d, 1H, $J_{H\text{-}H}$ = 6.12 Hz, *p*-cymene), 4.58 - 4.53 (q, 2H, N - (CH_2)CH_3), 2.30 (s, 3H, *p*-cymene), 1.42 (t, 3H, N - CH_2(CH_3)), 1.04 (d, 3H, $J_{H\text{-}H}$ = 6.88 Hz, *p*-cymene), 0.98 (d, 3H, $J_{H\text{-}H}$ = 6.88 Hz, *p*-cymene). ^{13}C NMR (100 MHz, DMSO-d_6, 25 °C, ppm) δ = 165.31 (imine C-H), 156.39, 154.85, 139.77, 129.40, 128.26 (Py), 144.37, 140.53, 139.97, 126.81, 122.02, 121.95, 121.62, 120.76, 119.60, 114.24, 109.86, 109.51 (Carb), 105.93, 102.17, 86.13, 86.03, 85.97, 85.64 (Ph, *p*-cymene), 37.38 (CH_2, N - CH_2CH_3), 30.63 (CH, ($CH(CH_3)_2$), *p*-cymene), 21.86, 21.34 (($CH_3)_2$ ($CH(CH_3)_2$), *p*-cymene), 18.82 (CH_3, *p*-cymene), 13.82 (CH_3, N - CH_2CH_3). FT-IR (γ/cm^{-1}): 3054, 2984, 2965, 2932, 1629, 1598 (s, C=N), 1484, 1476, 1461, 1234 (s), 841, 834 (s, P-F), 767, 745, 557. HR-MS (TOF MS ES^+) $C_{30}H_{31}BrN_3Ru$ Calculated: 614.0745, Found: 614.0724. Anal. Calcd for $C_{30}H_{31}BrF_6N_3PRu$: C, 47.44; H, 4.11; N, 5.53; Found: C, 47.61; H, 4.25; N, 5.26.

4.2.2.9 [(η^6-p-cymene)RuI(**L**)] (**6c**)

($RuI_2(\eta^6$-*p*-cymene))$_2$ (100 mg, 0.10 mmol), Schiff base carbazole ligand (60 mg, 0.20 mmol) and NH_4PF_6 (34 mg, 0.20 mmol). Yield (145 mg, 0.21 mmol, 88%). Mp. 240.0 °C (dec.). ^{1}H NMR (400 MHz, DMSO-d_6, 25 ºC, ppm) δ = 9.57 (d, 1H, $J_{H\text{-}H}$ = 5.56 Hz, α proton of Py), 8.95 (s, 1H, imine CH), 8.66 (d-d, 1H, $J_{H\text{-}H}$ = 1.68 Hz, Carb 3rd ring), 8.32-8.23 (m, 3H, Py and Carb 1st ring), 8.08 (d-d, 1H, $J_{H\text{-}H}$ = 1.80 Hz, Carb 3rd ring), 7.85-7.79 (m, 2H, Py), 7.74 (d, 1H, $J_{H\text{-}H}$ = 8.28 Hz, Carb 3rd ring), 7.59 (t, 1H, Carb 1st

ring), 7.34 (t, 1H, Carb 3rd ring), 6.06 (d, 1H, J_{H-H} = 6.24 Hz, *p*-cymene), 5.82 (d, 1H, J_{H-H} = 6.20 Hz, *p*-cymene), 5.68 (d, 1H, J_{H-H} = 6.24 Hz, *p*-cymene), 5.61 (d, 1H, J_{H-H} = 6.08 Hz, *p*-cymene), 4.58 - 4.53 (q, 2H, N - $(CH_2)CH_3$), 2.43 (s, 3H, *p*-cymene), 1.41 (t, 3H, N - $CH_2(CH_3)$), 1.05 (d, 3H, J_{H-H} = 6.84 Hz, *p*-cymene), 0.96 (d, 3H, J_{H-H} = 6.88 Hz, *p*-cymene). ^{13}C NMR (100 MHz, DMSO-d_6, 25 °C, ppm) δ = 164.81 (imine C-H), 155.68, 154.88, 139.54, 129.55, 127.90 (Py), 144.69, 140.56, 140.09, 126.83, 122.13, 122.00, 121.92, 120.72, 119.63, 114.68, 109.88, 109.44 (Carb), 107.70, 101.27, 86.85, 86.55, 85.80, 85.51 (Ph, *p*-cymene), 37.39 (CH_2, N - CH_2CH_3), 30.98 (CH, $(CH(CH_3)_2)$, *p*-cymene), 21.98, 21.23 ($(CH_3)_2$ $(CH(CH_3)_2)$, *p*-cymene), 19.89 (CH_3, *p*-cymene), 13.81 (CH_3, N - CH_2CH_3). FT-IR (γ/cm^{-1}): 3058, 2982, 2962, 1629, 1599 (s, C=N), 1485, 1475, 1461, 1241, 1233 (s), 841, 832 (s, P-F), 821, 767, 743, 557. HR-MS (TOF MS ES$^+$) $C_{30}H_{31}IN_3Ru$ Calculated: 662.0606, Found: 662.0579. Anal. Calcd for $C_{30}H_{31}BrF_6N_3PRu$: C, 44.68; H, 3.87; N, 5.21; Found: C, 44.60; H, 3.56; N, 5.13.

4.2.3.0 [(η^6-C_6H_6)OsCl(**L**)] (**7c**)

$(OsCl_2(\eta^6\text{-}C_6H_6))_2$ (100 mg, 0.15 mmol), Schiff base carbazole ligand (90 mg, 0.30 mmol) and NH_4PF_6 (50 mg, 0.30 mmol). Yield (143 mg, 0.19 mmol, 65%). Mp. 283.0 °C (dec.). ^{1}H NMR (400 MHz, DMSO-d_6, 25 ºC, ppm) δ = 9.62 (d, 1H, J_{H-H} = 5.48 Hz, α proton of Py), 9.36 (s, 1H, imine CH), 8.51 (d-d, 1H, J_{H-H} = 1.24 Hz, Carb 3rd ring), 8.41 (d, 1H, J_{H-H} = 7.64 Hz, Carb 1st ring), 8.31 - 8.23 (m, 2H, Py), 7.94 (d, 1H, J_{H-H} = 8.64 Hz, Carb 3rd ring), 7.85 - 7.81 (m, 2H, Py and Carb 3rd ring), 7.74 (d, 1H, J_{H-H} = 8.24 Hz, Carb 3rd ring), 7.59 (t, 1H, Carb 1st ring), 7.33 (t, 1H, Carb 3rd ring), 6.13 (s, 6H, C_6H_6), 4.58 - 4.53 (q, 2H, N - $(CH_2)CH_3$), 1.41 (t, 3H, N - $CH_2(CH_3)$). ^{13}C NMR (100 MHz, DMSO-d_6, 25 °C, ppm) δ = 166.93 (imine C-H), 156.24, 155.86, 139.88, 129.39, 129.31 (Py), 144.08, 140.49, 140.30, 126.79, 121.99, 121.92, 121.82, 120.86, 119.58, 114.37, 109.86, 109.53 (Carb), 78.85 (C_6H_6), 37.39 (CH_2, N - CH_2CH_3), 13.85 (CH_3, N - CH_2CH_3). FT-IR (γ/cm^{-1}): 3062, 2973, 1598 (s, C=N), 1492, 1482, 1233 (s) 833 (s, P-F), 809, 779, 750. HR-MS (TOF MS ES$^+$) $C_{27}H_{23}ClN_2Os$ Calculated: 602.1165, Found: 602.1151. Anal. Calcd for $C_{26}H_{23}ClF_6N_3OsP$: C, 41.74; H, 3.10; N, 5.62; Found: C, 41.62; H, 3.41; N, 5.39.

4.2.3.1 [(η^6-p-cymene)OsCl(**L**)] (**8c**)

$(OsCl_2(\eta^6\text{-}p\text{-cymene}))_2$ (100 mg, 0.13 mmol), Schiff base carbazole ligand (76 mg, 0.26 mmol) and NH_4PF_6 (42 mg, 0.32 mmol). Yield (170 mg, 0.21 mmol, 84%). Mp. 262.0 °C (dec.). ^{1}H NMR (400 MHz, DMSO-d_6, 25 ºC, ppm) δ = 9.53 (d, 1H, J_{H-H} = 5.52 Hz, α proton of Py), 9.39 (s, 1H, imine CH), 8.52 (d, 1H, J_{H-H} = 1.56 Hz, Carb 3rd ring), 8.42 (d, 1H, J_{H-H} = 7.64 Hz, Py), 8.30-8.25 (m, 2H, Carb 1st ring and Py), 7.89 (d-d, 1H, Carb 3rd ring), 7.84-7.82 (m, 2H, Py and Carb 3rd ring), 7.74 (d, 1H, J_{H-H} =

8.24 Hz, Carb 3rd ring), 7.57 (t, 1H, Carb 1st ring), 7.36 (t, 1H, Carb 3rd ring), 6.40 (d, 1H, J_{H-H} = 5.80 Hz, *p*-cymene), 6.00 (d, 1H, J_{H-H} = 5.76 Hz, *p*-cymene), 5.86 (d, 1H, J_{H-H} = 5.72 Hz, *p*-cymene), 5.78 (d, 1H, J_{H-H} = 5.76 Hz, *p*-cymene), 4.58 - 4.53 (q, 2H, N - $(CH_2)CH_3$), 2.29 (s, 3H, *p*-cymene), 1.42 (t, 3H, N - $CH_2(CH_3)$), 0.96 (d, 3H, J_{H-H} = 6.88 Hz, *p*-cymene), 0.93 (d, 3H, J_{H-H} = 6.88 Hz, *p*-cymene). ^{13}C NMR (100 MHz, DMSO-d_6, 25 °C, ppm) δ = 166.48 (imine C-H), 156.25, 155.62, 139.98, 129.26, 126.82 (Py), 144.16, 140.51, 140.08, 121.97, 121.32, 120.71, 120.83, 119.61, 114.47, 109.85, 109.56 (Carb), 96.81, 96.59, 78.55, 78.04, 75.97, 75.90 (Ph, *p*-cymene), 37.39 (CH_2, N - CH_2CH_3), 30.68 (CH, $(CH(CH_3)_2)$, *p*-cymene), 21.98, 21.80 ($(CH_3)_2$ $(CH(CH_3)_2)$, *p*-cymene), 18.26 (CH_3, *p*-cymene), 13.84 (CH_3, N - CH_2CH_3). FT-IR (γ/cm^{-1}): 3063, 2976, 1597 (s, C=N), 1491, 1473, 1242, 1234, 830 (s, P-F), 779, 754, 556. HR-MS (TOF MS ES$^+$) $C_{30}H_{31}ClN_3Os$ Calculated: 660.1821, Found: 660.1802. Anal. Calcd for $C_{30}H_{31}ClF_6N_3PRu$: C, 44.80; H, 3.89; N, 5.22; Found: C, 44.75; H, 3.43; N, 5.48.

4.2.3.2 [(η^6-p-cymene)OsI(**L**)] (**9c**)

$(OsI_2(\eta^6$-*p*-cymene$))_2$ (100 mg, 0.9 mmol), Schiff base carbazole ligand (52 mg, 0.18 mmol) and NH_4PF_6 (30 mg, 0.18 mmol). Reddish brown solid. Yield (124 mg, 0.21 mmol, 81%). Mp. 187.0 °C (dec.). ^{1}H NMR (400 MHz, DMSO-d_6, 25 ºC, ppm) δ = 9.53 (d, 1H, J_{H-H} = 5.52 Hz, α proton of Py), 9.32 (s, 1H, imine CH), 8.59 (s, 1H, Carb 3rd ring), 8.44 (d, 1H, J_{H-H} = 7.72 Hz, Py), 8.24-8.20 (m, 2H, Py and Carb 1st ring), 8.01 (d, 1H, J_{H-H} = 8.84 Hz, Carb 3rd ring), 7.84 (d, 1H, J_{H-H} = 8.80 Hz, Carb 3rd ring), 7.77 - 7.72 (m, 2H, Py and Carb 3rd ring), 7.59 (t, 1H, Carb 1st ring), 7.34 (t, 1H, Carb 3rd ring), 6.33 (d, 1H, J_{H-H} = 5.88 Hz, *p*-cymene), 6.02 (d, 1H, J_{H-H} = 5.84 Hz, *p*-cymene), 5.86 (d, 1H, J_{H-H} = 5.80 Hz, *p*-cymene), 5.79 (d, 1H, J_{H-H} = 5.80 Hz, *p*-cymene), 4.58 - 4.53 (q, 2H, N - $(CH_2)CH_3$), 2.52 (s, 3H, *p*-cymene), 1.41 (t, 3H, N - $CH_2(CH_3)$), 0.99 (d, 3H, J_{H-H} = 6.88 Hz, *p*-cymene), 0.90 (d, 3H, J_{H-H} = 6.88 Hz, *p*-cymene). ^{13}C NMR (100 MHz, DMSO-d_6, 25 ºC, ppm) δ = 165.53 (imine C-H), 156.78, 156.18, 139.63, 129.34, 128.65 (Py), 144.88, 140.56, 140.17, 126.85, 122.49, 121.96, 121.92, 120.74, 119.63, 115.05, 109.88, 109.45 (Carb), 98.88, 94.36, 78.14, 77.91, 77.79, 77.73 (Ph, *p*-cymene), 37.38 (CH_2, N - CH_2CH_3), 30.97 (CH, $(CH(CH_3)_2)$, *p*-cymene), 21.94, 21.37 ($(CH_3)_2$ $(CH(CH_3)_2)$, *p*-cymene), 20.02 (CH_3, *p*-cymene), 13.82 (CH_3, N - CH_2CH_3). FT-IR (γ/cm^{-1}): 3039, 2975, 1628, 1610, 1596 (s, C=N), 1491, 1473, 1441, 1233, 832 (s, P-F), 769, 753, 556. HR-MS (TOF MS ES$^+$) $C_{30}H_{31}IN_3Os$ Calculated: 752.1178, Found: 752.1147. Anal. Calcd for $C_{30}H_{31}ClF_6N_3PRu$: C, 40.23; H, 3.49; N, 4.69; Found: C, 40.15; H, 3.23; N, 4.55.

4.2.3 Crystallography

Details of the crystal structures of complexes **2c** and **6c** are given in Table 4.1. A suitable crystal for single crystal XRD was grown by slow evaporation of hexane into an acetonitrile, methanol (1:1) mixture. The crystal was selected and glued onto the tip of a glass fibre, then mounted in a stream of cold nitrogen at 100 (1) K and centred in the X-ray beam by using a video camera. The crystal refinement and data collection were performed on a Bruker Smart *APEX11* diffractometer using graphite crystal monochromatised Mo - Kα radiation (ʎ = 0.71073 Å) at 100 (1) K. The intensity data was collected by the ω scan mode within 3.44° < Θ > 65.08° for *hkl* (-15 ≤ h ≤13, -22 ≤ k ≤22, -28 ≤ l ≤ 27) (**2c**) in the orthorhombic system and 1.47 < Θ > 28.70° for -28≤h≤28, -36≤k≤36, -13≤l≤14 (**6c**) in the monoclinic system. The structure of the crystal was resolved by using, the SHELX program. The full-matrix least-squares on F^2 refinement method with the SHELX program package was used to refine the positions and thermal parameters of all non-hydrogen atoms in the crystals [36]. For the structures and graphics, *ORTEP-3* [37] and DIAMOND [38] programs were used.

4.2.4 Cells and culture conditions

The human breast cancer MCF-7 cell line was obtained from the National Centre of Cell Science (Pune, India). The cells were maintained in Dulbecco's Modified Eagles medium supplemented with 2 mM l-glutamine and Earle's BSS adjusted to contain 1.5 g L^{-1} Na bicarbonate, 0.1 mM nonessential amino acids, and 1.0 mM of Na pyruate in a humidified atmosphere containing 5% CO_2 at 37 °C.

4.2.5 Cell viability assay

Cell viability was determined by 3-(4,5-dimethylthiazol-2yl)-2,5-diphenyltetrazolium bromide (MTT) assay [39]. Briefly, exponentially growing cells ($1x10^4$ cells/well) were seeded into a 96 well plate and allowed to attach overnight. Cells were treated with the various concentrations of complexes in at least six replicate wells and left in contact for 48 h. 500 μM mL^{-1} of MTT was added to each well, and the plate was further incubated at 37 °C for another 4 h. The formazan crystals formed were dissolved in DMSO. Cell viability was expressed as follows:

$$\text{Cell viability (\%)} = \frac{\text{Test}}{\text{Control}} \text{ X } 100\%$$

4.2.6 Morphological study

The MCF-7 cells that were grown on cover slips (1×10^5 cells/cover slip) were incubated for 6-24 h with compounds at the IC_{50} concentration, and they were then fixed in an ethanol:acetic acid solution (3:1 v/v). The cover slips were gently mounted on glass slides for the morphometric analysis. Three monolayers per experimental group were photo micrographed. The morphological changes of the MCF-7 cells were analyzed using Nikon (Japan) bright field inverted light microscopy at 40x magnification.

4.2.7 Fluorescence microscopic analysis of cell death

Approximately 1 µL of a dye mixture of 100 mg/mL acridine orange (AO) and 100 mg/mL ethidium bromide (EtBr) in distilled water was mixed with 9 mL of cell suspension (1×10^5 cells/mL) on clean microscope cover slips. The MCF-7 cells were collected, washed with phosphate buffered saline (PBS) (pH 7.2) and stained with 1 mL of AO/EtBr. After incubation for 2 min, the cells were washed twice with PBS (5 min each) and visualized under a fluorescence microscope (Nikon Eclipse, Inc, Japan) at 400x magnification with an excitation filter at 480 nm. The percentage of apoptotic cells was determined using the following formula

$$\% \text{ of apoptotic cells} = \frac{\text{Total number of apoptotic cells}}{\text{Total number of normal and apoptotic cells}} \text{ X } 100$$

4.2.8 Flow cytometric analysis of cell cycle

The DNA content during the cell cycle steps were evaluated with flow cytometric analysis. In brief, 5×10^6 cells were treated with complexes **1c-3c** at a specific concentration. After 24 hr, the cell pellets were washed and resuspended in 2 mL of 1% paraformaldehyde in PBS and incubated for 15 min at 4°C. Then, the cells were centrifuged and 1 mL of cold perm buffer III solution was added and incubated for 30 min at 4 °C followed by washing with PBS twice. Next, 500 µg of Propidium Iodide (PI) (Sigma-Aldrich, Steinbeim, Germany) staining buffer (50 µg/mL PI, 10 µg/mL RNase in PBS) was added and incubated for 1 hr at room temperature in the dark. After DNA staining by PI, samples were evaluated by a flow cytometer using Partec FloMax software (Version 2.3).

4.2.9 Statistical analysis

All the experiments were performed in triplicates for each group. The data are expressed as mean ± standard deviation. Differences with p value < 0.05 were considered to be statistically significant.

4.3 Computational studies

4.3.0.1 Molecular Docking

This study was performed using AutoDock 4v software which performs docking calculations to identify the binding orientation or conformation of a complex in the active site of the protein [40]. The crystal structure of the cyclooxygenase-2 (COX-2) protein (PDB ID: 1CX2) was retrieved from the protein data bank. Complexes **1c-3c** were sketched using Chemdraw software [41]. The geometry optimization and minimization for both protein and ligand was performed with the AM1-BCC charge method using AMBER software to obtain the correct bond length, bond angles and dihedral angles [42, 43]. The minimized complexes **1c-3c** and protein were saved in pdbqt format in AutoDock software. The active site residues of the protein, COX-2 was taken from the literature and grid was generated. Docking was performed using the Lamarckian genetic algorithm with default parameters and the best conformation or pose was chosen based on binding energy (kcal/mol).

4.3 Results and discussion

4.3.1 Synthesis of the ligand and complexes

In the present work, the new half sandwich metal complexes **1c-9c** have been synthesised using the new N,N' carbazole bidentate ligand (Scheme 4.1). A reaction between the chloro bridged dimer $(MCl_2Cp^*)_2$ (M = Ir and Rh) with N, N' 9-ethyl-N-(pyridine-2-yl methylene)-9H-carbazole-3-amine (**L**) and NH_4PF_6 afforded the new $[(\eta^5\text{-}C_5Me_5)MCl(L)]PF_6$ (M = Ir (**1c**) and Rh (**2c**)) complexes in good yields in methanol (72% and 84%). Furthermore, a reaction between the chloro-bridged arene dimer $(MX_2(\eta^6\text{-arene}))_2$ (M = Ru or Os; arene = benzene or *p*-cymene; X = Cl or Br or I) with N, N' 9-ethyl-N-(pyridine-2-yl methylene)-9H-carbazole-3-amine (L) and NH_4PF_6, afforded the new $[(\eta^6\text{-arene})MX(\mathbf{L})]PF_6$ complexes in good yields (65-88%). Complexes **1c-8c** are orange-red crystalline solids (complex **9c** = reddish brown color) and are air stable, non-hygroscopic and soluble in common polar solvents such as DMSO, DMF, acetonitrile, dichloromethane, acetone and partially soluble in water, chloroform, methanol, ethanol. These complexes are insoluble in diethyl ether, petroleum ether and hexane.

Characterisation of the ligand and metal complexes **1c-9c** was carried out by NMR, 2D NMR (COSY, NOESY), IR spectroscopy, melting point analysis, HR-MS spectroscopy and elemental analyses. The structures of the complexes **2c** and **6c** have been further authenticated by single crystal X-ray crystallography.

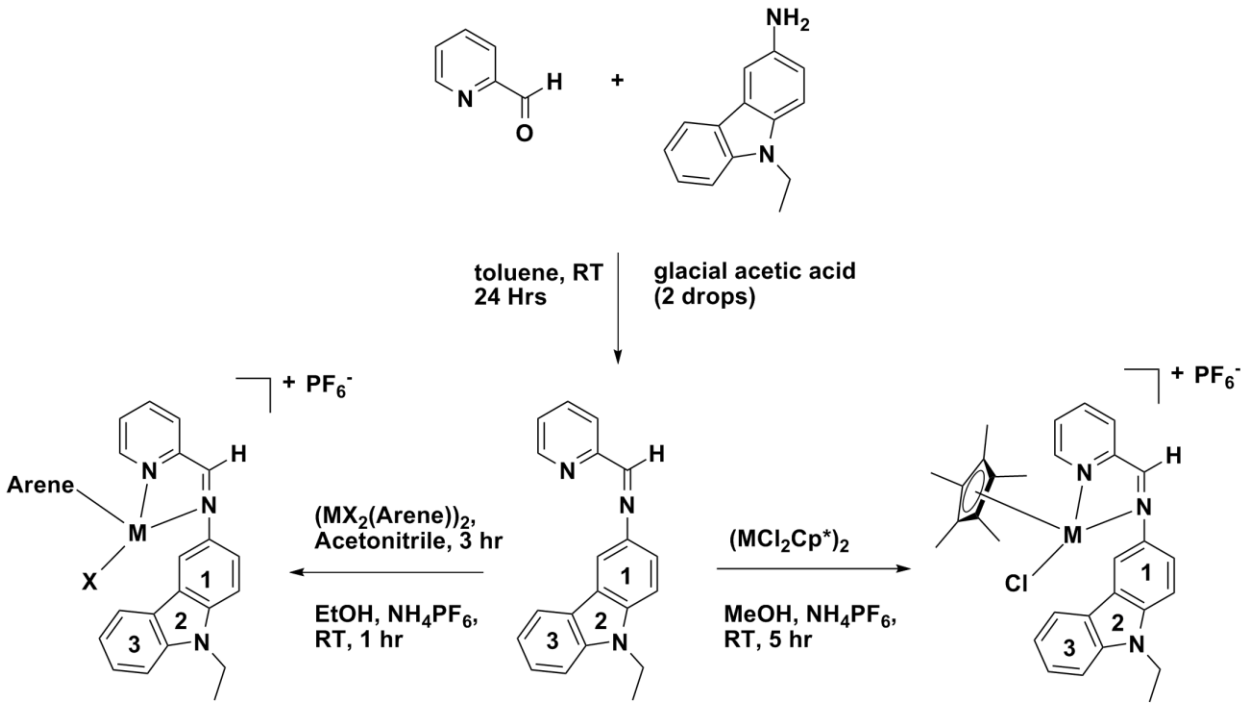

Complex	Metal	Arene	X
3c	Ru	Benzene	Cl
4c	Ru	*p*-cymene	Cl
5c	Ru	*p*-cymene	Br
6c	Ru	*p*-cymene	I
7c	Os	Benzene	Cl
8c	Os	*p*-cymene	Cl
9c	Os	*p*-cymene	I

Scheme 4.1: Schematic diagram of ligand and complexes **1c**-**9c** synthesis routes.

4.3.2 NMR studies

The spectral data of the ligand and metal complexes have been summarized in the Experimental section. The ^{1}H NMR spectrum of the free N,N' carbazole ligand (**L**) showed a -CH imine proton singlet signal at 8.83 ppm and a doublet signal of the α proton in the pyridine ring appeared at 8.73 ppm. When the N,N' carbazole ligand was coordinated with the iridium, rhodium and ruthenium metal precursor, the singlet peak of the imine proton signal shifted further down-field to 9.44 (**1c**), 9.04 (**2c**), 8.99 (**3c**), 8.99 (**4c**), 8.98 (**5c**), 8.95 (**6**), 9.38 (**7**), 9.39 (**8c**) and 9.32 (**9c**) ppm respectively and the doublet peak of the α proton in the pyridine ring shifted down-field to 9.06 (**1c**), 9.08 (**2c**), 9.68 (**3c**), 9.59 (**4c**), 9.58 (**5c**), 9.57 (**6c**), 9.62 (**7c**), 9.53 (**8c**) and 9.53 (**9c**) ppm respectively. The signals of the aromatic region of all metal

complexes **1c**-**9c** were shifted down-field compared to the respective free ligand signals. The ^{13}C NMR signals of the ligand imine carbon and α proton carbon in the pyridine ring appeared at 157.5 and 149.6 ppm respectively, whilst the corresponding signals of the complexes **1c**-**9c** shifted downfield to 167.0 and 155.7 ppm for (**1c**), 165.6 and 154.1 ppm for (**2c**), 165.9 and 156.1 ppm for (**3c**), 165.5 and 156.9 ppm for (**4c**), 165.3 and 156.4 ppm for (**5c**), 164.8 and 155.7 ppm for (**6c**), 166.9 and 155.9 ppm for (**7c**), 166.5 and 155.6 ppm for (**8c**) and 165.5 and 156.8 ppm for (**9c**), respectively. The ^{1}H NMR and ^{13}C NMR shifts confirmed that the N,N' carbazole ligand was coordinated with the respective metal centers and hence the formation of the respective complexes **1c**-**9c**.

4.3.3 Infrared spectroscopy

IR spectra of the N,N' carbazole ligand exhibits a characteristic peak for the (C=N) stretching frequency at 1581 cm^{-1} and the stretching frequency of the carbazole moiety aliphatic ethyl group attached to the nitrogen atom (N-CH_2CH_3) appeared in the range of 2932 - 3050 cm^{-1}. In complexes **1c**-**9c**, these bands are shifted to higher frequencies at 1596 cm^{-1} (**1c**), 1595 cm^{-1} (**2c**), 1595 cm^{-1} (**3c**), 1598 cm^{-1} (**4c**), 1598 cm^{-1} (**5c**), 1599 cm^{-1} (**6c**), 1598 cm^{-1} (**7c**), 1597 cm^{-1} (**8c**) and 1596 cm^{-1} (**9c**), which are attributed to the N,N' carbazole nitrogen atom of the (C=N) group coordinated with the respective metal centers. The stretching frequency of the aliphatic ethyl group attached to the nitrogen atom (N-CH_2CH_3) was shifted to higher frequencies in all metal complexes 2941 to 3069 cm^{-1} (**1c**), 2939 to 3094 cm^{-1} (**2c**), 2980 to 3089 cm^{-1} (**3c**), 2979 to 3054 cm^{-1} (**4c**), 2932 to 3054 cm^{-1} (**5c**), 2962 to 3058 cm^{-1} (**6c**), 2973 to 3062 cm^{-1} (**7c**), 2976 to 3063 cm^{-1} (**8c**) and 2975 to 3039 cm^{-1} (**9c**). The characteristic peak of the PF_6 counter ion appeared at 826 cm^{-1} (**1c**), 833 cm^{-1} (**2c**), 822 cm^{-1} (**3c**), 829 cm^{-1} (**4c**), 834 cm^{-1} (**5c**), 832 cm^{-1} (**6c**), 833 cm^{-1} (**7c**), 830 cm^{-1} (**8c**) and 832 cm^{-1} (**9c**).

4.3.4 Stability of the complexes (1c-9c) in DMSO-d_6 and DMSO-d_6 / D_2O solvent system

The stability of metal complexes is important in biological drug delivery systems. DMSO is a widely used solvent in preparing metal complexes stock solutions for therapeutic studies. DMSO acts as a good ligand for coordination with metal ions in some transition metal complexes via S or O atoms [44]. In order to confirm the stability of complexes **1c**-**9c**, they were dissolved in DMSO-d_6 and monitored via ^{1}H NMR for 48 h at 25 °C (see SI). New peaks were not observed in the ^{1}H NMR spectra indicating that complexes **1c**-**9c** are stable in DMSO-d_6 solution.

Time dependent hydrolysis ^{1}H NMR studies of complexes **1c**-**9c** were carried out in a DMSO-d_6 / D_2O (20:80) solvent system for 72 h at 25 °C (See SI for complexes **4c**-**9c**). The iridium complex is stable over a period of 72 h in the DMSO-d_6 / D_2O system at 25 °C (Fig. 4.1). No specific spectral changes were

observed for complex **1c** during this study, whilst after 48 h, the aqua complex was evident for complex **2c** (Fig. 4.2), which also appeared in less than an hour for complex **3c**. Complex **3c** thus hydrolyzed faster than the other two complexes (Fig. 4.3). To confirm the hydrolysis of complex **3c**, NaCl was added to equilibrium solutions containing the chloride complex and their aqua adducts to final concentrations of 1 mM, 2 mM and 3 mM NaCl, mimicking the chloride concentrations in the cell nucleus, cell cytoplasm and blood plasma, respectively [45]. The ^{1}H NMR spectra were recorded 15 min after addition of NaCl to the equilibrium solution. The intensity of the aqua complex peaks decreased with increase in the concentration of NaCl in the equilibrium solution.

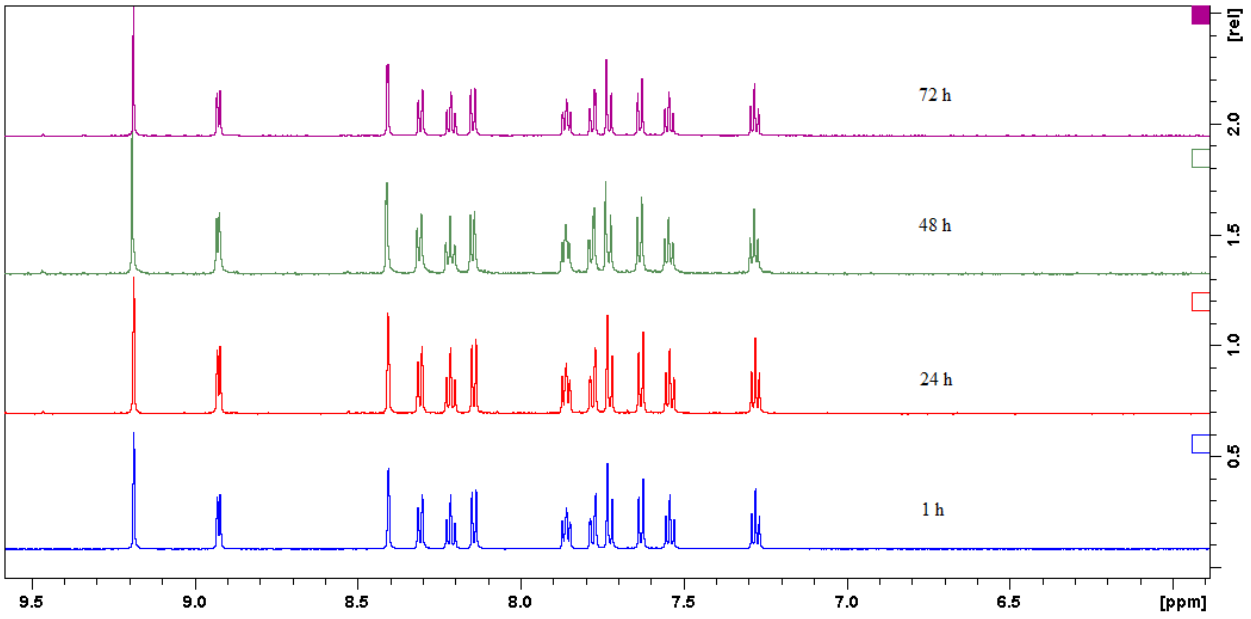

Fig. 4.1 Time dependent hydrolysis ^{1}H NMR spectra of the iridium complex **1c** in DMSO-d_6 / D_2O at 25 °C.

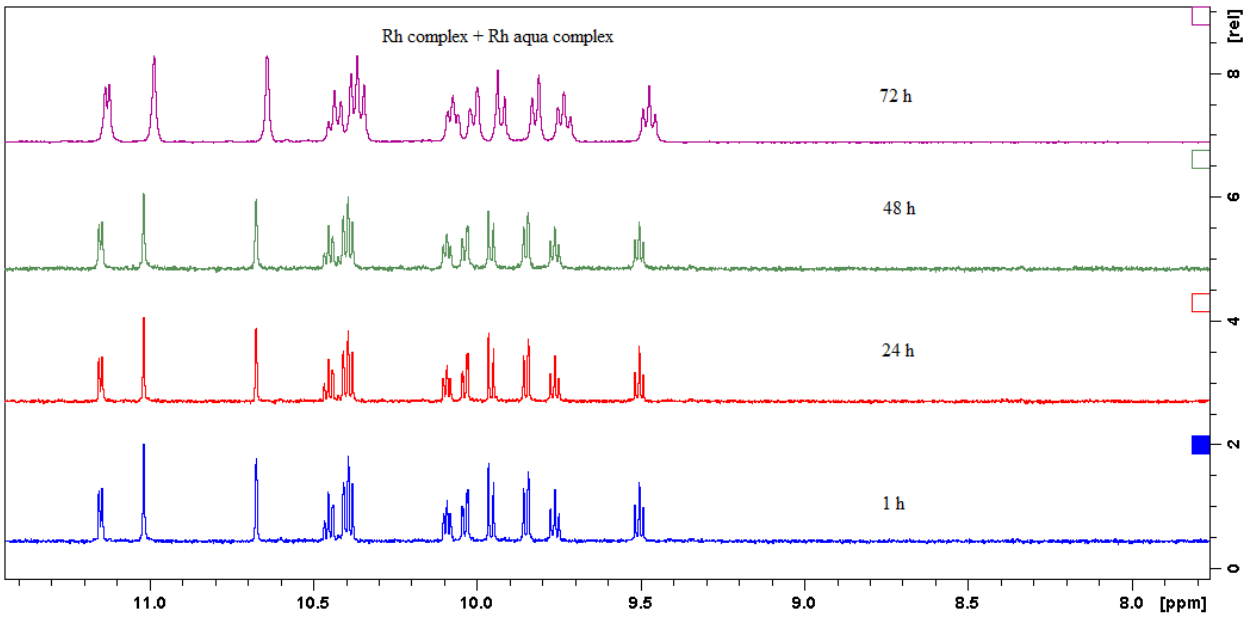

Fig. 4.2 Time dependent hydrolysis ^{1}H NMR spectra of the rhodium complex (**2c**) in DMSO-d_6 / D_2O at 25 °C.

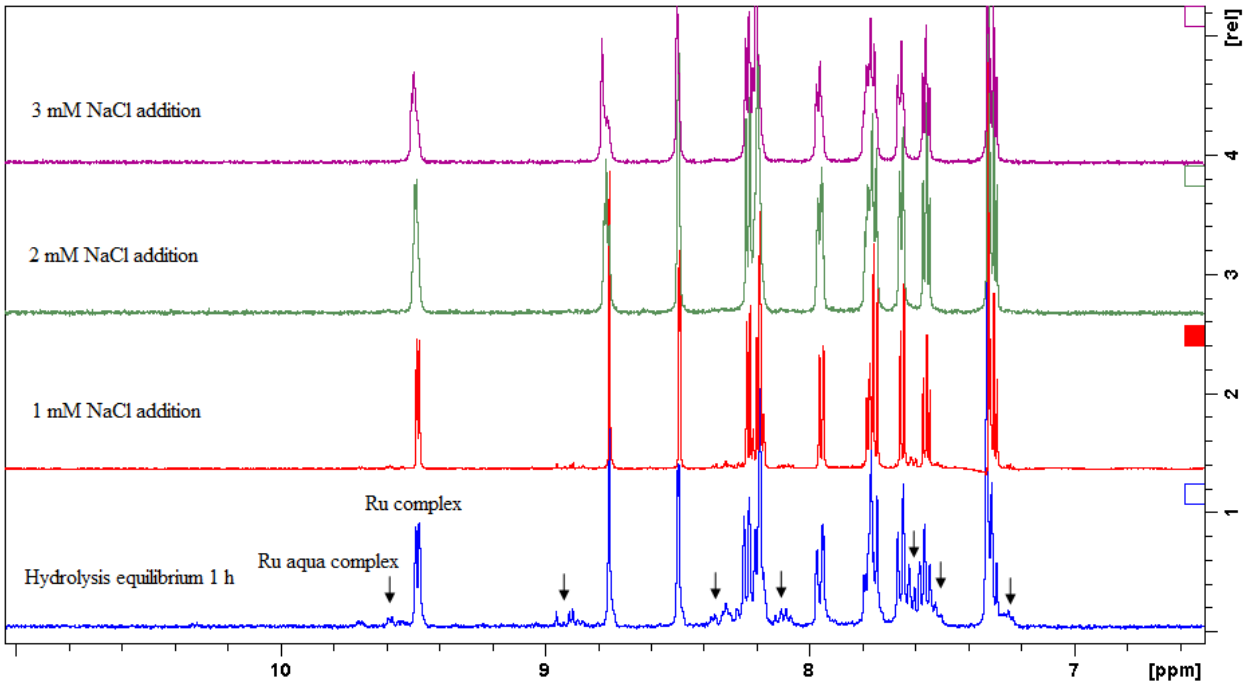

Fig. 4.3 Confirmation of the ruthenium complex (**3c**) hydrolysis by 1, 2 and 3 mM of NaCl addition to an equilibrium solution (1 mM) of the complex in DMSO-d_6 / D_2O at 25°C.

4.3.5 Structural information

Structural refinement and crystal data (Table 4.1), and selected bond angles and distances of the complexes **2** and **6** (Table 4.2) are presented. The perspective view of complexes **2c** and **6c** are shown in Figs. 4.4 and 4.5. The complexes are arranged in the orthorhombic / crystal system with the $P2_12_12_1$ / C 2/c space group respectively. The crystal structure of the complexes **2c** and **6c** showed typical pseudo-octahedral "piano-stool" geometry with the rhodium / ruthenium coordinated to an η^5-cyclopentadienyl / η^6-*p*-cymene (Rh(1)-centroid = 1.79 Å / Ru(1)-centroid = 1.70 Aº), a chloride / iodide atom (Rh(1)-Cl(1) = 2.41 Å / Ru(1)-I(1) = 2.71 Å) and the N,N' carbazole ligand in a bidentate manner forming a 5 or 6 membered metallocycle respectively.

The bond distances of the N(1)-Rh(1) = 2.09 Å, N(2)-Rh(1) = 2.11 Å, Cl(1)-Rh(1) = 2.41 Å and centroid-Rh(1) = 1.79 Å, whilst N(1)-Ru(1) = 2.08 Å, N(2)-Ru(1) = 2.08 Å, I(1)-Ru(1) = 2.70 Å and centroid-Ru(1) = 1.70 Å also consistent with reported literature [46] [35]. The angles of the N(1)-Rh(1)-Cl(1) = 88.00°, N(2)-Rh(1)-Cl(1) = 90.53° and N(2)-Ru(1)-I(1) = 89.61º are close to 90° is also consistent with literature data [35, 46, 47]. The rhodium complex **2c** exhibits a head to tail arrangement, non-covalent C-H···F (Table 4.3) and C-H···π interactions in the crystal packing (Fig. 4.6).

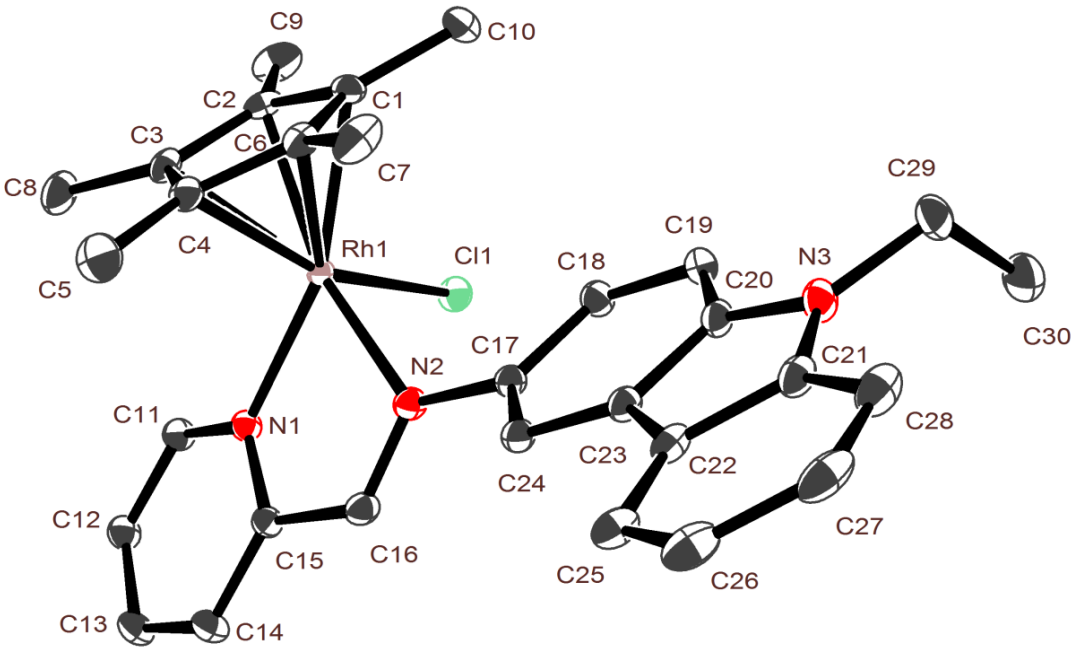

Fig. 4.4 The *ORTEP* diagram of the rhodium complex **2c**. Displacements of the ellipsoids are drawn at 50% probability. PF_6 and hydrogen atoms are omitted for clarity.

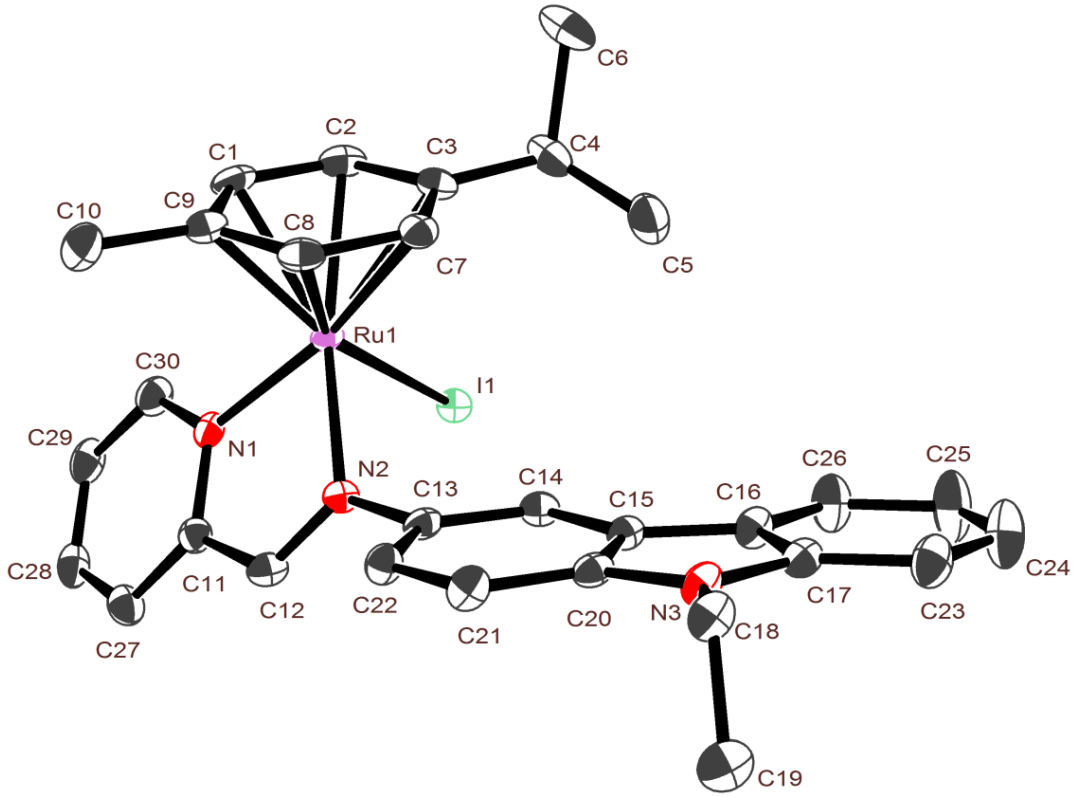

Fig. 4.5 The *ORTEP* diagram of the ruthenium complex **6c**. Displacements of the ellipsoids are drawn at 50% probability. PF_6 and hydrogen atoms are omitted for clarity.

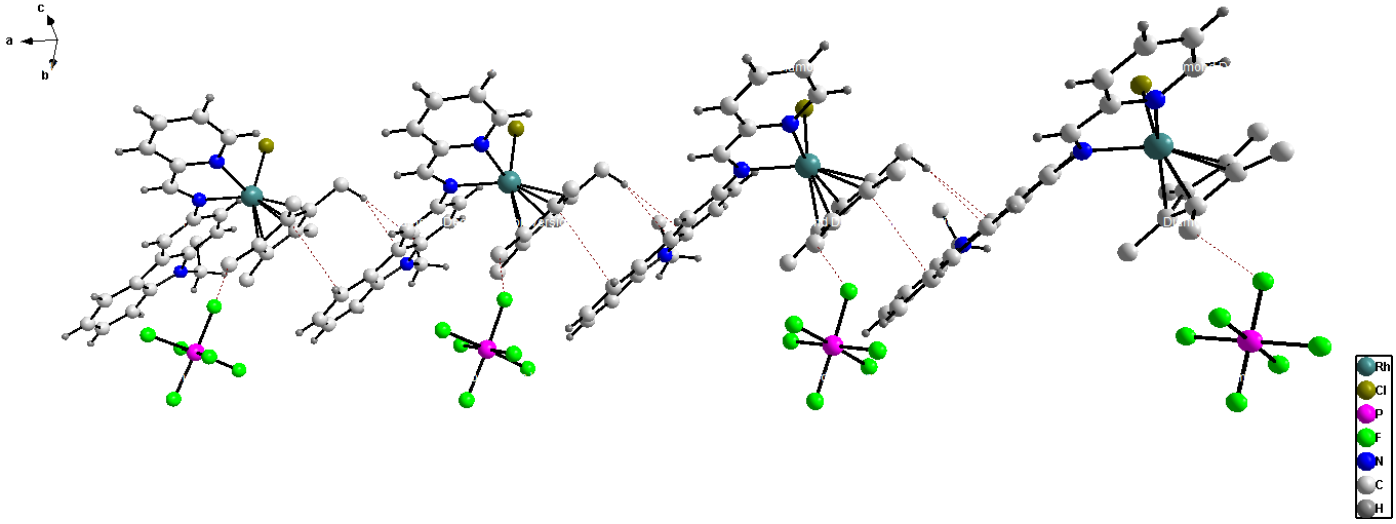

Fig. 4.6 Head to tail arrangement and noncovalent C-H···F and C-H···π interactions of the rhodium complex **2c**.

Table 4.1 Structure refinement and crystal data of complexes **2c** and **6c**

Complex	**2c**	**6c**
Empirical formula	$C_{30}H_{32}ClF_6N_3PRh$	$C_{30}H_{31}IN_3Ru$, 0.5(F6P), 0.5(F6 P1.90)
Formula weight	717.92	820.15
Temperature/K	100.02	100.02
Crystal system	orthorhombic	monoclinic
Space group	$P2_12_12_1$	C 1 2/c 1
a/Å	10.1972(4)	21.5315(13)
b/Å	15.0901(6)	27.6362(17)
c/Å	19.0469(8)	10.4424(6)
α/°	90	90
β/°	90	103.079(3)
γ/°	90	90
Volume/$Å^3$	2930.9(2)	6052.5(6)
Z	4	8
$\rho_{calc}g/cm^3$	1.6269	1.775
μ(Mo Kα)/mm^{-1}	0.793	
F(000)	1456.0	3200
Crystal size/mm^3	0.331 × 0.283 × 0.268	0.110 x 0.176 x 0.184
Radiation	Mo Kα (λ = 0.71073)	Mo Kα (λ = 0.71073)
2ϴ range for data collection/°	3.44 to 65.08	1.47 to 28.70
Index ranges	$-15 \le h \le 13$, $-22 \le k \le 22$, $-28 \le l \le 27$	$-28 \le h \le 28$, $-36 \le k \le 36$, $-13 \le l \le 14$
Reflections collected	58813	64503
Independent reflections	9644 [R_{int} = 0.0277, R_{sigma} = 0.0200]	7665 [R_{int} = 0.0406]
Data/restraints/parameters	9644/0/384	7665/0/392
Goodness-of-fit on F^2	1.110	1.051
Final R indexes [I>=2σ (I)]	R_1 = 0.0280, wR_2 = 0.0730	R_1 = 0.0816, wR_2 = 0.2225
Final R indexes [all data]	R_1 = 0.0294, wR_2 = 0.0749	R_1 = 0.0936, wR_2 = 0.2334
Largest diff. peak/hole / e $Å^{-3}$	1.30/-1.14	4.178/-9.348
Flack parameter	0.006(18)	

Table 4.2 Selected bond distances (Å) and angles (°) of the complexes **2c** and **6c**

Complex 2c		**Complex 6c**	
Selected bond distances (Å)			
N(1) – Rh(1)	2.091(16)	N(1) – Ru(1)	2.080(3)
N(2) – Rh(1)	2.108(17)	N(2) – Ru(1)	2.078(3)

Cl(1) – Rh(1)	2.408(5)	I(1) – Ru(1)	2.707(4)
C(1) – Rh(1)	2.154(18)	C(1) – Ru(1)	2.188(4)
C(2) – Rh(1)	2.166(19)	C(2) – Ru(1)	2.209(4)
C(3) – Rh(1)	2.179(2)	C(3) – Ru(1)	2.260(4)
C(4) – Rh(1)	2.147(2)	C(7) – Ru(1)	2.221(4)
C(6) – Rh(1)	2.180(19)	C(8) – Ru(1)	2.173(4)
Centroid – Rh(1)	1.787	C(9) – Ru(1)	2.208(4)
		Centroid – Ru(1)	1.696
Selected bond angles (°)			
N(1) – Rh(1) – N(2)	76.65(6)	N(1) – Ru(1) – N(2)	76.43(12)
N(1) – Rh(1) – C(1)	161.93(7)	N(1) – Ru(1) – C(1)	94.80(14)
N(1) – Rh(1) – C(2)	123.97(7)	N(1) – Ru(1) – C(2)	118.21(14)
N(1) – Rh(1) – C(3)	97.31(7)	N(1) – Ru(1) – C(3)	154.58(13)
N(1) – Rh(1) – C(4)	103.76(7)	N(1) – Ru(1) – C(7)	161.59(14)
N(1) – Rh(1) – C(6)	139.07(7)	N(1) – Ru(1) – C(8)	123.71(14)
N(1) – Rh(1) – Centroid	129.58	N(1) – Ru(1) – C(9)	96.38(14)
N(1) – Rh(1) – Cl(1)	88.00(5)	N(1) – Ru(1) – I(1)	84.07(9)
N(2) – Rh(1) – Cl(1)	90.53(5)	N(2) – Ru(1) – I(1)	89.61(9)
N(2) – Rh(1) – C(1)	119.67(7)	N(2) – Ru(1) – C(1)	146.60(15)
N(2) – Rh(1) – C(2)	158.60(7)	N(2) – Ru(1) – C(2)	165.15(13)
N(2) – Rh(1) – C(3)	143.88(7)	N(2) – Ru(1) – C(3)	128.49(13)
N(2) – Rh(1) – C(4)	106.97(8)	N(2) – Ru(1) – C(7)	98.86(13)
N(2) – Rh(1) – C(6)	96.65(7)	N(2) – Ru(1) – C(8)	90.29(13)
N(2) – Rh(1) – Centroid	129.82	N(2) – Ru(1) – C(9)	110.18(14)
Cl(1) – Rh(1) – Centroid	126.39	N(1) – Ru(1) – Centroid	132.13
Cl(1) – Rh(1) – C(1)	98.89(5)	N(2) – Ru(1) – Centroid	129.57
Cl(1) – Rh(1) – C(2)	95.47(6)	I(1) – Ru(1) – Centroid	127.67
Cl(1) – Rh(1) – C(3)	125.18(5)	I(1) – Ru(1) – C(1)	121.93(12)
Cl(1) – Rh(1) – C(4)	160.65(6)	I(1) – Ru(1) – C(2)	94.24(11)
Cl(1) – Rh(1) – C(6)	132.79(6)	I(1) – Ru(1) – C(3)	90.52(10)
		I(1) – Ru(1) – C(7)	113.92(10)
		I(1) – Ru(1) – C(8)	151.28(11)
		I(1) – Ru(1) – C(9)	159.80(11)

Table 4.3 C-H···F interaction in the complex **2c**

C-H···F	D-H	H···A	D···A	D-H···A
C(8)-H(8A) ···F(3)	0.981(16)	2.485(17)	3.412(4)	157.4(6)
C(16)-H(16) ···F(5)	0.950(3)	2.450(3)	3.189(3)	134.5(2)
C(28)-H(28) ···F(5)	0.950(3)	2.520(3)	3.263(3)	135.2(2)

4.3.6 Cytotoxic Activity

The aim of the present study is to investigate the *in vitro* potential of the synthesized complexes **1c**-**3c** on the viability of MCF-7 human breast cancer cells for 48 h. The experimental results indicated that complexes **1c**-**3c** inhibited cell proliferation in a dose dependent manner (Fig. 4.7). The determined IC_{50} value of the tested complexes are Ir(III) (5 μM) (**1c**), Rh(III) (6 μM) (**2c**), and Ru(II) (8 μM) (**3c**) against MCF-7 breast cancer cells by MTT assay. All the three complexes (**1c**-**3c**) inhibited MCF-7 cancer cells by dose and in a time-dependent manner. The IC_{50} value of the complexes **1c**-**3c** reveals that inhibition of MCF-7 cells depends on the mode of interaction of the complexes with MCF-7 cell lines. The activity of the complexes **1c**-**3c** falls in the following order **1c** > **2c** > **3c**, which may be due to the hydrophobicity of Cp* being higher than the benzene ring and therefore effective in penetrating the cell membrane [48]. Morris *et al*. reported $[Ru(arene)(ethylenediamine)Cl]^+$ compounds containing arene as a η^6-benzene (IC_{50}:17.0 μM) or η^6-*p*-cymene (IC_{50}:9.0 μM) moiety which showed different cytotoxicity effects on A2780 human ovarian cancer cells. These results supported the hydrophobicity nature of the complexes which could play a role against penetration in the cell membrane [14]. Very recently, Yellol *et al*. also reported a Cp* moiety containing [Ir(Cp*)(methyl-1-butyl-2-phenyl-1*H*-benzo[*d*]imidazole-5-carboxylate)Cl]$^+$ complex showing better potential anti-cancer activity against the HT29 (IC_{50}:0.98 μM), T47D (IC_{50}:2.27 μM), A2780 (IC_{50}:1.87 μM) and A2780cisR (IC_{50}:1.77 μM) human cancer cell lines compared to $[Ru(arene)(benzimidazole)Cl]^+$ and $[Rh(Cp^*)(benzimidazole)Cl]^+$ complexes, due to the mode and greater extent of interaction of the iridium complex with DNA and protein, as well as the effective penetrating nature into the cell membrane [19]. Gupta *et al*. also reported similar trend of the *in vitro* anticancer activity of Ir(III), Rh(III) and Ru(II) complexes against the Dalton lymphoma cell line [49]. The lower levels of toxicity of metal based drugs were well explained by Bergamo *et al*. [50]. The IC_{50} value of a free carbazole ligand was higher than 100 μM in the studied cancer cell line (MCF-7).

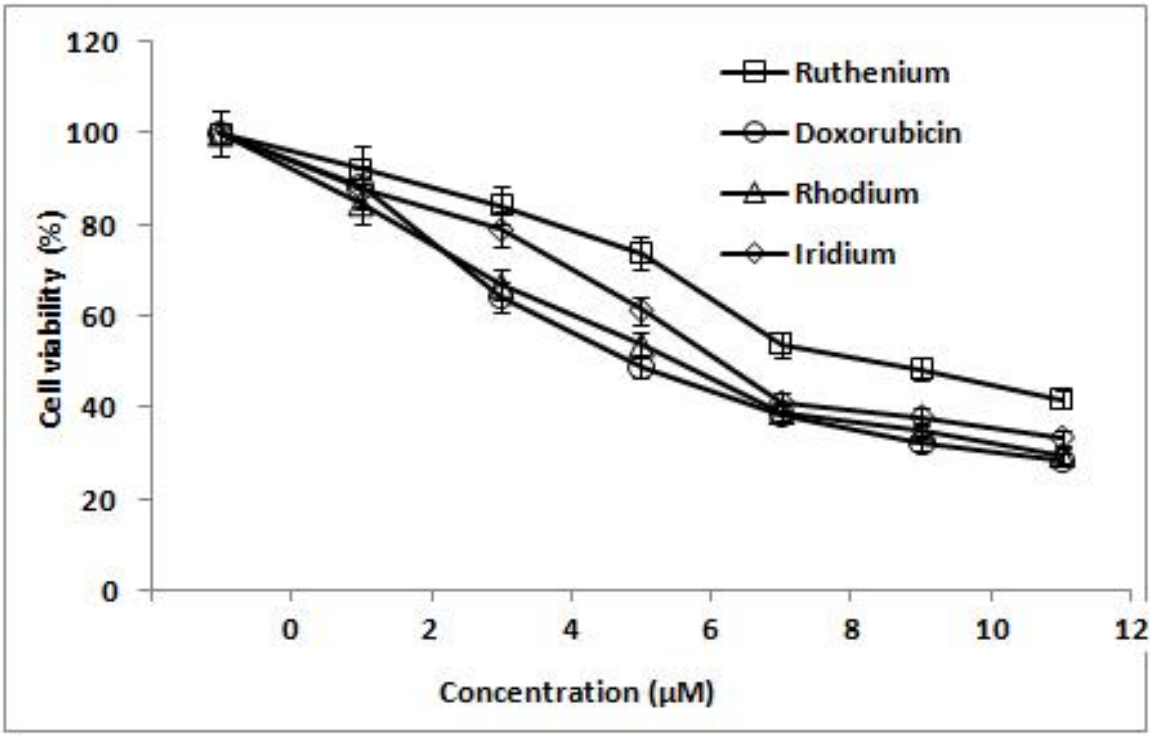

Fig. 4.7 *In vitro* cytotoxicity of complexes **1c-3c** against MCF-7 human breast cancer cells after incubation for 48 h.

4.3.7 Cell morphology analysis

Fig. 4.8 shows morphological changes in MCF-7 human breast cancer cells after treatment with complexes **1c-3c** for 24 h. Phase-contrast micrographs reveal that the Ir(III) (**1c**) complex induces increased cell shrinkage, membrane blebbing and forms floating cells, compared to the Rh(III) (**2c**) and Ru(II) (**3c**) complexes in a dose-dependent manner. Cytological investigations elucidate the antiproliferative effect routed through membrane blebbing, membrane instability and disturbing the cytoskeleton of the cells by the complexes. In Fig. 4.8, the arrows indicate the appearance of membrane blebbing and formation of floating cells in the treated MCF-7 breast cancer cells. All three complexes **1c-3c** showed significant cytotoxicity and anti-proliferative effects on selected human breast cancer MCF-7 cells.

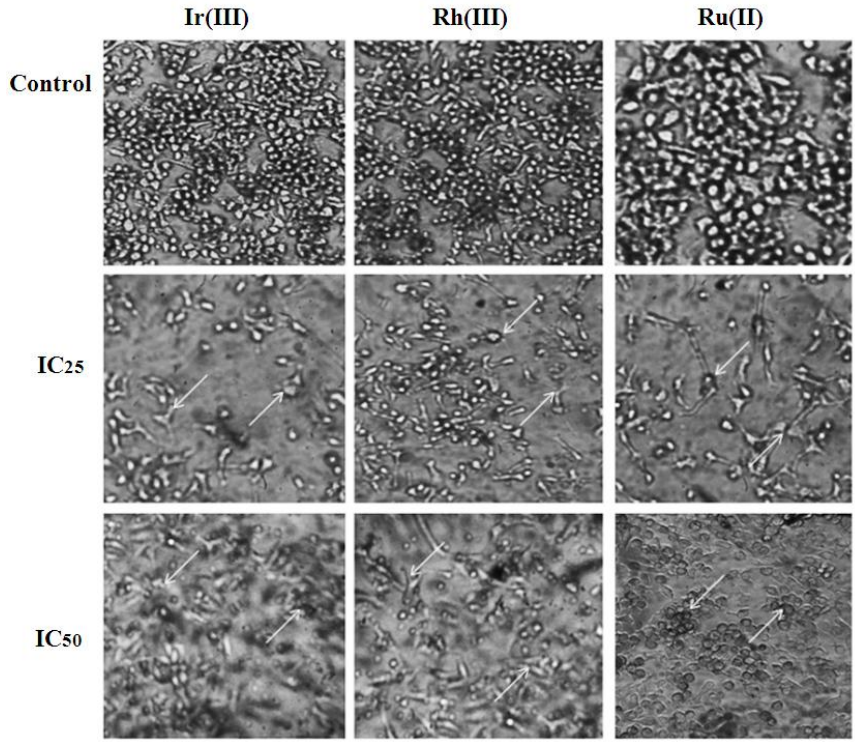

Fig. 4.8 Images of complexes **1c**-**3c** treated MCF-7 cells after 24 h exposure to the complexes at the IC_{25} & IC_{50} concentrations.

4.3.8 Fluorescence microscopy analysis of nuclear fragmentation

4.3.8.1 Acridine orange / Ethidium bromide (AO/EtBr) staining Method

The fluorescence microscopic studies reveal that concentration effects of complexes **1c**-**3c** significantly induce the apoptosis in MCF-7 human breast cancer cells. A control cell did not show any significant change compared to the treated MCF-7 breast cancer cells (Fig. 4.9). The complexes **2c** and **3c** required increased concentration relative to complex **1c** to induce apoptosis and the nuclear condensation effect on the cells. The arrows in Fig. 4.9 show the significant nuclear fragmentation, and induced apoptosis was observed in treated MCF-7 cells by complexes **1c**-**3c**. However, lower to moderate levels of induce apoptosis and nuclear fragmentation was observed in cells treated with complexes **2c** and **3c**, when compared to complex **1c**.

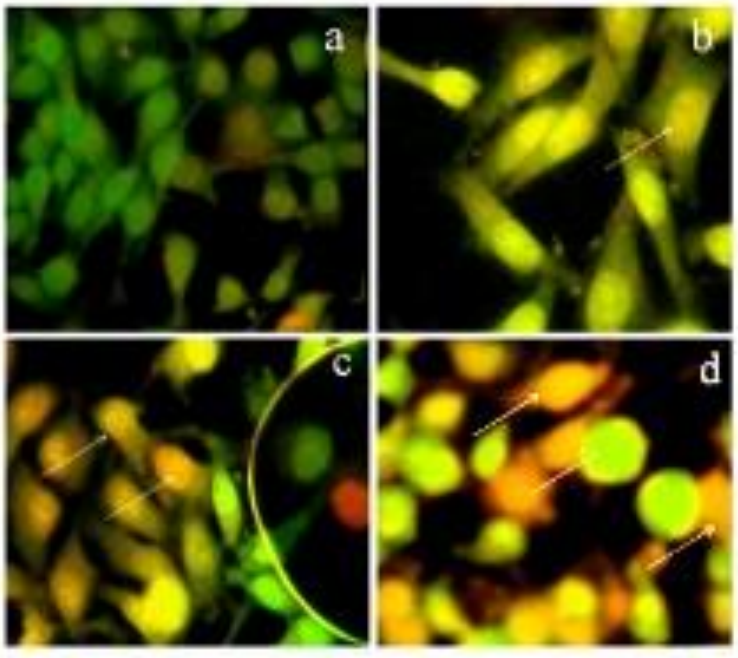

Fig. 4.9 Fluorescence microscopy images of MCF-7 breast cancer cells. (a) Control (untreated cells), (b) 5 µM (**1c**), (c) 6 µM (**2c**), (d) 8 µM (**3c**) for 24 h stained with DAPI. The fluorescent spectrum was detected at 360 nm/470 nm excitation/emission.

4.3.8.2 DAPI staining Method

Similarly, DAPI staining also revealed a significant level of nuclear fragmentation for complex **1c** treated MCF-7 cancer cells when compared to complexes **2c** and **3c** (Fig. 4.10). Many mechanisms have been proposed to explain MCF-7 inhibition through activation apoptosis [51]. However, the mitochondrial pathways of both intrinsic and extrinsic related efficacy of complexes have thus far not been reported explicitly. Herein, the complexes **1c**-**3c** caused significant reduction of viability in human MCF-7 breast cancer cells through activation of apoptotic related pathways (Fig. 4.10). The pharmacological target of antitumor ruthenium, rhodium and iridium complexes has not been unequivocally identified, but it is generally accepted that their cytotoxicity is related to their ability to bind DNA, although some exceptions have been reported [52, 53].

A chemotherapeutic anticancer drug should be able to inhibit uncontrolled cell growth or cause death to the affected metastatic cells. On the other hand, the drug has to have few weak side effects and show no genotoxicity on living normal cells in the host body. Complexes **1c**-**3c** appear to have a high affinity to interact with biomolecules like DNA, protein and RNA. Through this interaction with DNA, the synthesized complexes **1c**-**3c** have been shown to disrupt DNA synthesis, and thereby inhibit cell

viability. In Fig. 4.10, the bright fetch indicates the condensed chromatins and nuclear fragmentations in the MCF-7 cancer cells, marked by arrows. The fluorescence microscopy analysis reveals the nuclear changes and shrinking morphology in the drug treated MCF-7 cancer cells, which is another important hallmark of apoptosis.

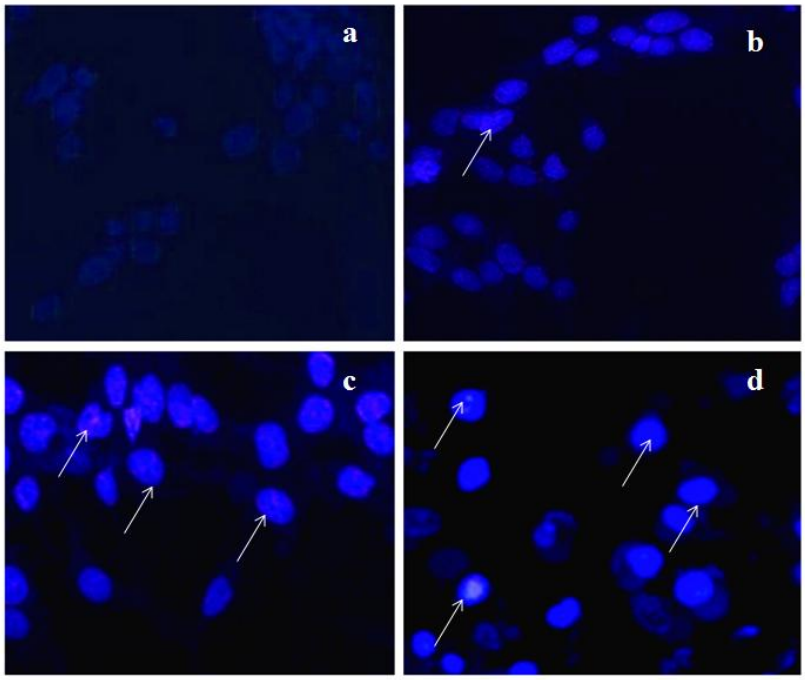

Fig. 4.10 Fluorescence microscopy images of the complexes **1c**-**3c** treated MCF-7 breast cancer cells after 24 h stained with DAPI. (a) Control (untreated cells), (b) 5 µM (**1c**), (c) 6 µM (**2c**), (d) 8 µM (**3c**). The fluorescent spectrum was detected at 360 nm/470 nm excitation/emission.

4.3.9 Cell cycle analysis

To investigate the effect of the new complexes **1c**-**3c** on the cell growth of cancer cell lines, the cell cycle distribution was analyzed after exposure of these cells to the complexes **1c**-**3c**. As shown in Fig. 4.11, the untreated control cells were mainly in G0/G1 phase and with the treatment of the complexes **1-3** (5-8 µM) for 24 hr, the percentage of S phase cells was significantly reduced to 33% (**1c**), 41% (**2c**) and 38% (**3c**) (in the case of control 44%), that of G2/M phase cells was also decreased to 10% (**1c**), 19% (**2c**) and 12% (**3c**). The synthesized complexes **1c**-**3c** have different effects on the cell cycle status in MCF-7 cell lines. These results show that these complexes **1c**-**3c** are able to arrest the S cell cycle.

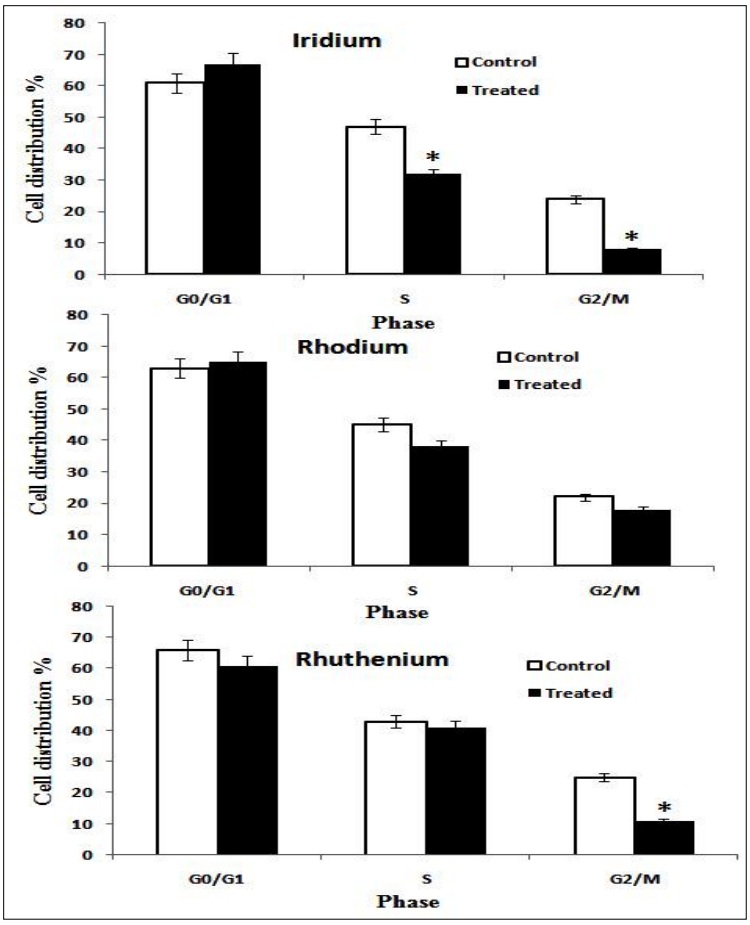

Fig. 4.11 Flow cytometric analysis effects of complexes **1c**-**3c** on cell cycle distribution in human breast cancer MCF-7 cells.

4.4.0 Docking studies

Docking studies were performed for all three complexes (**1c-3c**) to identify the mode of binding and binding affinity with the COX-2 receptor (PDB ID: 1CX2) (see Fig. 4.12 and SI). This study reveals that all three complexes bind in the active site of COX-2 via H-bonding and a hydrophobic contact with binding energy of -7.13 to -8.18 kcal/mol (Table 4.4). Among the three complexes, the iridium complex (**1c**) shows high binding energy with the selective amino acid (N2 --- OH of val 523) H-bond interaction of the COX-2 receptor, which initiates conformational changes to access the hydrophobic pocket of COX-2. Furthermore, the iridium complex (**1c)** shares H-bond interaction with the surrounding amino acid Glu-524 (N3 --- OH of Glu-524) of COX-2 receptor. The rhodium complex (**2c**) shares a H-bond interaction with the active site residue His-90 (N3 --- NH of His-90) and Ser-353 (N3 --- OH of Ser-353), whilst the ruthenium complex (**3c**) shares a similar interaction with His-90 of the COX-2 receptor like the rhodium complex (**2c**).

The prime region of COX-2 is the hydrophobic pocket where binding of the inhibitor will result in the inhibition of COX-2 [54]. The ligand moiety of the complexes **1c**-**3c** is crucial for establishing hydrophobic interactions in the active site of COX-2. The molecular docking results clearly show that the iridium complex (**1c**) is closer to the hydrophobic pocket, comprising of residues of Val 523, Tyr 355, Tyr 385, Ser 530, Gly 526 and Ala 527, than complexes **2c** and **3c**. Additionally, the iridium complex (**1**) also shares another H-bond interaction with the surrounding amino acid residue Glu 524 (N3 --- OH of Glu 524) of the active site, indicating that the iridium complex (**1c**) is highly stable in the hydrophobic pocket of COX-2. The docking study correlates with the experimental results which indicate that the iridium complex (**1c**) actively inhibits the COX-2 receptor compared to the other two complexes.

Table 4.4 Binding energy, H-bond and hydrophobic interactions of the complexes **1c**-**3c** with the COX-2 receptor

Complexes	**Binding energy (kcal/mol)**	**H-bond interaction**	**Hydrophobic interaction**
1c	-8.18	N2 --- OH of Val-523 N3 --- OH of Glu-524	Val 523, Tyr 355, Tyr 385, Ser 530, Gly 526 and Ala 527.
2c	-7.34	N3 --- NH of His-90 N3 --- OH of Ser-523	Val 523 and Leu 352
3c	-7.13	N3 --- NH of His-90	Val 523 and Leu 352

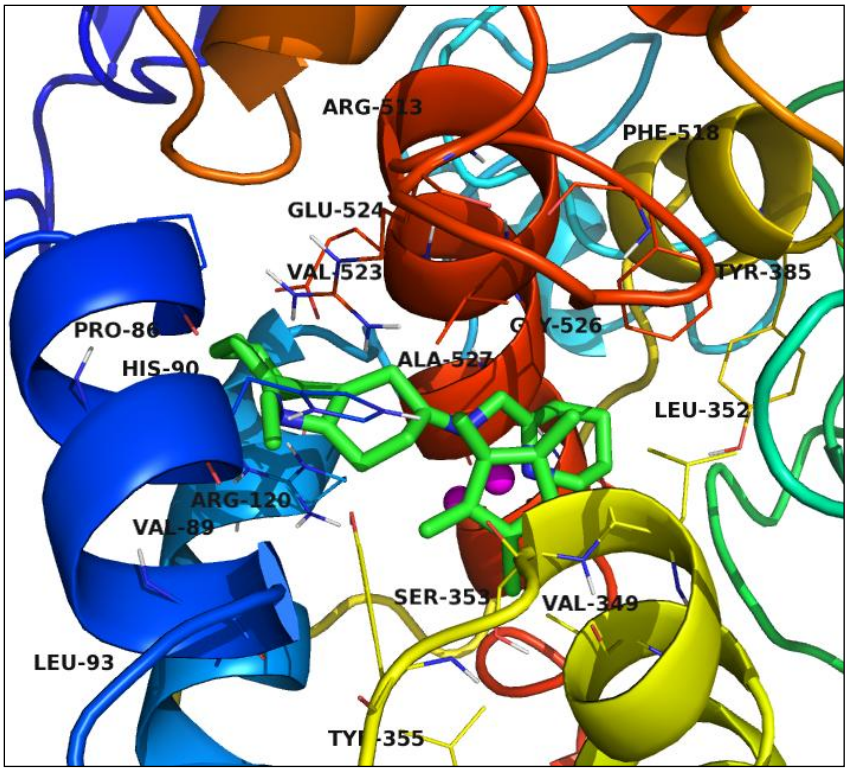

Fig. 4.12 Binding mode of complex **1c** in the active site of COX-2 receptor.

4.4 Conclusions

In conclusion, the synthesis and characterisation of new half sandwich Ir(III), Rh(III), Ru(II) and Os(II) complexes coordinated with a N,N' carbazole bidentate ligands have been shown. The rhodium and ruthenium complexes displayed the pseudo octahedral "piano-tool" geometry in the crystal structure. NMR studies reveal that all complexes are stable in DMSO-d_6. On the other hand, the Ru(II) (**3c**) complex hydrolyzed faster than the Ir(III) and Rh(III) complexes in a DMSO-d_6 / D_2O (2:8) solvent system due to formation of the respective aqua complexes.

Anticancer study clearly demonstrated that the new half sandwich Ir(III), Rh(III) and Ru(II) (**1c**-**3c**) complexes displayed potent anticancer properties against human breast cancer cells (MCF-7) at very low concentrations. Among the three complexes, the Ir(III) complex showed the best and most promising results, in all the experiments conducted, at a lower dose (5 µM). Overall studies concluded that all three synthesized complexes very effectively inhibit the cancer cell growth by causing damage to nuclear material, as well as membrane integrity. Molecular docking studies revealed that the ligand moiety is important for the binding of all three complexes in the hydrophobic pocket of the COX-2 receptor and the iridium complex actively inhibits the COX-2 receptor more than the rhodium and ruthenium complexes. Furthermore, anti-cancer studies for the Ru(II) and Os(II) complexes are in progress and also need to be

aimed at elucidating the molecular mechanism of the complexes M(III) (M = Ir and Rh) and M(II) (M = Ru and Os) for anti-cancer drug development.

Acknowledgements

The authors would like to thank the NRF, THRIP (Grant no. TP 1208035643) and the University of KwaZulu-Natal, Durban, South Africa for financial support. We also would like to thank Mr. Michael Nivendran Pillay for solving the X-ray crystal structures.

Appendix A. Supplementary Information

The ^{1}H and ^{13}C NMR, 2D NMR, NMR stability data, HR-MS spectroscopy, molecular docking pictures and crystal data of the complexes are also shown in the SI.

References

[1] V. Cepeda, M.A. Fuertes, J. Castilla, C. Alonso, C. Quevedo, J.M. Perez, Anticancer Agents Med. Chem. 7 (2007) 3-18.

[2] N. Cutillas, G.S. Yellol, C. de Haro, C. Vicente, V. Rodríguez, J. Ruiz, Coord. Chem. Rev. 257 (2013) 2784-2797.

[3] L. Kelland, Nat. Rev. Cancer 7 (2007) 573-584.

[4] D. Wang, S.J. Lippard, Nature reviews. Drug Discovery 4 (2005) 307-320.

[5] G. Gupta, A. Garci, B.S. Murray, P.J. Dyson, G. Fabre, P. Trouillas, F. Giannini, J. Furrer, G. Suss-Fink, B. Therrien, Dalton Trans. 42 (2013) 15457-15463.

[6] I. Ott, K. Schmidt, B. Kircher, P. Schumacher, T. Wiglenda, R. Gust, J. Med. Chem. 48 (2004) 622-629.

[7] B.M. Zeglis, V. Divilov, J.S. Lewis, J. Med. Chem. 54 (2011) 2391-2398.

[8] F. Lentz, A. Drescher, A. Lindauer, M. Henke, R.A. Hilger, C.G. Hartinger, M.E. Scheulen, C. Dittrich, B.K. Keppler, U. Jaehde, Anti-cancer drugs 20 (2009) 97-103.

[9] I. Bratsos, S. Jedner, T. Gianferrara, E. Alessio, CHIMIA Int. J. Chem. 61 (2007) 692-697.

[10] P. Nowak-Sliwinska, J.R. van Beijnum, A. Casini, A.A. Nazarov, G. Wagnières, H. van den Bergh, P.J. Dyson, A.W. Griffioen, J. Med. Chem. 54 (2011) 3895-3902.

[11] M.L.B. Tobe, J, in: A. Bakac (Ed.), Physical Inorganic Chemistry: Reactions, Processes, and Applications, Addison Wesley Longman Inc, UK, 1999.

[12] A.L. Noffke, A. Habtemariam, A.M. Pizarro, P.J. Sadler, Chem. Commun. 48 (2012) 5219-5246.

[13] R.E. Aird, J. Cummings, A.A. Ritchie, M. Muir, R.E. Morris, H. Chen, P.J. Sadler, D.I. Jodrell, Br. J. Cancer. 86 (2002) 1652-1657.

[14] R.E. Morris, R.E. Aird, P. del Socorro Murdoch, H. Chen, J. Cummings, N.D. Hughes, S. Parsons, A. Parkin, G. Boyd, D.I. Jodrell, P.J. Sadler, J. Med. Chem. 44 (2001) 3616-3621.

[15] Y. Fu, R. Soni, M.J. Romero, A.M. Pizarro, L. Salassa, G.J. Clarkson, J.M. Hearn, A. Habtemariam, M. Wills, P.J. Sadler, Chem. Eur. J. 19 (2013) 15199-15209.

[16] Z. Liu, A. Habtemariam, A.M. Pizarro, S.A. Fletcher, A. Kisova, O. Vrana, L. Salassa, P.C.A. Bruijnincx, G.J. Clarkson, V. Brabec, P.J. Sadler, J. Med. Chem. 54 (2011) 3011-3026.

[17] Z. Liu, L. Salassa, A. Habtemariam, A.M. Pizarro, G.J. Clarkson, P.J. Sadler, Inorg. Chem. 50 (2011) 5777-5783.

[18] R.K. Gupta, R. Pandey, G. Sharma, R. Prasad, B. Koch, S. Srikrishna, P.-Z. Li, Q. Xu, D.S. Pandey, Inorg. Chem. 52 (2013) 3687-3698.

[19] G.S. Yellol, A. Donaire, J.G. Yellol, V. Vasylyeva, C. Janiak, J. Ruiz, Chem. Commun. 49 (2013) 11533-11535.

[20] C. Asche, W. Frank, A. Albert, U. Kucklaender, Bioorg. Med. Chem. 13 (2005) 819-837.

[21] C. Guillonneau, A. Pierré, Y. Charton, N. Guilbaud, L. Kraus-Berthier, S. Léonce, A. Michel, E. Bisagni, G. Atassi, J. Med. Chem. 42 (1999) 2191-2203.

[22] A. Bombrun, P. Gerber, G. Casi, O. Terradillos, B. Antonsson, S. Halazy, J. Med. Chem. 46 (2003) 4365-4368.

[23] T. Indumathi, F.R. Fronczek, K.J. Rajendra Prasad, J. Mol. Struct. 1016 (2012) 134-139.

[24] M. Stiborová, J. Sejbal, L. Bořek-Dohalská, D. Aimová, J. Poljaková, K. Forsterová, M. Rupertová, J. Wiesner, J. Hudeček, M. Wiessler, E. Frei, Cancer Res. 64 (2004) 8374-8380.

[25] S. Butler, R. Wang, S.L. Wunder, H.-Y. Cheng, C.S. Randall, Biophys. Chem. 119 (2006) 307-315.

[26] A.A. Pieper, S. Xie, E. Capota, S.J. Estill, J. Zhong, J.M. Long, G.L. Becker, P. Huntington, S.E. Goldman, C.H. Shen, M. Capota, J.K. Britt, T. Kotti, K. Ure, D.J. Brat, N.S. Williams, K.S. MacMillan, J. Naidoo, L. Melito, J. Hsieh, J. De Brabander, J.M. Ready, S.L. McKnight, Cell 142 (2010) 39-51.

[27] D. Crich, S. Rumthao, Tetrahedron 60 (2004) 1513-1516.

[28] B.P. Bandgar, L.K. Adsul, H.V. Chavan, S.S. Jalde, S.N. Shringare, R. Shaikh, R.J. Meshram, R.N. Gacche, V. Masand, Bioorg. Med. Chem. Lett. 22 (2012) 5839-5844.

[29] Y. Hieda, T. Choshi, S. Kishida, H. Fujioka, S. Hibino, Tetrahedron Lett. 51 (2010) 3593-3596.

[30] D.D.A. Perrin, W. L. F.; Perrin, D. R, Purification of laboratory Chemicals, Pergamon: Oxford, UK, 1986.

[31] C.W. Cheung, D.S. Surry, S.L. Buchwald, Org. Lett. 15 (2013) 3734-3737.

[32] R. Lenz, S. V. Ley, J. Chem. Soc., Perkin Trans. 1 (1997) 3291-3292.

[33] C. White, A. Yates, P.M. Maitlis, Inorg. Synth. 29 (1992) 228-234.

[34] M.A. Bennett, A.K. Smith, J. Chem. Soc., Dalton Trans. (1974) 233-241.

[35] A.F.A. Peacock, A. Habtemariam, R. Fernández, V. Walland, F.P.A. Fabbiani, S. Parsons, R.E. Aird, D.I. Jodrell, P.J. Sadler, J. Am. Chem. Soc. 128 (2006) 1739-1748.

[36] G.M.Sheldrick, Acta. Crystallogr. A64 (2008) 112-122.

[37] L. J. Farrugia, *ORTEP-3* for Windows. J. Appl. Crystallogr. 30 (1997) 565.

[38] K. Brandenburg, H. Putz, DIAMOND Crystal Impact GbR, Bonn (2005).

[39] T. Mosmann, J. Immunol. Methods 65 (1983) 55-63.

[40] G.M. Morris, D.S. Goodsell, R.S. Halliday, R. Huey, W.E. Hart, R.K. Belew, A.J. Olson, J. Comput. Chem. 19 (1998) 1639-1662.

[41] A.D. Hunter, J. Chem. Educ. 74 (1997) 905.

[42] J. Wang, W. Wang, P.A. Kollman, D.A. Case, J. Mol. Graph. Mod. 25 (2006) 247-260.

[43] E.F. Pettersen, T.D. Goddard, C.C. Huang, G.S. Couch, D.M. Greenblatt, E.C. Meng, T.E. Ferrin, J. Comput. Chem. 25 (2004) 1605-1612.

[44] M. Patra, T. Joshi, V. Pierroz, K. Ingram, M. Kaiser, S. Ferrari, B. Spingler, J. Keiser, G. Gasser, Chem. Eur. J. 19 (2013) 14768-14772.

[45] Z. Liu, A. Habtemariam, A.M. Pizarro, G.J. Clarkson, P.J. Sadler, Organometallics 30 (2011) 4702-4710.

[46] M. Yadav, A.K. Singh, D.S. Pandey, Organometallics 28 (2009) 4713-4723.

[47] R.K. Gupta, G. Sharma, R. Pandey, A. Kumar, B. Koch, P.-Z. Li, Q. Xu, D.S. Pandey, Inorg. Chem. 52 (2013) 13984-13996.

[48] M. Ganeshpandian, R. Loganathan, E. Suresh, A. Riyasdeen, M.A. Akbarsha, M. Palaniandavar, Dalton Trans. 43 (2014) 1203-1219.

[49] G. Gupta, G. Sharma, B. Koch, S. Park, S.S. Lee, J. Kim, New J. Chem. 37 (2013) 2573-2581.

[50] A. Bergamo, A. Masi, P.J. Dyson, G. Sava, Int. J. Oncol. 33 (2008) 1281-1289.

[51] J. Zhang, M. Xu, Trends Cell Biol. 12 (2002) 84-89.

[52] S. Frühauf, W.J. Zeller, Cancer Res. 51 (1991) 2943-2948.

[53] E. Gallori, Vettori, C., Alessio, E., Vilchez, F.G., Vilaplana, R., Orioli, P., Casini, A., Messori, L, in: N.M.-N. Gérard Jaouen (Ed.), Med. Organomet. Chem., Springer, New York, USA, 2000.

[54] R.G. Kurumbail, A.M. Stevens, J.K. Gierse, J.J. McDonald, R.A. Stegeman, J.Y. Pak, D. Gildehaus, J.M. Miyashiro, T.D. Penning, K. Seibert, P.C. Isakson, W.C. Stallings, Nature 384 (1996) 644-648.

Chapter 5

Binding interaction, conformational change, and molecular docking study of N-(pyridin-2-ylmethylene)aniline derivatives and carbazole Ru(II) complexes with human serum albumin

Abstract

New [$RuCl_2$(COD)(L1)] (**1d**)**,** [$RuCl_2$(COD)(L2)] (**2d**), [$RuCl_2$(COD)(L3)] (**3d**), [$RuCl_2$(COD)(L4)] (**4d**), [$RuCl_2$(COD)(L5)] (**5d**) (**L** = (*p*-R-N-(pyridin-2-ylmethylene)aniline), R = H (**L1**), Cl (**L2**), OCH_3 (**L3**), CH_3 (**L4**), **L5** = (9-ethyl-N-(pyridin-2-ylmethylene)9H-carbazole-3-amine and COD = η^4-cyclooctadiene) complexes were synthesized and characterized by ^{1}H and ^{13}C NMR, melting point analysis, elemental analysis, HR-MS spectrometry, FT-IR and UV-vis spectroscopy. The single crystal X-ray structures of complexes **1d**, **2d** and **3d** revealed coordination of the ligands to the Ru(II) centre in a bidentate manner via the N atoms. The geometry around the Ru(II) centre is pseudooctahedral with the two Cl atoms and the π-bonds of the cyclooctadiene occupying the coordination sites. Interactions of Ru(II) complexes **1d**-**5d** with human serum albumin (HSA) were investigated using UV-vis, synchronous emission and circular dichroism spectroscopy. The results demonstrated that the Ru(II) complexes **1d**-**5d** have significantly strong interaction with HSA proteins. Complexes **1d**, **3d** and **5d** showed high binding constants (K_b) 1.77 × 10^5 dm^3 mol^{-1} (**1d**), 1.07 × 10^5 dm^3 mol^{-1} (**3d**) and 1.07 × 10^5 dm^3 mol^{-1} (**5d**) respectively. Circular dichroism (CD) studies revealed decreased α-helix content within HSA upon interaction with complexes **1d**-**5d**, suggesting a conformational change of the HSA secondary structure. Also, molecular docking studies were carried out to identify the binding models of the HSA-Ru complexes and binding energy of complexes **1d**-**5d** in HSA, which further revealed the contribution of amino acid residues of HSA in Ru(II) complex binding.

Keywords: Ru(II) complexes; N,N' chelated ligands; human serum albumin; synchronous fluorescence spectroscopy; circular dichroism; molecular docking

5.1 Introduction

Metal-mediated drug discovery is of great interest for biological system applications and to pharmaceutical industries, since these molecules can strongly bind and cleave DNA or proteins under physiological conditions for use as therapeutic agents [1-3]. Over the last decades, platinum metal complexes such as cisplatin, carboplatin and oxaliplatin have been studied in clinical trials as anticancer agents, but due to high resistance to the metal complexes and severe side effects, alternative transition metal complexes are required as new therapeutic drugs [4, 5]. Highly active ruthenium(II) organometallic complexes have recently been reported in anticancer studies to replace the platinum metal drugs [6, 7]. Thus KP1019 (indazolium trans-[tetrachloridobis(1H-indazole)ruthenate(III)]) and NAMI-A (imidazolium trans-[tetrachlorido(dimethyl sulfoxide)(1H-imidazole)ruthenate-(III)]) are pioneering ruthenium drugs for potential anticancer and antitumor activity in biological systems [8, 9]. In recent years, organo-ruthenium scaffold (arene) modified drugs such as RAPTA-T, RAPTA-C and RM175 (Fig. 5.1) showed promising anticancer activities in preclinical studies [10-12].

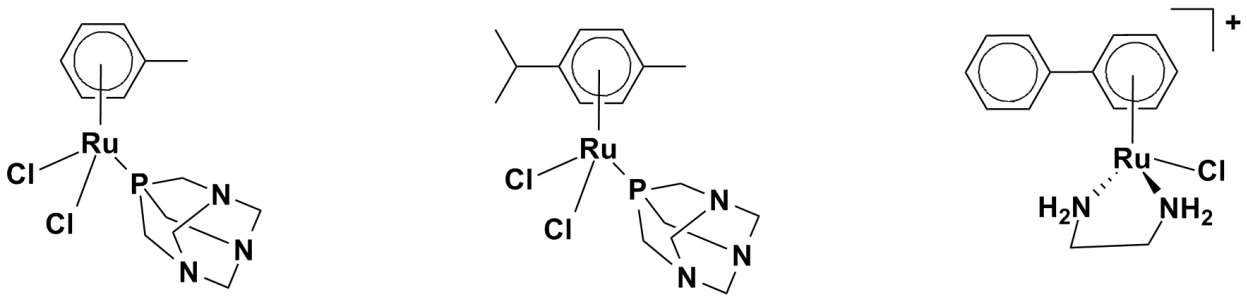

RAPTA-T RAPTA-C RM 175

Fig. 5.1 Structure of ruthenium based anticancer compounds.

The interactions of metallo-drugs with macromolecular blood components have been recognized as crucial for their bio distribution and efficacy. Studies on the interaction mechanism of Ru-based drugs to serum albumins are of great interest due to their potential biological applications. It is known that the distribution, excretion and efficiency of a drug are related to its ability to interact with serum proteins [13-16]. In particular, ruthenium complexes of known anticancer activity have been shown to interact with human serum albumin (HSA) [17-19]. Serum albumins are extensively used in biophysical and biochemical studies as a model system for protein folding, aggregation and drug delivery. HSA is one of the most abundant proteins present in the blood plasma, which assists in the disposition and transportation of various exogenous and endogenous ligands to specific targets [20]. HSA acts as a plasma carrier by nonspecific binding through several hydrophobic steroid hormones across organ-circulatory interfaces such as the liver, intestine, kidney, and brain [21].

Structural aspects of HSA have been well explored. The primary structure of HSA has about 580 amino acid residues in a single peptide chain, which assumes a solid equilateral triangular shape with sides of ~80 Å and depth of ~30 Å [22, 23]. The secondary and tertiary structure of HSA is composed of three α-helical domains I, II and III and each domain contains two subdomains, stabilized by disulfide bridges[22, 23]. Besides domains I (site I) and II (site II), a third (III) domain was recently identified as a binding pocket in subdomain IB [24]. The binding affinity offered by site I is mainly through hydrophobic interaction, while site II involves a combination of hydrophobic, hydrogen bonding and electrostatic interactions [25-28]. It has been reported that aromatic and hetero cyclic ligands possessing higher affinity for serum albumins and showing preferential binding at site II exhibit efficient therapeutic applications [29]. Most of the drugs bind to these site I and II with an affinity of 10^{-4} and 10^{-6} M^{-1} [28]. Therefore, the study of compounds with serum albumins is essential to establish pharmacokinetic behaviour in biological systems. It is widely accepted in the pharmaceutical industry that the overall distribution, metabolism, and efficacy of many drugs can be altered based on their affinity to serum albumin [30]. Obviously, understanding drug-protein interactions can suggest new approaches to drug therapy and design.

In this study, we report the synthesis and characterization of $Ru(COD)Cl_2$ coordinated with ligands (*p*-R-N-(pyridin-2-ylmethylene)aniline) (R = H (**L1**), Cl (**L2**), OCH_3 (**L3**), CH_3 (**L4**)) and 9-ethyl-N-(pyridine-2-ylmethylene)-9H-carbazole-3-amine (**L5**). Their interaction with HSA is also investigated by UV-vis, emission, synchronous emission circular dichroism spectroscopy and molecular docking studies.

5.2 Experimental section

5.2.1 Reagents and general procedures

Unless otherwise stated, all manipulations were performed using standard Schlenk tube techniques under argon atmosphere. The reagents 2-pyridinecarboxaldehdye, aniline, substituted anilines, 1,5-cyclooctadiene (COD), hydrated $RuCl_3 \cdot xH_2O$ (≥99% purity) and solvents were purchased from Sigma-Aldrich, Capital Labs, South Africa and were used without further purification. The NMR solvent $CDCl_3$ was purchased from Merck, Germany. Solvents were dried by standard procedures and distilled prior to use [31]. The metal precursor $Ru(COD)Cl_2$ and 3-amino-9-ethyl-9*H*-carbazole were synthesised as per reported procedures [30, 32, 33].

Melting points were recorded on a Stuart™ scientific apparatus SMP 3 and are uncorrected. ^1H (400 MHz) and ^{13}C (100 MHz) NMR were recorded in $CDCl_3$ and recorded on a Bruker Topspin 400

spectrometer. Elemental analyses were performed on a Thermo-Scientific Flash 2000 CHNS/O analyser. Solid and liquid state infrared spectra were recorded using an FT-IR Perkin Elmer Spectrum 100 spectrophotometer between 4000 - 400 cm^{-1}. High resolution mass spectra were recorded using a Waters Micromass LCT Premier TOF-MS instrument. Single crystal XRD analysis of suitable crystals was performed on a Bruker Smart *APEX11* Nonius Kappa-CCD diffractometer equipped with graphite monochromated Mo - Kα radiation (λ = 0.71073 Å). The electronic absorption spectroscopy (UV/Vis) studies were recorded using a Perkin Elmer precisely Lambda35 and JASCO V-630 instrument.

5.2.2 Synthesis and characterization of the ligands

The ligands (**L1-L4**) were synthesized by using reported procedures and the spectral data of the ligands **L1-L4** match reported data [34, 35]. The following procedure was used to synthesise ligand **L5**: A mixture of 9-ethyl-9H-carbazole-3-amine (2.5 mmol, 530 mg), 2-pyridinecarboxaldehyde (2.5 mmol, 0.25 mL) and 2 drops of glacial acetic acid, in toluene (10 mL), was stirred at room temperature for 24 h. The reaction was monitored by TLC. Once the reaction was completed, the solvent was distilled *in vacuo* to leave the crude product. This was dissolved in diethyl ether (30 mL), and the organic layer was washed with brine (15 mL) and dried over anhydrous $MgSO_4$. The combined organic layer was concentrated *in vacuo*, resulting in a brown oil. Yield (700 mg, 88%). ^{1}H NMR (400 MHz, $CDCl_3$, 25 ºC, ppm) δ = 8.87 (s, 1H, imine CH), 8.75- 8.74 (d, 1H, α proton of Py), 8.31 (d, 1H, J_{H-H} = 7.88 Hz, Py), 8.18 (d, 1H, J_{H-H} = 2.08 Hz, Carb 1st ring), 8.14 (d, 1H, J_{H-H} = 7.72 Hz, Carb 3rd ring), 7.87 (t, 1H, Py), 7.61 (d-d, 1H, Carb 1st ring), 7.53 - 7.49 (m, 1H, Carb 3rd ring), 7.46 (t, 2H, Carb), 7.39 - 7.39 (m, 1H, Py), 7.29 (t, 1H, Carb 3rd ring), 4.42 - 4.37 (q, 2H, N - CH_2), 1.49 (t, 3H, N -CH_3). ^{13}C NMR (100 MHz, $CDCl_3$, 25 °C, ppm) δ = 157.49 (imine C-H), 149.50 (C, Py), 136.76 (C, Py), 126.03 (Carb 3rd ring), 124.67 (Py), 121.62 (Py), 120.61 (Carb 3rd ring), 120.05 (Carb 1st ring), 119.11 (Carb 3rd ring), 113.54, 108.86 (Carb 1st ring), 108.74 (Carb 3rd ring), 37.75 (C, N - $(CH_2)CH_3$), 13.87 (C, N - $CH_2(CH_3)$). FT-IR (γ/cm^{-1}): 3050, 2974, 2931, 1733, (C=N) 1581 (s), 1478 (s), 1469 (s), 1234 (s) 744 (s), 728 (s). UV-Vis (dichloromethane, v/v): λ_{max}(nm) = 242, 291, 321, 377.

5.2.3 Synthesis and characterization of the complexes

The following common procedure was followed for the syntheses of complexes **1d-5d**:
A mixture of the ligand (0.36 mmol) and $Ru(COD)Cl_2$ (0.36 mmol) was dissolved in dry ethanol (10 mL) and the resulting mixture was refluxed for 2 h. The reaction volume was concentrated to a third of its original volume and the suspension was kept at 4 ºC overnight to give brick red solid which was filtered

off, washed with cold ethanol and then diethyl ether. The solid was dissolved in chloroform and excess of *n*-hexane was added to induce the precipitation of the brick red solid product.

5.2.3.1 [$RuCl_2$(COD) (**L1**)] (**1d**)

L1 (0.36 mmol, 66 mg) and Ru(COD)Cl_2 (0.36 mmol, 100 mg). Yield: 72 % (120 mg). Mp. 220.0 °C (dec. turns black without melting). ^{1}H NMR (400 MHz, $CDCl_3$, 25 ºC, ppm) δ = 8.45 (s, 1H, imine CH), 8.25 (d, 1H, J_{H-H} = 5.16 Hz, α proton of Py), 8.01 -7.94 (m, 2H, Py), 7.58 - 7.54 (m, 1H, Py), 7.82 (d, 2H, J_{H-H} = 7.56 Hz, Ph), 7.39 - 7.34 (m, 3H, Ph), 4.75 - 4.74 (m, 2H, -CH, COD), 4.15 - 4.11 (m, 2H, -CH, COD), 2.74 - 2.57 (m, 4H, -CH_2, COD), 2.20 - 2.14 (m, 2H, -CH_2, COD), 2.06 - 2.00 (m, 2H, -CH_2, COD). ^{13}C NMR (100 MHz, $CDCl_3$, 25 °C, ppm) δ = 168.04 (imine C-H), 156.70 (Py), 150.60 (Py), 149.44 (Py), 138.11 (Py), 135.94 (Py), 129.02 (Ph), 128.93 (Ph), 127.88 (Ph), 127.80 (Ph), 120.81 (Ph), 92.25, 91.87 (C, -CH, COD), 29.64, 29.22 (C, -CH_2, COD). FT-IR (γ/cm^{-1}): (COD, C=C) 3038 - 2829 (m), (C=N) 1594 (s), 1203 (s), 767 (s), 702 (s). UV-Vis (dichloromethane, v/v): λ_{max} (nm) = 229, 292, 345, 439. HR-MS (TOF MS ES$^+$) $C_{20}H_{22}N_2Ru$ calculated: 393.0810, found: 393.0815. Anal. Calcd for $C_{20}H_{22}Cl_2N_2Ru$: C, 51.95; H, 4.80; N, 6.06; Found: C, 51.87; H, 5.10; N, 6.33.

5.2.3.2 [$RuCl_2$(COD)(**L2**)] (**2d**)

L2 (0.36 mmol, 78 mg) and Ru(COD)Cl_2 (0.36 mmol, 100 mg). Yield: 82 % (147 mg). Mp. 230.0 °C (dec. turns black without melting). ^{1}H NMR (400 MHz, $CDCl_3$, 25 ºC, ppm) δ = 8.42 (s, 1H, imine CH), 8.25 (d, 1H, J_{H-H} = 5.20 Hz, α proton of Py), 8.00 - 7.95 (m, 2H, Py), 7.59 - 7.56 (m, 1H, Py), 7.43 - 7.42 (d, 1H, J_{H-H} = 2.16 Hz, Ph), 7.41 (t, 1H, Ph), 7.39 (t, 1H, Ph), 7.40 - 7.36 (d, 1H, J_{H-H} = 2.20 Hz, Ph), 4.75 - 4.73 (m, 2H, -CH, COD), 4.11 - 4.10 (m, 2H, -CH, COD), 2.73 - 2.58 (m, 4H, -CH_2, COD), 2.20 - 2.14 (m, 2H, -CH_2, COD), 2.07 - 2.00 (m, 2H, -CH_2, COD). ^{13}C NMR (100 MHz, $CDCl_3$, 25 °C, ppm) δ = 168.50 (imine C-H), 156.46 (Py), 150.67 (Py), 147.73 (Py), 138.17 (Py), 133.67 (Py), 129.20 (Ph), 129.15 (Ph), 128.07 (Ph), 122.22 (Ph), 92.32, 91.86 (C, -CH, COD), 29.61, 29.20 (C, -CH_2, COD). FT-IR (γ/cm^{-1}): (COD, C=C) 3030 - 2830 (m), (C=N) 1595 (s), 1478 (s), 770 (s), 747 (s). UV-Vis (dichloromethane, v/v): λ_{max} (nm) = 229, 292, 347, 445. HR-MS (TOF MS ES$^+$) $C_{20}H_{20}ClN_2Ru$ calculated: 425.0358, found: 425.0350. Anal. Calcd for $C_{20}H_{21}Cl_3N_2Ru$: C, 48.35; H, 4.26; N, 5.64; Found: C, 48.50; H, 4.10; N, 5.45.

5.2.3.3 [$RuCl_2$(COD)(**L3**)] (**3d**)

L3 (0.36 mmol, 77 mg) and Ru(COD)Cl_2 (0.36 mmol, 100 mg). Yield: 87 % (154 mg). Mp. 233.0 °C (dec. turns black without melting). ^{1}H NMR (400 MHz, $CDCl_3$, 25 ºC, ppm) δ = 8.32 (s, 1H, imine CH), 8.15 (d, 1H, J_{H-H} = 5.24 Hz, α proton of Py), 7.91 - 7.83 (m, 2H, Py), 7.47 - 7.44 (m, 1H, Py), 7.31 -

7.29 (d, 2H, J_{H-H} = 8.72 Hz, Ph), 6.83 - 6.81 (d, 2H, J_{H-H} = 8.80 Hz,Ph), 4.65 - 4.64 (m, 2H, -CH, COD), 4.10 - 4.09 (m, 2H, -CH, COD), 2.65 - 2.50 (m, 4H, -CH_2, COD), 2.23 (s, 3H, OCH_3), 2.11 - 2.05 (m, 2H, -CH_2, COD), 1.97 - 1.92 (m, 2H, -CH_2, COD). ^{13}C NMR (100 MHz, $CDCl_3$, 25 °C, ppm) δ = 167.97 (imine C-H), 159.09 (Py), 156.81 (Py), 150.55 (Py), 142.95 (Py), 138.05 (Py), 128.81 (Ph), 127.71 (Ph), 122.03 (Ph), 114.01 (Ph), 92.33, 91.77 (C, -CH, COD), 55.49 (C, OCH_3), 29.65, 29.22 (C, -CH_2, COD). FT-IR (γ/cm^{-1}): (COD, C=C) 2949 - 2829 (m), (C=N) 1595 (s), 1500 (s), 1029 (s), 836 (s) 767 (s). UV-Vis (dichloromethane, v/v): λ_{max} (nm) = 229, 281, 360, 454. HR-MS (TOF MS ES$^+$) $C_{21}H_{24}N_2ORu$ calculated: 421.0854, found: 421.0842. Anal. Calcd for $C_{21}H_{24}Cl_2N_2Ru$: C, 52.94; H, 5.08; N, 5.88; Found: C, 52.80; H, 5.10; N, 5.95.

5.2.3.4 [$RuCl_2$(COD)(**L4**)] (**4d**)

L4 (0.36 mmol, 75 mg) and Ru(COD)Cl_2 (0.36 mmol, 100 mg). Yield: 80 % (140 mg). Mp. 227.0 °C (dec. turns black without melting). ^{1}H NMR (400 MHz, $CDCl_3$, 25 ºC, ppm) δ = 8.41 (s, 1H, imine CH), 8.25 - 8.24 (d, 1H, J_{H-H} = 5.16 Hz, α proton of Py), 7.98 - 7.92 (m, 2H, Py), 7.56 - 7.53 (m, 1H, Py), 7.35 - 7.33 (d, 2H, J_{H-H} = 8.12 Hz, Ph), 7.20 - 7.18 (d, 2H, J_{H-H} = 8.00 Hz, Ph), 4.74 - 4.73 (m, 2H, -CH, COD), 4.16 - 4.15 (m, 2H, -CH, COD), 2.70 - 2.59 (m, 4H, -CH_2, COD), 2.37 (s, 3H, CH_3), 2.19 - 2.13 (m, 2H, -CH_2, COD), 2.05-1.99 (m, 2H, -CH_2, COD). ^{13}C NMR (100 MHz, $CDCl_3$, 25 °C, ppm) δ = 167.90 (imine C-H), 156.77 (Py), 150.57 (Py), 147.15 (Py), 138.06 (Py), 137.71 (Py), 129.44 (Ph), 128.86 (Ph), 127.76 (Ph), 120.62 (Ph), 92.28, 91.86 (C, -CH, COD), 29.64, 29.23 (C, -CH_2, COD), 21.11 (C, CH_3). FT-IR (γ/cm^{-1}): (COD, C=C) 2950 - 2830 (m), (C=N) 1594 (s), 1499 (s), 1298 (s), 770 (s). UV-Vis (dichloromethane, v/v): λ_{max} (nm) = 229, 291, 350, 432. HR-MS (TOF MS ES$^+$) $C_{21}H_{23}N_2Ru$ calculated: 405.0905, found: 405.0897. Anal. Calcd for $C_{21}H_{24}Cl_2N_2ORu$: C, 51.22; H, 4.91; N, 5.69; Found: C, 51.10; H, 5.10; N, 5.77.

5.2.3.5 [$RuCl_2$(COD)(**L5**)] (**5d**)

L5 (0.36 mmol, 108 mg) and Ru(COD)Cl_2 (0.36 mmol, 100mg). Yield: 67 % (138 mg). Mp. 246.0 °C (dec. turns black without melting). ^{1}H NMR (400 MHz, $CDCl_3$, 25 ºC, ppm) δ = 8.54 (s, 1H, imine CH), 8.28(d, 1H, J_{H-H} = 5.24 Hz, α proton of Py), 8.15 (s, 1H, Carb, 1st ring), 8.13(d, 1H, J_{H-H} = 2.08 Hz Carb, 3rd ring), 8.01 - 7.95 (m, 2H, Py), 7.63(d-d, 1H, Carb, 1st ring), 7.58 - 7.54 (m, 1H, Ph), 7.52 (d-d, 1H, Carb, 1st ring),7.45 (d,1H, J_{H-H} = 8.16 Hz Carb, 3rd ring), 7.40 (d,1H, J_{H-H} = 8.60 Hz Carb, 3rd ring), 7.27 (t, 1H, Carb, 3rd ring) 4.77 - 4.76 (m, 2H, -CH, COD), 4.42 - 4.37 (m, 2H, -CH, COD), 4.25 (q, 2H, N - CH_2), 2.74 - 2.58 (m, 4H, -CH_2, COD), 2.20 - 2.14 (m, 2H, -CH_2, COD), 2.02 - 1.96 (m, 2H, -CH_2, COD),1.49 (t, 3H, N - CH_3). ^{13}C NMR (100 MHz, $CDCl_3$, 25 °C, ppm) δ = 168.13 (imine C-H), 157.04 (Py), 150.56 (Py), 138.07 (Py), 128.82 (Py), 127.64, 126.41 121.08, 119.27, 119.05, 112.51, 108.76,

108.32(Carb), 92.39, 91.78 (C, -CH, COD), 37.78 (C, N - CH_2), 29.64, 29.27 (C, -CH_2, COD), 13.89 (C, N - CH_3).FT-IR (γ/cm^{-1}): (COD, C=C) 2951 - 2879 (m), (C=N) 1595 (s), 1468 (s), 1285 (s), 775 (s). UV-Vis (dichloromethane, v/v): λ_{max} (nm) = 239, 268, 297, 336, 351, 422. HR-MS (TOF MS ES^+) $C_{28}H_{28}N_3Ru$ calculated: 508.1327, found: 508.1334. Anal. Calcd for $C_{28}H_{29}Cl_2N_3Ru$: C, 58.03; H, 5.04; N, 7.25; Found: C, 57.95; H, 5.10; N, 7.33.

5.2.4 X-ray crystal structure determination of complexes 1d, 2d and 3d

Suitable crystals for X-ray analysis were grown by slow evaporation of hexane into an acetone solution for **1d**, and slow evaporation of chloroform into an ethanol solution for **2d** and **3d**. The crystals were selected and glued onto the tip of glass fibers, then mounted in a stream of cold nitrogen at 173 ($\pm$2) K and centered in the X-ray beam by using a video camera. The crystal refinement and data collection were performed on a Bruker Smart *APEX11* diffractometer using graphite crystal monochromatised Mo - Kα radiation (λ= 0.71073 Å) and a diffractometer to crystal distance of 4.00 cm. The initial cell matrix was obtained from three series of scans at different starting angles. Each series consisted of 12 frames collected at intervals of 0.5° in a 6° range with the exposure time of about 10 seconds per frame. The reflections were successfully indexed by an automated indexing routine built in the APEXII program suite. The final cell constants were calculated from a set of 6460 strong reflections from the actual data collection. The data collection method involved ω scans of width 0.5°. Data reduction was carried using the program *SAINT+* [36]. The structure was solved by direct methods using *SHELXS* and refined by *SHELXL* [37]. All structures were checked for solvent-accessible cavities using *PLATON* [38] and the graphics were performed with the *DIAMOND* [39] visual crystal structure information system software and *ORTEP-3* [40]. Non-H atoms were first refined isotropically and then by anisotropic refinement with full-matrix least-squares calculations based on F^2 using *SHELXS*. All H atoms were positioned geometrically and allowed to ride on their respective parent atoms. All H atoms were refined isotropically. The absorption correction was based on fitting a function to the empirical transmission surface as sampled by multiple equivalent measurements [38]. Crystal data and structure refinement information for compounds **1d**, **2d** and **3d** are summarized in SI.

5.2.5 HSA binding studies

Human serum albumin (HSA (Fatty acid and Globulin free), fraction V, Product No: A3782) was purchased from Sigma-Aldrich, USA and used without further purification. The stock solution of HSA was prepared by using phosphate buffer saline (PBS) of pH = 7.2. An incubation time of 10 minutes was used to achieve a homogeneous and uniform of mixing of both the HSA and the complexes. The

concentration of HSA (1×10^{-3} mol dm^{-3}) was measured spectrophotometrically by a reported procedure [41].

UV-vis absorption measurements were carried out by using a JASCO V-630 UV-vis spectrophotometer. Quartz cuvettes of path length 1 cm were used to record the absorption spectra. The emission spectral studies were performed with a JASCO FP-6600 spectrofluorometer. All the titration experiments were carried out by adding appropriate amounts of Ru(II) complexes **1d-5d** into 1 mL of HSA solution in a 5 mL standard measuring flask and then made up to the mark with phosphate buffer solution. The solution was allowed to equilibrate for 10 minutes before recording the spectra in a quartz cuvette (1 cm). Blank experiments of complexes with PBS buffer and HSA solutions with PBS buffer were carried out to determine any influence of the buffer solution. No shift in the absorption peaks of either the complex or the protein were observed. It seems the complexes were relatively stable in buffer solution. HSA was excited at 295 nm and the emission was monitored in the absorption region between 300 nm to 500 nm. The emission and excitation slit widths used throughout the experiment were 5 nm and 2 nm, respectively. The synchronous fluorescence spectra were recorded at $\Delta\lambda$ = 15 nm and $\Delta\lambda$ = 60 nm. Stock solutions of serum albumins and Ru(II) complexes were always freshly prepared before use at ambient temperature.

5.2.6 Circular dichroism studies

Circular dichroism (CD) measurements were performed with a JASCO-180 spectropolarimeter using a 0.1 cm path length quartz cell. The CD spectra were recorded in the range of 200–300 nm with 0.1 nm step resolution and averaged over two scans at a speed of 50 nm min^{-1}. All observed spectra were baseline subtracted for buffer solution and the α-helical content was calculated on the basis of change of molar ellipticity values.

5.2.7 Molecular docking studies for complexes 1d-5d

Molecular docking studies were performed for complexes **1d-5d** with human serum albumin protein, to identify the binding mode and the crucial functional groups interacting with the human serum albumin protein using Autodock v4 [42]. Crystal structure of human serum albumin with PDB ID: 1H9Z was taken from protein data bank [43]. The water molecules and the crystal ligand were removed from the crystal structure of protein. Ligands and protein were prepared by adding the Gasteiger charges and polar hydrogen bonds using AutoDock 4.0 and saved as PDBQT files. For the Ruthenium atom the van der Waals and other parameters were obtained from the Autodock website. The grid was generated for the active site residues of the human serum albumin protein using Autogrid. The size of the grid was set up with the spacing 0.375 Å and x, y and z dimensions of 56 x 54 x 40. In the docking tab, docking

calculations were carried out using Lamarckian genetic algorithm to generate the possible conformations of the ligand in the active site of human serum albumin. The best conformation was selected with the lowest binding energy (kcal/mol).

5.3 Results and discussion

5.3.1 Characterization of the ligands and complexes

The ligands **L1**-**L5** and complexes **1d**-**5d** were synthesized and characterized by different spectral techniques. The metal complexes are soluble in solvents such as DMSO, DMF, dichloromethane, ethyl acetate, chloroform, acetonitrile and 3 mg per mL in water at pH 7.20. They are insoluble in petroleum ether, hexane and diethyl ether.

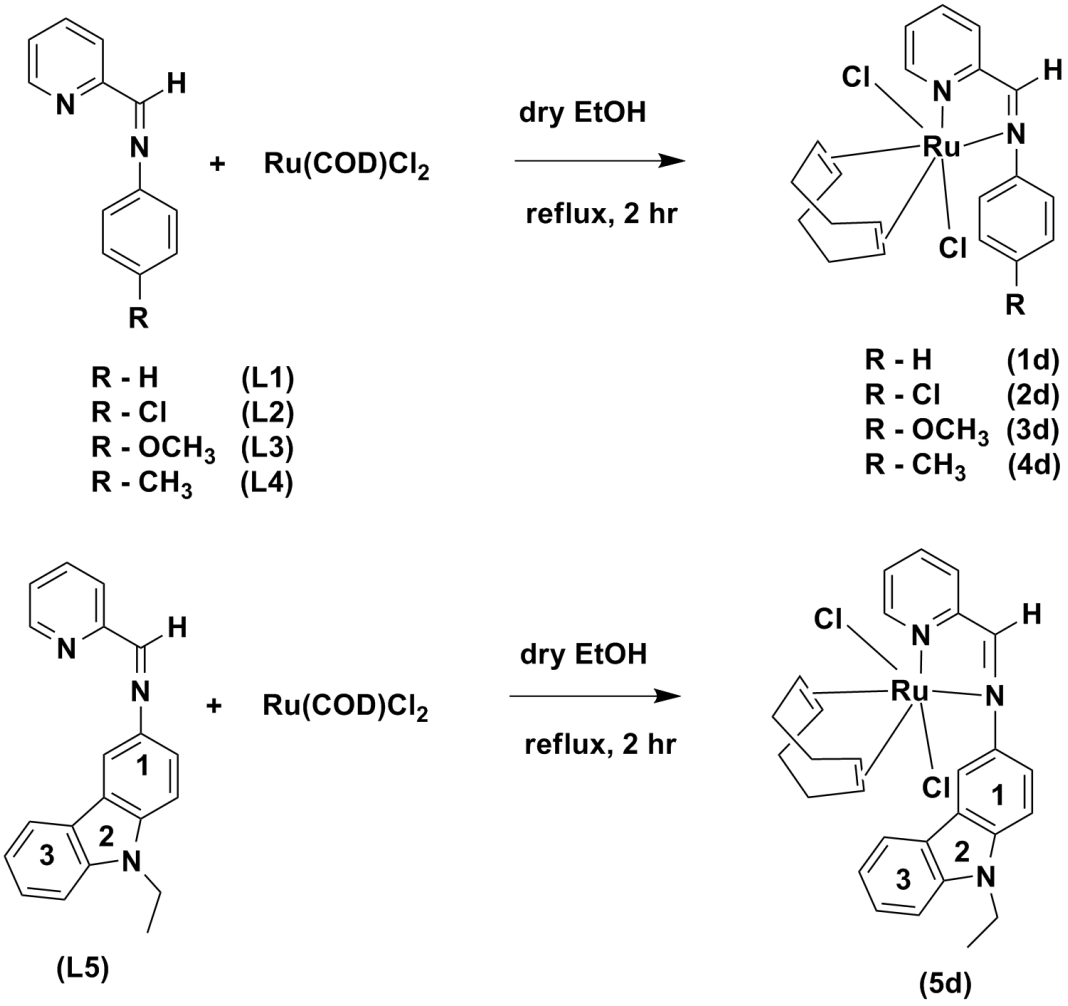

Scheme 5.1: Synthesis of the ruthenium(II) complexes **1d**-**5d**.

5.3.2 NMR studies

The ^{1}H NMR spectra of the free Schiff base ligands **L1-L5**, show a -CH imine proton singlet in the range of 8.67 - 8.87 ppm and the doublet of the α proton of the pyridine ring appeared in the range of 8.77 - 8.75 ppm. When the Schiff base ligands were coordinated with the ruthenium precursor, the singlet peak of the imine proton signal shifted up-field to 8.44 - 8.54 ppm and the doublet peak of the α proton of the pyridine ring shifted up-field to 8.28 - 8.26 ppm. The signals in the aromatic region for all the metal complexes shifted up-field compared to their respective ligand signals. On the other hand, the ^{13}C NMR signals of the imine carbon and the α proton carbon of the pyridine ring of **L5** appeared at 157.5 and 149.5 ppm respectively, whilst in complex **5d** the signals were shifted down-field to 168.1 and 150.6 ppm, respectively. A similar trend was found for all complexes. The ^{1}H and ^{13}C NMR confirms that the Schiff base ligands were coordinated to the ruthenium center through the N atoms.

5.3.3 Infrared spectroscopy

IR spectra of the all ligands **L1-L5** exhibit a sharp peak for C=N stretching in the range 1579 - 1585 cm^{-1}, but for the complexes **1d-5d**, these bands were shifted to higher frequencies in the range of 1594 - 1595 cm^{-1}. This is attributed to the nitrogen atom of the C=N group now being coordinated to ruthenium. The unsaturated cyclic (C=C) stretching frequency was observed for all the complexes at around 2829 - 2957 cm^{-1}, which indicates that the 1,5-cyclooctadiene group is present in the metal complexes. Thus, IR data show that the Schiff base ligands were coordinated to ruthenium through the N atoms.

5.3.4 UV-vis spectroscopy

UV-vis spectra of the ligands **L1-L5** and complexes **1d-5d** were obtained at 10 μM concentrations, in dichloromethane. The spectra of the ligands exhibit one band in the range of 239 - 242 nm, which is attributed to a π-π* transition. Two other bands appeared in the range of 278 - 291 nm and 319 - 338 nm, which are assigned to n-π* transitions of the C=N group in the ligands. The low energy bands for the complexes appeared at 438 nm (**1d**), 445 nm (**2d**), 453 nm (**3d**), 432 nm (**4d**), and 422 nm (**5d**) and the bands at 344 nm (**1d**), 346 nm (**2d**), 359 nm (**3d**), 350 nm (**4d**) and 351 nm (**5d**) may be attributed for the metal to ligand charge transfer (MLCT) transitions. The conjugated intra ligand based π-π* transitions appeared in the UV region at 292 nm (**1d**), 292 nm (**2d**), 281 nm (**3d**), 290 nm (**4d**), and 296 nm (**5d**). The observed band shift variations in the complexes were due to the different donor strengths of the Schiff base nitrogen atoms.

5.3.5 HR-MS spectral studies

The mass spectra of the complexes **1d-5d** were recorded to understand the composition of the metal complexes. The accurate mass of the most abundant peaks present in the metal complexes matched M^{2+} (*m/z*) 393.0815 (**1d**), 425.0350 (**2d**), 421.0842 (**3d**), 405.0897 (**4d**), 508.1334 (**5d**), thus indicating the loss of two chloro groups from the respective metal complexes. It seems that the chloro group is more labile than the other groups present in the metal complexes.

5.3.6 Structural characterization studies

Suitable crystals for structural analysis were grown by vapour diffusion of hexane into an acetone solution for **1d**, and vapour diffusion of chloroform into ethanol solution for **2d** and **3d**. The respective *ORTEP* diagrams for **1d**, **2d** and **3d** are given in Figs. 5.2-5.4, while selected bond distances and bond angles are given in Table 5.1.

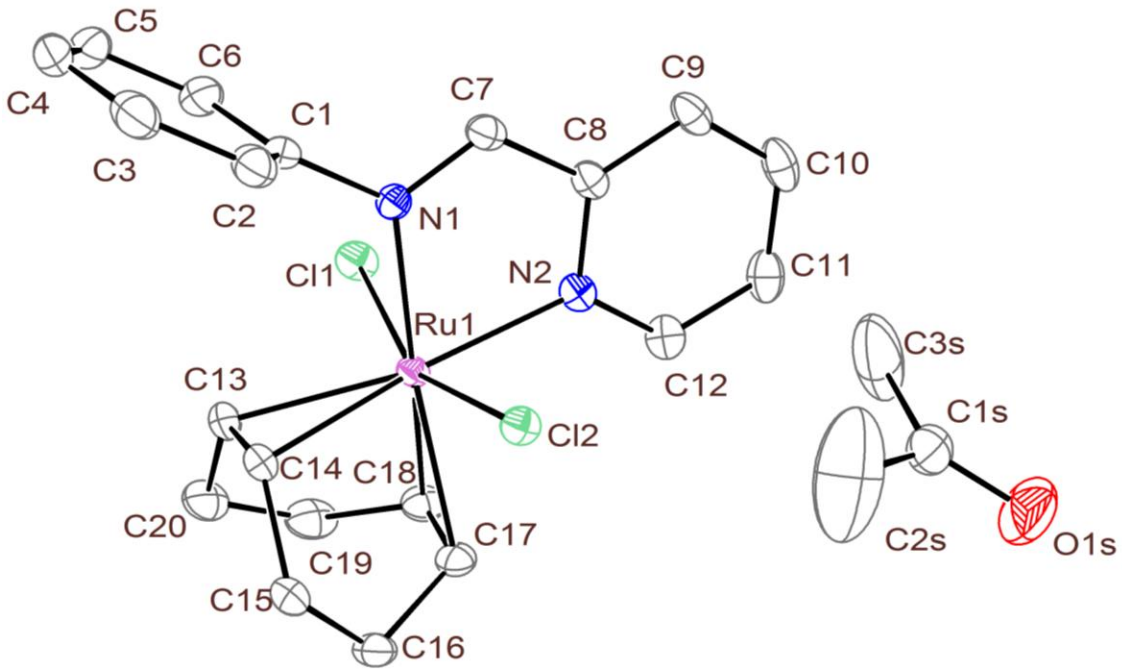

Fig. 5.2 The *ORTEP* diagram of complex **1d**. Displacements of the ellipsoids are drawn by 50% probability and hydrogen atoms are omitted for the clarity.

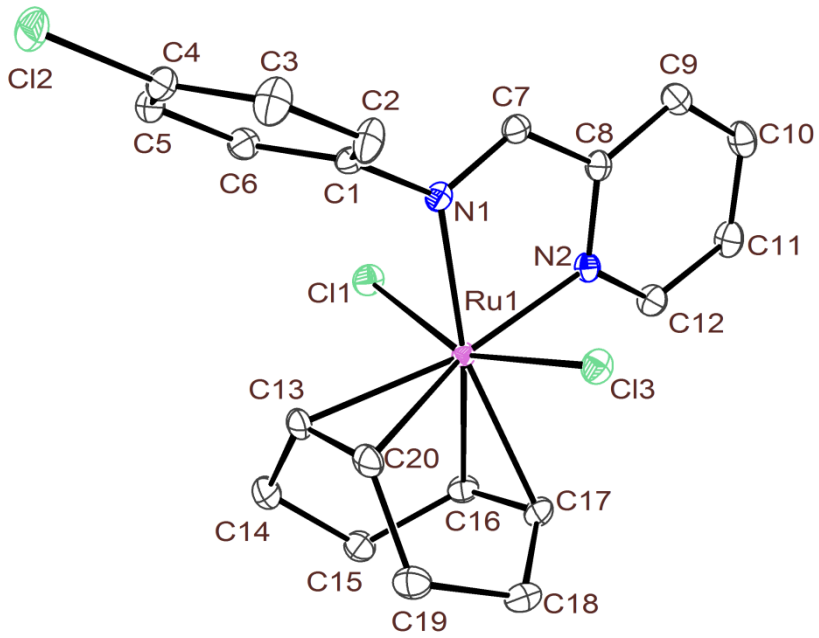

Fig. 5.3 The *ORTEP* diagram of complex **2d**. Displacements of the ellipsoids are drawn by 50% probability and hydrogen atoms are omitted for the clarity.

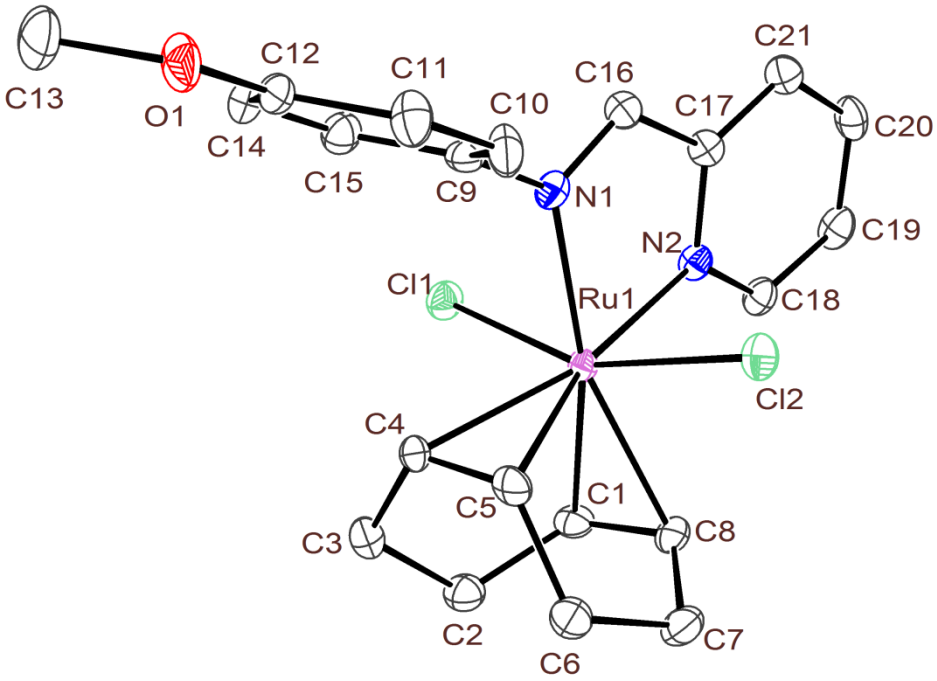

Fig. 5.4 The *ORTEP* diagram of complex **3d**. Displacements of the ellipsoids are drawn by 50% probability and hydrogen atoms are omitted for the clarity.

Whereas the asymmetric unit of complex **1d** has the ruthenium complex and an acetone solvent molecule, the asymmetric units for **2d** and **3d** only contain the complexes. The molecular structures of all three complexes consist of the *N*-pyridinylmethylene aniline (**1d**) or a methoxy (**2d**) or chloro (**3d**) substituted ligand which coordinates to the Ru(II) center via the two N atoms in a bidentate manner forming 5 member metallocycles. The geometry around the Ru(II) center can be described as pseudooctahedral in which four coordination sites are occupied by two Cl atoms and N atoms from the ligand and the remaining by π-bonds of the cyclooctadiene moiety. Cyclooctadiene is bonded to Ru(II) with an η^4 mannered π-olefin bond similar to what is observed in literature [44, 45]. The pseudooctahedral compounds are comparable to piano stool type complexes in which Ru(II) compounds are coordinated to 5 member rings in an η^5 manner [44-47]. The angles around the centre range between 77.90º and 177.28º.

There are two distinct planes in the complex described by (i) the pyridine aryl ring, the C=N imine and the Ru(II) centre, and (ii) the phenyl ring (chloro and methoxy substituted in **2d** and **3d** respectively)**.** The angle between these two planes in all three complexes differ, where in **1** it is 89.53°, in **2d** it is 72.32° and in **3d** it is 78.29°. This correlates to the deviation of the Ru atom from the 5 member metallacycle which is 0.007 Å in complex **1d**, 0.095 Å in complex **2d** and 0.303 Å in complex **3d**. This supports that the bite angles between the N_{aryl} and N_{phenyl} mean planes (ligand) affect the binding nature of the complexes with HSA**.** In addition, the torsion angles of $C_7 - C_8 - N_2 - Ru$ in complexes **1d** and **2d** crystal structures fall at -0.88° and -4.52° and for complex **3d**, the torsion angle of $C_{16} - C_{17} - N_2 - Ru$ was -8.21°, which indicates the N_{aryl} ring of complex **1** is more co-planner to ruthenium than the others. The Ru - $C_{(COD)}$ and Cl - Ru - Cl distances and bond angles of the complexes **1d**-**3d** were in good agreement with reported values in related complexes [45-47]. Non covalent C-H···X and C-H···Cg (Cg = Centroid of the phenyl ring) inter-molecular interactions are observed in the crystal structure of the complexes **1d**-**3d** (SI S12).

Table 5.1 Selected bond distances (Å) and bond angles (°) for complexes **1d**, **2d** and **3d**

Complex 1	**Crystal data**	**Complex 2d**	**Crystal data**	**Complex 3d**	**Crystal data**
Distances (Å)		Distances (Å)		Distances (Å)	
Ru(1) – M1	2.100	Ru(1) – M3	2.092	Ru(1) – M5	2.105
Ru(1) – M2	2.115	Ru(1) – M4	2.100	Ru(1) – M6	2.105
Ru(1) – Cl(1)	2.432(7)	Ru(1) – Cl(1)	2.441(4)	Ru(1) – Cl(1)	2.447(10)
Ru(1) – Cl(2)	2.438(6)	Ru(1) – Cl(3)	2.428(4)	Ru(1) – Cl(2)	2.437(9)
Ru(1) – N(1)	2.093(2)	Ru(1) – N(1)	2.108(12)	Ru(1) – N(1)	2.105(3)
Ru(1) – N(2)	2.113(2)	Ru(1) – N(2)	2.096(12)	Ru(1) – N(2)	2.098(4)
Angles (°)		Angles (°)		Angles (°)	
N(1)-Ru(1)-N(2)	77.96(8)	N(1)-Ru(1)-N(2)	77.99(5)	N(1)-Ru(1)-N(2)	78.22(12)
N(1)-Ru(1)-Cl(1)	81.25(6)	N(1)-Ru(1)-Cl(1)	82.95(3)	N(1)-Ru(1)-Cl(1)	83.10(8)
N(1)-Ru(1)-Cl(2)	82.89(6)	N(1)-Ru(1)-Cl(3)	80.28(3)	N(1)-Ru(1)-Cl(2)	80.69(8)
N(2)-Ru(1)-Cl(1)	82.85(6)	N(2)-Ru(1)-Cl(1)	82.04(3)	N(2)-Ru(1)-Cl(1)	82.17(10)
N(2)-Ru(1)-Cl(2)	80.53(6)	N(2)-Ru(1)-Cl(3)	81.97(3)	N(2)-Ru(1)-Cl(2)	81.21(10)
Cl(1)-Ru(1)-Cl(2)	159.05(2)	Cl(1)-Ru(1)-Cl(3)	158.86(2)	Cl(1)-Ru(1)-Cl(2)	158.80(3)
Cl(1)-Ru(1)-M1	97.18	Cl(1)-Ru(1)-M3	98.16	Cl(1)-Ru(1)-M5	97.63
Cl(2)-Ru(1)-M1	98.49	Cl(3)-Ru(1)-M3	97.53	Cl(2)-Ru(1)-M5	97.65
N(1)-Ru(1)-M1	97.96	N(1)-Ru(1)-M3	175.09	N(1)-Ru(1)-M5	176.10
N(2)-Ru(1)-M1	175.88	N(2)-Ru(1)-M3	97.39	N(2)-Ru(1)-M5	98.06
Cl(1)-Ru(1)-M2	97.96	Cl(1)-Ru(1)-M4	98.99	Cl(1)-Ru(1)-M6	98.91
Cl(2)-Ru(1)-M2	97.25	Cl(3)-Ru(1)-M4	96.42	Cl(2)-Ru(1)-M6	96.81
N(1)-Ru(1)-M2	177.28	N(1)-Ru(1)-M4	177.28	N(1)-Ru(1)-M6	98.91
N(2)-Ru(1)-M2	99.38	N(2)-Ru(1)-M4	98.99	N(2)-Ru(1)-M6	176.72

M1 = Midpoint of C14-C13 (**1d**); M2 = Midpoint of C17-C18 (**1d**); M3 = Midpoint of C16-C17 (**2d**); M4 = Midpoint of C13-C20 (**2d**); M5 = Midpoint of C1-C8 (**3d**); M6 = Midpoint of C4-C5 (**3d**).

5.3.7 Emission spectral studies of HSA in the presence of complexes 1d-5d

HSA possess intrinsic emission properties owing to the tryptophan (Trp), tyrosine (Tyr), and phenylalanine (Phe) residues. The interaction of complexes with HSA often leads to changes in the intrinsic emission property of the protein with respect to the complexes concentration. As a result, fluorimetric titrations have been frequently used to study the interactions of proteins with metal complexes. In the present study, the effect of Ru(II) complexes **1d**-**5d** on the intrinsic emission property of HSA was monitored using emission spectroscopy. The emission spectra recorded for HSA with different concentrations of complexes **1d**-**5d** are shown in Fig. 5.5. The emission spectrum of HSA in the absence of complexes **1d**-**5d** shows an emission maximum at 345 nm, when excited at 295 nm. The excitation wavelength of 295 nm was chosen to avoid any contribution from the Tyr residue and the resulting emission spectrum is exclusively ascribed to the intrinsic Trp fluorophore [48]. As an example, Fig. 5.5 shows the emission spectra resulting from the addition of complex **1d** to HSA. The addition of increasing concentrations of complexes **1d**-**5d** notably reduces the intrinsic emission of HSA without any significant shift in the emission maximum (SI S15). Since the emission spectrum of HSA depends on the degree of exposure of the Trp residues to the solvent polarity and upon its proximity to specific quenching groups, the observed decrease in emission intensity could be attributed to the binding of complexes **1d**-**5d** with HSA. The above interpretation shows that the binding site of complexes **1d**-**5d** on HSA is most probably located near the Trp residue of HSA (Trp-214) [49]. It is well known that quenching of a fluorescent macromolecule can occur due to inner-filter effect, collisional quenching, and binding-related quenching. The mechanism of quenching is obtained from the emission intensity data and not from the emission maximum value. The binding-related quenching is further subdivided into ground-state complex formation between the ligand and the macromolecule, excited-state quenching in the complex (e.g. energy transfer), or structural changes around the fluorophores [50]. To rule out the influence of an inner filter effect, a correction was applied to all the fluorescence data, by the use of equation 1 [50].

$$F_{Corr} = F_{Obs} \times e^{\frac{(A_{exi}+A_{emi})}{2}} \qquad (1)$$

F_{obs} and F_{corr} are the observed and corrected emission intensities, and A_{exi} and A_{emi} are the solution absorption at the excitation and emission wavelengths.

Since the concentrations of the complexes **1d**-**5d** used in the titration experiments were low, most compounds had minimum correction factors. Although overall inner-filter effects were minimal, corrected values were used in all the data treatment and analysis.

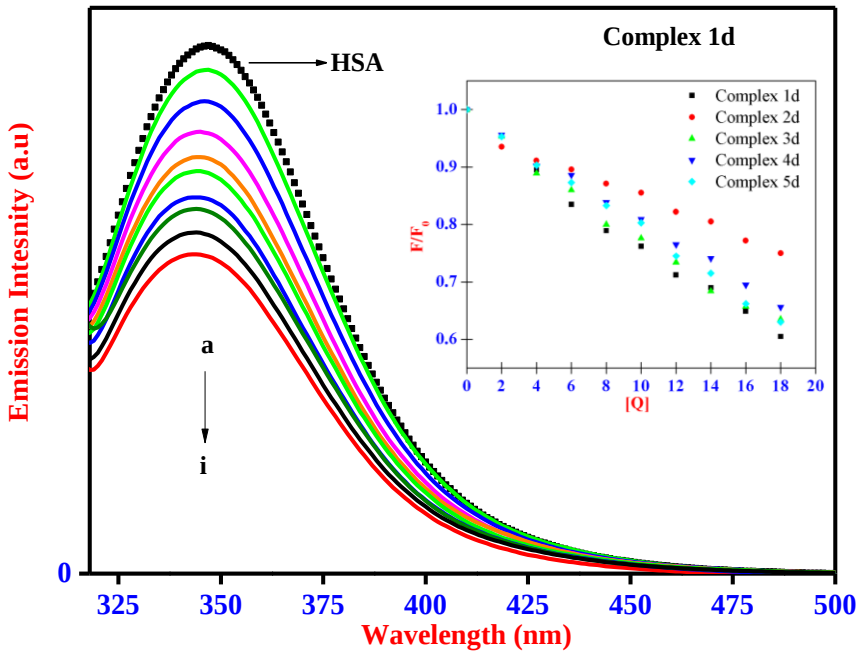

Fig. 5.5 Emission spectra of HSA (1.00×10^{-6} mol dm^{-3}) at various concentrations of complexes **1d-5d**. (a) 0, (b) 2.00×10^{-7}, (c) 4.00×10^{-7}, (d) 6.00×10^{-7}, (e) 8.00×10^{-7}, (f) 10.00×10^{-7}, (g) 12.00×10^{-7}, (h) 14.00×10^{-7} and (i) 16.00×10^{-7} mol dm^{-3}. The arrow shows that emission intensity decreases while increasing the concentration of complex **1d**.

5.3.8 Quenching Mechanism of HSA in the presence of complexes 1d-5d

Fluorescence quenching refers to any process that results in a decrease of fluorescence intensity of a fluorophore. A variety of molecular interactions can result in quenching, including excited-state reactions, molecular rearrangements, energy transfer, ground-state complex formation, and collisional quenching. In order to gain insight into the quenching mechanism, the fluorescence quenching data for complexes **1d-5d** were analyzed by using the Stern-Volmer equation (2) [50],

$$F_0/F = 1 + K_q\,\tau_0\,[Q] = 1 + K_{SV}\,[Q] \qquad (2)$$

where, F_0 and F are the relative corrected emission intensities in the absence and presence of quencher. K_q is the bimolecular quenching rate constant; τ_0 is the average lifetime of the fluorophore in the absence of quencher and [Q] is the concentration of the quencher. K_{sv} is the Stern-Volmer quenching constant which measures the efficiency of quenching.

Fig. 5.6 shows the plot of relative corrected emission intensity at maximum wavelength of HSA *vs* the concentration of complexes **1d-5d**. It demonstrates a good linear relationship within the experimental concentrations of complexes **1d-5d**. The values of the Stern-Volmer quenching constant K_{sv} were obtained from the slope and intercept of the linear plot (Fig. 5.6). The K_q values for the quenching of HSA by the Ru(II) complexes were calculated and are given in Table 5.2. It can be noted that the K_q values of all the complexes **1d-5d** were higher than the accepted limit for diffusion controlled bimolecular quenching constants [50], providing further evidence for the occurrence of static quenching. These combined data strongly suggests that the complexes **1d-5d** bind to HSA and form a dark protein-complex in ground state.

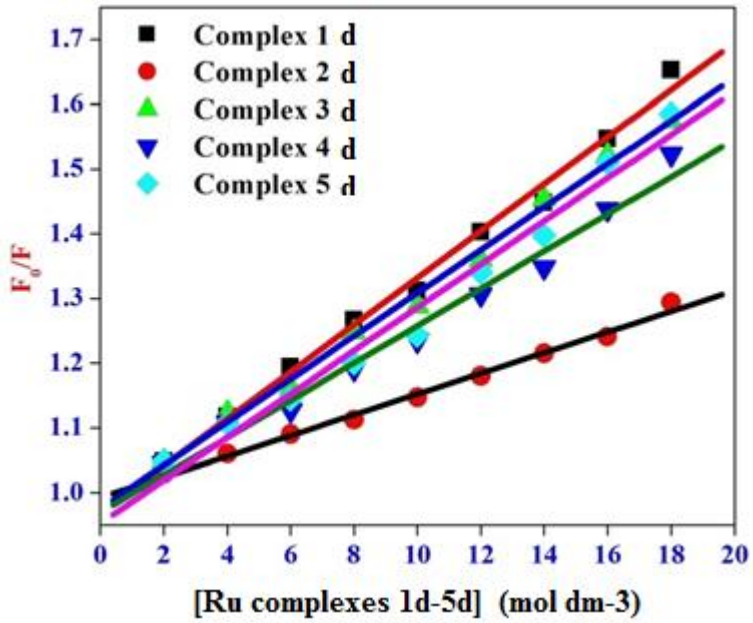

Fig. 5.6 Stern-Volmer plot for HSA with complexes **1d-5d**.

5.3.9 Binding constants and the number of binding sites

The fluorescence quenching data obtained from the interaction of complexes **1d-5d** with HSA were further analyzed to obtain binding constants and the number of binding sites (n) by using the modified double logarithm regression equation (3) [28, 51]. Equation 3 is valid for determining both dynamic and static quenching processes, and the use of equation 3 can give information on the binding site and degree of cooperativity of complexes of HSA [28].

$$\log\left[\frac{F_0-F}{F}\right] = \log K_b + n \log [Q] \quad (3)$$

where, F_0 and F are the corrected emission intensities of HSA in the absence and presence of the complexes **1d**-**5d**, where *n* is the average binding number for complexes **1d**-**5d**, K_b is the binding constant. In Fig. 5.7, the plots of log[(F_0-F)/F] against log(Ru complexes **1d**-**5d**) showed linear relationship with the slope equal to *n*. The average binding site for the complexes **1d**-**5d** is almost equal to 1 for HSA. Moreover, the binding between HSA and complexes **1d**-**5d** is in a 1:1 stoichiometric ratio. The double logarithmic plot for complexes **1d**-**5d** is shown in Fig. 5.7, and obtained data for all the complexes are given in Table 5.2.

HSA consists of three homologous domains (I, II and III) and each domain contains two sub domains labelled as "A" and "B". The primary regions of the ligand or complex binding sites of HSA are located in hydrophobic cavities in sub domains IIA and IIIA [50]. The higher binding constant (K_b) and binding sites (*n*) of the complexes are 1.77×10^5 dm^3 mol^{-1}, 1.14 (**1d**), 1.07×10^5 dm^3 mol^{-1}, 1.11 (**3d**) and 1.07×10^5 dm^3 mol^{-1}, 1.11 (**5d**) respectively, demonstrating stronger affinity to HSA than complexes **2d** and **4d**. It may be attributed to the electron withdrawing chlorine group and electron releasing methyl group present on the phenyl ring of complexes **2d** and **4d** which may affect the planarity of the complexes. In the case of the complex **1d** there is no substitution on the phenyl ring which may assist complex planarity and high interaction with HSA that correlates with experimental results. However, the electron releasing methoxy group present in complex **3d** showed better binding capability with HSA than complex **2d**. The carbazole ligand moiety present in complex **5d** also showed good binding affinity with HSA that may be due to planarity of the carbazole moiety in the complex. The planarity of the complexes **1d**-**3d** were discussed in Section 3.6

Recently, the binding nature of Ru(II) and Cu(II) complexes with DNA or protein were shown to be dependent on the aromatic ring planarity present in the ligands, as reported by Rajendiran *et al*. and Ramakrishnan *et al*. respectively [52, 53]. The binding constants of these synthesized complexes are close to those of reported Ru(II) complexes [54, 55]. These values suggest that these ruthenium complexes bind with HSA in a 1:1 stoichiometric ratio.

Binding interaction of Ru(II) complexes with HSA also depends on the nature of the metal, COD and other groups present in the complex. From the experimental results, in complex **3d** the *p*-methoxy (OCH_3) group might show better interaction compared to the *p*-Cl present in complex **2d**. Complex **5d** shows both electronic and steric effects in the HSA binding studies. The electronic effect of the pyridine ring and the steric effect of the fused carbazole rings of complex **5d** played an important role during the binding study with HSA. According to the experimental studies, the steric effect plays a major role in decreasing the biological activity of complex **5d** compared to complex **1d**.

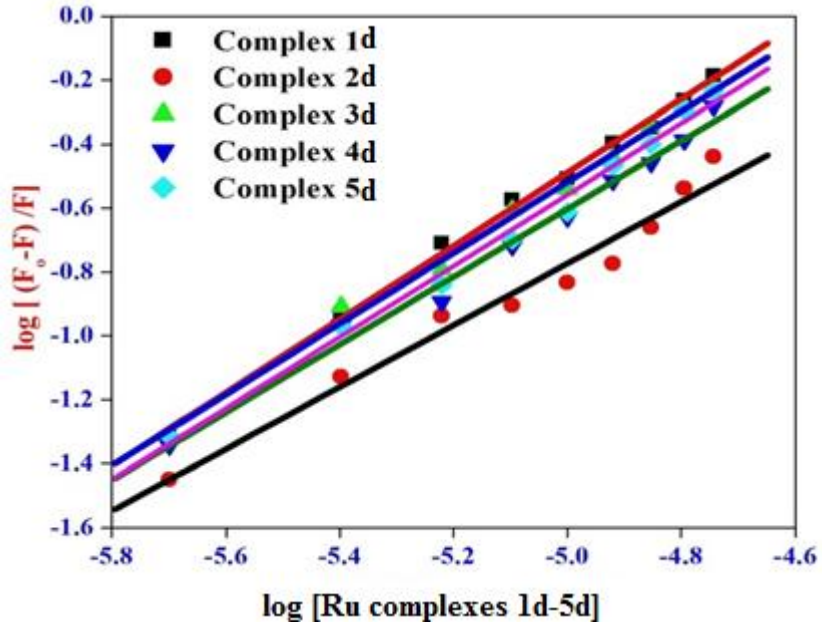

Fig. 5.7 Double logarithmic plot for HSA-complexes **1d-5d**.

Table 5.2 Calculated Stern-Volmer constants (K_{sv}), bimolecular quenching constants (k_q), binding constants (K_b), and number of active sites (*n*) for the interaction of HSA with complexes **1d-5d**

Ru(II) complexes	K_{sv}[a] ($dm^3\ mol^{-1}$) (± 0.20)	K_q ($dm^3 mol^{-1} s^{-1}$) (± 0.17)	K_b[a] ($dm^3\ mol^{-1}$) (± 0.12)	*n*
1d	3.62×10^4	3.62×10^{12}	1.77×10^5	1.14
2d	1.59×10^4	[b]1.59×10^{12}	0.14×10^5	0.98
3d	3.33×10^4	3.33×10^{12}	1.07×10^5	1.11
4d	2.88×10^4	[b]2.88×10^{12}	0.52×10^5	1.06
5d	3.33×10^4	3.33×10^{12}	1.07×10^5	1.11

[a] The mean value of the three individual experiments. [b] ± 0.20.

5.4.0 Conformational studies of HSA in the presence of complexes 1d-5d

Further changes in the serum albumin secondary structure imparted by the presence of the complexes are confirmed by UV-vis absorption, synchronous fluorescence and circular dichroism analyses.

5.4.1 Absorption spectral studies of HSA with complexes 1d-5d

UV-vis absorption is a simple but efficient technique to explore structural changes and to show complex formation. The absorption profile of HSA is characterized by a strong absorption at 208 nm which is ascribed to the π-π^* transition of the polypeptide backbone structure C=O of HSA [30, 56]. In addition the absorption peak at 278 nm mainly originates from the aromatic amino acid residues, viz Trp, Tyr, and Phe. It is well known that the absorption maximum of HSA is highly sensitive to the surrounding micro environment and it displays a substantial spectral shift upon changes in protein conformation [57]. In order to explore the structural changes of HSA and to establish the quenching mechanism, the absorption spectra of HSA was recorded in the presence of increasing concentrations of complexes **2d-5d** (See SI S16). As depicted in Fig. 5.8, the absorption intensity of HSA at 208 nm and 278 nm increased simultaneously with the incremental addition of complex **1d**. It is pertinent to note that the absorption maximum at 278 nm is red shifted to 283 nm. It is widely reported that the interaction between serum proteins and complexes leads to perturbation of the protein absorption spectrum [56]. It is believed that the increase in absorption maxima of HSA at 208 nm and 278 nm is solely due to the interaction of complexes **1d-5d** with HSA and increase in the hydrophobicity around Trp residues of HSA. It is widely reported that the formation of the ground state complex between the protein and complex often leads to alteration in the absorption spectrum of the proteins [30, 56]. Blank UV-vis experiments were done to allow comparison of the spectra of HSA alone, complex **1d** alone and HSA with complex **1d**. No significant overlap was observed in the range of 220-310 nm in UV-vis spectra, as shown in SI S16.

Subsequently, the perturbation in the absorption spectra of serum protein suggests that complexes **1d-5d** are primarily initiated by the static quenching process and this corroborates well with the results obtained from the emission spectral studies.

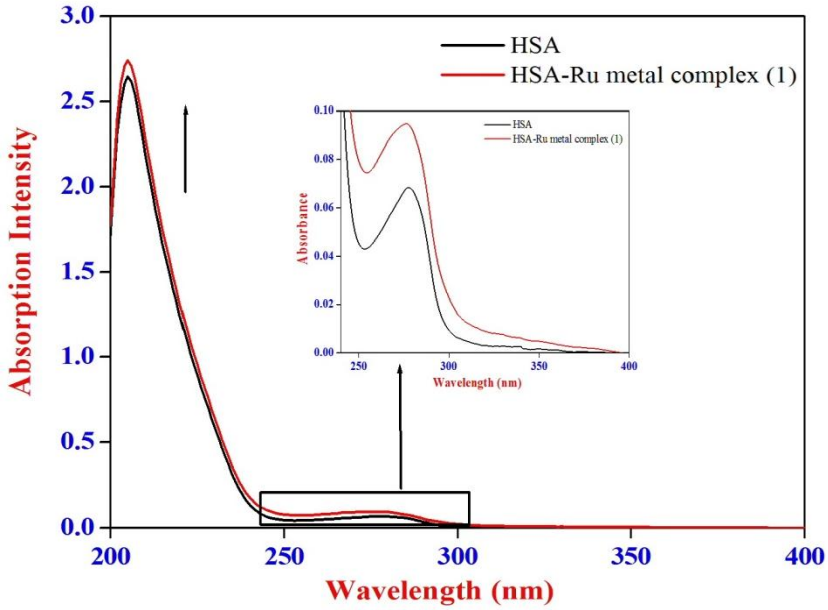

Fig. 5.8 Absorption spectra of HSA = HSA-Complex **1d** = 1.0×10^{-6} mol dm^{-3}.

5.4.2 Synchronous fluorescence spectroscopy of HSA with complexes 1d-5d

Synchronous fluorescence spectroscopy, introduced by Lloyd [58, 59], involves a simultaneous scanning of the excitation and the emission monochromators while maintaining a constant wavelength interval between them. It is used to study the conformation change of proteins and gives information about the molecular environment in the vicinity of Tyr and Trp residues. According to the theory of Miller [60], when $\Delta\lambda$ between excitation and emission wavelength is stabilized at 15 nm or 60 nm, the spectral characteristics of the protein Tyr or Trp residues are observed. The synchronous fluorescence spectrum of HSA in the presence of complex **1d** is shown in Fig. 5.9 (For complexes **2d-4d** See SI S17). As can be seen from Fig. 5.9, the maximum emission wavelength of Trp in HSA has a slight blue shift from 344 nm to 341 nm and a slight red shift from 301 nm to 303 nm for HSA. The above results indicate that in the presence of complexes **1d-5d** the conformation of HSA was altered and the polarity around the Trp residues was decreased with increase in hydrophobicity [49, 61]. It is apparent from the above analysis that the synchronous emission intensity of both Tyr and Trp decreased instantaneously upon the addition of complexes **1d-5d** and this corroborates the occurrence of emission quenching in the binding process. The results from these synchronous fluorescence studies further suggest that the binding regions of complexes **1d-5d** are located in the vicinity of both Tyr and Trp residues of HSA, since a distant event cannot cause the synchronous emission quenching of both Tyr and Trp residues. Therefore, from synchronous fluorescence experiments it can be concluded that the binding site of complexes **1d-5d** in HSA is located adjacent to both Tyr and Trp residues.

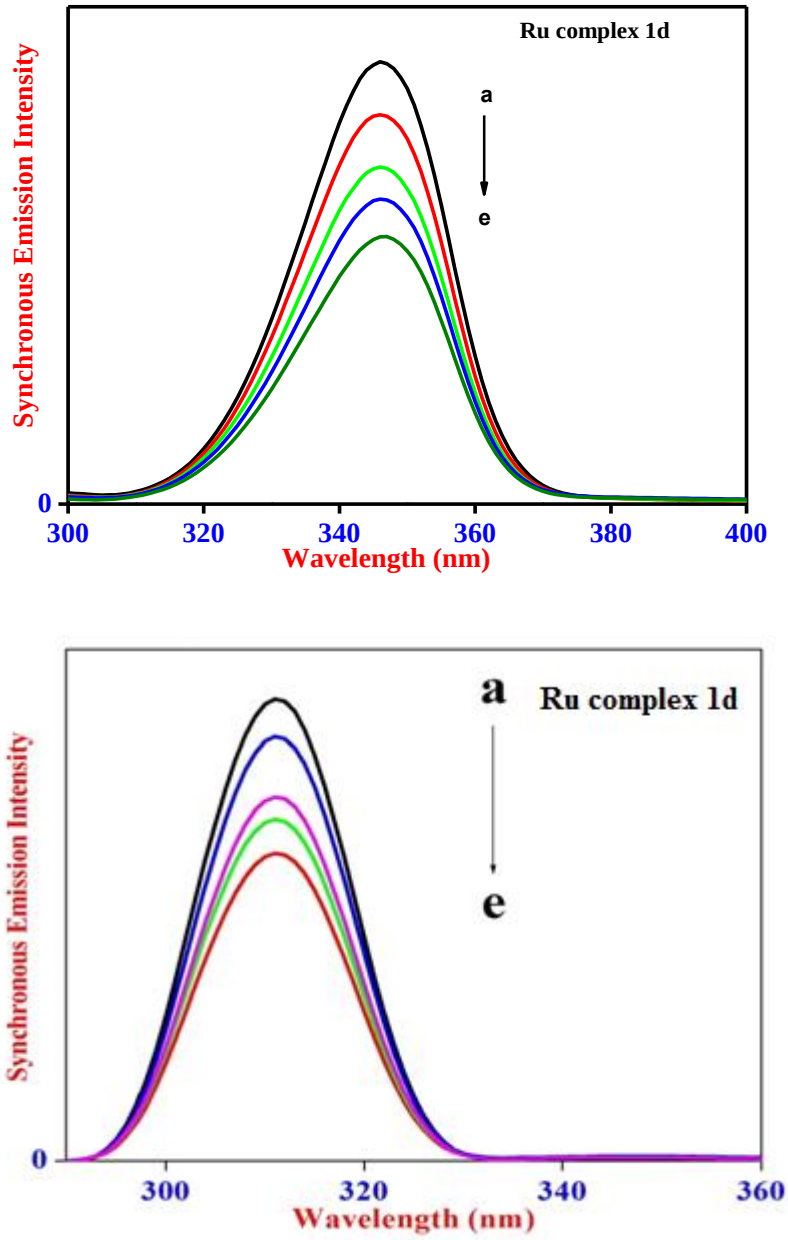

Fig. 5.9 Synchronous emission spectra of HSA (2 x 10^{-6} mol dm^{-3}) at $\Delta\lambda$ = 60 nm at various concentrations of complex **1d**. (a) 0, (b) 4.00 × 10^{-7}, (c) 8.00 × 10^{-7}, (d) 12.00 × 10^{-7} and (e) 16.00 × 10^{-7}mol dm^{-3}.

5.4.3 Circular dichroism spectroscopy of HSA-Complexes 1d-5d

To gain a better understanding of the conformational behavior of the HSA-complexes system, the CD spectra of HSA in the absence and presence of complexes **1d-5d** were obtained. The observed CD

results were first transformed into mean residue ellipticity (MRE) according to the following equation [62],

$$\mathrm{MRE} = \frac{\mathrm{ObservedCD(mdeg)}}{[\mathrm{Cpn}lx10]} \qquad (4)$$

where, C_P is the molar concentration of the protein, n is the number of amino acid residues (585 amino acids for HSA) and *l* is the path length of the cell.

The helicity content of the protein is then determined from the calculated MRE values at 222 nm using the following equation,

$$\alpha - \text{Helix content } (\%) = \left[\frac{-\mathrm{MRE}_{208} - 4000}{33000 - 4000}\right] \text{x } 100 \qquad (5)$$

where, MRE 208 is the observed MRE value at 208 nm, 4000 is the MRE of the β-form and random coil conformation cross at 208 nm and 33000 is the MRE value of a pure α-helix at 208 nm.

In free HSA, the secondary structure consists of ~58% α-helix, ~20% β-sheets and ~22% random coils. The CD spectrum of HSA exhibits two negative peaks in the ultraviolet region at 208 and 222 nm, which are characteristic of the α-helix structure in proteins. The binding of complex **4d** (Fig. 5.10 and for complexes **1d**-**3d** & **5d** SI S19) to HSA caused a decrease in band intensity at all wavelengths of the CD spectra without any significant shift of the peaks, which indicates a decrease of the α-helix content in the protein structure at molar ratio of the complexes to HSA of 1:1. The acting force of these HSA-complex interactions might be hydrophobic or hydrophilic interactions, as well as hydrogen bonding. The decreasing α-helix content suggests that the binding of complexes with HSA induces a slight unfolding of the constituent polypeptides of the protein, some secondary-structure changes in HSA, and the exposure of some hydrophobic regions increased [63]. It is possible that the hydrophobic interaction occurred in the region of the IB sub domain due to the presence of the L-Trp and L-Tyr hydrophobic amino acid residues in this sub domain of HSA [64]. This is consistent with the results of the synchronous fluorescence spectroscopy.

Thus complexes **1d-5d** cause a conformational change of the protein, with the loss of α-helical stability. The quantitative analyses of the α-helix content was determined by using Eqns. 4 and 5 and the obtained results are reported in Table 5.3, which show the decrease in the α-helix content in HSA upon addition of complexes **1d**-**5d**. The difference in CD spectral values of HSA protein conformation upon binding with Ru(II) complexes may be attributed to different substituent groups in the ligand moieties of the complexes. The carbazole ligand containing complex **5d** showed highest α-helix stability, which decreased from values of 57.84 to 52.36%, which may be due to the additional phenyl rings present in the

carbazole moiety. The Ru(II) complex bound to HSA causes the conformational change in α-helix stability, due to the inherent flexibility at the IIA domain [28].

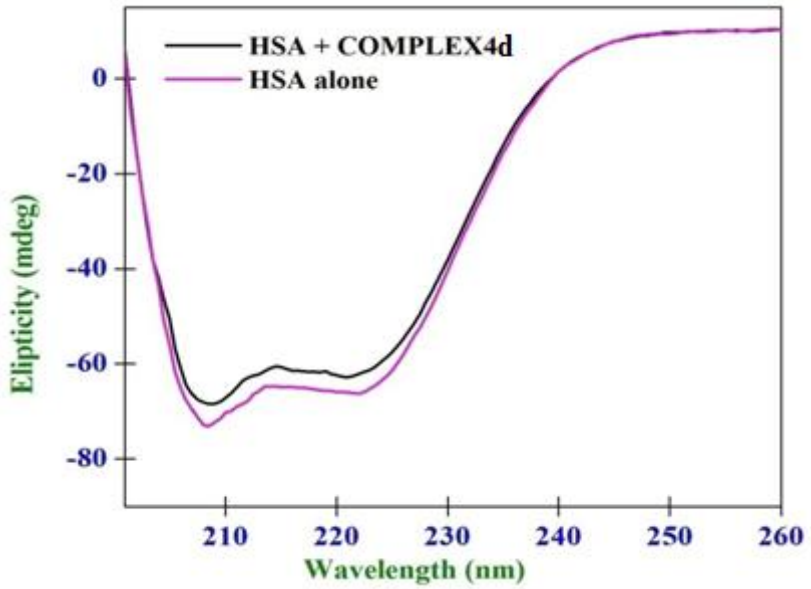

Fig. 5.10 Circular dichroism of HSA in the presence and absence of complex **4d**. HSA = complex **4d** = 1.0×10^{-6} mol dm^{-3}.

Table 5.3 Circular dichroism spectral values (±2) % of HSA and complexes **1d-5d**

System	Complex 1d	Complex 2d	Complex 3d	Complex 4d	Complex 5d
% of α-Helix content in HSA	57.15	57.97	57.06	57.73	57.84
% of α-Helix content in HSA + Complex	53.78	54.64	53.87	53.06	52.36

5.4.4 Molecular docking studies

A molecular docking study was performed to understand the possible binding conformation and binding location of complexes **1d-5d** in the protein environment, which is important [57]. The lowest binding energy conformation of the complexes was used for docking analysis, out of 10 different possible conformations. During the docking analysis, possible binding sites of complex **1d** were obtained, of which the lowest free energy for HSA has been shown in Fig. 5.11. The diagram (Fig. 5.11) of the docking study reveals that HSA subdomain IIA has more favourable binding sites for complexes **1d-5d**.

The HSA subdomain IIA entrance pocket is surrounded by Trp 214, Arg 222, His 242, Leu 238 and Ala 291. These amino acid residues are responsible for the hydrophobic and van der Waals interaction with complexes **1d-5d**. Docking studies reveal that complexes **1d-5d** are located closer to the active site residues of Trp 214, Arg 222, His 242, Leu 238 and Ala 291 in HSA subdomain IIA. The phenyl group of complexes **1d-5d** forms π-π stacking with Trp 214 and His 242. The secondary interactions between Ru metal and His 242 nitrogen for complexes **1d-5d** are given in the SI S19. This interaction indicates that the phenyl groups of the complexes are crucial for inducing conformational changes in the protein [49]. These complexes bind in the drug binding pocket of HSA subdomain IIA in a similar fashion to the warfarin [43]. The binding energies of complexes **1d-5d** were obtained in the range of -5.73 to -6.67 kcal/mol, listed in Table 5.4. Complex **1** shows the highest binding energy among complexes **1d-5d,** with a binding energy of -6.67 kcal/mol. The hydrophobic interaction within the protein active sites is increased, which leads to the stabilization of the HSA-complexes.

Table 5.4 Binding energy values of the complexes **1d-5d**

Complexes	Binding energy (kcal/mol)
1d	-6.67
2d	-5.94
3d	-6.23
4d	-5.73
5d	-6.24

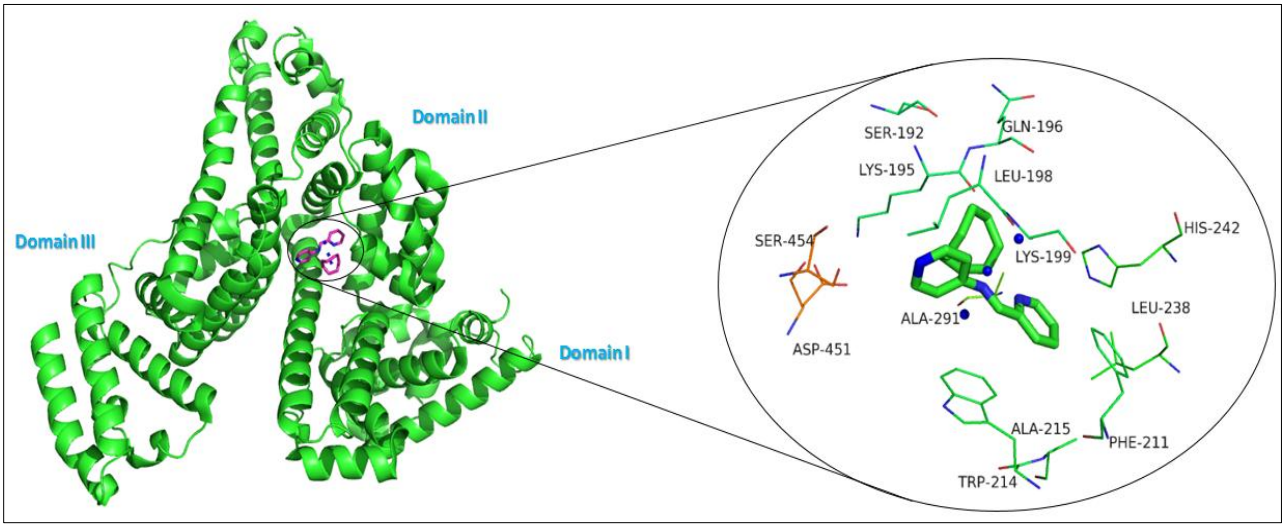

Fig. 5.11 Molecular docking of the complex **1d** with HSA.

5.5 Conclusions

In conclusion, new Ru(II) aniline and amine complexes were synthesized and characterized. Single crystal X-ray studies showed the expected pseudooctahedral geometry in the crystal structures. The emission spectra revealed that interactions of complexes **1d-5d** occurred with HSA and caused an increase in the hydrophobicity around the Trp residues of HSA. Fluorescence quenching of HSA is induced by the Ru(II) complexes following the static quenching mechanism. The binding constant study revealed that the planarity and substitution of the ligands present in the complexes were responsible for the binding affinity with HSA.

In synchronous emission spectra, blue and red shifts for complexes **1d-5d** confirmed that the binding site of the complexes in HSA are most probably located adjacent to both Trp and Tyr residues. The circular dichroism study further confirmed the loss of α-helix stability during the addition of the complexes **1d-5d** to HSA, whilst the binding of the Ru(II) complexes with HSA initiates the secondary structure change and increases hydrophobic interactions in HSA. Furthermore, the molecular docking study revealed that the amino acid residue Trp-214 in the HSA subdomain IIA is the most favourable binding location for complexes **1d-5d**. Further, the binding energies of complexes **1d-5d** were found between -5.73 to -6.67 kcal/mol.

Acknowledgements

Authors would like to thank the NRF and University of KwaZulu - Natal, Durban, South Africa for financial support and facilities. We also would like to thank Dr. Sukesh Kalva for valuable guideline during the molecular docking study.

Appendix A. Supplementary Information

^{1}H and ^{13}C NMR data, HR-MS, UV-vis, emission spectra, synchronous emission spectra, and circular dichroism spectra for complexes **1d-5d** are also shown in the SI. Selected intermolecular interactions in the crystalline structures of Ru(II) complexes **1d-3d** can be consulted in the SI. CCDC-1408763 (**1d**), CCDC-1408764 (**2d**), and CCDC-1408765 (**3d**) contain the supplementary crystallographic data in this paper. These data can be obtained free of charge from the Cambridge crystallographic data center via *www.ccdc.cam.ac.uk/data_request/cif.* Supplementary data associated with this article can be found, in the online version, at http://dx.doi.org/10.1016/j.poly.

References

[1] O. Zelenko, J. Gallagher, Y. Xu, D.S. Sigman, Inorg. Chem. 37 (1998) 2198-2204.

[2] M. Hanif, A.A. Nazarov, A. Legin, M. Groessl, V.B. Arion, M.A. Jakupec, Y.O. Tsybin, P.J. Dyson, B.K. Keppler, C.G. Hartinger, Chem. Commun. 48 (2012) 1475-1477.

[3] A. Kurzwernhart, W. Kandioller, S. Bächler, C. Bartel, S. Martic, M. Buczkowska, G. Mühlgassner, M.A. Jakupec, H.-B. Kraatz, P.J. Bednarski, V.B. Arion, D. Marko, B.K. Keppler, C.G. Hartinger, J. Med. Chem. 55 (2012) 10512-10522.

[4] L. Kelland, Nat. Rev. Cancer 7 (2007) 573-584.

[5] S.B. Howell, R. Safaei, C.A. Larson, M.J. Sailor, Mol. Pharmacol. 77 (2010) 887-894.

[6] R.E. Morris, R.E. Aird, P. del Socorro Murdoch, H. Chen, J. Cummings, N.D. Hughes, S. Parsons, A. Parkin, G. Boyd, D.I. Jodrell, P.J. Sadler, J. Med. Chem. 44 (2001) 3616-3621.

[7] S. Schäfer, I. Ott, R. Gust, W.S. Sheldrick, Eur. J. Inorg. Chem. 2007 (2007) 3034-3046.

[8] S.K. Stevens, A.P. Strehle, R.L. Miller, S.H. Gammons, K.J. Hoffman, J.T. McCarty, M.E. Miller, L.K. Stultz, P.K. Hanson, Mol. Pharmacol. 83 (2013) 225-234.

[9] G. Sava, S. Zorzet, C. Turrin, F. Vita, M. Soranzo, G. Zabucchi, M. Cocchietto, A. Bergamo, S. DiGiovine, G. Pezzoni, L. Sartor, S. Garbisa, Clin. Cancer. Res. 9 (2003) 1898-1905.

[10] C. Scolaro, A. Bergamo, L. Brescacin, R. Delfino, M. Cocchietto, G. Laurenczy, T.J. Geldbach, G. Sava, P.J. Dyson, J. Med. Chem. 48 (2005) 4161-4171.

[11] K.J. Kilpin, S. Crot, T. Riedel, J.A. Kitchen, P.J. Dyson, Dalton Trans. 43 (2014) 1443-1448.

[12] P. Nowak-Sliwinska, J.R. van Beijnum, A. Casini, A.A. Nazarov, G. Wagnières, H. van den Bergh, P.J. Dyson, A.W. Griffioen, J. Med. Chem. 54 (2011) 3895-3902.

[13] I. Ascone, L. Messori, A. Casini, C. Gabbiani, A. Balerna, F. Dell'Unto, A.C. Castellano, Inorg. Chem. 47 (2008) 8629-8634.

[14] M. Groessl, M. Terenghi, A. Casini, L. Elviri, R. Lobinski, P.J. Dyson, J. Anal. At. Spectrom. 25 (2010) 305-313.

[15] A.Y. Shmykov, V.N. Filippov, L.S. Foteeva, B.K. Keppler, A.R. Timerbaev, Anal. Biochem. 379 (2008) 216-218.

[16] A.R. Timerbaev, C.G. Hartinger, S.S. Aleksenko, B.K. Keppler, Chem. Rev. 106 (2006) 2224-2248.

[17] L. Messori, P. Orioli, D. Vullo, E. Alessio, E. Iengo, Eur. J. Biochem. 267 (2000) 1206-1213.

[18] I.N. Stepanenko, A. Casini, F. Edafe, M.S. Novak, V.B. Arion, P.J. Dyson, M.A. Jakupec, B.K. Keppler, Inorg. Chem. 50 (2011) 12669-12679.

[19] I. Romero-Canelón, L. Salassa, P.J. Sadler, J. Med. Chem. 56 (2013) 1291-1300.

[20] T. Peters, in: T. Peters (Ed.), Biochemistry, Genetics and Medical Applications, Academic Press, San Diego, USA, 1995, pp. 76-132.

[21] P. Banerjee, S. Pramanik, A. Sarkar, S.C. Bhattacharya, J. Phys. Chem. B 113 (2009) 11429-11436.

[22] M.K. Helms, C.E. Petersen, N.V. Bhagavan, D.M. Jameson, FEBS Lett. 408 (1997) 67-70.

[23] M. El-Kemary, M. Gil, A. Douhal, J. Med. Chem. 50 (2007) 2896-2902.

[24] F. Zsila, Mol. Pharm. 10 (2013) 1668-1682.

[25] X.M. He, D.C. Carter, Nature 358 (1992) 209-215.

[26] T. Peters, in: Yoshinori Mine, Fereidoon Shahidi (Eds.), Nutraceutical Proteins and Peptides in Health and Disease, CRC press, NewYork, 1985, pp. 161 - 245.

[27] V. Lhiaubet-Vallet, Z. Sarabia, F. Boscá, M.A. Miranda, J. Am. Chem. Soc. 126 (2004) 9538-9539.

[28] D.P. Yeggoni, M. Gokara, D. Mark Manidhar, A. Rachamallu, S. Nakka, C.S. Reddy, R. Subramanyam, Mol. Pharm. 11 (2014) 1117-1131.

[29] T. Patrice, Photodynamic Therapy, Royal Society of Chemistry Cambridge, UK, 2004.

[30] Y.-J. Hu, Y. Liu, X.-H. Xiao, Biomacromolecules 10 (2009) 517-521.

[31] D.D.A. Perrin, W. L. F.; Perrin, D. R, Purification of laboratory chemicals, Pergamon: Oxford, UK, 1986.

[32] M.O. Albers, T.V. Ashworth, H.E. Oosthuizen, E. Singleton, J.S. Merola, R.T. Kacmarcik, Inorg. Synth. 2007, pp. 68-77.

[33] C.W. Cheung, D.S. Surry, S.L. Buchwald, Org. Lett. 15 (2013) 3734-3737.

[34] C.-H. Chien, S. Fujita, S. Yamoto, T. Hara, T. Yamagata, M. Watanabe, K. Mashima, Dalton Trans. (2008) 916-923.

[35] T.S. Basu Baul, S. Kundu, H. Höpfl, E.R.T. Tiekink, A. Linden, Polyhedron 55 (2013) 270-282.

[36] Bruker-AXS, Bruker-AXS, Madison, Wisconsin, USA, 2009.

[37] G.M.Sheldrick, Acta. Crystallogr. A64 (2008) 112-122.

[38] A.L. Spek, Acta. Crystallogr. D65 (2009) 148-155.

[39] K. Brandenburg, H. Putz, DIAMOND Crystal Impact GbR, Bonn (2005).

[40] L. J. Farrugia, *ORTEP-3* for Windows. J. Appl. Crystallogr. 30 (1997) 565.

[41] B.K. Hoefelschweiger, A. Duerkop, O.S. Wolfbeis, Anal. Biochem. 344 (2005) 122-129.

[42] G.M. Morris, D.S. Goodsell, R.S. Halliday, R. Huey, W.E. Hart, R.K. Belew, A.J. Olson, J. Comput. Chem. 19 (1998) 1639-1662.

[43] I. Petitpas, A.A. Bhattacharya, S. Twine, M. East, S. Curry, J. Biol. Chem. 276 (2001) 22804-22809.

[44] H. Chiririwa, R. Meijboom, Acta Crystallogr., Sect. E: Struct. Rep. Online 67 (2011) m1336-m1336.

[45] J. Gómez, G. García-Herbosa, J.V. Cuevas, A. Arnáiz, A. Carbayo, A. Muñoz, L. Falvello, P.E. Fanwick, Inorg. Chem. 45 (2006) 2483-2493.

[46] J.A. Widegren, H. Weiner, S.M. Miller, R.G. Finke, J. Organomet. Chem. 610 (2000) 112-117.

[47] H. Chiririwa, R. Meijboom, S.O. Owalude, U.B. Eke, C. Arderne, Acta Crystallogr., Sect. E: Struct. Rep. Online 67 (2011) m1096-m1096.

[48] M.R. Eftink, C.A. Ghiron, Biochem. 15 (1976) 672-680.

[49] F. Li, M. Feterl, J.M. Warner, A.I. Day, F.R. Keene, J.G. Collins, Dalton Trans. 42 (2013) 8868-8877.

[50] J.R. Lakowicz, Principles of Fluorescence Spectroscopy, 3 ed., Springer, US, 2006.

[51] E. Lissi, C. Calderón, A. Campos, Photochem. Photobiol. 89 (2013) 1413-1416.

[52] V. Rajendiran, M. Murali, E. Suresh, M. Palaniandavar, V.S. Periasamy, M.A. Akbarsha, Dalton Trans. (2008) 2157-2170.

[53] S. Ramakrishnan, V. Rajendiran, M. Palaniandavar, V.S. Periasamy, B.S. Srinag, H. Krishnamurthy, M.A. Akbarsha, Inorg. Chem. 48 (2009) 1309-1322.

[54] T.S. Morais, F.C. Santos, L. Corte-Real, M.H. Garcia, J. Inorg. Biochem. 129 (2013) 94-101.

[55] F. Beckford, J. Thessing, J. Woods, J. Didion, N. Gerasimchuk, A. Gonzalez-Sarrias, N.P. Seeram, Metallomics 3 (2011) 491-502.

[56] A.S. Sharma, S. Anandakumar, M. Ilanchelian, RSC Adv. 4 (2014) 36267-36281.

[57] A. Selva Sharma, S. Anandakumar, M. Ilanchelian, J. Lumin. 151 (2014) 206-218.

[58] J. B. F. Lloyd, NPhS. 231 (1971) 64-65.

[59] J.B.F. Lloyd, J. Forensic. Sci. Soc. 11 (1971) 83-94.

[60] J. N. Miller, Proc. Anal. Div. Chem. Soc. 16 (1979) 203-208.

[61] S. Naveenraj, S. Anandan, J. Photoch. Photobio. C. : Photochem. Rev. 14 (2013) 53-71.

[62] Y.-J. Hu, Y. Ou-Yang, C.-M. Dai, Y. Liu, X.-H. Xiao, Biomacromolecules 11 (2009) 106-112.

[63] H. Liu, X. Shi, M. Xu, Z. Li, L. Huang, D. Bai, Z. Zeng, Eur. J. Med. Chem. 46 (2011) 1638-1647.

[64] J. Ezzati Nazhad Dolatabadi, V. Panahi-Azar, A. Barzegar, A.A. Jamali, F. Kheirdoosh, S. Kashanian, Y. Omidi, RSC Adv. 4 (2014) 64559-64564.

Chapter 6

Synthesis and characterization of C,N cyclometalated new half sandwich Ir(III) and Rh(III) complexes

Abstract

Six new complexes [(η^5-C_5Me_5)IrCl(*para*-R-N-benzylidene-9-ethyl-9H-carbazol-3-amine)] (R = F (**1e**), CH_3 (**2e**), OCH_3 (**3e**)), and [(η^5-C_5Me_5)RhCl(*para*-R-N-benzylidene-9-ethyl-9H-carbazol-3-amine)] (R = F (**4e**), CH_3 (**5e**), OCH_3 (**6e**)) containing carbazole C,N ligands have been synthesized and characterized by ^{1}H NMR, ^{13}C NMR, 2D NMR, melting point analysis, infrared spectroscopy, HR-MS and elemental analyses. The crystal structures of **2e** and **5e** have been determined by single crystal XRD.

Keywords: Half sandwich; Ir(III), Rh(III) complexes; C,N ligands

6.1 Introduction

C-H activation is a popular field in organometallic chemistry due to it is important potential for producing functionalized hydrocarbons and direct arylation and alkenylation in chemical reactions [1]. Intra-molecular C-H functionalized platinum metal complexes were first reported by Cope and Siekman in 1965 [2] and have since shown promise in different fields of catalysis [3]. Cyclometallation in platinum metal complexes is well known and adding of $Pd(OAc)_2$ salt to a $PdCl_2$ complex can induce the cyclometallation of the ligand [4]. In 2003, Davies *et al.* reported sodium acetate salts which were used to promote cyclometalation of nitrogen donor C,N ligands at room temperature [4]. Cyclometalated arene ruthenium complexes coordinated to N,N'-dimethylbenzylamine are well known and are versatile and active catalysts for C-C bond forming reactions with ethene and alkynes [4]. Furthermore, C,N donor ligands also improve the nature of the complexes by enhancing the electron density at the metal center which stabilizes the oxidation states of metal and promotes the rapid hydrolysis of the labile chloro group attached to the metal [5].

In recent years, half sandwich complexes with cyclometalated ligands containing nitrogen donors have become an important emerging field in organometallic chemistry. Octahedral Ir(III) and Rh(III) complexes with C,N ligands have significantly improved the scope of applications in biological studies

and catalysis [6, 7]. Their photochemical and electrochemical properties are of interest in various applications, such as photodynamic therapy, photovoltaic cells, luminescent sensors and anticancer studies [8]. Also, a number of iridium and rhodium cyclometalated catalysts are reported for transfer hydrogenation, hydrogenation, oxidation reactions, reductive amination, imine hydrogenation and olefin hydrogenation reactions [9-11].

In medicinal chemistry, half sandwich Ir(III) and Rh(III) complexes containing C,N ligands have shown promising anticancer activity through intercalation with the target DNA in the cancer cells [6]. The fine tuning of the functional groups present in the ligands and varying metal centers can have a definite effect on biological systems [6, 12]. Furthermore, Ru, Ir, Rh and Os complexes containing cyclometalated ligands are appropriate for anticancer compounds due to their favorable kinetic aspects, rate of ligand exchange, variable oxidation states, low toxicity and intercalating target in DNA in the cancer cells. Thus, they could resolve many of the negative aspects which exist with platinum based anticancer drugs [13-17].

This work describes the synthesis and characterization of new half sandwich complexes containing C,N Schiff base carbazole chelating ligands. The prepared complexes **1e**-**6e** were characterized by ^{1}H NMR, ^{13}C NMR, 2D NMR, IR spectroscopy, HR-MS spectroscopy, single crystal XRD and elemental analysis.

6.2 Experimental Section

6.2.1 Reagents and Methods

Unless otherwise noted, all manipulations were performed using standard Schlenk tube techniques under nitrogen atmosphere. Reagents such as the substituted benzaldehydes, sodium acetate, $IrCl_3 \cdot 3H_2O$ (≥99% purity) and $RhCl_3 \cdot 3H_2O$ (≥99% purity) and solvents were purchased from Sigma-Aldrich, Capital Labs, South Africa and were used without further purification. The NMR solvent $CDCl_3$ was purchased from Merck Germany. The solvents were dried by standard procedures and distilled prior to use [18]. Melting points were recorded on a Stuart^{TM} Scientific apparatus SMP 3 and are uncorrected. ^{1}H NMR (400 MHz) and ^{13}C (100 MHz) NMR were recorded in $CDCl_3$ using a Bruker Topspin 400 MHz spectrometer. Elemental analyses were performed on a Thermo-Scientific Flash 2000 CHNS/O analyser. Solid and liquid state infrared spectra were recorded using an FT-IR Perkin Elmer Spectrum 100 spectrophotometer between 4000 - 400 cm^{-1}. High resolution mass spectra were recorded using a Waters Micromass LCT Premier TOF-MS instrument. X-ray single crystal intensity data were collected on a Bruker Smart *APEX11* Nonius Kappa-CCD diffractometer using graphite monochromated MoKα

radiation (λ = 0.71073 Å). The ligand precursor 3-amino-9-ethyl-9*H*-carbazole [19], ligands (*p*-R- N-benzylidene-9-ethyl-9H-carbazol-3-amine) (R = F (**L1**), CH_3 (**L2**) & OCH_3 (**L3**)) [20] and metal precursors $(IrCl_2Cp^*)_2$ and $(RhCl_2Cp^*)_2$ were prepared according to literature methods [21-23].

6.2.2 Synthesis of the complexes 1e-6e

A common procedure was followed to synthesize the complexes [(η^5-C_5Me_5)IrCl(*para*-R-N-benzylidene-9-ethyl-9H-carbazol-3-amine)] (R = F (**1e**), CH_3 (**2e**), OCH_3 (**3e**)), and [(η^5-C_5Me_5)RhCl(*para*-R-N-benzylidene-9-ethyl-9H-carbazol-3-amine)] (R = F (**4e**), CH_3 (**5e**), OCH_3 (**6e**)).

A mixture of $(MCl_2Cp^*)_2$ (M = Ir / Rh), the Schiff base carbazole ligands (**L1-L3**) and sodium acetate was stirred at room temperature in dichloromethane (15 mL) for 48 hours. The solvent was then removed under vacuum and the residue was dissolved in dichloromethane (10 mL), and filtered through a pad of celite. Evaporation of the solvent in vacuo, followed by the addition of diethyl ether, produce a yellow powder corresponding to complexes **1e**-**6e**.

6.2.2.1 [(η^5-C_5Me_5)IrCl(**L1**)] (**1e**)

$(IrCl_2Cp^*)_2$ (100 mg, 0.13 mmol), Schiff base carbazole ligand **L1** (80 mg, 0.26 mmol) and CH_3COONa (53 mg, 0.65 mmol). Yield (140 mg, 0.21 mmol, 82%). Mp. 332 °C (dec.). ^{1}H NMR (400 MHz, $CDCl_3$, 25 ºC, ppm) δ = 8.40 (s, 1H, imine CH), 8.23 (d, 1H, J_{H-H} = 1.88 Hz), 8.16 (d, 1H, J_{H-H} = 7.68 Hz), 7.84 (d-d, 1H, J_{H-H} = 2.04 Hz), 7.67 (m, 1H), 7.56 (m, 2H), 7.48 (d, 1H, J_{H-H} = 8.20 Hz), 7.42 (d, 1H, J_{H-H} = 8.56 Hz), 7.30 (m, 1H), 6.79 (t, 1H), 4.45 - 4.40 (q, 2H, N - CH_2), 1.51 (m, 18H, C_5Me_5 & N -CH_3). ^{13}C NMR (100 MHz, $CDCl_3$, 25 °C, ppm) δ = 170.21 (imine C-H), 164.76, 162.18, 143.47, 142.80, 138.98, 130.37, 130.27, 126.23, 122.82, 122.76, 122.56, 120.88, 120.69, 119.16, 113.35, 108.86, 108.54, 89.04 (C, C_5Me_5), 37.82 (CH_2, N - CH_2CH_3), 13.84 (CH_3, N - CH_2CH_3), 8.98 (CH_3, C_5Me_5). FT-IR (γ/cm^{-1}): 3040, 2977, 2911, 1625, 1592 (s, C=N), 1538, 1480, 1470, 1460, 1234, 1173, 1147, 1027, 813, 747, 428. HR-MS (TOF MS ES$^+$) $C_{31}H_{31}FIrN_2$ Calculated: 643.2101, Found: 643.2110. Anal. Calcd for $C_{31}H_{31}ClFIrN_2$: C, 54.90; H, 4.61; N, 4.13; Found: C, 54.54; H, 4.62; N, 4.01.

6.2.2.2 [(η^5-C_5Me_5)IrCl(**L2**)] (**2e**)

$(IrCl_2Cp^*)_2$ (100 mg, 0.13 mmol), Schiff base carbazole ligand **L2** (79 mg, 0.26 mmol) and CH_3COONa (53 mg, 0.65 mmol). Yield (146 mg, 0.22 mmol, 86%). Mp. 342 °C (dec.). ^{1}H NMR (400 MHz, $CDCl_3$, 25 ºC, ppm) δ = 8.38 (s, 1H, imine CH), 8.24 (d-d, 1H, J_{H-H} = 1.92 Hz), 8.16 (d, 1H, J_{H-H} =

7.72 Hz), 7.86 (d-d, 1H, J_{H-H} = 2.00 Hz), 7.70 (s, 1H), 7.56 (m, 2H), 7.48 (d, 1H, J_{H-H} = 8.20 Hz), 7.41 (d, 1H, J_{H-H} = 8.68 Hz), 7.30 (m, 1H), 6.89 (d, 1H, J_{H-H} = 7.48 Hz), 4.45 - 4.40 (q, 2H, N - CH_2), 2.49 (s, 3H, CH_3), 1.50 (m, 18H, C_5Me_5 & N -CH_3). ^{13}C NMR (100 MHz, $CDCl_3$, 25 °C, ppm) δ = 174.19 (imine C-H), 169.60, 144.97, 144.54, 142.44, 140.65, 138.85, 135.77, 128.97, 126.11, 123.13, 122.87, 122.68, 121.19, 120.68, 119.07, 116.24, 113.86, 108.80, 108.55, 108.34, 89.03 (C, C_5Me_5), 37.80 (CH_2, N - CH_2CH_3), 22.16 (C, CH_3), 13.85 (CH_3, N - CH_2CH_3), 8.84 (CH_3, C_5Me_5). FT-IR (γ/cm^{-1}): 3041, 2974, 2908, 1583 (s, C=N), 1532, 1481, 1471, 1459, 1230, 1174, 1147, 1028, 814, 747, 728, 567. HR-MS (TOF MS ES$^+$) $C_{32}H_{34}IrN_2$ Calculated: 639.2351, Found: 639.2360. Anal. Calcd for $C_{32}H_{34}ClIrN_2$: C, 57.00; H, 5.08; N, 4.15; Found: C, 56.94; H, 4.93; N, 4.04.

6.2.2.3 [(η^5-C_5Me_5)IrCl(**L3**)] (**3e**)

($IrCl_2Cp^*$)$_2$ (100 mg, 0.13 mmol), Schiff base carbazole ligand **L3** (83 mg, 0.26 mmol) and CH_3COONa (53 mg, 0.65 mmol). Yield (141 mg, 0.20 mmol, 82%). Mp. 315 °C (dec.). ^{1}H NMR (400 MHz, $CDCl_3$, 25 ºC, ppm) δ = 8.32 (s, 1H, imine CH), 8.22 (d-d, 1H, J_{H-H} = 1.44 Hz), 8.15 (D, 1H, J_{H-H} = 7.72 Hz), 7.85 (d-d, 1H, J_{H-H} = 1.44 Hz), 7.61 (d, 1H, J_{H-H} = 8.28 Hz), 7.54 (t, 1H), 7.46 (d, 1H, J_{H-H} = 8.08 Hz), 7.42 (m, 2H), 7.29 (m, 1H), 6.64 (d-d, 1H, J_{H-H} = 2.20 Hz), 4.45 - 4.40 (q, 2H, N - CH_2), 2.49 (s, 3H, CH_3), 1.50 (m, 18H, C_5Me_5 & N -CH_3). ^{13}C NMR (100 MHz, $CDCl_3$, 25 °C, ppm) δ = 173.13 (imine C-H), 171.93, 162.27, 144.55, 140.97, 140.63, 138.74, 130.66, 126.07, 122.87, 122.67, 121.30, 120.65, 119.45, 119.02, 113.86, 108.78, 108.44, 108.32, 89.01 (C, C_5Me_5), 55.07 (C, OCH_3), 37.79 (CH_2, N - CH_2CH_3), 13.84 (CH_3, N - CH_2CH_3), 8.84 (CH_3, C_5Me_5). FT-IR (γ/cm^{-1}): 3046, 3024, 2979, 2910, 1623, 1587 (s, C=N), 1527, 1480, 1470, 1454, 1256, 1240, 1206, 1169, 1147, 1030, 861, 748, 731, 607. HR-MS (TOF MS ES$^+$) $C_{32}H_{34}IrN_2O$ Calculated: 655.2301, Found: 655.2312. Anal. Calcd for $C_{32}H_{34}ClIrN_2O$: C, 55.68; H, 4.96; N, 4.06; Found: C, 55.49; H, 4.81; N, 3.89.

6.2.2.4 [(η^5-C_5Me_5)RhCl(**L1**)] (**4e**)

($RhCl_2Cp^*$)$_2$ (100 mg, 0.16 mmol), Schiff base carbazole ligand **L1** (102 mg, 0.32 mmol) and CH_3COONa (66 mg, 0.80 mmol). Yield (176 mg, 0.28 mmol, 93%). Mp. 249 °C (dec.). ^{1}H NMR (400 MHz, $CDCl_3$, 25 ºC, ppm) δ = 8.27 (m, 1H), 8.25 (s, 1H, imine CH), 8.18 (d, 1H, J_{H-H} = 8.04 Hz), 7.91 (d-d, 1H, J_{H-H} = 1.96 Hz), 7.59-7.52 (m, 3H), 7.48 (d, 1H, J_{H-H} = 8.12 Hz), 7.43 (d, 1H, J_{H-H} = 8.64 Hz), 7.31 (m, 1H), 6.80 (t, 1H), 4.45 - 4.40 (q, 2H, N - CH_2), 1.51 (m, 3H, N -CH_3). 1.45 (s, 15H, C_5Me_5). ^{13}C NMR (100 MHz, $CDCl_3$, 25 °C, ppm) δ = 170.20 (imine C-H), 164.79, 160.21, 143.46, 142.83, 140.71, 138.99, 130.28, 126.23, 122.85, 122.75, 122.57, 120.84, 120.69, 119.16, 113.39, 110.33, 110.10, 108.86, 108.53, 96.42, 96.36 (C, C_5Me_5), 37.81 (CH_2, N - CH_2CH_3), 13.82 (CH_3, N - CH_2CH_3), 8.96 (CH_3,

C_5Me_5). FT-IR (γ/cm^{-1}): 3045, 2978, 2911, 1590 (s, C=N), 1574, 1550, 1481, 1470, 1460, 1372, 1238, 1173, 1149, 1024, 815, 747, 453. HR-MS (TOF MS ES$^+$) $C_{31}H_{31}FN_2Rh$ Calculated: 553.1526, Found: 553.1522. Anal. Calcd for $C_{31}H_{31}ClFN_2Rh$: C, 63.22; H, 5.31; N, 4.76; Found: C, 63.10; H, 4.92; N, 4.61.

6.2.2.5 [(η^5-C_5Me_5)RhCl(**L2**)] (**5e**)

($RhCl_2Cp^*$)$_2$ (100 mg, 0.16 mmol), Schiff base carbazole ligand **L2** (101 mg, 0.32 mmol) and CH_3COONa (66 mg, 0.80 mmol). Yield (160 mg, 0.27 mmol, 85%). Mp. 259 °C (dec.). ^{1}H NMR (400 MHz, $CDCl_3$, 25 ºC, ppm) δ = 8.28 (s, 1H, imine CH), 8.26 (d, 1H, J_{H-H} = 3.84 Hz), 8.18 (d, 1H, J_{H-H} = 7.72 Hz), 7.95 (d-d, 1H, J_{H-H} = 1.96 Hz), 7.70 (s, 1H), 7.55 (m, 1H), 7.47 (m, 2H), 7.43 (d, 1H, J_{H-H} = 8.64 Hz), 7.30 (m, 1H), 6.90 (d, 1H, J_{H-H} = 7.40 Hz), 4.45 - 4.40 (q, 2H, N - CH_2), 2.49 (s, 3H, CH_3), 1.51 (t, 3H, N-CH_3), 1.44 (s, 15H, C_5Me_5). ^{13}C NMR (100 MHz, $CDCl_3$, 25 °C, ppm) δ = 171.05 (imine C-H), 144.08, 143.76, 141.38, 140.64, 138.90, 137.07, 128.67, 126.12, 123.86, 122.90, 122.81, 121.03, 120.71, 119.08, 113.35, 108.80, 108.48, 96.14, 96.08 (C, C_5Me_5), 37.81 (CH_2, N - CH_2CH_3), 22.24 (C, CH_3), 13.85 (CH_3, N - CH_2CH_3), 9.02 (CH_3, C_5Me_5). FT-IR (γ/cm^{-1}): 3039, 2975, 2906, 1624, 1599, 1579 (s, C=N), 1481, 1471, 1460, 1230, 1175, 1147, 1024, 816, 747, 731, 562. HR-MS (TOF MS ES$^+$) $C_{32}H_{34}N_2Rh$ Calculated: 549.1777, Found: 549.1776. Anal. Calcd for $C_{32}H_{34}ClN_2Rh$: C, 65.70; H, 5.86; N, 4.79; Found: C, 65.98; H, 5.70; N, 4.61.

6.2.2.6 [(η^5-C_5Me_5)RhCl(**L3**)] (**6e**)

($RhCl_2Cp^*$)$_2$ (100 mg, 0.16 mmol), Schiff base carbazole ligand **L3** (106 mg, 0.32 mmol) and CH_3COONa (66 mg, 0.80 mmol). Yield (130 mg, 0.22 mmol, 67%). Mp. 283 °C (dec.). ^{1}H NMR (400 MHz, $CDCl_3$, 25 ºC, ppm) δ = 8.25 (s, 1H, imine CH), 8.19 (m, 2H), 7.92 (d, 1H, J_{H-H} = 8.28 Hz), 7.54 - 7.40 (m, 5H), 7.30 (t, 1H), 6.63 (d, 1H, J_{H-H} = 8.00 Hz), 4.44 - 4.39 (q, 2H, N - CH_2), 3.94 (s, 3H, OCH_3), 1.50 (t, 3H, N-CH_3), 1.45 (s, 15H, C_5Me_5). ^{13}C NMR (100 MHz, $CDCl_3$, 25 °C, ppm) δ = 170.19 (imine C-H), 160.99, 143.79, 140.63, 140.04, 138.77, 130.17, 126.07, 122.89, 122.79, 121.17, 121.09, 120.68, 119.03, 113.37, 109.01, 108.79, 108.47, 96.15, 96.08 (C, C_5Me_5), 55.16 (C, OCH_3), 37.79 (CH_2, N - CH_2CH_3), 13.85 (CH_3, N - CH_2CH_3), 9.04 (CH_3, C_5Me_5). FT-IR (γ/cm^{-1}): 3046, 2980, 2909, 1624, 1584 (s, C=N), 1541, 1531, 1480, 1470, 1460, 1239, 1205, 1168, 1147, 1088, 1033, 859, 748, 586. HR-MS (TOF MS ES$^+$) $C_{32}H_{34}N_2ORh$ Calculated: 565.1726, Found: 565.1725. Anal. Calcd for $C_{32}H_{34}ClN_2ORh$: C, 63.95; H, 5.70; N, 4.66; Found: C, 63.98; H, 5.70; N, 4.79.

6.3 Results and discussion

6.3.1 Synthesis of the ligands and complexes

In this work, new half sandwich metal complexes **1**-**6** have been synthesized using C,N carbazole bidentate ligands (Scheme 6.1). The reaction between the chloro bridged dimer $(MCl_2Cp^*)_2$ (M = Ir and Rh) with C, N [*para*-R-N-benzylidene-9-ethyl-9h-carbazol-3-amine)] (R = F (**L1**), CH_3 (**L2**) and OCH_3 (**L3**)] ligands afforded the new [(η^5-C_5Me_5)MCl(**L**)] (M = Ir and Rh; L = **L1**-**L3**) complexes **1e**-**6e** in good yield in dichloromethane (67% to 93%). Complexes **1e**-**6e** are orange-red crystalline solids and are air stable, non-hygroscopic and soluble in common polar solvents such as DMSO, DMF, acetonitrile, dichloromethane, acetone, chloroform, methanol, ethanol and partially soluble in water. These complexes are insoluble in diethyl ether, petroleum ether and hexane.

Characterisation of the ligands **L1**-**L3** and metal complexes **1e**-**6e** was carried out by NMR, 2D NMR (COSY, NOESY), IR spectroscopy, melting point analysis, HR-MS spectroscopy and elemental analyses. The structures of the complexes **2e** and **5e** have been further authenticated by single crystal X-ray crystallography.

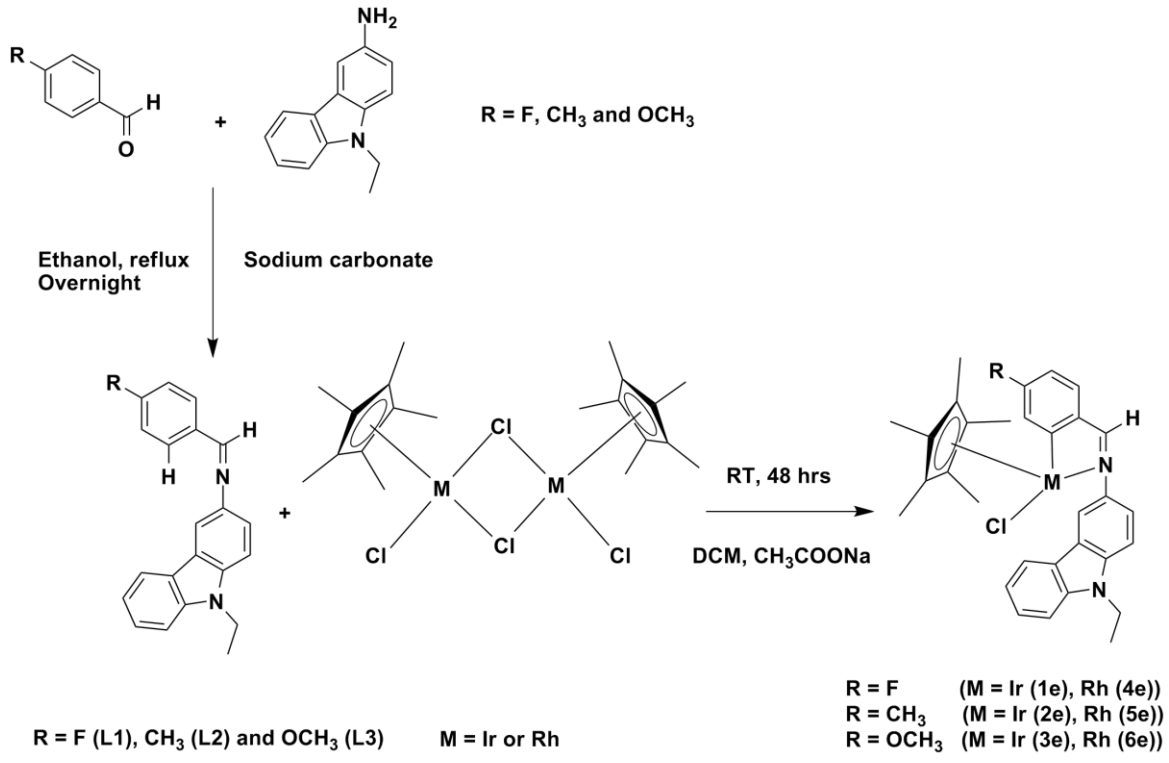

Scheme 6.1: Schematic diagram for the synthesis of ligands (**L1**-**L3**) and complexes **1e**-**6e**.

6.3.2 NMR spectral studies

The spectral data of the ligands and metal complexes have been summarized in the Experimental section. The ^{1}H NMR spectra of the free C,N Schiff base carbazole ligands **L1-L3** showed a CH imine proton singlet signal at 8.65 (**L1**), 8.53 (**L2**) and 8.61 (**L3**) ppm respectively. When the C,N Schiff base carbazole ligands were coordinated with the iridium and rhodium metal precursors, the singlet peak of the imine proton signal shifted up-field to 8.40 (**1e**), 8.38 (**2e**), 8.32 (**3e**) for the Ir complexes and to 8.26 (**4e**), 8.28 (**5e**) and 8.23 (**6e**) ppm for the Rh complexes, respectively. The signals of the aromatic region of all metal complexes **1e-6e** were shifted up-field compared to the respective free ligands signals. The corresponding signals of the benzaldehyde protons in complexes **1e-6e** shifted further up-field to 6.79 for (**1**), 6.89 for (**2**), 6.64 for (**3**), 6.80 for (**4e**), 6.90 for (**5e**) and 6.63 (**6e**) ppm respectively. The electron density around the imine hydrogen was increased by metal-carbon bond, while C-H activated carbon formed five-membered metallocycle with metal. Electron density around the imine hydrogen was further increased by the para-substituents presented in the benzaldeyde moiety. On the other hand, the nitrogen (N) coordination with the metal center might not influence an electron density on the imine ligand as per the ^{1}H NMR and IR shifts. Due to an increasing electron density around the imine hydrogen, both ^{1}H NMR and IR frequencies were shifted to up-field in iridium and rhodium complexes. Both rhodium and iridium metals showed similar trend of coordination to C,N ligands. The rhodium complexes showed more ^{1}H NMR and IR upfield shifts compared to the iridium complexes, due to the smaller atom size of the rhodium atom. The ^{1}H NMR shifts confirmed that the C,N Schiff base carbazole ligands were coordinated to the respective metal centers and hence the formation of the respective complexes **1e-6e**.

6.3.3 Infrared spectroscopy

The IR spectra of the C,N Schiff base carbazole ligands **L1-L3** exhibit a characteristic peak for the (C=N) stretching frequency at 1595 cm^{-1} (**L1**), 1609 cm^{-1} (**L2**) and 1602 cm^{-1} (**L3**) and the stretching frequency of the carbazole moiety aliphatic ethyl group attached to the nitrogen atom (N-CH_2CH_3) appeared in the range of 2835 - 2998 cm^{-1}. In complexes **1e-6e**, these bands are shifted to lower frequencies at 1592 cm^{-1} (**1e**), 1583 cm^{-1} (**2e**), 1587 cm^{-1} (**3e**), 1590 cm^{-1} (**4e**), 1579 cm^{-1} (**5e**) and 1584 cm^{-1} (**6e**), which are attributed to the C,N Schiff base carbazole nitrogen atom of the (C=N) group coordinated with the respective metal centers. The stretching frequency of the aliphatic ethyl group attached to the nitrogen atom (N-CH_2CH_3) was shifted to higher frequencies in all metal complexes, from 2911 to 3040 cm^{-1} (**1e**), 2908 to 3041 cm^{-1} (**2e**), 2910 to 3046 cm^{-1} (**3e**), 2911 to 3045 cm^{-1} (**4e**), 2906 to 3039 cm^{-1} (**5e**) and 2909 to 3046 cm^{-1} (**6e**), respectively. The IR stretching frequency shifts confirmed that

the C,N Schiff base carbazole ligands were coordinated to the respective metal centers and hence the formation of the respective complexes **1e**-**6e**.

6.3.4 HR-MS spectral studies

The mass spectra of the complexes **1e**-**6e** were recorded to confirm the composition of the complexes. The accurate mass of the most abundant peaks present in the metal complexes matched M - Cl (*m/z*) 641.1827, 643.1855 (**1e**), 637.2231, 639.2254 (**2e**), 653.2072, 655.2103 (**3e**), 553.1523, 555.1517 (**4e**), 549.2016, 549.2018 (**5e**) and 565.1760, 566.1796 (**6e**), thus indicating the loss of a chloro group from the respective metal complexes. It seems that the chloro group is more labile than the other groups present in the metal complexes.

6.3.5 Structural information

Selected crystallographic and refinement data (Table 6.1) along with selected bond angles and distances (Table 6.2) of the iridium **2e** and rhodium **5e** complexes are presented. The perspective view of complexes **2e** and **5e** are shown in Figs. 6.1 and 6.2. The complexes **2e** and **5e** are arranged in the monoclinic crystal system with the $P2_1/n$ space group. The crystal structures show typical pseudo-octahedral "piano-stool" geometry with the iridium / rhodium coordinated to an η^5-cyclopentadienyl ligand (Ir(1)-centroid = 1.82 Å / Rh(1)-centroid = 1.83 Å), a chloride atom (Ir(1)-Cl(1) = 2.40 Å / Rh(1)-Cl(1) = 2.27 Å) and the C,N Schiff base carbazole ligand in a bidentate manner forming a five membered metallocycle.

The bond distances of the N(1)-Ir(1) = 2.11 Å, C(11)-Ir(1) = 2.04 Å, Cl(1)-Ir(1) = 2.40 Å, N(1)-Rh(1) = 2.12 Å, C(11)-Rh(1) = 2.03 Å and Cl(1)-Rh(1) = 2.27 Å are consistent with similar bonds reported in the literature [4, 6, 7, 24-26]. The bond angles of the N(1)-Ir(1)-Cl(1) = 88.02°, N(1)-Rh(1)-Cl(1) = 90.57°, C(11)-Ir(1)-Cl(1) = 87.85° and C(11)-Rh(1)-Cl(1) = 88.87° are close to 90°, whilst the centroid of the Cp* ring to iridium and rhodium distances = 1.82 and 1.83 Å respectively, which are also consistent with reported data [4, 24, 25, 27].

Table 6.1 Crystallographic data and summary of structural refinement of the metal complexes **2e** and **5e**

Complex	**2e**	**5e**
Empirical formula	$C_{33}H_{36}Cl_3IrN_2$	$C_{33}H_{36}Cl_3N_2Rh$
Formula weight	759.24	669.90
Temperature/K	173(2)	173(2)
Crystal system	Monoclinic	Monoclinic
Space group	$P2_1/n$	$P2_1/n$
a/Å	11.5604(4)	11.5862(2)
b/Å	14.3378(3)	14.3937(2)
c/Å	18.4761(4)	18.4023(2)
α/°	90	90
β/°	101.3710(10)	101.3800(10)
γ/°	90	90
Volume/$Å^3$	3002.31(14)	3008.59(7)
Z	4	4
$\rho_{calc}g/cm^3$	1.680	1.479
μ(Mo Kα)/mm^{-1}	4.740	0.860
F(000)	1504.0	1376
Crystal size/mm^3	0.21 x 0.16 x 0.14	0.281 x 0.247 x 0.190
Radiation	Mo Kα (λ = 0.71073)	Mo Kα (λ = 0.71073)
2ɵ range for data collection/°	3.62 to 55.94	1.81 to 28.63
Index ranges	-13≤ h ≤15, -18≤ k ≤18, -24≤ l ≤23	-15≤ h ≤14, -19≤ k ≤19, -24≤ l ≤24
Reflections collected	49723	71253
Independent reflections	7077 [R_{int} = 0.0217]	7650 [R(int) = 0.0174]
Data/restraints/parameters	7077/0/359	7650/0/359
Goodness-of-fit on F^2	1.347	1.108
Final R indexes [I>=2σ (I)]	R1 = 0.0185, wR2 = 0.0403	R1 = 0.0227, wR2 = 0.0564
Final R indexes [all data]	R1 = 0.0214, wR2 = 0.0412	R1 = 0.0242, wR2 = 0.0577
Largest diff. peak/hole / e $Å^{-3}$	0.564/-0.781	0.871/-0.975

Table 6.2 Selected bond lengths (Å) and bond angles (°) data for metal complexes **2e** and **5e**

Complex **2e**	Crystal data	Complex **5e**	Crystal data
Bond distances (Å)		Bind distances (Å)	
Ir(1) – C1 (Cp*)	2.269(2)	Rh(1) – C1 (Cp*)	2.271(14)
Ir(1) – C2 (Cp*)	2.259(2)	Rh(1) – C3 (Cp*)	2.262(14)
Ir(1) – C3 (Cp*)	2.158(2)	Rh(1) – C4 (Cp*)	2.154(14)
Ir(1) – C5 (Cp*)	2.159(2)	Rh(1) – C6 (Cp*)	2.171(15)
Ir(1) – C6 (Cp*)	2.149(2)	Rh(1) – C8 (Cp*)	2.145(15)
Ir(1) – Centroid (Cp*)	1.828	Rh(1) – Centroid (Cp*)	1.832
Ir(1) – Cl(1)	2.401(5)	Rh(1) – Cl(1)	2.395(4)
Ir(1) – N(1)	2.111(17)	Rh(1) – N(1)	2.117(12)
Ir(1) – C(11)	2.041(2)	Rh(1) – C(11)	2.030(14)
Bond angles (°)		Bond angles (°)	
N(1)-Ir(1)-C(11)	78.05(7)	N(1)-Rh(1)-C(11)	78.79(5)
N(1)-Ir(1)-Cl(1)	88.02(5)	N(1)- Rh(1)-Cl(1)	90.57(3)
N(1)-Ir(1)-C(1)	103.82(7)	N(1)- Rh(1)-C(1)	102.81(5)
N(1)-Ir(1)-C(2)	132.10(7)	N(1)- Rh(1)-C(3)	131.16(5)
N(1)-Ir(1)-C(3)	166.89(7)	N(1)- Rh(1)-C(4)	165.50(5)
N(1)-Ir(1)-C(5)	134.57(8)	N(1)- Rh(1)-C(6)	133.75(6)
N(1)-Ir(1)-C(6)	103.22(7)	N(1)- Rh(1)-C(8)	102.17(5)
N(1)-Ir(1)-Centroid (Cp*)	132.43	N(1)-Rh(1)-Centroid (Cp*)	131.20
C(11)-Ir(1)-Cl(1)	87.85(6)	C(11)-Rh(1)-Cl(1)	88.87(4)
C(11)-Ir(1)-C(1)	155.39(8)	C(11)-Rh(1)-C(1)	152.96(6)
C(11)-Ir(1)-C(2)	149.76(8)	C(11)-Rh(1)-C(3)	149.99(6)
C(11)-Ir(1)-C(3)	112.08(8)	C(11)-Rh(1)-C(4)	111.80(6)
C(11)-Ir(1)-C(5)	97.11(8)	C(11)-Rh(1)-C(6)	95.51(6)
C(11)-Ir(1)-C(6)	117.01(8)	C(11)-Rh(1)-C(8)	114.60(6)
C(11)-Ir(1)-Centroid (Cp*)	131.61	C(11)-Rh(1)-Centroid (Cp*)	129.97

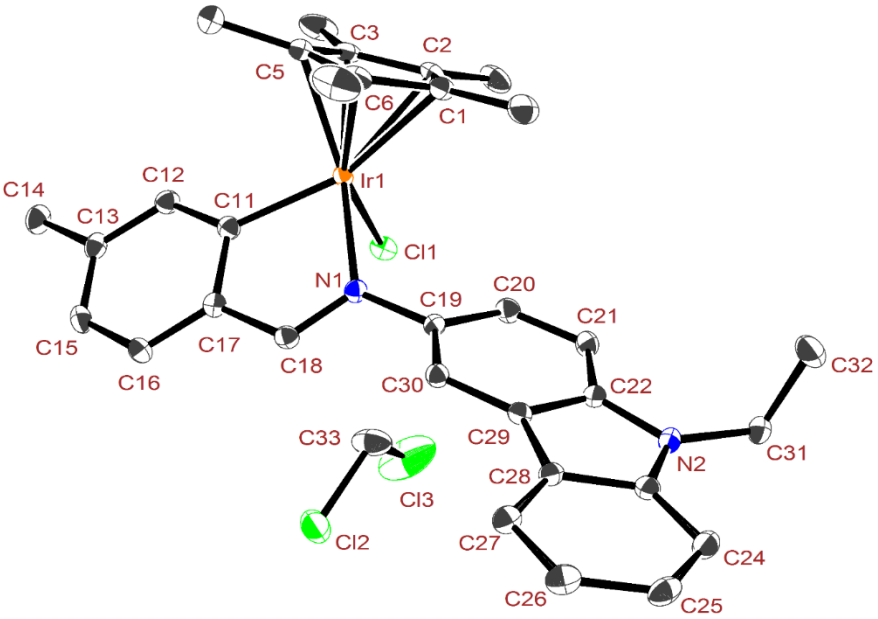

Fig. 6.1 The *ORTEP* diagram of iridium complex **2e**. Displacements of the ellipsoids are drawn at 50% probability and hydrogen atoms are omitted for clarity.

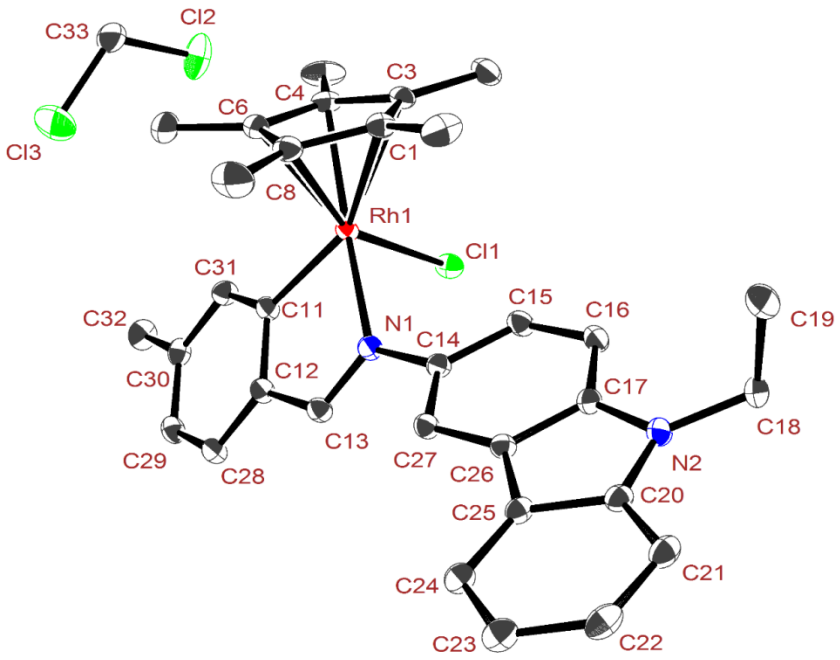

Fig. 6.2 The *ORTEP* diagram of rhodium complex **5e**. Displacements of the ellipsoids are drawn at 50% probability and hydrogen atoms are omitted for clarity.

6.4 Conclusions

In conclusion, the new half sandwich Ir(III) and Rh(III) complexes were synthesized and characterized. ^{1}H NMR, IR spectroscopy, HR-MS spectroscopy and elemental analysis further confirmed the formation of the Ir(III) and Rh(III) complexes. The crystal structures confirm that the synthesized Ir(III) and Rh(III) complexes exhibit a "piano-stool" pseudooctahedral geometry in their crystal structures.

Acknowledgements

Authors would like to thank the NRF, THRIP Grant (Grant no. TP 1208035643) and the University of KwaZulu - Natal, Durban, South Africa for financial support.

Appendix A. Supplementary Information

The ^{1}H and ^{13}C NMR, 2D NMR, HR-MS spectroscopy and crystal data of the complexes are also shown in the SI.

References

[1] A.E. Shilov, G.B. Shul'pin, Chem. Rev. 97 (1997) 2879-2932.

[2] A.C. Cope, R.W. Siekman, J. Am. Chem. Soc. 87 (1965) 3272-3273.

[3] V. Ritleng, C. Sirlin, M. Pfeffer, Chem. Rev. 102 (2002) 1731-1770.

[4] D.L. Davies, O. Al-Duaij, J. Fawcett, M. Giardiello, S.T. Hilton, D.R. Russell, Dalton Trans. (2003) 4132-4138.

[5] Z. Liu, I. Romero-Canelón, B. Qamar, J.M. Hearn, A. Habtemariam, N.P.E. Barry, A.M. Pizarro, G.J. Clarkson, P.J. Sadler, Angew. Chem. 126 (2014) 4022-4027.

[6] S. Mukhopadhyay, R.K. Gupta, R.P. Paitandi, N.K. Rana, G. Sharma, B. Koch, L.K. Rana, M.S. Hundal, D.S. Pandey, Organometallics 34 (2015) 4491-4506.

[7] K.-i. Fujita, T. Yoshida, Y. Imori, R. Yamaguchi, Org. Lett. 13 (2011) 2278-2281.

[8] Y. You, W. Nam, Chem. Soc. Rev. 41 (2012) 7061-7084.

[9] S. Gruber, M. Neuburger, A. Pfaltz, Organometallics 32 (2013) 4702-4711.

[10] Y. Wei, D. Xue, Q. Lei, C. Wang, J. Xiao, Green Chem. 15 (2013) 629-634.

[11] E. Féghali, L. Barloy, J.-T. Issenhuth, L. Karmazin-Brelot, C. Bailly, M. Pfeffer, Organometallics 32 (2013) 6186-6194.

[12] Z. Liu, P.J. Sadler, Acc. Chem. Res. 47 (2014) 1174-1185.

[13] G.S. Yellol, A. Donaire, J.G. Yellol, V. Vasylyeva, C. Janiak, J. Ruiz, Chem. Commun. 49 (2013) 11533-11535.

[14] N. Cutillas, G.S. Yellol, C. de Haro, C. Vicente, V. Rodríguez, J. Ruiz, Coord. Chem. Rev. 257 (2013) 2784-2797.

[15] F. Lentz, A. Drescher, A. Lindauer, M. Henke, R.A. Hilger, C.G. Hartinger, M.E. Scheulen, C. Dittrich, B.K. Keppler, U. Jaehde, Anti-cancer drugs 20 (2009) 97-103.

[16] Z. Liu, L. Salassa, A. Habtemariam, A.M. Pizarro, G.J. Clarkson, P.J. Sadler, Inorg. Chem. 50 (2011) 5777-5783.

[17] B. Boff, C. Gaiddon, M. Pfeffer, Inorg. Chem. 52 (2013) 2705-2715.

[18] D.D.A. Perrin, W. L. F.; Perrin, D. R, Purification of laboratory Chemicals, Pergamon: Oxford, UK, 1986.

[19] C.W. Cheung, D.S. Surry, S.L. Buchwald, Org. Lett. 15 (2013) 3734-3737.

[20] A. Bytyqi-Damoni, H. Genç, M. Zengin, S. Beyaztas, N. Gençer, O. Arslan, Artif. Cell. Blood. Sub. 40 (2012) 369-377.

[21] R. Lenz, S. V. Ley, J. Chem. Soc., Perkin Trans. 1. (1997) 3291-3292.

[22] C. White, A. Yates, P.M. Maitlis, Inorg. Synth 29 (1992) 228-234.

[23] M.A. Bennett, A.K. Smith, J. Chem. Soc., Dalton Trans. (1974) 233-241.

[24] M. Yadav, A.K. Singh, D.S. Pandey, Organometallics 28 (2009) 4713-4723.

[25] L. Li, W.W. Brennessel, W.D. Jones, Organometallics 28 (2009) 3492-3500.

[26] R.K. Gupta, R. Pandey, G. Sharma, R. Prasad, B. Koch, S. Srikrishna, P.-Z. Li, Q. Xu, D.S. Pandey, Inorg. Chem. 52 (2013) 3687-3698.

[27] R.K. Gupta, G. Sharma, R. Pandey, A. Kumar, B. Koch, P.-Z. Li, Q. Xu, D.S. Pandey, Inorg. Chem. 52 (2013) 13984-13996.

Chapter 7

General Conclusion

7.1 Chapter 2

The preparation of a N,N' (N-(pyridin-2-ylmethylene)aniline) bidentate imine ligand was successful. The N,N' ligand was characterized by ^{1}H NMR, ^{13}C NMR, IR spectroscopy and UV-vis spectroscopy and the successful complexation of the ligand to iridium, rhodium and ruthenium was achieved. The Ir(III), Rh(III) and Ru(II) complexes were characterized by ^{1}H NMR, ^{13}C NMR, IR spectroscopy, UV-vis spectroscopy, mass spectroscopy, melting point analysis and elemental analyses. The crystal structures of complexes [Cp*MCl(N-(pyridin-2-ylmethylene)aniline)]PF_6 (M = Ir (**1a**) and Rh(**2a**)) and [(η^6-arene)RuCl(N-(pyridin-2-ylmethylene)aniline)]PF_6 (**3a**) were determined by single crystal XRD confirming that the N,N' ligands were coordinated to the metal center via the nitrogen atoms. The catalytic performance of these complexes for the dehydrogenation of primary alcohols to their respective aldehydes with different bases and solvents was demonstrated. The complexes of iridium (**1a**) and ruthenium (**3a**) gave a good conversion in different alkaline solutions.

A theoretical approach using DFT and Gibbs free energy calculations unambiguously explained the reactivity of the complexes and a reaction mechanism was proposed. The energy difference between the HOMO and LUMO for complexes **1a**-**3a** are 120.59 kcal\mol, 130.67 kcal/mol and 124.49 kcal/mol respectively, which indicates that the lower energy gap of the iridium complex makes it more reactive than the latter complexes. The calculations thus supported the experimental results. Also, the NPA analysis for the iridium complex clearly shows that N,N' bidentate ligand donor strength on the iridium (N1 = -0.441 & N2 = -0.405) is higher than on rhodium and ruthenium, which facilitated the iridium complex to be more reactive than the other two.

The Gibbs free energy (ΔG) calculation of the reaction intermediates of the proposed rhodium catalytic cycle clearly shows that the catalytic cycle progressed through a metal-hydride intermediate. The Gibbs free energy for the Rh-H is -8.50 kcal/mol, which is much lower than the transition states Rh-benzyloxo A (21.41 kcal/mol), Rh-dihydride complex C (20.34 kcal/mol) and 16e$^-$ Rh complex D (31.85 kcal/mol). The Rh-benzyloxo to Rh-H formation step is attributed to the rate determining step of the

proposed reaction mechanism. Additionally, the reaction mechanism which goes via C as compared to D, is explained by the free energy barrier of the transition states.

7.2 Chapter 3

A series of N,N' bidentate amine ligands have been synthesized successfully and characterized by ^{1}H NMR, ^{13}C NMR and IR spectroscopy. All ligands were successfully coordinated to iridium and rhodium. The resultant six new complexes [Cp*IrCl(*para*-R-N-(pyridin-2-ylmethyl)aniline)]PF_6 (R = H (**1b**); F (**2b**); OCH_3 (**3b**)) and [Cp*RhCl(*para*-R-N-(pyridin-2-ylmethyl)aniline)]PF_6 (R = H (**4b**); F (**5b**); OCH_3 (**6b**)) were characterized by different spectral techniques. The crystal structures (R_M, S_{N-H}) of [Cp*IrCl(N-(pyridin-2-ylmethyl)aniline)]PF_6 (**1b)** and [Cp*RhCl(*para*-OCH_3-N-(pyridin-2-ylmethyl)aniline)]PF_6 (**6b**) were unambiguously determined by single crystal X-ray diffraction. Interestingly, the iridium and rhodium complexes showed diastereomers and cross interactions between the CH_2 to Cp* moiety, as well as the CH_2 to the phenyl ring in solution, which was further confirmed by ^{1}H NMR and 1D NOE NMR analysis.

The catalytic transfer hydrogenation of aromatic ketones and aldehydes in water was demonstrated for these complexes under pH dependent acidic reaction conditions. Generally, the Ir(III) amine complexes (**1b**-**3b**) required longer reaction times (4 to 6 hr) than the Rh(III) amine complexes (**4b**-**6b**) under the specified reaction conditions. This is due to the highly acidic N-H proton, which promoted the formation of imine Ir(III) complexes in the reaction. Though the Ir(III) imine complexes remain active in the reaction medium, they required a longer reaction times to reduce the aromatic ketones. Overall, the Rh(III) amine and imine complexes proved to be most efficient catalysts, as they gave significantly higher conversions as compared to the Ir(III) amine complexes. Another feature of this system is that the catalyst was recovered and that the recovered catalyst was active for at least three catalytic cycles.

7.3 Chapter 4

New carbazole N,N' imine ligand has been synthesized successfully and characterized by ^{1}H NMR, ^{13}C NMR and IR spectroscopy. New carbazole N,N' imine ligand successfully coordinated with iridium, rhodium, ruthenium and osmium metals via nitrogen atoms. The resultant nine new complexes [(η^5-C_5Me_5)MCl(**L**)]PF_6, (M = Ir (**1c**) and Rh (**2c**)) and [(η^6-C_6H_6)RuCl(**L**)]PF_6 (**3c**), [(η^6-*p*-cymene)RuX(**L**)]PF_6 (X = Cl (**4c**), Br (**5c**), I (**6c**)), [(η^6-C_6H_6)OsCl(**L**)]PF_6 (**7c**), [(η^6-*p*-cymene)OsX(**L**)]PF_6 X = Cl (**8c**), I (**9c**)) (**L** = 9-ethyl-N-(pyridine-2-yl methylene)-9H-carbazole-3-amine) were completely characterized by ^{1}H NMR, ^{13}C NMR, 2D NMR, melting point analysis, IR spectroscopy, HR-MS spectroscopy and elemental analyses. The crystal structures of [(η^5-

C_5Me_5)RhCl(**L**)]PF_6 (**3c**) and [(η^6-*p*-cymene)RuI(**L**)]PF_6 (**6c**) further confirmed that the N,N' imine ligands were coordinated to the metal center via nitrogen atoms.

Anticancer study of the synthesized complexes **1c**-**3c** clearly showed them to be potent inhibitors of human breast cancer cells (MCF-7) under *in vitro* conditions. The inhibitory concentrations (IC_{50}) of the complexes **1c**-**3c** were determined at low (5, 6 and 8 μM) concentration against the MCF-7 human breast cancer cell line. The activity of the complexes **1c**-**3c** were explained by the hydrophobicity of the Cp* ring, higher than that of the benzene ring, which was effective in penetrating the cell membrane. Experimental results for complexes **1c**-**3c** showed the mode of interaction and that a greater extent of interaction occurred with the iridium complex with DNA and protein, and that it had a higher effective penetrating nature into the cell membrane than the other two complexes. Furthermore, the docking studies for complexes **1c**-**3c** with the COX-2 receptor showed that the iridium complex binding energy (-8.18 kcal/mol) was higher than those of the rhodium (-7.34 kcal/mol) and ruthenium (-7.13 kcal/mol) complexes, which indicated that the iridium complex is most stable in the hydrophobic pocket active site of COX-2.

7.4 Chapter 5

New [$RuCl_2$(COD)(**L1**)] (**1d**), [$RuCl_2$(COD)(**L2**)] (**2d**), [$RuCl_2$(COD)(**L3**)] (**3d**), [$RuCl_2$(COD)(**L4**)] (**4d**), [$RuCl_2$(COD)(**L5**)] (**5d**) (**L** = (*p*-R-N-(pyridin-2-ylmethylene)aniline), R = H (**L1**), Cl (**L2**), OCH_3 (**L3**), CH_3 (**L4**), **L5** = (9-ethyl-N-(pyridin-2-ylmethylene)9H-carbazole-3-amine and COD = η^4-cyclooctadiene) complexes containing N,N' bidentate ligands were successfully synthesized and characterized by various spectral techniques. The crystal structure of complexes **1d**-**3d** showed coordination of the ligands to the Ru(II) centre in a bidentate manner via the N atoms and exhibited pseudooctahedral geometry.

The complexes **1d**-**5d** showed binding interaction with human serum albumin (HSA). Among the complexes **1d**-**5d**, complex **1d** showed strongest binding interaction with HSA compared to the other complexes, which is explained by the planarity of the complexes. In the case of complex **1d** there is no substitution on the phenyl ring present in the ligand which may assist complex planarity which gives the high interaction with HSA as seen in the experimental results. Complex **3d** with the *p*-methoxy (OCH_3) group showed better interaction compared to complex **2d** with the *p*-Cl group. Complex **5d** showed both electronic and steric effects in the HSA binding studies. A molecular docking study of complexes **1d**-**5d** with HSA confirmed that complex **1d** (-6.67 kcal/mol) showed the highest binding energy among the complexes **1d**-**5d**. Overall, docking studies confirmed that complexes **1d**-**5d** are located close to the active site residues of Trp 214, Arg 222, His 242, Leu 238 and Ala 291 in HSA subdomain IIA.

7.5 Chapter 6

A series of the C,N bidentate Schiff base ligands [*para*-R-N-benzylidene-9-ethyl-9H-carbazol-3-amine] (R = F (**1e**), CH_3 (**2e**), OCH_3 (**3e**) have been synthesized successfully and characterized by ^1H NMR, ^{13}C NMR and melting point analysis. These three ligands were successfully cyclometalated with iridium and rhodium. The resultant six new complexes [Cp*IrCl(**L**)] [**L** = (*para*-R-N-benzylidene-9-ethyl-9h-carbazol-3-amine)] R = F (**1e**), CH_3 (**2e**), OCH_3 (**3e**)), and [Cp*RhCl(**L**)] R = F (**4e**), CH_3 (**5e**), OCH_3 (**6e**) were characterized by ^1H NMR, ^{13}C NMR, IR spectroscopy and elemental analysis. The crystal structure of the complexes **2e** and **5e** showed a pseudooctahedral geometry in their crystal structures.

Finally, it can be concluded that the main goals of this study were achieved because the complexes were successfully synthesized, characterized and investigated for their catalytic activities in oxidation of primary alcohols and transfer hydrogenation of aromatic ketones under green conditions. Some of the metal complexes were also investigated in an anti-cancer cytotoxicity study and in binding interactions with human serum albumin. All the synthesized complexes showed excellent catalytic activities for their respective catalytic systems as well as in biological applications. The majority of the synthesized bidentate half sandwich complexes exhibited the common “piano-stool” geometry. The geometries around the metal centers of the complexes is “piano-stool” in which the N,N' / C,N atoms and a Cl group form the base, while the π-bonds of the Cp* / arene ring form the apex of a piano stool.

Appendix

Appendix for each chapter 2-6 given in the disk